

Experimental and simulation-based investigation of the performance of a 100 % methanol port-injected spark-ignited engine.

J.J. Bosklopper

Supervisors:

ir. Klaas Visser

prof.dr. Dirk Roekaerts

prof.dr.ir. Robert van de Ketterij

ir. Harsh Sapra

PE report number 3029



Experimental and simulation-based investigation of the performance of a 100 % methanol port-injected spark-ignited engine.

by

J.J. Bosklopper

to obtain the degree of Master of Science
at the Delft University of Technology,
to be defended on Monday August 24, 2020 at 09:00 AM.

Student number:	1178334	
Project duration:	November 11, 2019 – August 24, 2020	
Thesis committee:	Ir. Klaas Visser	TU Delft, supervisor
	Prof. dr. Dirk Roekaerts	TU Delft, chairman
	Prof. dr. ir. Robert van de Ketterij	NLDA
	Prof. dr. ir. Wiebren de Jong	TU Delft
	ir. Harsh Sapra	TU Delft

An electronic version of this thesis is available at <http://repository.tudelft.nl/>.

Abstract

The maritime sector faces major challenges with increasing regulations from the International Maritime Organization (IMO) and national regulations for CO₂, SO_x and NO_x. Innovative fuel types for maritime use are now under development by various stakeholders. Methanol shows considerable potential as one of the most promising for implementation in the short to medium term, based on the potential availability, emission reduction, and energy density. The Green maritime methanol (GMM) project is Netherlands based collaboration of important stakeholders such as shipbuilders, engine manufacturers and universities. Within this project, methanol is researched as a potential alternative combustion fuel for maritime vessels. For this purpose, the "Dutch Caterpillar engine dealer" PON Power provided a G3508A engine available as a retrofit option. The engine is a turbocharged spark-ignited natural gas (NG) engine with 8 cylinders and a rated power of 500 kW_e at 1500 rpm. After six months of rebuilding the engine, the spark-ignited (SI), port fuel injected (PFI) engine runs on 100% methanol. Tests with stable engine operation were achieved with 100% methanol at 25%, 50%, and 75% engine loading and a constant engine speed of 1500 rpm.

In this research, experiments and modelling have been performed to study combustion using 100% PFI methanol. Measurements are realized with varying: ignition timings, NO_x emission settings, and manifold temperatures. Data collected during these measurements such as in-cylinder pressures, emissions, and temperatures, provided a comparison between running the engine on methanol or natural gas. In this comparison combustion stability is determined with the coefficient of variation (COV) of P_{max} and of imep, optimum ignition timing is determined and engine efficiency is calculated and compared to NG. Modelling is accomplished with a TU Delft model of the G3508A SI engine adjusted for the use of 100% methanol as a fuel. A modified sub-model for the PFI and vaporization of methanol has been developed. These engine data will be used to validate the methanol engine model and to optimise the engine performance for further experimental runs and better understanding the use of methanol as a fuel.

The effect on the performance and the combustion when 100% methanol is used as fuel for a SI PFI engine compared to premixed injection of natural gas is shown in this work. The engine operates stably on methanol at 50% and 75% load within ignition timings of 16-24 °CA BTDC, but less stable than with NG. Heat release indicates an almost similar combustion duration, but shorter combustion duration is shown for methanol. Also with methanol, the crank angle where 50% of fuel is burnt (CA50) is shown earlier compared to NG. The faster premixed combustion, combined with a better found fuel consumption operating point, resulted in higher efficiencies for methanol compared to NG for the tested 50% and 75% load at comparable operating conditions.

Preface

Proudly I introduce my thesis "Experimental and simulation-based investigation of the performance of a 100 % methanol port-injected spark-ignited engine". This thesis is written to obtain the degree of Master of Science at the Delft University of Technology. Assisted by PON Power in Papendrecht, I have been working on this thesis from November 2019 until August 2020. It has been a challenge to continue studying after finishing my Bsc degree in 2009 at the Netherlands Defence Academy (NLDA) on Military Platform systems. Tight planning and perseverance enabled me to finish the Master's program within the given time frame.

First of all, I want to express my gratitude to the Royal Dutch Navy for providing access to this 2-year Master's program. Furthermore, I sincerely appreciated the excellent academic guidance and counselling of my supervisors: Ir Visser, Prof. Van de Ketterij and Prof. Roekaerts. Thank you for allowing me to do my research in this very interesting project. Ir. H. Sapra, thank you for the daily discussions and guidance. Also, I do owe sincere appreciation to various people at Pon Power: Joost Schapendonk for giving me the opportunity to work at your company. Edwin Spoelder and Wim van Sluijs for all interesting discussion and hard work throughout the project. And last but not least, I would like to thank my friends and family for their support and encouragement. Especially gratitude to my fiancée, Edmée de Vries, taking almost full responsibility in caring for our two children, thus enabling me to work continuously on my study and thesis.

Please enjoy reading.

*Jurian Bosklopper
Delft, August 2020*

Contents

List of Figures	xi
List of Tables	xv
Nomenclature	xix
1 Introduction	1
1.1 Background	1
1.2 Thesis objective & research questions	2
1.3 Methodology	2
1.4 Thesis outline	2
2 Literature study	3
2.1 Background of methanol	3
2.1.1 Current use of methanol in internal combustion engines (ICEs)	3
2.1.2 Alternative fuel in a maritime environment	4
2.1.3 Recent methanol projects in the maritime sector	4
2.2 Methanol production	4
2.2.1 Production from coal	4
2.2.2 Production from natural gas	5
2.2.3 Production from natural biomass and municipal solid waste	5
2.2.4 A synthesised methanol production method from CO ₂ and renewable H ₂	5
2.2.5 Conclusion of methanol production	6
2.3 Fuel properties	6
2.3.1 Boiling temperature.	6
2.3.2 Auto-ignition temperature	6
2.3.3 Liquid density	7
2.3.4 Lower heating value	7
2.3.5 Oxygenated Fuel	7
2.3.6 Latent heat of vaporization	7
2.3.7 Flammability limits	7
2.3.8 Flame speed	7
2.3.9 Sulfur content.	7
2.3.10 Cetane number	7
2.3.11 Octane number	8
2.3.12 Lubricity and viscosity	8
2.4 Methanol in ICE.	8
2.4.1 Direct injection (DI) of methanol blends with diesel.	8
2.4.2 Port fuel injection (PFI) of methanol and DI of (pilot) diesel	8
2.4.3 M100 Port fuel injection (PFI)	9
2.4.4 M100 Direct injection (DI)	9
2.4.5 Challenges of methanol in ICE.	9
2.4.6 Emissions	10
2.5 Methanol versus ethanol	10
2.6 Methanol in ICE models	11
2.6.1 Types of models	11
2.6.2 Investigated aspects of ICE (sub-)models:	11
2.6.3 Flame speed	11
2.6.4 In-cylinder heat transfer	13
2.6.5 Fuel evaporation time	13
2.6.6 Wall-wetting effect	13

2.6.7	Knock and misfire	14
2.6.8	Heat release	15
2.7	Hypotheses	17
3	The experimental setup	19
3.1	The engine	19
3.1.1	Modifications on the engine	20
3.2	The test setup	21
3.2.1	Schematic overview of the fuel and air system	21
3.3	The test plan	22
3.3.1	Performance runs on NG.	23
3.3.2	Performance runs on methanol	23
3.4	Sensor sensitivity	24
4	Analysis of the experiments	27
4.1	Methanol compared to NG	27
4.1.1	Cycle-to-cycle pressure variations	27
4.1.2	Cylinder-to-cylinder variations	30
4.1.3	Mean cylinder pressure	31
4.2	Ignition variation	32
4.2.1	Cylinder pressure with changing ignition timing	32
4.2.2	COV_{pmax} and COV_{imep} with changing ignition timing	33
4.2.3	COV values from Kibox with changing ignition timing	34
4.2.4	COV values from Kibox for methanol compared to NG	35
4.3	Aftercooler temperature variation	36
4.4	Combustion duration	38
4.5	Effective (brake) engine efficiency	39
4.6	Experimental sub-conclusions	40
5	The model	43
5.1	The in-cylinder HR-model	43
5.1.1	Volume	43
5.1.2	Temperature	44
5.1.3	Air excess ratio	44
5.1.4	Mass and composition balance	45
5.1.5	Properties library	46
5.1.6	Heat of combustion	47
5.1.7	Heat loss to cylinder walls (Woschni model)	47
5.1.8	Energy of fuel	48
5.1.9	Heat release calculations	48
5.1.10	Spark-ignited (SI) engine.	49
5.2	Modifications in the model for the engine on methanol	49
5.2.1	Modifications for the fuel	50
5.2.2	New sub-model: Heat loss to liquid fuel h-u (methanol)	51
5.2.3	The vaporization factor	53
5.3	Assumptions & pre-calculations used in model	56
6	Analysis of the model	59
6.0.1	Methanol compared to NG	59
6.0.2	Ignition variation	59
6.0.3	Aftercooler temperature variation	59
6.1	Pressure	59
6.1.1	The chosen cylinder	60
6.1.2	Methanol compared to NG	60
6.1.3	Ignition sweep	61
6.1.4	Aftercooler temperature variation	61
6.1.5	Conclusion pressure	62

6.2	Power	62
6.2.1	TDC shift	62
6.2.2	Methanol compared to NG	64
6.2.3	Ignition variation	64
6.2.4	Aftercooler temperature variation	65
6.2.5	Conclusion Power	65
6.3	Heat release	66
6.3.1	Methanol compared to NG	66
6.3.2	Ignition variation	68
6.3.3	Aftercooler temperature variation	71
6.3.4	Conclusion heat release	71
6.4	Temperature	72
6.4.1	Methanol compared to NG	72
6.4.2	Ignition variation	73
6.4.3	Aftercooler temperature variation	74
6.4.4	Conclusion Temperature	75
6.5	Validation of the models with Kibox HR & HRR	75
6.5.1	Validation of the NAHR for the methanol model.	75
6.5.2	Validation of the NAHR for the NG model	77
6.5.3	Heat release rate validation	78
6.6	Modelling sub-conclusions	79
7	Conclusions & recommendations	81
7.1	Conclusions	81
7.2	Recommendations	83
A	Engine modifications	85
A.1	Fuel system	86
A.1.1	Fuel hoses / piping	86
A.1.2	Fuel storage	87
A.1.3	Fuel pump	87
A.1.4	Fuel filters	88
A.1.5	Fuel rail	88
A.1.6	Fuel injection & ignition.	88
A.1.7	Fuel injectors	88
A.1.8	Spark plug	88
A.1.9	Safety and control valves	89
A.2	Cooling system	89
A.2.1	Charged air cooling system before modifications	89
A.2.2	Modification on the air cooling system.	89
A.2.3	Engine cooling system	90
A.3	Control system	90
A.3.1	Woodward LECM.	90
A.3.2	Engine PLC	90
A.4	Safety system.	90
A.4.1	Vapor detection system	90
A.4.2	Inert gas system: Nitrogen	91
A.4.3	Extra safety systems	91
A.5	Measurement systems	91
A.5.1	Dewetron measurement & adjust sensors	91
A.5.2	Kibox	92
A.5.3	Testo-350	92

B Extra analysis	93
B.1 Stable load runs	93
B.2 NO _x variation	94
B.3 Efficiency	94
B.3.1 Methanol compared to NG	96
B.3.2 Ignition variation	96
B.3.3 Aftercooler temperature variation	97
B.3.4 Conclusion efficiency	97
C Validations and deviations	99
C.0.1 Validation COV values calculated compared to Kibox COV values.	99
C.0.2 Stability increase after replacement of the injector of cylinder 4	103
C.0.3 Check the influence of 2 degrees difference in IVO	104
D Test plan for the engine on methanol	107
E Sensors and calibrationreports	111
F Task risk analysis	115
G Engine and Generator datasheet	119
H refprop datasheets	123
I Natural gas analyse	125
Bibliography	129

List of Figures

2.1	Methanol storage capacity worldwide [25]	3
2.2	Synthetic methanol production [28]	5
2.3	Fuel properties [25]	6
2.4	Example of a port fuel injection system [26]	8
2.5	NO _x emissions vs temperature [15]	10
2.6	Trade-off between NO _x and CO emissions [26]	10
2.7	Methanol flame speed vs temperature [23]	12
2.8	Methanol flame speed vs equivalence ratio [23]	12
2.9	Flame speed of various fuels vs equivalence ratio [46]	12
2.10	Wall effect with PFI [49]	14
2.11	Wall effect mass balance [49]	14
2.12	Kibox HR figure showing knock in cylinder 4 during tests	14
2.13	Operating window of a Wartsila 9L50DF [9]	14
2.14	Typical heat release curve of DE [37]	15
2.15	Cycle to cycle difference in heat flux curve shown [15]	15
2.16	Heat release of a natural gas engine with changing injection timings [50]	16
2.17	P and HRR of a 4 cylinder, 2L, 18:1, engine with 100% methanol at 1400 rpm with changing ignition timings [48]	16
3.1	The G3508A Spark-ignited gas engine	19
3.2	fuel line	20
3.3	injector holders	20
3.4	injectors	20
3.5	Testbed	21
3.6	Control room	21
3.7	Schematic of the test setup	22
4.1	Cycle-to-cycle variation of cylinder 4 with NG	28
4.2	Cycle-to-cycle variation of cylinder 4 with methanol	28
4.3	Mean pressure cylinder-to-cylinder variation with NG	30
4.4	Mean pressure cylinder-to-cylinder variation with methanol	31
4.5	Mean pressure of NG compared to methanol at 375 kWe	31
4.6	Mean pressure of all cylinders with changing ignition timing at 250 kWe on 100 % methanol	32
4.7	Mean pressure of all cylinders with changing ignition timing at 375 kWe on 100 % methanol	32
4.8	COV values with methanol of cyl 4 from Kibox with varying ignition timing at 375 kWe (M=30 for every COV point)	34
4.9	COV values of NG and methanol at 375 kWe and 20 °CA BTDC ignition from Kibox (M=30 for every COV point)	35
4.10	Temperature aftercooler variation between 40 °C and 60 °C	36
4.11	No _x emission during temperature increase to 60°C	37
4.12	Mean in-cylinder pressure plots at a T _{manifold} of 40 °C and 60 °C	38
5.1	Blockdiagram of the "Heat release calculation model [8]"	43
5.2	The coefficients for the polynomial to calculate C _p for methanol"	50
5.3	Scheme of the control volume of the in-cylinder model [34]"	52
5.4	Temperature dependence of heat of combustion for diesel [9]	52
5.5	Modifications in the Simulink sub-model "heat loss to liquid fuel"	53
5.6	Control volume used to calculate x _{vapor}	54

6.1	Pressure plot of cylinder 4 for NG and methanol at 375 kWe, both at an ignition timing of 20 °CA BTDC.	60
6.2	Pressure plot of cylinder 4 for methanol at 375 kWe with changing ignition timings.	61
6.3	Pressure plot of cylinder 4 with varying manifold temperature at 375 kWe, both at an ignition timing of 20 °CA BTDC.	61
6.4	Pressure signal of methanol with three TDC shifts.	63
6.5	Indicated power plot of cylinder 4 for NG compared to methanol at 375 kWe.	64
6.6	Indicated power of cylinder 4 with changing ignition timings at 375 kWe.	64
6.7	Indicated power plot of cylinder 4 with varying manifold temperature.	65
6.8	Heat-release during combustion for DI diesel [15].	66
6.9	HRR plot of cylinder 4 with NG and Methanol at 375 kWe both at an ignition timing of 20 °CA BTDC.	67
6.10	RCO plot of cylinder 4 with NG and methanol at 375 kWe both at an ignition timing of 20 °CA BTDC	67
6.11	The fuel mass burn fraction (RCO) with changing ignition timing, with a closer look at the start of ignition	68
6.12	The fuel mass burn fraction (RCO) for changing ignition timing, with a closer look at EOC	69
6.13	The fuel mass burn fraction (RCO) for changing ignition timings	70
6.14	The heat release flow for changing ignition timing	70
6.15	The fuel mass burn fraction (RCO) for varying aftercooler temperatures	71
6.16	Temperature plot of cylinder 4 with NG vs M100 at 375 kWe	72
6.17	Temperature plot of cylinder 4 with changing ignition timings at 375 kWe	73
6.18	Temperature plot of cylinder 4 with changing temperature manifold at 375 kWe	74
6.19	Net apparent heat release methanol model compared to Kibox hr	76
6.20	Net apparent heat release methanol model compared to Kibox hr. close look around TDC	77
6.21	Net apparent heat release NG model compared to kibox HR	77
6.22	Net apparent heat release rate methanol model compared to Kibox HRR	78
6.23	Net apparent heat release rate NG model compared to Kibox HRR	79
A.1	Test bed	85
A.2	Schematic of the fuel system	86
A.3	Rubber hose	86
A.4	Stainless steel fuel lines	86
A.5	Dip tray with Methanol IBC container used as fuel tank	87
A.6	Port fuel injection holders	88
A.7	Fuel injectors	88
A.8	Available spark plugs	88
A.9	Cooling three-way valve	89
A.10	Cooling three-way valve placed with electric motor	89
A.11	Used nitrogen bottles with pressure regulator	91
A.12	Dewetron measurement system	92
A.13	Testo-350	92
B.1	Mean pressure of all cylinders with changing NO _x settings at a load of 250 kWe	94
B.2	Energy losses in an engine (taken from Klein Woud et al. [18])	96
C.1	Kibox settings of IMEP	100
C.2	COV values with NG at 375ekW	101
C.3	COV values with Methanol at 375 ekW	101
C.4	Kibox settings of IMEP	102
C.5	Mean pressure of cylinder 4 compared to the mean pressure of cylinders 3,4,5, and 6	104
C.6	COV values of cylinder 4 from Kibox before and after replacement.	104
E.1	Calibratie sensoren dewetron(1/2)	112
E.2	Calibratie seonsoren dewetron (2/2)	113
F.1	Task risk analyse (1/6)	115

F.2	Task risk analyse (2/6)	116
F.3	Task risk analyse (3/6)	116
F.4	Task risk analyse (4/6)	117
F.5	Task risk analyse (5/6)	117
F.6	Task risk analyse (6/6)	118
G.1	Motor datasheet	120
G.2	Generator datasheet	121
H.1	refprop used data	123
I.1	Analyse of used NG (1/2)	126
I.2	Analyse of used NG (2/2)	127

List of Tables

3.1	Engine Specifications	20
3.2	Overview of executed performance tests	23
3.3	Overview of the sensors	24
4.1	COV_{pmax} at 250 kWe for 100 % methanol at different ignition timings	33
4.2	COV_{imep} at 250 kWe for 100 % methanol at different ignition timings	33
4.3	COV_{imep} at 375 kWe for 100 % methanol at different ignition timings	33
4.4	Mean of kibox COV_{imep} values of cylinder 4 with varying ignition timing	35
4.5	Important parameters with increasing aftercooler temperature at 375 kWe and constant fuel consumption	37
4.6	Mean of kibox CA10 CA50 and CA90 values in °CA ATDC of the four measured cylinders with methanol with varying ignition timing compared to natural gas	38
4.7	Engine efficiency (η_e) of methanol with varying ignition timing compared with NG	40
5.1	Significantly changed model values from changing mass fractions	51
6.1	CA10 CA50 and CA90 values of the cylinder 4 from the RCO for NG compared to methanol	67
6.2	Combustion duration (CA90-CA10) from NAHRR with methanol compared to the Kibox calculations	68
6.3	CA10, CA50 and CA90 values of the cylinder 4 from the model with varying ignition timings	71
6.4	Heat release per cycle comparison between model and Kibox	76
B.1	Efficiency values of cylinder 4 from the model for NG compared to methanol at 375 kWe	96
B.2	Efficiency values of cylinder 4 from the model with methanol and ignition variation	97
B.3	Efficiency values of cylinder 4 from the model for varying the aftercooler temperature	97
C.1	COV_{imep} at 375ekW for 100%methanol with own calculations and (standard) Kibox calculations	100
C.2	COV_{imep} at 375 ekW for 100 % methanol with own calculations and (standard) Kibox calculations	102
C.3	COV_{imep} at 375 ekW for 100 % methanol before and after replacement of injector cylinder 4	103
C.4	COV_{pmax} at 375 ekW for 100 % methanol before and after replacement of injector cylinder 4	103
C.5	Influence of 2 degrees change in IVO	105
C.6	Influence of 2 degrees change in IVO on final results of the model	105
D.1	Overview of performance tests	108

Nomenclature

Acronyms

AFR	Air-to-fuel ratio
ATDC	After top dead centre
BTDC	Before top dead centre
BTE	Brake thermal efficiency
CAT	Caterpillar
CI	Compression ignited
CYL	Cylinder
DAC	Direct air capture
e.g.	Example given
E100	100 % Ethanol
GHG	Green house gas
GMM	Green maritime methanol
H-NG	Hydrogen-natural gas
HCHO	Formaldehyde
HFO	Heavy fuel oil
ICE	Internal combustion engine
IFO	Intermediate fuel oil
IMO	International Maritime organisation
IVC	Inlet valve close
IVO	Inlet valve open
LNG	Liquefied Natural Gas
LSFO	Low sulfur fuel oil
M100	100% methanol
mbf	Mass burned fuel
MDO	Marine diesel oil
MGO	Marine gas oil
NG	Natural gas
PFI	Port fuel injected
PPM	Parts per million
RPM	Rounds per minute
SI	Spark-ignited
SOC	Start of combustion
STP	Standard temperature and pressure
Syngas	Synthetic gas
TC	Thermocouple
TDC	Top Dead Center
UHC	Unburned hydrocarbons
viz.	Videlicet
WGS	Water gas shift
WP	Work plan

Greek symbol

α	Crank angle	°
ϵ	Geometric compression ratio	
η	Efficiency	
γ	Ratio of specific heats	
λ	Air excess ratio	
λ_{cr}	Radius to length ratio	
π	Compression ratio	
ρ	Density	kg/m ³

σ	Stoichiometric air/fuel ratio	
Other Symbols		
A	Area	m ²
BSFC	Brake (power) specific fuel consumption	g/kWh
C ₂ H ₅ OH	Ethanol	
c_m	Mean piston speed	m/s
CA	Crank angle	°
CH ₃ OH	Methanol	
CO ₂	Carbon dioxide	
COV	Coefficient of variation	
CRR	Combustion reaction rate	kg/s
GAHR	Gross apparent heat release	J
GAHRR	Gross apparent heat release rate	J/s
h	Enthalpy per unit of mass	kJ/kg
H ₂	Hydrogen	
H ₂ O	Water	
H ₂ S	Hydrogen sulfide	
h^L	Lower heating value	kJ/kg
HR	Heat release	J
HRR	Heat release rate	J/s
i	Number of cylinders	
IMEP	Indicated mean effective pressure	Pa
isfc	Indicated specific fuel consumption	g/kWh
L	Length	m
LHV	Lower heating value	kJ/kg
M	Molecular weight	g/mol
m	Mass	kg
\dot{m}	Massflow	kg/s
N	Engine speed	rpm
NAHR	Net apparent heat release	J
NAHRR	Net apparent heat release rate	J/s
NO _x	Nitrogen oxides	
P	Power	kW
p	In-cylinder pressure	Pa
Q	Heat	kJ
\dot{Q}	Heatflow	kJ/s
R	Gas constant	kJ/kgK
R	Radius	m
RCO	Reaction coordinate	kg
SFC	Specific fuel consumption	g/kWh
SO _x	Sulphur oxides	
T	Temperature	°C
t	Time	s
u	Internal energy per unit of mass	kJ/kg
v	Volume	m ³
W	Watt	J/s
x	Mass fraction	
y	Molar fraction	
Zn-Cr	Zinc-chromium	
Sub- & Superscript		
a	Air	
b	Bore	
bld	Blowdown	
C	Carbon	
comb	Combustion	
CR	Connecting rod	

da	Dry air
e	Effective
e	Engine
e	Exponent
EO	Exhaust open
f	Fuel
ft	Fuel trapped
H	High
H	Hydrogen
hl	Heat loss
i	Indicated
IC	Inlet closes
ind	Induction
IO	Inlet open
L	Low
m	Mass
m	Mechanical
max	Maximum
norm	Normal
O	Oxygen
p	Pressure
q	Heat input
rg	Residual gas
s	Stroke
sg	Stoichiometric gas
t	Tangential
t	Trapped
td	Thermodynamic
tot	Total
v	Volume

Introduction

1.1. Background

During this thesis, work is being carried out within the green maritime methanol (GMM) project on a Caterpillar (CAT) G3508A sparked-ignited natural gas (SI NG) engine at the company PON Power in Papendrecht. The GMM project has been set up because the maritime sector is fronting a major challenge. The economy keeps globally growing, increasing freight transport by ship. Meanwhile, the goals from the Paris climate agreement and the subsequent agreement in IMO require a 50% reduction of CO₂ emissions from maritime transport by 2050. Development of new fuel types for shipping, such as methanol, hydrogen, various bio-fuels, and battery-electric are carried out. However, the solution to this challenge is still uncertain. Different ship segment may have different recommendations, this also applies to the short and long term solutions. The use of methanol is considered one of the most promising solutions for the implementation in the short to medium term, based on the potential availability, emission reduction and energy density [41].

This research assignment is part of the GMM project with a 2-year duration where the goal is to investigate the uptake of methanol as an alternative shipping fuel for maritime vessels. The objectives of the project have been subdivided into two themes:

- The technical development of the power train and associated emissions and efficiency.
- The economic/technical competitiveness with respect to the alternatives, e.g. MGO and LNG.

To achieve these objectives the project consisted of 6 work plans (WP's). In WP3, called the technical analysis, the sub-objectives are as follows:

- Show feasibility of the use of methanol, by performing tests for a number of retrofit options and new build at the facilities of the Netherlands Defence Academy (NLDA).
- Provide a high quality, reliable and independent data set on engine performance and emissions for the 3 most feasible retrofit combustion solutions with methanol. These 3 retrofit technologies are methanol emulsification in diesel, spark-ignited methanol combustion and dual-fuel methanol diesel solution.
- Analyse effects on CO₂ emission performance and on other emissions such as NO_x, SO_x and PM.
- Elaborate safe on-board storage and transshipment.

To achieve goals of WP3 the "Dutch CAT engine dealer" PON Power has provided G3508A SI NG engine as a retrofit option. The purpose is to change the SI NG engine to work with 100% methanol port fuel injected. The first performance tests on a testbed have been carried out in January 2020. The purpose of these initial performance tests was to run the engine stable at several loads and constant speed.

1.2. Thesis objective & research questions

The objective is to compare the performance and the combustion of methanol with Natural Gas (NG) in a spark-ignited (SI) internal combustion engine (ICE) with the purpose of using methanol in a maritime environment. A model is made of the G3508A SI engine with the use of methanol as a fuel. During this thesis a G3508A SI engine will run on methanol and performance data from that engine is collected. These engine data will provide input for the methanol engine model. During this thesis the following primary question will be answered:

"What is the effect on the engine performance when 100% methanol is used as fuel for a spark-ignited port fuel injected engine compared to premixed injection of natural gas?"

Response to this primary question will be provided by building a test setup, executing performance tests and using a modified model for further elaborating on methanol combustion. The following sub-questions, regarding the test setup and the performance tests, will be addressed:

- *Is it possible to run a CAT G3508A spark-ignited (SI) engine with port-injected methanol? What challenges are faced when running the engine on methanol?*
- *What data should be measured from the engine for modelling the in-cylinder combustion performance?*
- *What is the operation stability at 250 and 375 kWe with methanol compared to NG in terms of COV_{imep} and COV_{pmax} ?*
- *When running with methanol on constant NOx emissions of 500 mg/Nm³ what is the engine efficiency at 50 % and 75 % load compared to NG?*

And subsequently sub-questions need to be addressed with regards to modeling:

- *Which heat release model is used for the methanol engine and what needs to be changed in the model?*
- *Will the model give comparable heat release characteristics as found in the experimental data?*

1.3. Methodology

The thesis started with a literature study and simultaneously the engine is converted into a 100% methanol engine. After the literature study, a model of the engine has been built. After modifying the engine, a two week period of experimenting on a testbed at PON Power is conducted, including performance tests and data collection. The data is then analyzed and compared with the model. Sensitivity analyses have been carried out and the model is validated.

1.4. Thesis outline

In chapter 2, the literature study is described to understand the production of methanol, methanol as a fuel in ICE and to compare and understand the different types of models for modelling a methanol engine. At the end of the literature study, four hypotheses will be presented. After the literature study, the test setup is briefed in chapter 3. The engine, the placement of the engine and the test plan are discussed. Subsequently, in chapter 4, the analysis of the experiments is presented. Here the first (experimental) sub-questions of the thesis will be answered. Then, the heat release model that has been used and modified is discussed in chapter 5. Chapter 6 shows the analysis of the model. A comparison of the model data with the performance data is also made in this chapter. Finally, conclusions and recommendations are given in chapter 7.

2

Literature study

2.1. Background of methanol

Methanol, CH_3OH , is a widely traded chemical. Methanol has a lower heating value (LHV) of 19.9 MJ/kg, which is approximately half of the LHV of marine diesel oil (MDO) with 42.6 MJ/kg as shown in table 2.3 and is used as a fuel. Methanol is also produced to be used as a feedstock for production of pesticides, medicines, etc. Due to this multipurpose of methanol, it is already widely distributed around the world and has storage capacity at many ports as shown in figure 2.1 [25].

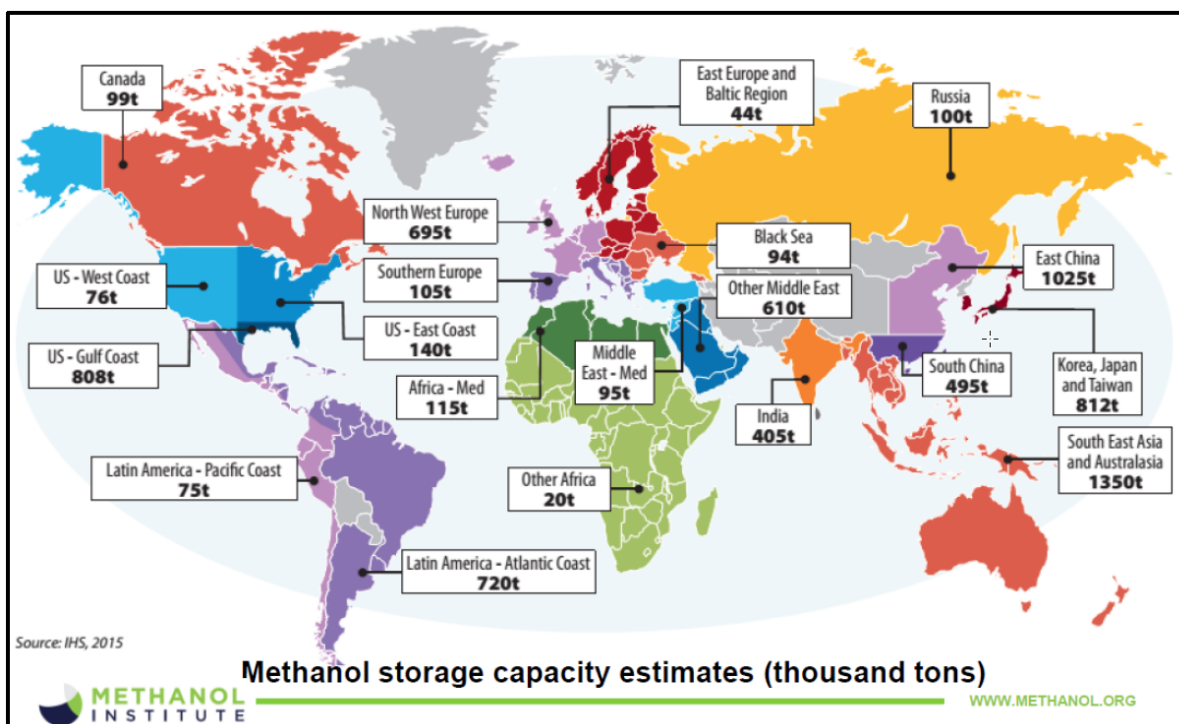


Figure 2.1: Methanol storage capacity worldwide [25]

2.1.1. Current use of methanol in internal combustion engines (ICEs)

The automotive industry is the first and foremost familiar with methanol. In car racing, it is used across Europe as fuel and it is also used as standard fuel in cars in China. China's use of methanol in the transport sector is mainly due to a lot of coal mining regions. The coal is used to produce methanol. Therefore, a lot of low-cost methanol is available in China. The methanol is used to blend with gasoline or to use in 100% methanol (M100) cars [42][19].

2.1.2. Alternative fuel in a maritime environment

Standard marine fuels are marine diesel oil (MDO), intermediate fuel oil (IFO)(a blend of gas oil and heavy oil), marine gas oil (MGO), low sulfur fuel oil (LSFO) and heavy fuel oil (HFO). These fuels show significant CO₂, SO_x and NO_x emissions. The CO₂ emissions are restricted by the IMO and must be reduced by 50% in 2050. In some areas, other emissions e.g. SO_x and NO_x are limited[17].

The maritime sector is searching for an alternative fuel due to the tightening emission regulations [16]. Various development projects are underway in the Netherlands for alternative fuels for methanol, hydrogen, liquefied natural gas, various biofuels and battery-electric. But methanol shows most potential due to potential availability, emission reduction and energy density [25].

2.1.3. Recent methanol projects in the maritime sector

Since 2011 at least seven methanol projects have been carried out in Europe before the GMM project started to investigate the use of methanol as a marine fuel, viz.: Effship, SPIRETH, Methanol: The marine fuel of the future, MethaShip, Waterfront Shipping, LeanShips, proFLASH and SUMMETH. These studies include paper-studies but also had real vessels modified with methanol engines, e.g. Ropax ferry Stean Germanica [11][27][6]. Within these projects, four engine-manufacturers work on the use of alcohol fuels in the engine, viz.: Wartsilla, MAN DieselTurbo, Scania and Caterpillar. Wherever the first two have the focus on a dual fuel concept, the latter two use 95% ethanol and 100% methanol engine. Two university research programs have been carried out focusing on using methanol as a fuel, viz.: Lund University (Sweden) and Ghent University (Belgium) [11].

2.2. Methanol production

Methanol is manufactured for fuel use and as feedstock for production of pesticides, medicines, etc. Methanol production primarily takes place in China followed by Saudi Arabia, Trinidad Tobago, Iran and Russia. China is by far the largest manufacturer and investor in methanol production plants worldwide with a production capacity of about 50 Million tonnes annually [25]. The global production capacity of about 110 million metric tons in 2015 is still small compared to the global gasoline production of approximately one billion metric tons in 2012 [42]. However, demand for methanol has doubled between 2009 and 2017[19]. To meet this demand methanol is produced by using various methods. The four most well-known production methods will be reviewed in the following sections.

2.2.1. Production from coal

Production of methanol from coal involves four steps: synthetic gas (syngas) generation, syngas purification, methanol synthesis and methanol rectification[19]. Coal slurry is supplied with oxygen under high pressure to the gasifier in order to generate syngas. This syngas is a mixture of hydrogen (H₂), carbon monoxide (CO), carbon dioxide (CO₂) and hydrogen sulfide (H₂S). Before the methanol synthesis, this syngas needs to be purified, meaning CO₂ and H₂S will be removed from the syngas. The syngas then needs a higher amount of H₂ or lower amount of CO to obtain stoichiometry. This is done with a shift reaction which produces CO₂ and H₂. The CO₂ will be removed again. The methanol can then be produced in a reactor at 300-350 bar and 300-400 °C. With these pressures and temperatures, the optimum methanol production is reached with a zinc-chromium (Zn-Cr) catalyst. In this reactor the following reactions are present:

Water gas shift (WGS) reaction:



Methanol synthesis reaction:



Methanol synthesis reaction:



Finally, the methanol must be separated from the water to obtain the purified methanol as a product.

2.2.2. Production from natural gas

Production from natural gas requires three steps: production of syngas, conversion of syngas and distillation. Syngas is produced with steam reforming and an auto-thermal reforming reaction. The syngas then contains H_2 , CO and CO_2 with an overcapacity of H_2 . The syngas is converted into crude methanol in a reactor at 50-100 bar and 200-300 °C. In this reactor equation 2.2 and 2.3 are present. These reactions are exothermic, thus require significant cooling. Due to a slow conversion process, large recycling and cooling are needed leading to high investment costs.

2.2.3. Production from natural biomass and municipal solid waste

The production process is comparable to that of producing methanol with natural gas, with only some different preparatory work. Before the production of syngas, first, the ferrous materials require removal with a magnet. Subsequently, biomass or waste is entering the gasification process. The gasification process is a thermochemical conversion process to convert the biomass or waste into gaseous form with the help of oxygen, steam and flue gases. Conversion of syngas and distillation, the next production steps, are similar to the production method from NG. Methanol production from biomass generally yields low efficiency [19].

2.2.4. A synthesised methanol production method from CO_2 and renewable H_2

The most promising and new production method is the production of methanol from recovered or air captured CO_2 and renewable H_2 . As shown in equation 2.2 and 2.3 the production of methanol has an ease chemical production method which needs hydrogen (H_2) and carbon dioxide (CO_2) as feed. Upon adding a renewable source, in order to obtain hydrogen from water by electrolysis, the hydrogen (H_2) is produced with the following reactions :



Then the reaction 2.3 only requires CO_2 to result into methanol. When the CO_2 is recovered from industry or captured from the air (e.g. the direct air capture (DAC) pilot plant from carbon engineering) this production method will reduce the CO_2 concentration in the air. Due to the fact that CO_2 is a green house gas (GHG), with a high concentration of 403.3 ppm in 2016 [19], this will prove to be a promising production method. A concept of Thyssenkrupp of using renewable energy and waste CO_2 to make renewable methanol is presented as an example in figure 2.2.

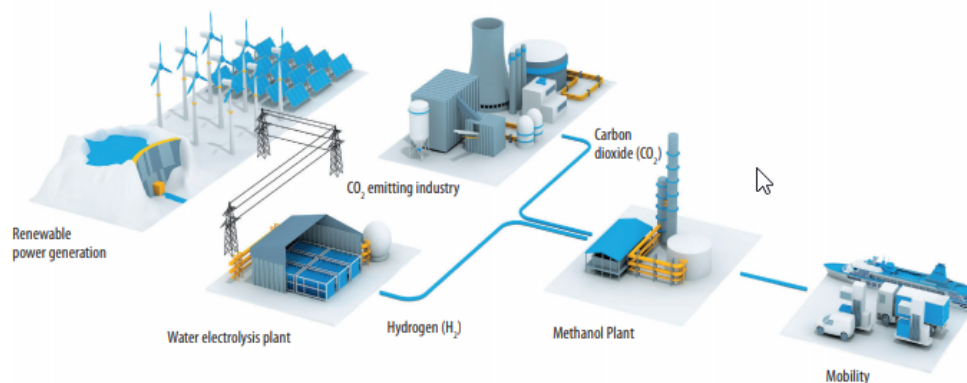


Figure 2.2: Synthetic methanol production [28]

When looking at reaction 2.3 synthesised methanol can directly be made from CO_2 and H_2 which has a higher economical and energetic efficiency with one reactor. If the plant were placed within a cheap electricity area, a two-step process might prove to be more economically efficient. The two-step process uses two reactors to first make CO from CO_2 with reaction 2.1 in the first reactor. After that methanol is made in reactor 2 with reaction 2.2. For both processes, an economical analysis has been made by B. Anicic et al.[2]. The electrolysis of H_2 is the highest cost element in this calculation. Both processes show an energy cost of around 11 kWh/kg methanol produced. With a methanol selling price

of 0.39 €/kg and a planned production of 25.000 kg/h both production processes show annual profits over 10M€/year when capital cost are taken over a period of 30 years. Although it seems economically feasible, the cost of this production process is still significantly higher than all other methanol production processes [13].

2.2.5. Conclusion of methanol production

Most methanol is currently produced using coal and natural gas. When looking at GHG solutions the synthesised methanol production method from CO₂ proves to be a promising production method. With this production method, a well to wheel near to zero-emission of CO₂ is possible. More will be discussed about emissions with methanol as a fuel in section 2.4.6.

2.3. Fuel properties

To run an engine on an alternative fuel, the properties of the alternative fuel must be known. In figure 2.3 the fuel properties of methanol are compared to common other fuel types. Diesel is the most common marine fuel. Liquefied Natural Gas (LNG) may best be compared to natural gas (NG) where the used test engine normally on operates. The most important properties of methanol will be discussed and compared with diesel and LNG in this chapter. The information about the properties is from Kumar unless stated otherwise [19].

Properties	Gasoline	Diesel	Methanol	LNG
Chemical structure	C ₄ H ₁₀ – C ₁₂ H ₂₆	C ₁₂ H ₂₆ – C ₁₄ H ₃₀	CH ₃ OH	CH ₄
Molecular weight	95-120	190–220	32.042	16
Density (kg/m ³)	740	830	790	419
Viscosity at 298.15 K (mPa s)	0.29	3.35	0.59	0.146
Boiling point (C)	27-245	180-360	65	-161.4
Freezing point (C)	-57	-1 to -4	-98	-182.5
Auto-ignition temperature (C)	228-470	220-260	450	585
Lower heating value (MJ/kg)	44.5	42.60	19.9	51.85
Vaporization heat (kJ/kg)	310	260	1110	-
Octane number	80-98	15-25	111	127
Cetane number	0-10	45–50	3	
Stoichiometric air/fuel ratio	14.6	14.5	6.5	17.2
Flame speed (cm/s)	37-43		45–52.3	40
Flammability limits (vol)	1.47-7.6	1.85-8.2	6.7-36	5-15
Adiabatic flame temperature (C)	2030	2054	1870	2197
Flash point (C)	-45	78	11	-136

Figure 2.3: Fuel properties [25]

2.3.1. Boiling temperature

The boiling point of methanol is 65°C. Therefore, methanol is a liquid at standard temperature and pressure (STP). It is the simplest molecule that is a liquid at STP. LNG has a boiling point of -161.4 °C and is therefore not a liquid at STP. Diesel has the highest boiling point with 180-360 °C.

2.3.2. Auto-ignition temperature

The auto-ignition temperature of methanol is 470°C. It has one specific auto-ignition temperature because it is a single component. Methanol and LNG have a high auto-ignition temperature compared to diesel and therefore are proper SI fuels.

2.3.3. Liquid density

The density of methanol in liquid form is 798 kg/m^3 . This is less than 10% lower than diesel. LNG has a density of 419 kg/m^3 , but due to its high lower heating value it still has comparable or less fuel storage capacity needed as compared to methanol.

2.3.4. Lower heating value

The lower heating value (LHV) is the most commonly used value for the calorific value of a fuel. However, the LHV may vary slightly when comparing different sources[19][25][42]. Therefore, the LHV is presented here in two significant figures. For methanol, it is 20 MJ/kg and about half as compared to diesel with 43 MJ/kg. LNG has even a higher LHV of 52 MJ/kg. The value of methanol is significantly lower due to its oxygen stored in the molecular structure. The lower LHV means more fuel must be injected to get an equivalent brake power output of an engine. And combined with the liquid density, it also means for the same range of a ship almost double the amount of fuel mass and volume must be stored in storage tanks when using methanol as a fuel compared to diesel[25]. LNG falls due to its lower density between methanol and diesel as it comes to required storage capacity. LNG requires some extra facilities for storage, like double-walled tanks, due to its boiling point.

2.3.5. Oxygenated Fuel

Methanol has inherent oxygen in its molecular structure, also known as oxygenated fuel. This means methanol has a lower stoichiometric air-to-fuel ratio (AFR). The lower added oxygen required for the complete burning of the fuel is due to the oxygen content that is already part of the fuel. This also facilitates achieving more complete combustion during the expansion stroke [19]. Therefore, methanol with an AFR of 6.5, requires 2.65 times less air for every kg fuel compared to LNG, with an AFR of 17.2. But methanol has 2.6 times lower LHV than LNG and therefore with every cylinder cycle a comparable amount of air is required for the engine to result into an equal power output.

2.3.6. Latent heat of vaporization

The heat of vaporization is the energy needed to vaporize the fuel. For methanol, the heat of vaporization is approximately 1100 kJ/kg and at least three times the heat of vaporization of gasoline and four times the heat of vaporization of diesel. This requirement for energy during vaporization provides a cooling effect and can contain desirable conditions at higher loads due to its improvements on brake thermal efficiency and power output. The high heat of vaporization has negative effects at the start, also well known as a cold start. The heat of vaporization for LNG is not important because it is already a gas at STP and therefore in gaseous form when it enters the engine as well as the combustion chamber.

2.3.7. Flammability limits

In addition to the heat of vaporization, a minimal amount of fuel is required to create an ignitable condition. In a mixture with too much fuel, the mixture is too rich to burn. Between these two flammability limits, the fuel will burn. Methanol is ignitable between 6.7 and 36% volume of fuel in a mixture. The range is wider than for all other comparable fuels [42].

2.3.8. Flame speed

The laminar flame speed is dependent on the air-to-fuel ratio. In table 2.3 the flame speed is given at an air excess ratio (λ) = 1. Methanol has the highest flame speed at $\lambda = 1$ and with the wide range of flammability limits which allows leaner mixtures to burn, could result in potentially higher efficiency [25].

2.3.9. Sulfur content

Methanol contains no sulfur. Therefore, the emissions of methanol as fuel will have no SO_x emissions. SO_x emissions are known to be responsible for acid rain.

2.3.10. Cetane number

The cetane number is used for the determination of ignition performance of diesel fuels. It is compared with iso-octane ($\text{C}_{16}\text{H}_{34}$) with cetane number 100 and α -methyl naphthalene ($\text{C}_{11}\text{H}_{10}$) with cetane number 0. Methanol has a cetane number of less than 5 [26].

2.3.11. Octane number

The octane number is used for the determination of ignition performance of gasoline fuels. It is defined with the iso-octane fraction (C_8H_{18}) with an octane number 100 and n-heptane (C_7H_{16}) with octane number 0. Methanol has an octane number of 109 [26].

2.3.12. Lubricity and viscosity

Methanol has poor lubricity properties and is also less viscous compared to diesel [19]. But LNG has even a lower viscosity at 298 K.

2.4. Methanol in ICE

In chapter 2.1.1 methanol has already been presented to be used in ICE's. Now the physical properties of methanol are known, the essentials of methanol in ICE will be explained in more detail. First, the different methods of using methanol in ICE's will be discussed. Next, the challenges of methanol in ICE are highlighted. Finally, the impact of the emissions of methanol used in ICE will be covered in this chapter.

2.4.1. Direct injection (DI) of methanol blends with diesel

The mixing of methanol with diesel is limited by its poor miscibility with diesel. Methanol is separated from diesel when more than 10% volume of methanol is blended with diesel. Using different additives can increase the miscibility. Experiments show that methanol-diesel blends can be used as fuel in diesel engines. At injection, the fuel will vaporize which causes a cooling effect. Methanol has a higher heat of vaporization compared to other fuels, therefore contains a better cooling effect. When cooling the air inside the cylinder, the maximum in-cylinder temperatures are reduced, which reduces NO_x emissions and change of knock. Emissions vary with the experiments, reduction of CO leads to increased NO_x and lower NO_x leads to increased CO emissions [19].

2.4.2. Port fuel injection (PFI) of methanol and DI of (pilot) diesel

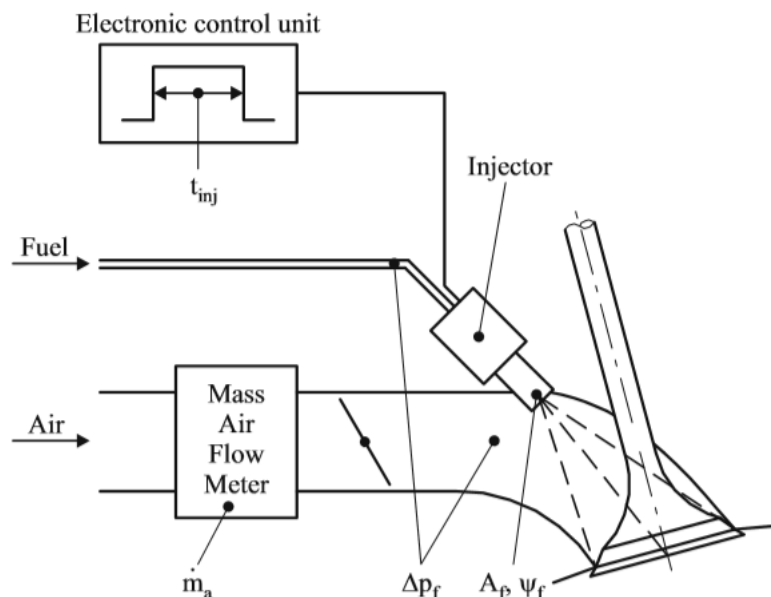


Figure 2.4: Example of a port fuel injection system [26]

On an existing (diesel) engine a port fuel injection system, as shown in figure 2.4, can be added to the engine. Port-injected methanol burns in the combustion chamber with the directly injected diesel. Compared to DI of methanol blends it may contain a higher quantity of methanol in the ICE. Research is carried out with quantities over 50% volume of methanol injected. PFI provides a proper fuel-air mixture before ignition compared to direct injection which minimizes the risk of droplets of fuel. This

better mixture is the result of longer mixing time before combustion. PFI also has the advantages to be able to operate at lower pressures (3-5 bar) as compared to common injection methods. At injection the fuel will vaporize causing a cooling effect. When cooling the air before the inlet more air, more fuel will be able to go into the cylinder. This results in higher power output. Furthermore, a decrease in NO_x has been demonstrated by several researchers with PFI of methanol combined with DI of diesel [19].

2.4.3. M100 Port fuel injection (PFI)

100% methanol (M100) engines can not be based on a diesel engine (with low to normal compression ratios) due to its low cetane number and high auto-ignition temperature compared to diesel. Therefore, a spark is required to burn the methanol. The PFI technique can therefore be used on a spark-ignited (SI) engine to get a M100 engine. Research on these types of engine has been executed by van Ghent university on a converted VW TDI Diesel engine with a 19.5:1 compression ratio [42]. This research proved that on high loads spark timing needed to be retarded due to knock. Peak brake thermal efficiency (BTE) of 42% on methanol compared to BTE of 40% on diesel were achieved and 20% CO_2 reduction was calculated.

2.4.4. M100 Direct injection (DI)

Direct injection of 100% methanol in a SI engine is used and researched. The effects of ignitions and injection timing have been investigated with a M100 engine by Jun Li, et al. [22]. With an 18.3 kW/2000rpm/16:1 compression ratio engine experiments were carried out. They showed a maximum thermal efficiency of 51% at an ignition timing of 18 °CA BTDC. Methanol injection and ignition timing can have effects of more than 10% on the brake-specific fuel consumption and also significantly effect on performance, combustion, and exhaust emissions. Research of DI of methanol with larger engines (>100kW) has not been found.

2.4.5. Challenges of methanol in ICE

Using methanol as a fuel in an ICE requires facing the following challenges.

Material compatibility

Alcohol fuels can be extremely aggressive toward magnesium, aluminium and copper. Steel and other ferrous metals are usually slightly affected. Components used for seals and fuel lines may also be attacked by methanol if not chosen properly [42]. Therefore, the use of these fast-wearing materials must be prevented.

Cold start

The use and research of M100 DI injection of methanol and M100 PFI injection is low due to the coldstart problems. Research of M100 PFI and DI in car engines show they have cold start problems starting around 0 °C and lower [42]. Therefore, most engines will use DI with blends or PFI with a pilot fuel.

For the maritime sector, the cold start problem is best solved by using preheating of the engine. With a high speed 3L Scania SI PFI engine, the operators experienced cold start problems in winter without an engine heater. With an engine heater and the engine temperature at 25 °C, outside temperatures of -15 °C proved not to be an issue [4]. It would be interesting to find this to also apply to bigger engines, but no research has been found about this problem for bigger engines.

Initially, in this project, natural gas can be used to heat the engine. Upon reaching the appropriate temperature the engine can be switched to methanol as a fuel. This project will undergo its first performance test in January, when outside temperatures around 0 °C may be expected. Inside the test-bed, slightly higher temperatures are expected. Monitoring at which temperatures this engine will have cold start problems will show to be interesting as far as it is possible to test in this setup.

Other challenges

Further challenges for the use of methanol in ICE's are:

- Pre-ignition due to overheated spark plug electrode.
- Increased thermo-mechanical stress in cylinder head due to increased evaporation cooling.
- The production of formaldehyde emissions, further explained in chapter 2.4.6 Emissions.
- Increased tank capacity for a similar range.

- Safety precautionary measures due to the toxicity and flammability of methanol.

2.4.6. Emissions

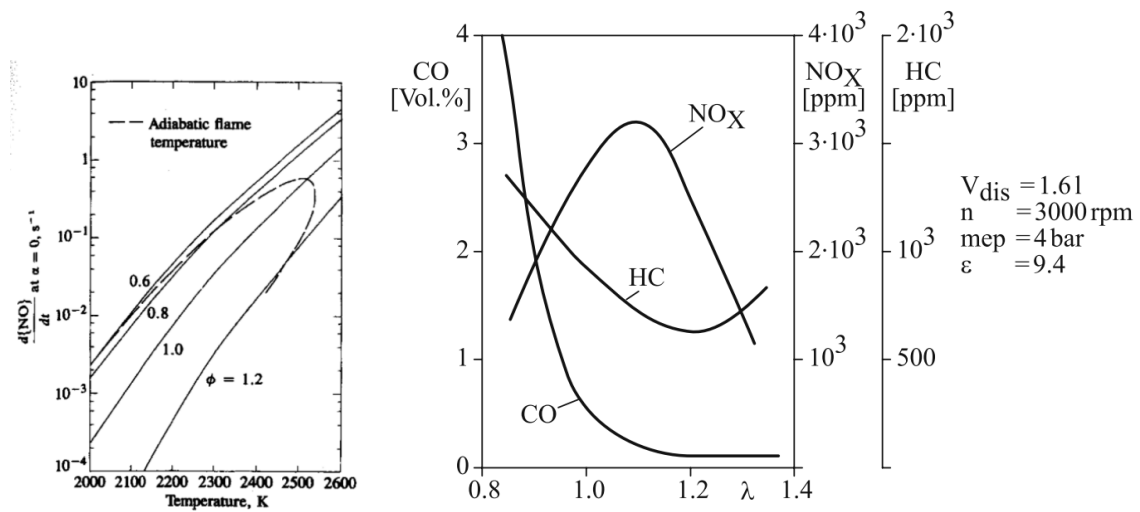


Figure 2.5: NO_x emissions vs temperature [15] - Figure 2.6: Trade-off between NO_x and CO emissions [26]

Previously described injection methods show advantages and disadvantages for the emissions. And this can be a study by itself. To give an applied impact of the use of methanol in an ICE to the emissions, only the 100% PFI SI methanol method will be compared with a regular marine fuel, in this case, marine diesel oil (MDO). Methanol in an ICE has no SO_x emissions due to the fact there is no sulfur in CH_3OH . The combustion characteristics of methanol and the single-carbon-molecule nature have the advantage that the emissions of particulate matter are significantly lower than for complex hydrocarbon fuels [42]. Methanol, just like MDO, produces NO_x and CO_2 emission. A trade-off exists between NO_x and CO_2 emissions in all ICE's, which can be influenced by the air excess ratio (λ), as shown in figure 2.6. With increasing λ , the flame temperature is lowered and therefore NO_x emissions are lowered. With rich mixtures ($\lambda < 1.0$) CO emissions increase due to the increase of unburned fuel. With lean mixtures ($\lambda > 1.2$), the combustion temperature decreases, so that NO_x drops, but unburned hydrocarbons (UHC) increases. Due to the high heat of vaporization of methanol, the flame temperature is expected to be lower and NO_x emission is lower as shown in figure 2.5 at similar engine operating conditions. All and all the CO/ CO_2 and NO_x emissions from the exhaust of the engine are equal to emissions from MDO or even higher than NG. The gain of CO_2 emissions with methanol as compared to MDO must be made in the production process as mentioned in chapter 2.2.5.

Unfortunately, methanol has one emission type that produces a higher degree of emission as compared to diesel, the emission of formaldehyde, HCHO. Formaldehyde is toxic and occupational exposure causes nasopharyngeal (a type of throat) cancer in humans. HCHO formations peak at temperatures around 727°C and is derived from unburned methanol. When methanol escapes from crevices during expansion the formation of formaldehyde can be expected. Therefore, more HCHO emissions are expected with PFI as compared to DI. To show an indication of the increase of emission a M85 is compared to pure gasoline and will have roughly 10 times more formaldehyde emissions [45]. After-treatment of formaldehyde can reduce up to 95% of the formaldehyde emissions [42].

2.5. Methanol versus ethanol

Ethanol ($\text{C}_2\text{H}_5\text{OH}$) has a higher LHV of 27 MJ/kg compared to 20 MJ/kg of methanol and similar density. This means it requires 35% less storage capacity onboard a ship fueled with ethanol instead of methanol. It has been used to blend with gasoline (E05 up to E85) or even 100% ethanol fuel (E100) to be used in fuel for cars. Compared with methanol it has comparable properties like boiling point, octane number and high heat of vaporization. It can therefore also be an alternative for fuel in marine

applications.

When looking at future production processes it can be produced on a similar synthetic process as methanol as shown in figure 2.2. In addition to the raw materials which also require methanol, ethanol requires the addition of water as feedstock. Ethanol can be produced directly from the syngas or it can be produced from methanol converted to ethanol via methanol homologation reaction [10]. But efficient synthetic production of ethanol is more difficult than for methanol due to the extra C-C bond. Therefore, research is carried out to yield more ethanol in synthetic processes with different catalysts and production methods [43]. A study between methanol and ethanol as fuel in ICEs is done by EMSA resulting in the conclusion that both fuels are attractive from an environmental perspective. Both fuels could work on heavy (diesel) engines. Methanol and ethanol are both globally available. Historically prices compared in USD/MWh of ethanol are a little bit higher than for those of methanol. But these prices are not comparable when considered within the perspective of future synthetic processes. Although the two fuels are equally potential, only methanol maritime projects are known to have been carried out whereas no ethanol maritime projects are known [11].

2.6. Methanol in ICE models

With the development of engines and increasing regulatory limitations on the engine efficiency and emission levels, the need for simulations of ICE in models increased. Therefore, the modelling of ICE is carried out frequently, where the input of alternative fuels in these models is still rather new and unknown. The modelling of ICE's will be categorized and discussed in section type of models. After that the investigated aspects with these models relevant to this research will be discussed.

2.6.1. Types of models

Verhelst shows a summary of research done with different types of models and distinguishes two types of models, quasi-dimensional and multidimensional models [42]. Xiang La explains up to four types of different models. Even within one model, different kind of sub-models may be used. The correct categorization can get mixed up or be misinterpreted due to the different kind of categorizations used. In this research the following four types of models according to Xiang La will be explained [47]:

- The mean value model, not intended for engine development, although efficient for research on system integration. Usually this model is based on a large amount of engine test data and cannot predict.
- Zero-dimensional model, the combustion chamber is divided in one zone. Combustion is simulated at every crank angle, assuming this all to be equal in the combustion chamber.
- Quasi-dimensional model, divides the combustion chamber in several zero-dimensional zones according to the distribution pattern of the flame or the injection. Specific physical and chemical processes are considered in each zone (e.g. fuel-air mixing, flame propagation, concentration changes to determine temperature and pressure in each individual zone).
- Multi-dimensional model, also known as computation fluid dynamics (CFD) model, provides the most in-cylinder details. Therefore, this model is the most time consuming and hardest to implement.

The model type that is used for research must be chosen based on the calculation speed and the depth of the research. The model that will be used in this thesis is a zero-dimensional, one zone, heat release model and will be further explained in chapter 5.

2.6.2. Investigated aspects of ICE (sub-)models:

In this section, the research done with (ICE) models relating to 100% methanol burning and effects in NG SI engines will be further investigated.

2.6.3. Flame speed

The velocity at which a flame spreads into a premixed, homogeneous, unburned mixture ahead of the flame, is called the laminar flame speed and is one of the most fundamental properties characterizing the combustion [15]. As mentioned in chapter 2.3.8, the flame speed of a fuel depends on the air excess ratio (λ). With increasing λ , or leaner burning, the flame speed will decrease. But the laminar

flame speed is also dependent on initial pressure and temperature. The engine that will be used in the test setup (further discussed in chapter 3) is known to operate with NG in lean conditions with a λ of around 1.6.

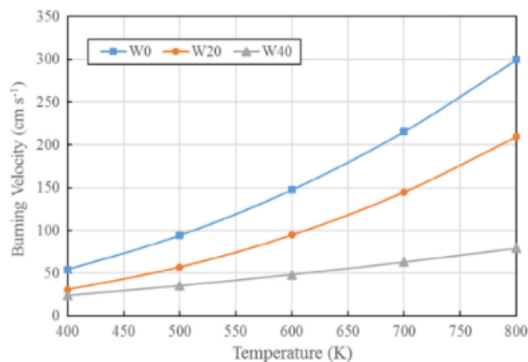


Figure 2.7: Methanol flame speed vs temperature [23]

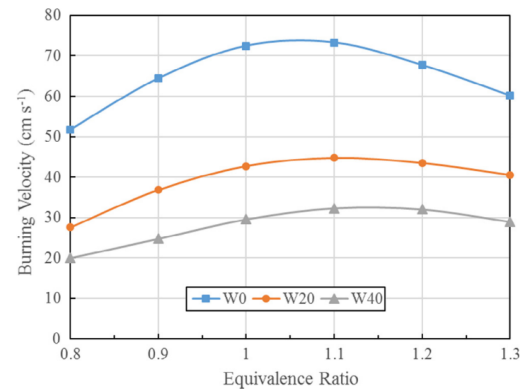


Figure 2.8: Methanol flame speed vs equivalence ratio [23]

Kun Liang conducted a study on the laminar burning velocity of (hydrous) methanol at elevated temperatures and pressures [23]. A multi-zone combustion model named BOMB program was used to calculate the burning velocity during the combustion. Kun Liang showed the correlations for the burning velocity against temperature increase with methanol as shown in figure in 2.7. This figure also shows that mixing with water will reduce the flame rate. Figure 2.8 shows that with increasing fuel/air equivalence ratio (actual fuel/air ratio compared to the stoichiometric fuel/air ratio) the flame speed will reduce.

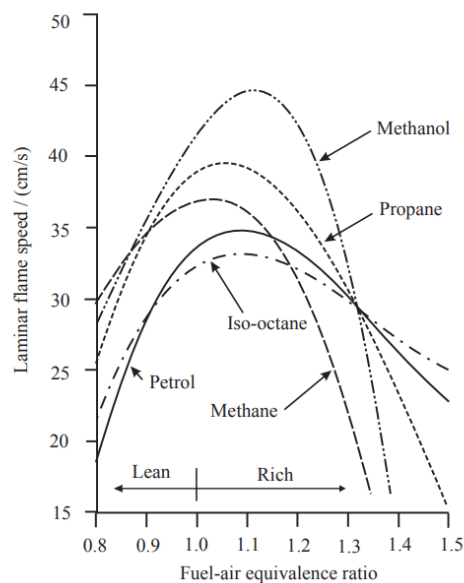


Figure 2.9: Flame speed of various fuels vs equivalence ratio [46]

In Winterbone [46] a comparison of laminar flame speed with changing fuel-to-air ratio has been given for several fuels, as shown in figure 2.9. It should be noted here that the fuel-air equivalence ratio is the inverse of the air excess ratio, λ , thus low fuel-air equivalence ratios indicate lean burning. Interesting to see here is that methanol in lean burn will cross the flame speed of methane (main component of NG). With a λ bigger than 1.17, equal to a fuel-air equivalence ratio of 0.85 in the figure, the laminar flame speed of NG is higher than the flame speed of methanol. This means that with the lean

burning test engine used in this research, at a λ of around 1.6, a lower laminar flame speed of methanol is expected compared to NG at similar operating conditions. Therefore, longer combustion duration is expected with methanol compared to NG. And due to the lower flame speed at lean burn conditions, an earlier ignition timing might be needed to get the same stable operating conditions compared to NG. The engine has on NG a standard ignition timing of 20 °CA BTDC. But it must also be mentioned that the effects of turbulence (and thus turbulent flame speed or u_t/u_l) are not taken into account in the figures 2.9 but will be expected in the cylinder of the ICE.

2.6.4. In-cylinder heat transfer

Two widely used in-cylinder heat transfer sub-models in ICE models are Annand and Woschni. Woschni is following up on Annand's heat transfer equation, presented in formula 2.5 [5].

$$q = A * D^{-0.2} * p^{0.8} * V^{0.8} * T^{-0.53} * (T_{gas} - T_{wall}) \quad (2.5)$$

The radiative heat does not show a separate term but is included or neglected. Convective heat is assumed to be quasi-steady. The heatflux (q) gives the convection coefficient with formula 2.6.

$$h = \frac{q}{(T_{gas} - T_{wall})} \quad (2.6)$$

The assumptions made by Woschni are only valid for air. Although the model seems to perform well for traditional fuels, they are not accurate for alternative fuels as methanol according to Stijn Broekaert, et al.[5]. In their research, they tried to present an alternative for Woschni's formula for alternative fuels. Their research identified four controllable factors; the throttle position, the compression ratio, the injected gas and ignition timing. For methanol, this improved model has not been evaluated yet and the paper could not conduct firm conclusion on the reviewed data. Therefore, the original Woschni formula will be used in this research. The used formula for Woschni's heatloss coefficient according to Stapersma is given in equation 2.7 [37, p824]:

$$\alpha = C_2 \cdot \frac{1}{D_b^{0.214}} \cdot \frac{p^{0.786}}{T^{0.525}} \cdot (C_3 \cdot c_m + C_4 \cdot \frac{p - p_0}{p_1} \cdot \frac{V_s}{V_1} \cdot T_1)^{0.786} \quad [W/m^2K] \quad (2.7)$$

The Woschni's formula applied to the model will be further explained in chapter 5, where In the work of Vogel and Huber new Woschni constants are given for C_4 when working with methanol as a fuel. Huber gives a C_4 constant of 0.004 for methanol in a SI engine[26, p152], but unknown is if this is also PFI or DI. C_4 is originally 0.00324 for DI according to Merker [26, p152] and the work of Stapersma. Stapersma [37, p825] gives also an alternative constant for C_4 pre-chamber constant, which is 0.00622. The effect of changing the C_4 value is interesting but will not be used in the model of this research, because the C_2 and T_{wall} parameters will be used as fine-tuning parameters and further explained in chapter 5.1.10.

2.6.5. Fuel evaporation time

Another view of the incorrect heat loss is given by Marriot et al. [42] The description of cylinder wall wetting and subsequent fuel evaporation for alcohol DI engines is needed to get correct predictions of wall heat transfer and volumetric efficiency. A so-called "puddling" sub-model takes account for the time needed for the alcohol fuel to evaporate. The sub-model gives better results in wall heat transfer than when fuel evaporation assumed to be instantaneous and complete on injection or at ignition.

For my research, the use of an evaporation sub-model must be considered. In the experimental setup, this effect will be reviewed by changing the temperature of the inlet receiver ($T_{manifold}$).

2.6.6. Wall-wetting effect

In the research of Yao et al. the influence of wall-wetting fuel film, especially its evaporation rate, upon the air-fuel ratio of in-cylinder mixtures (E0 - E30) is discussed [49]. Wall-wetting is due to the lower temperature in the intake port of PFI engines, the injected alcohol fuel has a tendency to adsorb on the intake port wall and form a wall-wetting fuel film on the surface as shown in figure 2.10. In steady-state operations, this effect will almost have no influence because of the mass balance as shown in figure 2.11. In this mass balance is shown, that with every cycle, the total injected mass stays constant. But in transient operations, the effect of wall-wetting needs to be considered.

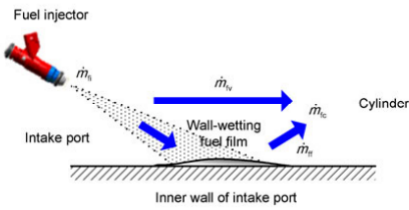


Figure 2.10: Wall effect with PFI [49]

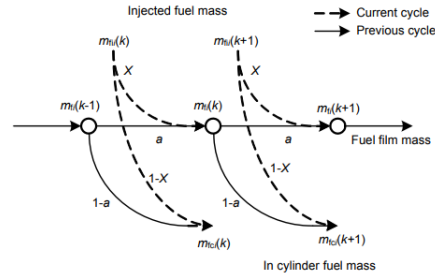


Figure 2.11: Wall effect mass balance [49]

The research concluded that the intake wall-wetting effect of PFI SI engines causes hysteresis errors of in-cylinder fuel mass flow, leading to air-fuel ratio deviations. The slower the fuel film evaporates, the larger and longer are the deviations. The engine in this research showed that, with an AFR change of 15% in 4 seconds, the AFR control error was less than 2% in steady-state conditions with compensation. Without compensation deviations from around 10% in AFR are shown in his graph [49].

For my research, these deviations with changing AFR will not be essential, due to constant rpm measurements, but the effect of wall-wetting needs to be known and considered. Especially with the placement of the flame arrestors in the air-intake, between the inlet valve and the PFI, the deviations might be a lot higher, due to a lot more wall area. However, at the first performance tests, no transient behaviour will be tested. Only tests at constant rpm and fixed loads will be conducted. Therefore in this research, these wall-wetting effects are not considered in the model or test plan.

2.6.7. Knock and misfire

Knocking is a sound transmitted through the engine which happens when the mixture of fuel, air and residual gas ignites spontaneously [15]. This means the mixture ignites before the ignition spark. An example of knock in a cylinder is given in figure 2.12. The knock results in an extremely rapid energy release, resulting in high local pressure. The pressure measured with the example given in figure 2.12 was 180 bar compared to a normal operating pressure of around 60 bar. Knock will normally appear in (too) rich mixtures.

Misfire is when the mixture in a cylinder fails to ignite. Misfire appears when the mixture is too lean to be burned. A too low flame speed combined with a weak mixture makes a misfire possible. Operating in partial-burn or misfire regimes is undesirable from the point of efficiency, emissions and torque variations [15]. An example of the operating range between the knocking and misfires is shown in figure 2.13.

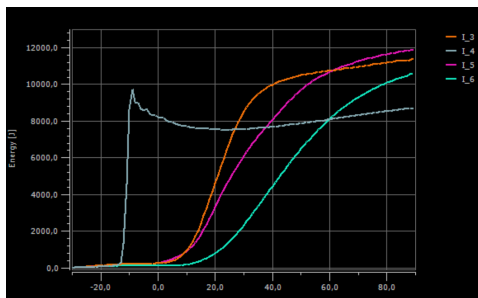


Figure 2.12: Kibox HR figure showing knock in cylinder 4 during tests

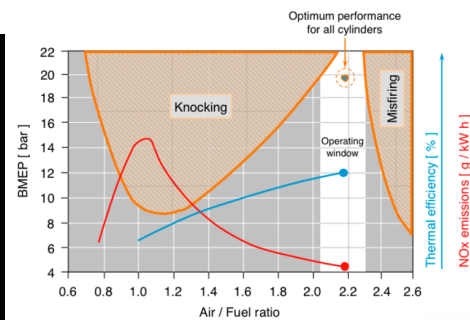


Figure 2.13: Operating window of a Wartsila 9L50DF [9]

A knocking prediction study with a two-zone combustion model NG SI engines has been done by La Xiang et al. [47]. In his study, he showed that with increasing compression ratios from 14 to 16 knocking will be expected earlier and also the knocking intensity will increase with increasing compression ratio. Also in this research is shown that retarding ignition timing is a good way to prevent knocking phenomenon in SI NG engines, but this will lead to lower efficiencies and higher fuel consumption. To

prevent damage from knock during the performance test the retarding ignition timing can be used.

2.6.8. Heat release

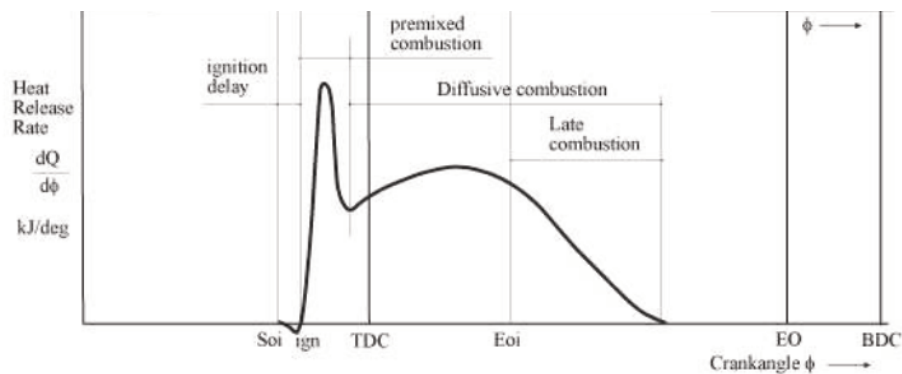


Figure 2.14: Typical heat release curve of DE [37]

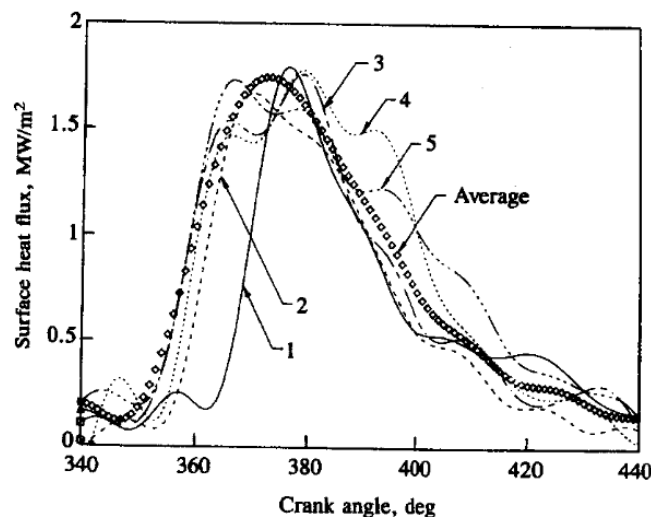


Figure 2.15: Cycle to cycle difference in heat flux curve shown [15]

In Stapersma [36] a typical heat release curve is given and in detail explained for a diesel engine. In figure 2.14 it shows clearly the different stages from ignition delay, premixed combustion, diffusive combustion and late combustion. For a spark-ignited engine a similar heat release curve can be shown. However, typical behaviour must be known. With spark-ignited engines the cycle-to-cycle variations are much bigger than with a diesel engine. Therefore, the heat flux for every cylinder cycle variate considerably more. This is well shown by Heywood in figure 2.15 [15], where 5 individual cycles are shown and the average heat flux of 198 cycles. When showing heat release curves for SI engines most of them will be an average of many cycles. With this average as shown in the figure the clear distinction between the different stages disappears. The average line is more smoothed due to the many cycle-to-cycle fluctuations.

A modelling and experimental study was done by Ke Zeng showed the impact on the in-cylinder heat release on a natural gas engine by changing fuel injection timings on a direct injected engine [50]. The effect of changing injection timings is shown in figure 2.16. It gives a clear picture of what range and variations can be expected in my heat release research. Although injection type and fuel are different compared to our study, the following can be taken from this study:

- Slow combustion rates are equal to low in-cylinder pressures.

- Optimum injection timing (or CA) is shown where heat release and pressure increase per CA is highest.

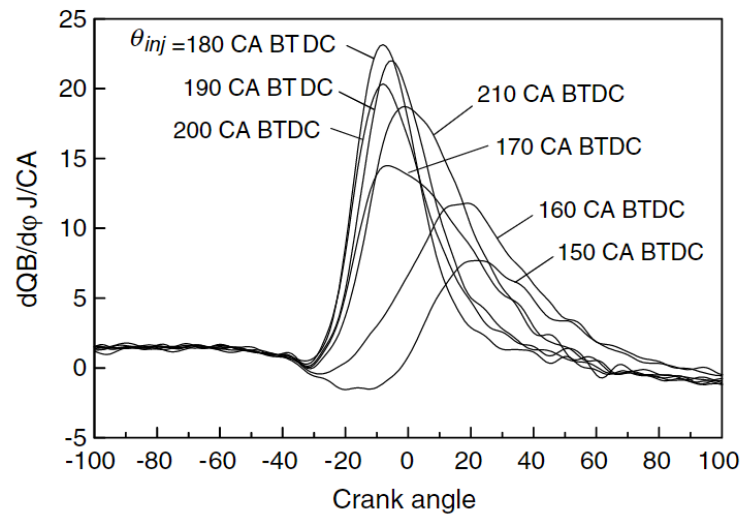


Figure 2.16: Heat release of a natural gas engine with changing injection timings [50]

To have a better understanding of the effect with methanol in the ICE a heat release curve with 100% methanol as a fuel is needed. Fang-Xi Xie et al. [48] have done a study on a SI engine with 100% methanol. This experimental study was with an automotive, much smaller, 2L, engine with a higher compression ratio of 18.0. The resulting pressure graph and HRR-curve from this study is shown in figure 2.17. It is visible that the heat release curves showed similar smooth curves as with SI NG heat release curves. Also can be seen that retarding ignition gives lower peak pressures and lower peaks in the HRR curve. The range of ignition timing from 12 to 18 °CA BTDC was the only range where stable engine operations were possible. This small operating range must be taken into account for my research. In this research brake (power) specific fuel consumption (BSFC) improvement was found with advanced ignition timing. The advanced ignition timing, meaning ignition at more CA BTDC, leads to higher peak pressure, peak temperature and peak heat release rate, and their corresponding crank angles are close to top dead centre (TDC).

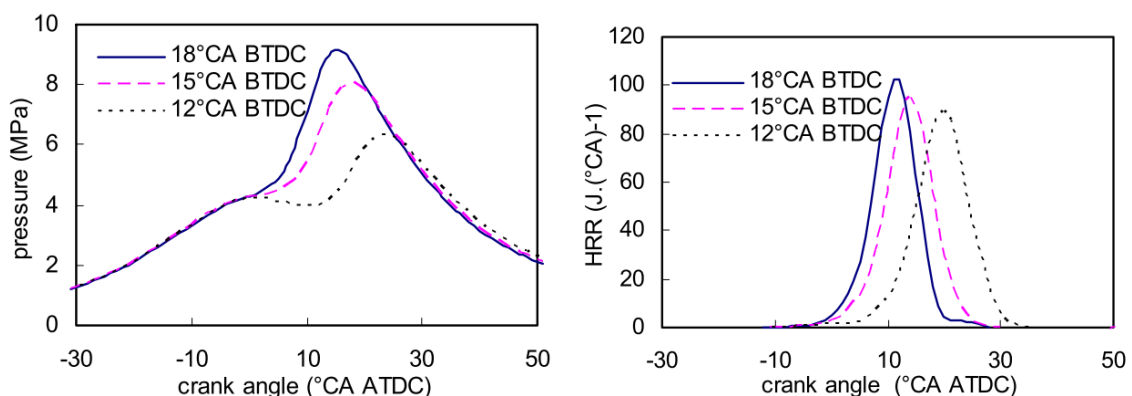


Figure 2.17: P and HRR of a 4 cylinder, 2L, 18:1, engine with 100% methanol at 1400 rpm with changing ignition timings [48]

The heat release modelling study of H. Sapra et al.[29] is done on the same engine as this research will be done. But the engine has been modified to be used with methanol as a fuel because his study

was with NG and hydrogen as a fuel. Therefore, the hr-model also must be changed. The hr-model will be further explained in chapter 5 and the modifications to this model in chapter 5.2.

2.7. Hypotheses

Now the literature study has been carried out, the hypotheses are described. Previous research has shown that the efficiency of the engine increases when using methanol. Nevertheless, other research has been conducted only on smaller engines. For the marine size 500 kWe test engine in this study, therefore, the first hypothesis will be: *"Engine efficiency is expected to be higher on methanol than on natural gas with the performed test loads of 50% and 75% load."*

The standard ignition timing for the test engine has an ignition timing of 20 °CA BTDC. Research shows that combustion generally becomes more stable with delayed ignition timing, but due to the following findings, it is predicted that stable operation is at a more advanced ignition timing: a.) The laminar flame speed of methanol is expected to be lower than of natural gas for lean burning operation with the test engine, indicating longer combustion duration for methanol. b.) Methanol is ignitable within a volume percentage of 6.7% and 36%, a much wider range compared to NG with 5-15%, thus a wider range for stable burning of the fuel. Research also shows that optimum fuel consumption is shown at advanced ignition timings, therefore, the following hypotheses are made: *"Better stability will be expected to be at an advanced ignition timing. With NG the standard ignition timing is at 20 °CA BTDC."* and *"Better bsfc will be reached at an advanced ignition timing on methanol than with NG. With NG the standard ignition timing is at 20 °CA BTDC."*

Methanol has a high heat of vaporization and will be port fuel injection in the test engine. Natural gas already is in a full gaseous state when entering the cylinder. However, the injected methanol will be partly in a gaseous state and partly in liquid state when entering the combustion chamber. This can be influenced by the temperature of air after the cooler. The initially used temperature after the cooler is maintained at 40 °C during the first experiments but can be changed with more or less cooling water. When entering the combustion chamber with a higher part in a gaseous state, or more methanol vapor, a more homogeneous mixture will be expected at the moment of ignition. A more homogeneous mixture will result in less hot spots and thus less NO_x emissions. This leads to the following hypothesis: *"With increasing temperature after the cooler, there will be more evaporation before the inlet valve, which causes better in-cylinder condition and therefore with constant efficiency, a lower NO_x emission can be realized"*

The hypotheses will now be summarized and given numbers:

1. *"Engine efficiency is expected to be higher on methanol than on natural gas with the performed test loads of 50 % and 75 % load."*
2. *"Better stability will be expected to be at an advanced ignition timing. With NG the standard ignition timing is at 20 °CA BTDC."*
3. *"Better efficiency will be reached at an advanced ignition timing on methanol than the standard used ignition timing of NG. With NG the standard ignition timing is at 20 °CA BTDC."*
4. *"With increasing temperature after the cooler, there will be more evaporation before the inlet valve, which causes better in-cylinder condition and therefore with constant efficiency, a lower NO_x emission can be realized"*

The hypotheses will be further investigated, in the test performances and with the model. The first three hypotheses will be tested in analysis from the experiments. The last hypothesis will be tested in the analysis from the model.

3

The experimental setup

This chapter describes the experimental setup for the initial performance tests with the SI PFI test engine on 100 % methanol. First, the specification of the test engine and the modification of the engine are explained. Next, the physical test setup and a schematic overview of the fuel and air system are discussed. Then, the test plan is briefly discussed. Finally, the sensor sensitivity is clarified in this chapter.

3.1. The engine

The engine used for this research is a Caterpillar (CAT) G3508A gas engine, as shown in figure 3.1. The engine is a turbocharged spark-ignited natural gas engine with 8 cylinders and a rated power of 500 kWe at 1500 rpm. Further engine specifications are shown in table 3.1. The engine has been used in 2018 for testing a hydrogen-natural gas (H-NG) fuel blend for the gasdrive project [29].

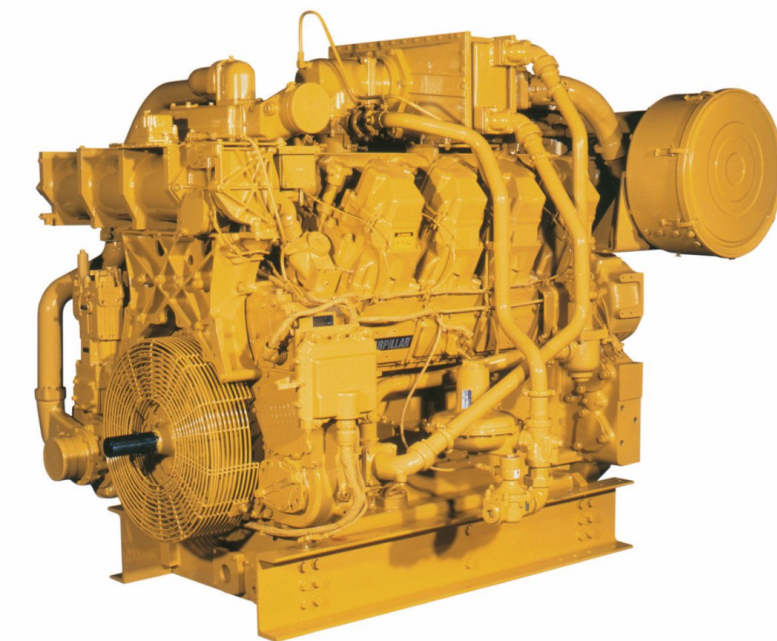


Figure 3.1: The G3508A Spark-ignited gas engine

Table 3.1: Engine Specifications

Parameter	Value	Units
Number of cylinders	8	-
Bore	170	mm
Stroke	190	mm
Displacement	34.5	L
Rated speed (N)	1500	rpm
Rated power (P)	500	kW
Compression ratio (ϵ)	12:1	-
Boost pressure	2.2	bar
Cycles	4	-
Firing order	1-2-7-3-4-5-6-8	-
IVO	6.7	$^{\circ}$ CA ATDC
IVC	158.5	$^{\circ}$ CA BTDC
EVO	20.1	$^{\circ}$ CA BBDC
EVC	11.8	$^{\circ}$ CA BTDC

3.1.1. Modifications on the engine

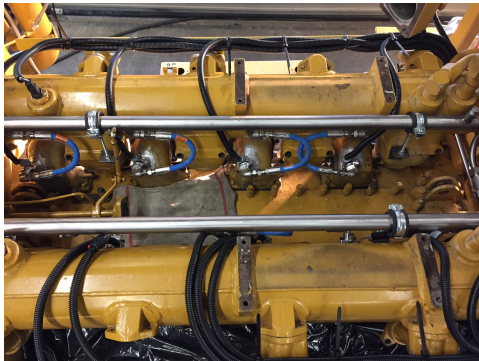


Figure 3.2: fuel line



Figure 3.3: injector holders



Figure 3.4: injectors

Several systems were modified for safe operation and measurements with 100 % methanol on CAT G3508A engine. The systems, that are retrofitted to operate a 100 % methanol engine with a port fuel injection (PFI) system, are divided by operation, safety, and measurements:

For operation:

- Modified fuel system

The modified fuel system includes modifications to fuel storage, fuel pump, filters, piping, specially designed fuel rail, adjusted PFI system with 2200 CC/min methanol injectors and valves. Methanol is corrosive to aluminium alloys, therefore chemical resistant materials such as stainless steel and rubber are used. The stainless steel fuel rail and port fuel injection system are shown in figure 3.2, 3.3 and 3.4.

- Modified charged air cooling system.

A new three-way valve and a modified charger air cooling control system were installed to control the temperature after the cooler. The standard system on the engine allows for constant temperature regulation after the cooler. However, the air temperature after the air cooler could not be kept constant with methanol injection. Due to the high evaporation energy requirements of methanol, the temperature after fuel injection at inlet port is load dependent. The modified charge air cooling system was installed because of concerns of reaching operating limits with the previous constant temperature regulator after the cooler at higher loads.

- New designed control system.

A primary and secondary control system is made for operating on methanol. The primary control

system controls fuel injection, airflow, engine speed, etc. The secondary control system to control the fuel supply system, charged air cooling system, purging system, and alarm handling.

For safety:

- Vapor detection system.
Two continuous methanol vapor detectors capable of measuring methanol content from 0-1000 ppm were installed inside the testbed. Such a detection system was necessary because methanol is toxic to humans beyond 200 ppm. Furthermore, human senses can detect methanol only when the concentration exceeds 10 times the 200 ppm safe limit [17].
- Fire detection system.
A fire detection system able to detect alcohol fires inside the testbed and outside at the fuel tank was installed.
- Inert gas system.
A nitrogen inert gas system was installed to reduce the amount of oxygen present in the fuel system and to clean the fuel system.
- Emergency stop system.
Emergency stop buttons and the vapor detection system was connected to the control system to instantly stop the engine and the fuel pump.

For measurements:

- A Testo-350 is used for exhaust gas measurements.
- A Kibox 2893A is used to determine the crank angle and in-cylinder pressure.
- A Dewetron Dewe-2600 is used to collect and store all sensor data excluding kibox data.

More details about the modifications on all these systems are given in appendix A.

3.2. The test setup



Figure 3.5: Testbed



Figure 3.6: Control room

The engine has been installed on a testbed at PON power, as shown in figure 3.5. The engine on the testbed is connected to a generator. The engine was installed including all control and measurement equipment that can be monitored in the control room just above the engine, as shown in figure 3.6.

3.2.1. Schematic overview of the fuel and air system

Figure 3.7 shows the engine test setup schematic with the premixed injection of natural gas (NG) (for 100 % NG operation), and methanol injection through port injectors (shown in green). The fuel filters, pressure sensors, and valves are left out of the overview for simplicity. Both fuel supply systems can operate simultaneously. The start of the engine was done by using NG. After knowing the engine's stable zero load running conditions on methanol, it was possible to start the engine using NG and run on 100 % methanol within 5 seconds after start.

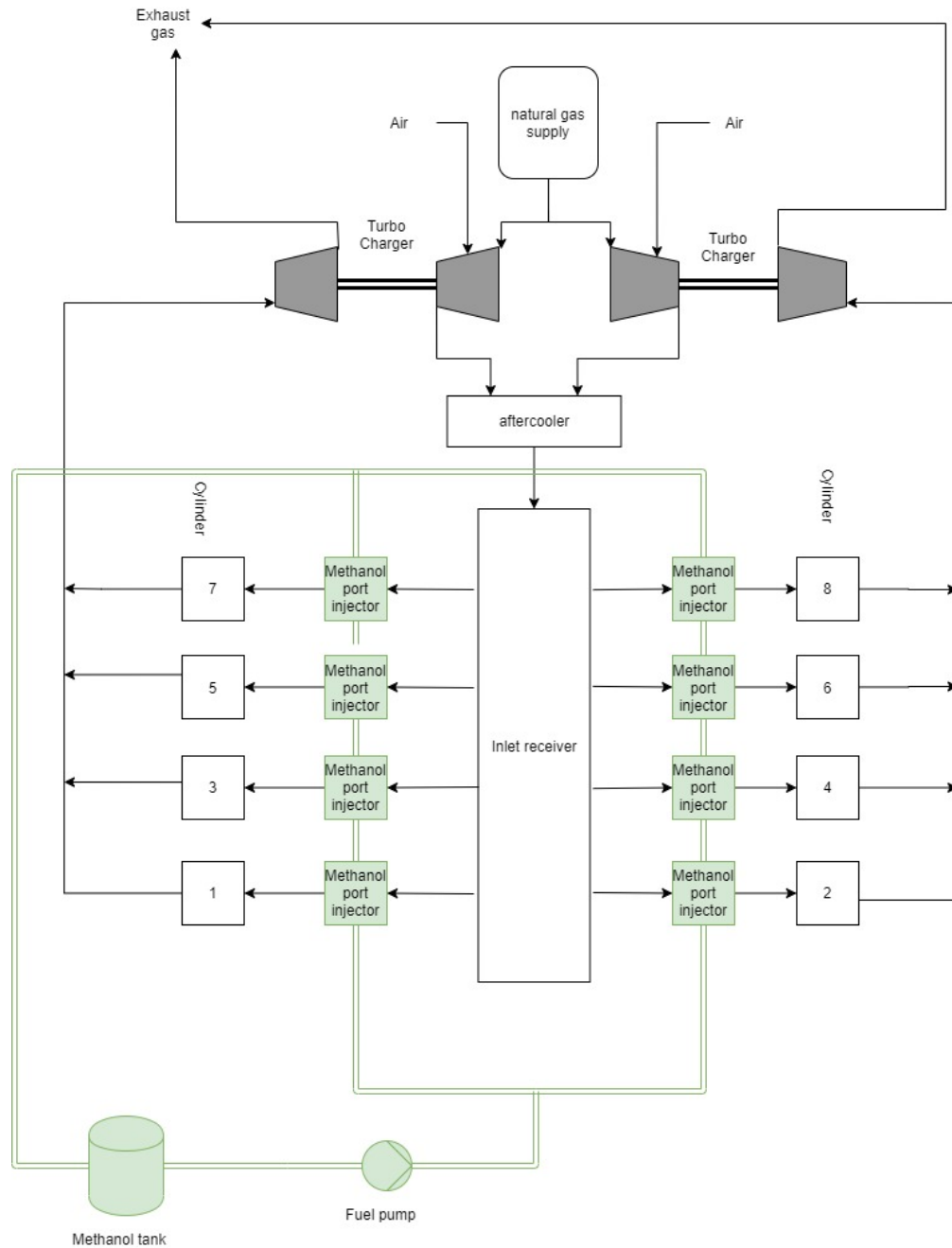


Figure 3.7: Schematic of the test setup

3.3. The test plan

Before the first performance tests with methanol on the engine are executed a full test plan is conducted and shown in appendix D. The tests were conducted safely and efficiently during the 2 weeks of testing on the engine. The plan is showing a step by step plan to be able to run the engine on constant engine speed on variable loads with changing variables. Due to the lack of fuel, time, and fuel pump capacity, not all tests of the full test plan could be executed. An overview of the executed tests is given in table 3.2.

Table 3.2: Overview of executed performance tests

	125 kWe (25 % load)	250 kWe (50 % load)	375 kWe (75 % load)
Performance runs on NG			
Ignition timing at 20 °CA BTDC		X	X
Performance runs on methanol			
Stable 0 % load run			
Stable load runs	X	X	X
<i>1th set of performance test: Ignition variation</i>			
Ignition timing at 16 °CA BTDC		X	X
Ignition timing at 18 °CA BTDC		X	X
Ignition timing at 20 °CA BTDC		X	X
Ignition timing at 22 °CA BTDC		X	X
Ignition timing at 24 °CA BTDC		X	X
<i>2nd set of performance test: NOx variation</i>			
NOx 250 mg/nm ³		X	X
NOx 500 mg/nm ³		X	X
NOx 1000 mg/nm ³		X	X
<i>3th set of performance test: Aftercooler temperature</i>			
Temperature variation ($T_{manifold}$)			X

3.3.1. Performance runs on NG

In this study, NG performance tests were performed for comparison with methanol performance. Two performance tests with natural gas (NG) are conducted on 250 kWe (50 % load) and 375 kWe (75 % load) with an ignition timing of 20 °CA BTDC. The NG used is from the Dutch grid, consisting of 80.5 % methane, where the full composition is detailed described in appendix I.

3.3.2. Performance runs on methanol

The performance runs on methanol are divided in two. First will be explained how the engine was able to run stable on methanol. Secondly will be described in which sets of performance tests are executed in this study.

Stable load runs

The first actual runs on 100 % methanol were done on 125 kWe load after slowly decreasing the NG supply and increasing the methanol fuel flow. This is not done as stated in the test plan on 0 % load, because combining the two fuel systems and control systems was found out to be best used with a small load. After running the engine stable with 100 % methanol on 125 kWe, the load was decreased to find 0 % load running condition, to find the amount of methanol and air needed for stable engine operation at 0 % load and 1500 rpm. This would allow switching from the NG to methanol at startup in 5 seconds. After running the engine with 100 % methanol at 0 % load, stable load conditions were found for 50 % and 75 % load conditions. The conditions for these stable load runs are:

- Pressure of fuel: 5 bar.
- Engine speed: 1500 RPM.
- Ignition moment: 20 °CA BTDC.
- End of injection was fixed at the middle between inlet valve open (IVO) and inlet valve closed (IVC).
- Injection duration was load dependent varying between 5 to 25 ms.
- Constant NOx emission of 500 mg/Nm³ at 5 % reference oxygen.
- $T_{manifold} = 40$ °C
- Air-excess ratio varied and was load dependent but close to 1.60.

Performance test sets on methanol

After the stable load runs a series of performance tests were executed as shown in table 3.2. During all three test sets fuel pressure, injection moment, and engine speed were kept constant as during the stable load run conditions. The first two sets of performance runs are executed on 50 % and 75 % load, the third set only on 75 % load. The third set, the temperature variation, could not be conducted anymore on 50 % load due to the limited time and due to limited fuel available on the testbed. The three sets of performance tests are further explained.

The first set of performance tests with methanol was changing the ignition variation. The ignition timing was varied by retarding the spark-timing by steps of 2 degrees, to study the impact of ignition timing sweep, while keeping the NO_x and load constant. This performance test was conducted at a constant NO_x emission of 500 mg/Nm³ at 5 % reference oxygen (equal to ± 340 ppm), with the main reason being the tightening emissions legislation. For the NG test engine, the 500 mg/Nm³ of NO_x value is lower but close to the NO_x IMO TIER-III limit for the engine, which is 2.08 g/kWh [31]. The air-excess ratio was varied to keep the NO_x emission constant.

The second set of performance tests was to change the NO_x emissions in three steps from 250, 500 and 1000 mg/Nm³ at 5 % reference oxygen. In the original test plan, it was planned to do more steps, but to be able to do the third performance set it is chosen to do only these 3 emission steps. The performance test was done at 50 % and 75 % load with varying fuel consumption and varying air-excess ratios.

The third set of performance tests was to study the impact of varying temperatures ($T_{manifold}$) on emissions and performance by increasing or decreasing the cooling in the aftercooler. By varying the manifold temperature the composition (liquid/vapor) of the fuel and air changes when entering the cylinder. With the third set of performance tests, the fuel consumption and load were kept constant with varying NO_x emissions. The temperature after the aftercooler was varied from 40 °C to 60 °C.

3.4. Sensor sensitivity

Table 3.3: Overview of the sensors

	use	range	accuracy
Kibox sensors			
In cylinder pressure sensor (Kistler 7061B)	in-cylinder pressure cylinder 3,4,5 and 6	0 - 250 bar	+/- 1.25 bar
Crank angle decoder (Kistler 2614C / 720)	determine CA	-360 : +360°	+/- 0.23 °CA
Dewetron sensors			
TC Model TE1260	air and exhaust gas temperatures	-40 °C : +1000 °C	+/- 1.5 °C +/- 0.004*(T)
PT100	lubrication oil and cooling water temperatures	-220 °C : + 600 °C	+/- 0.3 °C +/- 0.005*(T)
Pressure sensor 10 bar	air pressures	0 - 10 bar	+/- 0.02 bar
Testo-350 sensors			
CO	exhaust emission	0..10000 ppm	+/- 5 % (minimal 10 ppm)
CO ₂ (IR)	exhaust emission	0..50 vol %	+/- 0.3 vol %
No _x	exhaust emission	0..500 ppm	+/- 5 % (minimal 5 ppm)
Remaining sensors			
In-cylinder pressure sensor CAT	in-cylinder pressure cylinder 1 and 2	0-150 bar	+/- 9.75 bar
Flow sensor KRAL BEM 500	methanol flow	0 - 300 kg/s	+/- 0.3 kg/s (+/- 0.1 %)

The most important input sensors for the model are the in-cylinder pressure sensor and the CA sensor, without these the model will not work. But next to these two sensors a lot of other sensors are used during the performance tests and building the model of the engine. The most important data that is

received is in-cylinder pressure, crank angle, temperature measurements, pressure measurements, exhaust emissions (NO_x and CO_2), and fuel consumption. An overview of the range and sensitivity of these sensors is given in table 3.3. In addition to that, the sensors should be calibrated regularly to verify that they are still working properly. The Dewetron sensors are calibrated before testing, and the calibration report is shown in appendix E. The Testo-350 analyse box and the Kibox 2893A are calibrated prior to the testing, externally by the manufacturer.

4

Analysis of the experiments

In this chapter, the analysis of the experiments will be discussed. First, a comparison between 100 % methanol with 100 % NG is made by analysing the cycle-to-cycle variation, cylinder-to-cylinder variations and mean cylinder pressure at one similar operating condition. Next, the performance test sets: ignition variation and the aftercooler variation, as shown in table 3.2, are analysed and compared with the performance runs on NG. Performance tests that are conducted but had no contribution to the conclusions of this report are found in appendix B, e.g. the 2nd set of performance test, with varying NO_x emissions. After that, the combustion duration and the efficiency are determined over the full ignition sweep with methanol compared to NG at a singular operating point. And finally, the experimental sub-conclusions will be given.

4.1. Methanol compared to NG

4.1.1. Cycle-to-cycle pressure variations

Cycle-to-cycle pressure variations provide an indication of combustion stability. According to Merker, the relatively large fluctuations in the pressure path from cycle-to-cycle are a typical feature of SI engine combustion. Large cycle-to-cycle pressure variation can, in the worst case, lead to engine knocking or misfiring. The reduction of these variations in SI engine combustion can reduce specific fuel consumption (sfc) and/or emissions, and can be done by optimization of mixture formation, ignition and flame spreading [26, p68]. According to Heywood is the operating regime of the engine, determined by the cycle-to-cycle variation [15]. Therefore, in this section, the cycle-to-cycle pressure variation during the combustion will be investigated for methanol and NG at one similar operating condition.

The cycle-to-cycle variations pressure plots in figure 4.1 for NG and figure 4.2 for methanol are at 375kWe, 500 mg/nm³ NO_x, ignition at 20 °CA BTDC and 1500 rpm. These and following line graphs were made in Matlab, but the data is original from the Dewetron and the Kibox (pressure data). The pressure data is always measured from -360 °CA up to +360 °CA, but for clarity of the figures regularly fewer crank angles are shown on the x-axis. More cycle-to-cycle variation is already expected for methanol compared to NG when only looking at the maximum pressure variation of every cycle. The maximum pressure for methanol varied between 40 and 73 bar while NG varied from 45 to 70 bar. To determine the difference between the two cycle-to-cycle variations two coefficients of variation (COV) will be identified, one with the maximum pressure and one with the indicated mean effective pressure. The results of both COV calculations will first be given for cylinder 4 and then shown for all other cylinders. Prior to the experiments, the fuel injector of cylinder 4 is replaced due to dirt in the injector, therefore, this cylinder is looked at first with both COV calculations.

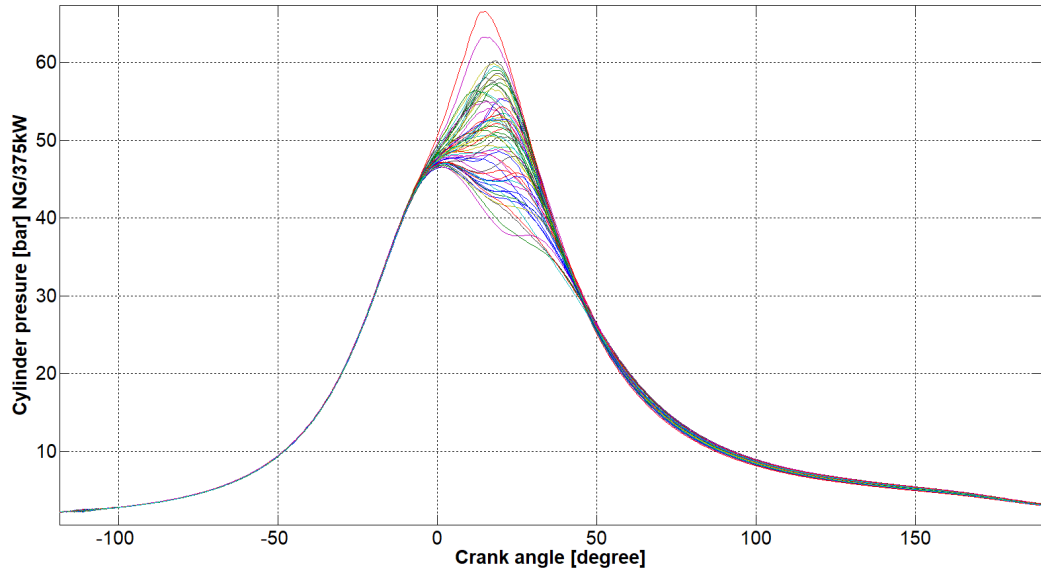


Figure 4.1: Cycle-to-cycle variation of cylinder 4 with NG

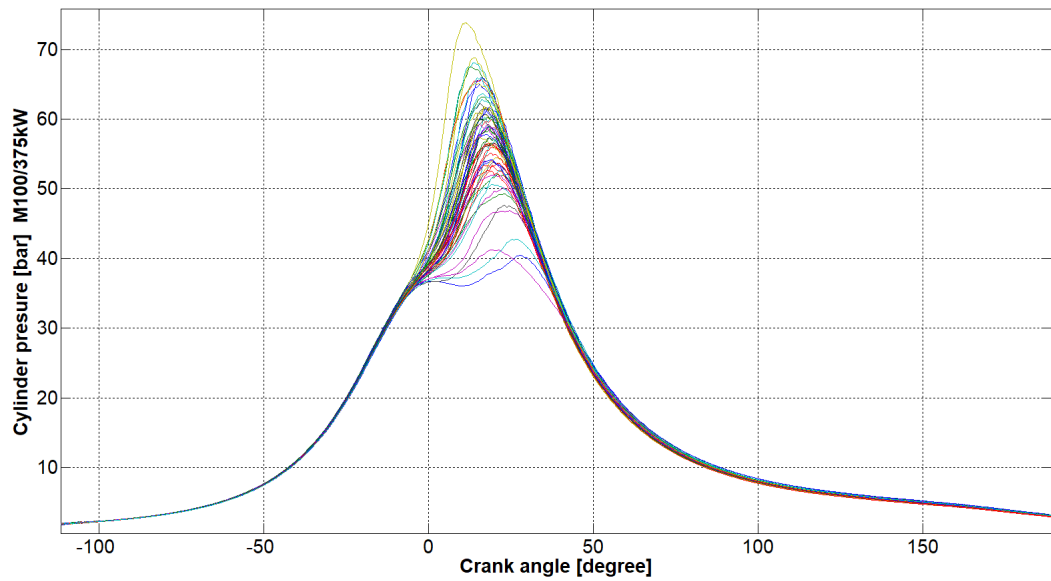


Figure 4.2: Cycle-to-cycle variation of cylinder 4 with methanol

Coefficient of variation for the maximum pressure (COV_{pmax})

First, the coefficient of variation for the maximum pressure (COV_{pmax}) is computed with formula 4.1 [48]:

$$COV_{pmax} = \frac{std_{pmax}}{Pmax_{avg}} \cdot 100\% \quad (4.1)$$

Where $Pmax_{avg}$ is the average of the maximum in-cylinder pressure and std_{pmax} is the standard deviation of the maximum in-cylinder pressure, shown in equation 4.2:

$$std_{pmax} = \sqrt{\frac{\sum_{i=1}^m (P_i max - Pmax_{avg})^2}{m - 1}} \quad (4.2)$$

Where $P_{max_{avg}}$ is the average of the maximum in-cylinder pressure over m cycles, $P_{i_{max}}$ is the maximum in-cylinder pressure of the i -th cycle, and m is the number of cycles taken = 60.

The standard deviation or COV changes with sample size. The more samples used, the smaller the standard deviation will be. Therefore, a critical view is needed when these COV values are matched with the COV measurements from other literature. However, with equal sample sizes the COV for methanol and NG can be compared and give a first estimate of the stability of the combustion. According to Lancaster a 99.9 % confidence level for the sample to stay within a 3 % difference of the mean is ensured with only 40 cycles, at highly stable operations [20]. But with less stable operations sample sizes can go up to 300 to achieve equal confidence levels. In this comparison, the sample size of the COV values for NG and for methanol are both 60 cycles.

Now for both pressure data sets the $COV_{p_{max}}$ is first taken for cylinder 4. With methanol, it shows for cylinder 4 a $COV_{p_{max}}$ of 11.41 %. And with NG it shows a $COV_{p_{max}}$ of 9.34 %. For the cylinders 3,5 and 6 with NG, the value of $COV_{p_{max}}$ varied between 7.63 % and 9.34 %. For methanol, these cylinders varied between 9.53 % and 14.82 %. This indicates higher cycle-to-cycle variations with methanol compared to NG. In Xie [48] similar results were found when running there engine on methanol. They found $COV_{p_{max}}$ values between 3.4 % and 14.0 %. F. Ma (F. Ma 2008) found values between 9.0 % and 11.0 % for NG for similar conditions [24]. The first impression of these results is that with methanol the $COV_{p_{max}}$ is slightly higher than running with NG, thus indicating less stable combustion with methanol.

Coefficient of variation for the indicated mean effective pressure (COV_{imep})

Another way to compare cycle-to-cycle variations between NG and methanol is to look at the COV of the indicated mean effective pressure (imep), which is more commonly used to determine the stability of the combustion [15, p.417]. The formula 4.3 shows the COV_{imep} calculation:

$$COV_{imep} = \frac{std_{imep}}{imep_{avg}} \cdot 100\% \quad (4.3)$$

Where std_{imep} is the standard deviation of the imep:

$$std_{imep} = \sqrt{\frac{\sum_{i=1}^m (imep_i - imep_{avg})^2}{m - 1}} \quad (4.4)$$

And where the imep is the work during one cycle divided by the stroke volume as shown in the following formula [35]:

$$imep = \frac{W_i}{V_s} = \frac{\int_{cycle} p \cdot dV}{V_s} \quad (4.5)$$

The full work cycle is taken in the formula, therefore W_H and W_L are combined in W_i . To validate the COV values a comparison is also made with the data from the Kibox. The COV values in the Kibox are calculated similar with formula 4.3, only the imep is defined alternative in the Kibox. To have the imep of the kibox comparable with formula 4.5 the total indicated mean effective pressure ($imep_N$) needs to be used, as shown in formula 4.6:

$$imep_{N,kibox} = imep_H + imep_L \quad (4.6)$$

Where $imep_H$ is the high part during the pressure cycle and $imep_L$ is the low part or pumping loop in the pressure cycle. Now for both pressure data sets the COV_{imep} is computed for cylinder 4 at 375 kWe and ignition timing of 20 °CA BTDC. With methanol, it shows for cylinder 4 a COV_{imep} of 3.72 %. And with NG a COV_{imep} of 2.21 % is shown. Therefore, it can be concluded that in cylinder 4 with methanol more cycle-to-cycle variations are shown compared to NG. For the other cylinders with methanol, the value of COV_{imep} varied between 3.72 % and 6.11 %. For NG the other cylinders varied between 1.76 % and 2.93 %. The COV_{imep} of the kibox shown similar results with a maximum error of 0.1 % as shown in appendix C.0.1.

In Heywood [15, p417] is stated that when COV_{imep} exceeds 10 % the ICE in automotive will cause driveability problems. This 10 % value was also exceeded when injector 4 needed to be replaced due to dirt in the injector as shown in appendix C.0.2. Furthermore, Sagra et al. [30], found that the current

test engine operation became rough and unstable when COV_{imep} crossed 10 % for 100 % natural gas. The 10 % value will, therefore, be seen as the misfire or stability limit. Both values for methanol and NG are far away from this unstable limit. Heywood also mentions that more accurate imep will be given with more than 100 cycles, but here again, the sample size was only 60 [15]. Thus, the standard deviation is negatively affected due to the low sample size. Both NG and methanol were measured with the same sample size. In conclusion, from the COV_{imep} comparison between methanol and NG at similar operating conditions, it can be concluded that combustion with methanol is less stable, but close to the stability of NG.

4.1.2. Cylinder-to-cylinder variations

According to Heywood is the operating regime of the engine limited by the extreme cycles [15]. These extreme cycles can appear in cycle-to-cycle variation, as discussed in the previous section, and can also appear due to cylinder-to-cylinder variations. Therefore, cylinder-to-cylinder variations in combustion are important and will be further investigated in this section for the combustion of NG and methanol.

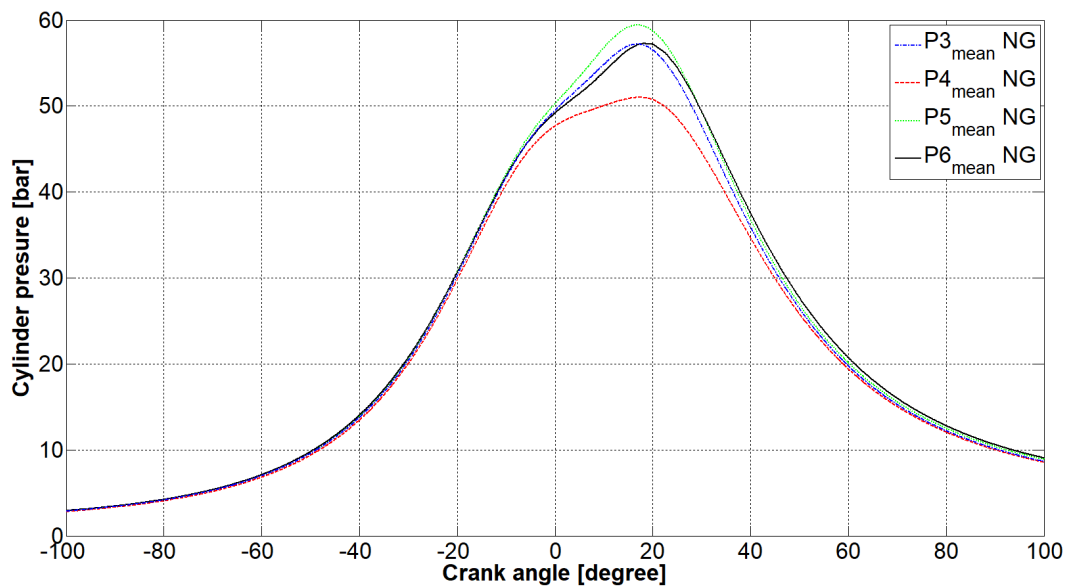


Figure 4.3: Mean pressure cylinder-to-cylinder variation with NG

The cylinder-to-cylinder variation for NG and methanol are shown in figures 4.3 and 4.4. The pressure data had some post-processing before it is shown. The in-cylinder data of every data-set consist of 60 cycles. The mean of these 60 cycles is taken to get a mean pressure of one cylinder. When the mean was taken of multiple data sets with similar conditions the pressure lines are on top of each other and only at the peak pressures minor differences are visible. Therefore, no further smoothing of the signal was necessary and only one of the data sets is used for this research.

The figures 4.3 for NG and 4.4 for methanol are at 375 kW_e, 500 mg/nm³ NO_x, ignition at 20 °CA BTDC and 1500 rpm. The graphs show the cylinder-to-cylinder mean pressure variation between the four cylinders (3,4,5 and 6) measured by the Kibox. Two interesting things to see from these figures is that:

- A difference is visible with NG between cylinder 5 and 6 of almost 10 bar at the maximum pressure. Because the fuel with NG is mixed with the air early in the engine, it is likely to assume that both cylinders will get the same percentage of fuel or equal AFR. Therefore, the difference here in cylinder-to-cylinder variations is most likely to come from other engine parameters, like how the manifold distributes the gas to the cylinders.
- With the methanol injection, it is visible that cylinder 3 and 4 have a higher pressure than cylinder 5 and 6. The difference between the highest and the lowest mean pressure between the cylinders about 3 bar more with methanol compared with NG. The injectors of cylinder 5 and 6 are closer

to the fuel pump than injectors of cylinder 3 and 4. This higher cylinder-to-cylinder variations with methanol can be caused by dirt in some of the injectors. This causes lower maximum pressures, which has also been seen before testing with the pressure of cylinder 4 with a dirty injector.

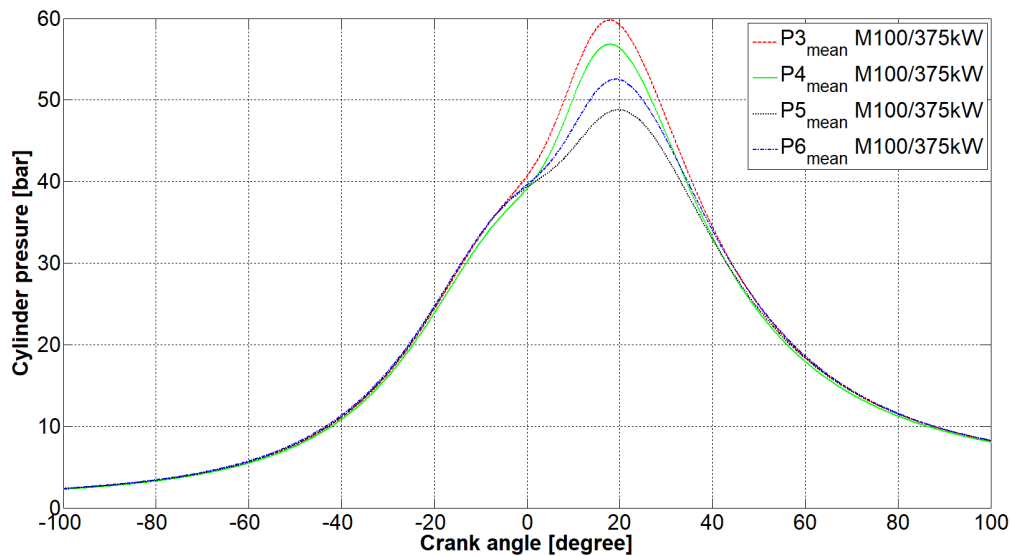


Figure 4.4: Mean pressure cylinder-to-cylinder variation with methanol

4.1.3. Mean cylinder pressure

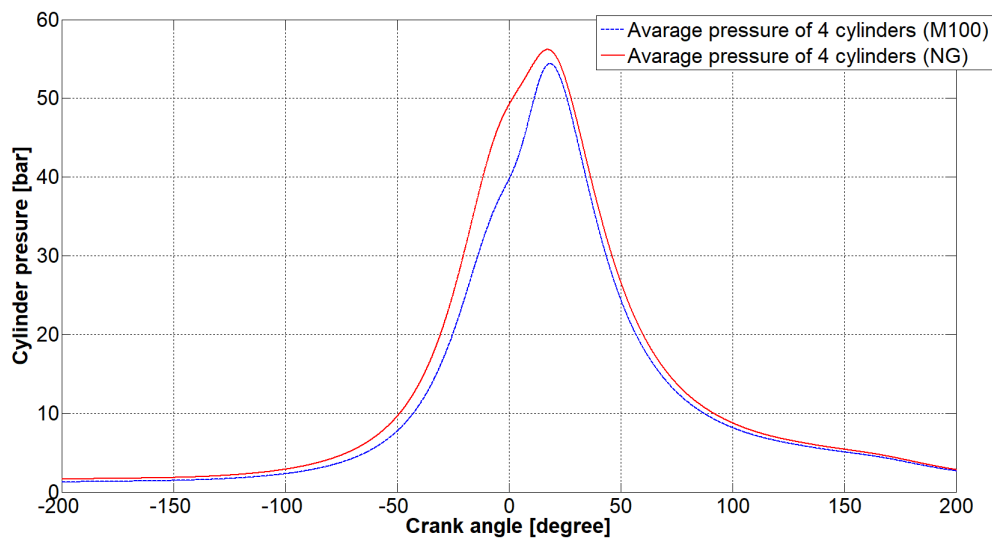


Figure 4.5: Mean pressure of NG compared to methanol at 375 kWe

The next step is to compare the mean cylinder pressures of NG with methanol. The average pressure of the 60 cylinder cycles for all the four measured cylinders is calculated as a function of crank angle. The engine settings corresponding to the measurements shown in figure 4.5 were 375 kWe power output, 500 mg/nm³ of NO_x, ignition at 20 °CA BTDC and 1500 rpm. As seen in figure 4.5, and based on an average of all four cylinders, methanol showed lower in-cylinder pressures compared to NG at the same engine operating conditions. However, it is vital to note that this was not the case for every single cylinder. For instance, cylinder 4 showed higher in-cylinder pressures with methanol compared to cylinder 4 with NG. It can also be seen that after TDC (0 degrees) the pressure rise with methanol is much steeper than with NG. This steeper rise of pressure can be an indication of faster combustion and will be further investigated with the model.

4.2. Ignition variation

In the previous section, the first comparisons are made between NG and methanol at similar operating conditions, the effect of changing ignition timing with methanol will be further investigated in this section. The ignition timing has a strong influence on efficiency and operating range [3]. With advanced ignition timings, knocking can be expected, with retarded ignition timing misfires can be expected [47]. Within these two limiting factors, the ignition timing will be varied, to determine stability. The efficiency is also influenced by changing ignition timing and will further investigated for every ignition timing in section 4.5. In this section, the cycle-to-cycle pressure variation and COV stability values will be investigated for methanol with an ignition variation from 16 °CA BTDC to 24 °CA BTDC.

4.2.1. Cylinder pressure with changing ignition timing

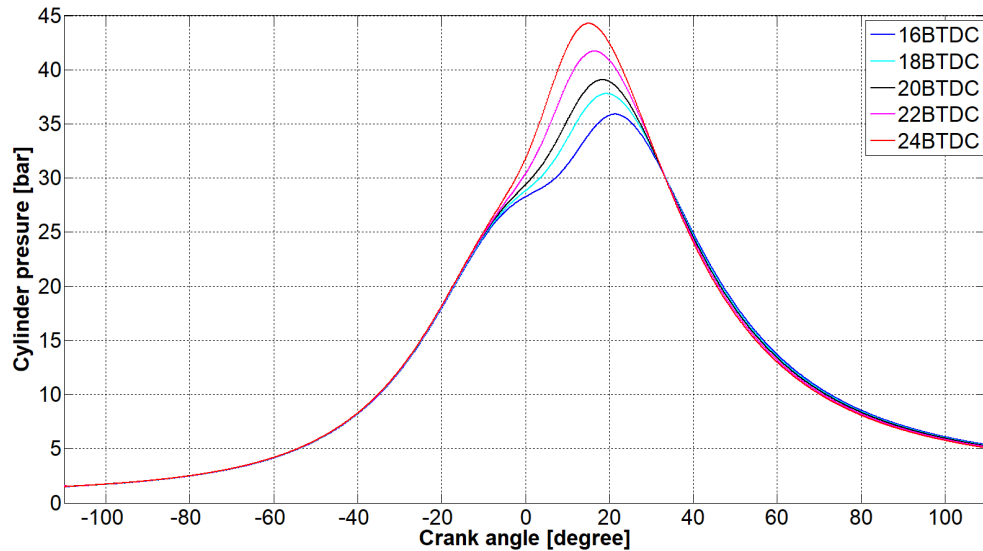


Figure 4.6: Mean pressure of all cylinders with changing ignition timing at 250 kW on 100 % methanol

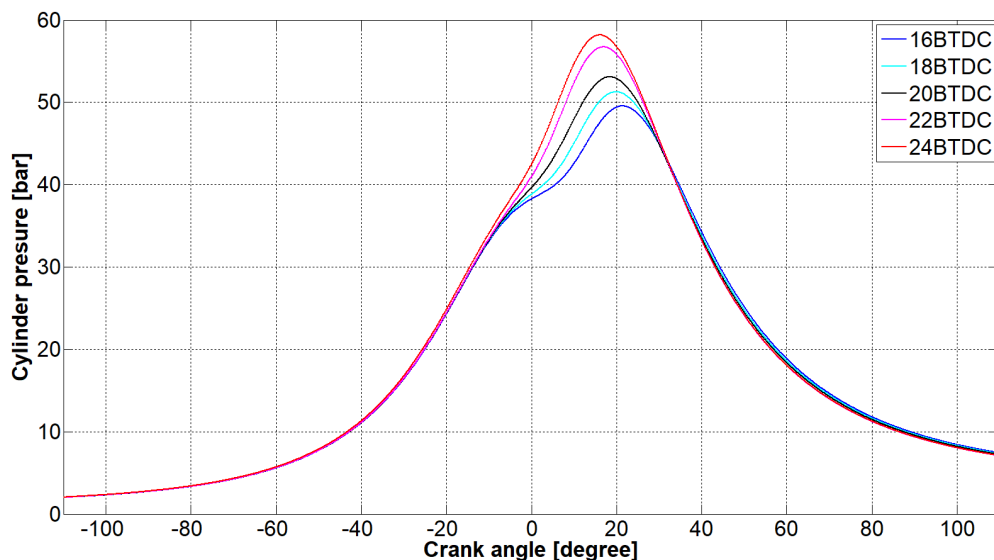


Figure 4.7: Mean pressure of all cylinders with changing ignition timing at 375 kW on 100 % methanol

The variations of ignition timing with methanol are done at 50 % and 75 % of maximum engine load. The ignition timing has been varied between 16 and 24 °CA BTDC in steps of 2 degrees. Normal

settings for NG and all other performance runs are at 20 °CA BTDC. Figure 4.6 shows the average pressures versus crank angle for various ignition timings at 50 % load and figure 4.7 at 75 % load. As expected the pressure peak comes earlier after TDC, as ignition timing advanced from 16 to 24 °CA BTDC. With advanced ignitions higher pressure rise and higher maximum pressure are achieved.

4.2.2. $COV_{p_{max}}$ and COV_{imep} with changing ignition timing

At rated power of 250 kWe the $COV_{p_{max}}$ of all cylinders are computed and shown in table 4.1 with the varying ignition timings. The $COV_{p_{max}}$ in this table are calculated with formula 4.1. It appears that the cycle-to-cycle variations do not change much with changing ignition timing for each cylinder. It does show again that the cylinder-to-cylinder variations are also visible in the $COV_{p_{max}}$. Cylinder 5 and 6 have higher $COV_{p_{max}}$ than cylinder 3 and 4. This means more fluctuations of the pressure, is shown in cylinder 5 and 6. Due to the higher $COV_{p_{max}}$, the average (peak) pressure of cylinder 5 and 6 will be lower than of cylinder 3 and 4 as also been shown at 375 kWe with 100 % methanol in figure 4.4.

Table 4.1: $COV_{p_{max}}$ at 250 kWe for 100 % methanol at different ignition timings

Ignition timing	$COV_{p_{max}}$ (CYL3)	$COV_{p_{max}}$ (CYL 4)	$COV_{p_{max}}$ (CYL 5)	$COV_{p_{max}}$ (CYL 6)
16 °CA BTDC	9.56 %	13.10 %	13.56 %	13.70 %
18 °CA BTDC	10.75 %	10.71 %	14.12 %	15.78 %
20 °CA BTDC	10.04 %	13.40 %	15.13 %	13.78 %
22 °CA BTDC	11.58 %	12.41 %	15.12 %	14.74 %
24 °CA BTDC	10.47 %	12.94 %	13.79 %	13.03 %

In table 4.2 the COV_{imep} , calculated with formula 4.3, is shown for the four measured cylinders with a variation of ignition timing. From these values, it is visible that the lowest COV_{imep} are at an ignition timing of 22 °CA BTDC. Indicating the most stable ignition timing is at 22 °CA BTDC at 250 kWe with methanol. Between 16 and 24 °CA BTDC the ignition timing all stays in a stable region, however, at 16 and 18 °CA BTDC significant less stable COV_{imep} are shown, closer to the 10 % unstable limit.

Table 4.2: COV_{imep} at 250 kWe for 100 % methanol at different ignition timings

Ignition timing	COV_{imep} (CYL3)	COV_{imep} (CYL 4)	COV_{imep} (CYL 5)	COV_{imep} (CYL 6)
16 °CA BTDC	4.50 %	3.98 %	5.45 %	6.15 %
18 °CA BTDC	3.77 %	4.08 %	6.04 %	9.13 %
20 °CA BTDC	3.35 %	3.49 %	5.05 %	6.57 %
22 °CA BTDC	3.00 %	3.18 %	5.5 %	4.73 %
24 °CA BTDC	3.47 %	3.95 %	5.8 %	4.97 %

The COV_{imep} has been determined on a similar way for 375 kWe as shown in table 4.3. In this table almost equal results are shown as found at 250 kWe. The most stable or lowest COV percentages are found at 22 and 24 °CA BTDC. Although, COV_{imep} at 16 and 18 °CA BTDC are showing here much lower values compared to 250 kWe. Again, cylinder 5 and 6 shown higher COV_{imep} than cylinder 3 and 4, indicating the earlier shown cylinder-to-cylinder variations with methanol.

Table 4.3: COV_{imep} at 375 kWe for 100 % methanol at different ignition timings

Ignition timing	COV_{imep} (CYL3)	COV_{imep} (CYL 4)	COV_{imep} (CYL 5)	COV_{imep} (CYL 6)
16 °CA BTDC	3.96 %	3.58 %	5.30 %	4.93 %
18 °CA BTDC	3.54 %	3.61 %	5.18 %	4.85 %
20 °CA BTDC	4.02 %	3.72 %	4.97 %	6.11 %
22 °CA BTDC	3.11 %	3.44 %	4.08 %	4.73 %
24 °CA BTDC	3.05 %	3.62 %	5.96 %	4.19 %

Section 4.1.1 concluded that methanol was less stable than NG at an ignition timing of 20 °CA BTDC. Now with the ignition variation shown in the tables 4.2 and 4.3, it becomes clear that the stability with

methanol for all used ignition timings was less stable than NG at 20°CA BTDC. The lower stability with methanol compared to NG could be due to one or a combination of the following reasons:

- **Dirty or blocked injectors.**

Prior to the experiments, the fuel injector of cylinder 4 is replaced due to dirt in the injector. In appendix C is shown that after replacing and fitting cylinder 4 with a clean injector, the COV_{imep} for that cylinder reduced from 10.59 % to 3.72 %, which is within the range of the above reported values found for methanol. It is vital to note that even when cylinder 4 indicated COV_{imep} value of 10.59 %, other cylinders had COV_{imep} in the acceptable range of 3.15 to 5.21 %. Furthermore, after replacing the injector of cylinder 4, the COV_{imep} value of 3.72 % was slightly lower than the 4.02 to 6.11 % values found for cylinder 3, 5 and 6. Thus, cleaning and replacing the cylinder clearly showed an improvement, however, the variations were still higher than those found for NG at the same operating condition. Given that dirt can cause injector blockage, which can lead to significantly high COV_{imep} values, the author would like to consider the possibility that the higher variations in COV_{imep} with methanol could be due to still remaining dirt particles in the injectors, originating from the production process of the new fuel system.

- **Higher evaporation energy.**

Another reason could be the 4 times higher evaporation energy requirement of methanol compared to diesel in combination with port injection instead of injection more upstream. In chapter 5.2 is calculated that at IVC the methanol is only for 18 % in a gaseous state, due to the low inlet temperatures, while NG is at IVC already 100 % in a gaseous state. The high evaporation energy requirement of methanol inside the cylinder could lead to non-uniform fuel evaporation before ignition, thus, leading to a non-homogeneous mixture formation with local air-excess ratios that are higher than 1.6, and, therefore, prone to cause combustion instability and higher in-cylinder pressure variations.

- **Lower flame speed.**

Lastly, Winterbone and Turan have reported that at lean air-excess ratios (approximately higher than 1.17) methanol can have a lower (laminar) flame speeds than that of methane, as shown in figure 2.3.8 [46]. The current test engine operates at much higher air-excess ratios of 1.6 when operating on 100 % methanol and 100 % natural gas. Reduced premixed flame speed of methanol at these leaner air-excess ratios could lead to slower combustion rates, which may contribute to higher cycle-to-cycle variations [12]. This hypothesis of lean methanol combustion causing lower combustion rates will be investigated chapter 6.3.

4.2.3. COV values from Kibox with changing ignition timing

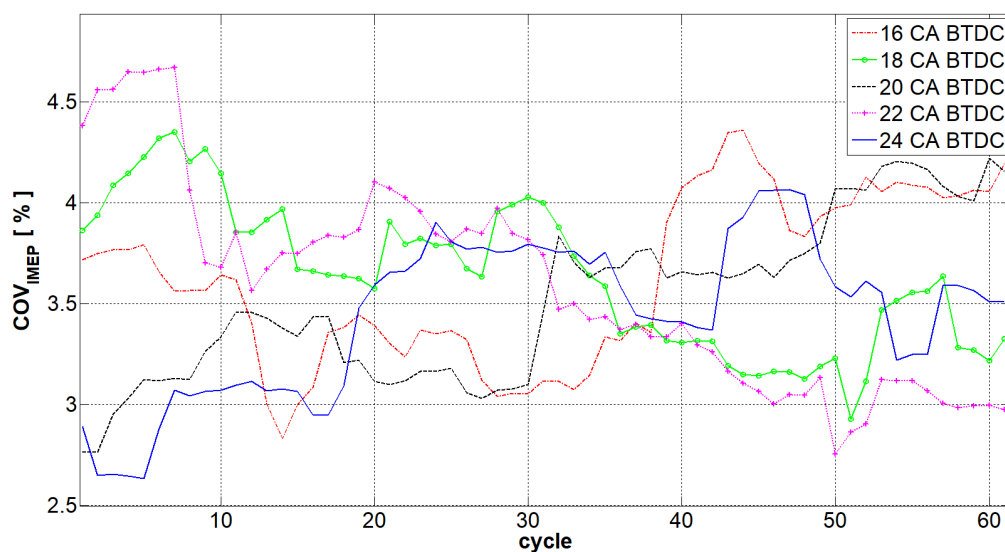


Figure 4.8: COV values with methanol of cyl 4 from Kibox with varying ignition timing at 375 kWe (M=30 for every COV point)

The own calculated COV values are now compared with the data from the Kibox. In appendix C.0.1 this is performed in detail for both COV values and Kibox settings. In the appendix the own calculated COV values are validated. In this section, only the results will be shown from the kibox COV values to find the ignition timing with the best stability.

In the results of the appendix C.0.1, it was found that the COV_{imep} in the Kibox is taken with 30 cycles instead of 60 cycles which has been used in formula 4.2 and 4.4. This will result in somewhat different values. However, the kibox stores more COV values, because it computes a new COV value over the last 30 cycles at every new cycle. The COV_{imep} from the Kibox of cylinder 4 is plotted in figure 4.8. To compare with table 4.3, the mean of these Kibox COV values is displayed in table 4.4.

Table 4.4: Mean of kibox COV_{imep} values of cylinder 4 with varying ignition timing

16 °CA BTDC	18 °CA BTDC	20 °CA BTDC	22 °CA BTDC	24 °CA BTDC
3.62 %	3.64 %	3.52 %	3.59 %	3.44 %

In table 4.4 it can be seen that the most stable and lowest COV percentages are shown at 24 °CA BTDC. Nevertheless, the values are close to each other. Especially the value of 16 °CA BTDC and 22 °CA BTDC are close together. When looking at figure 4.8, it shows that the COV_{imep} fluctuates between 2.5 % and 4.7 % and at some points in the figure the COV is lowest with an ignition timing of 16 or 18 °CA BTDC, thus the most stable ignition timing. Therefore, it is in the writer's opinion, not possible to determine optimum stability point. Because only one measurement of every varied ignition timing was taken. Combined with different results seen from the kibox compared to calculated COV values with formula 4.3. Concluding that hypothesis number 2 will not hold, which was:

"Better stability will be expected to be at an earlier ignition timing. With NG the standard ignition timing is at 20 °CA BTDC".

Although hypothesis number 2 will not hold still can be stated that between 16 and 24 °CA BTDC stable running of the engine with methanol is shown when taken an unstable limit of 10 %. Also the COV values show not many variation with ignition timings between 16 and 24 °CA BTDC.

4.2.4. COV values from Kibox for methanol compared to NG

Next, a comparison with the Kibox COV values will be performed for methanol compared to NG. Section 4.1.1 shows that methanol has higher COV values than NG at an ignition timing of 20 °CA BTDC, calculated with equation 4.3. In figure 4.9 the COV values are shown from the kibox for NG and methanol for all cylinders at 375 kWe at 20 °CA BTDC.

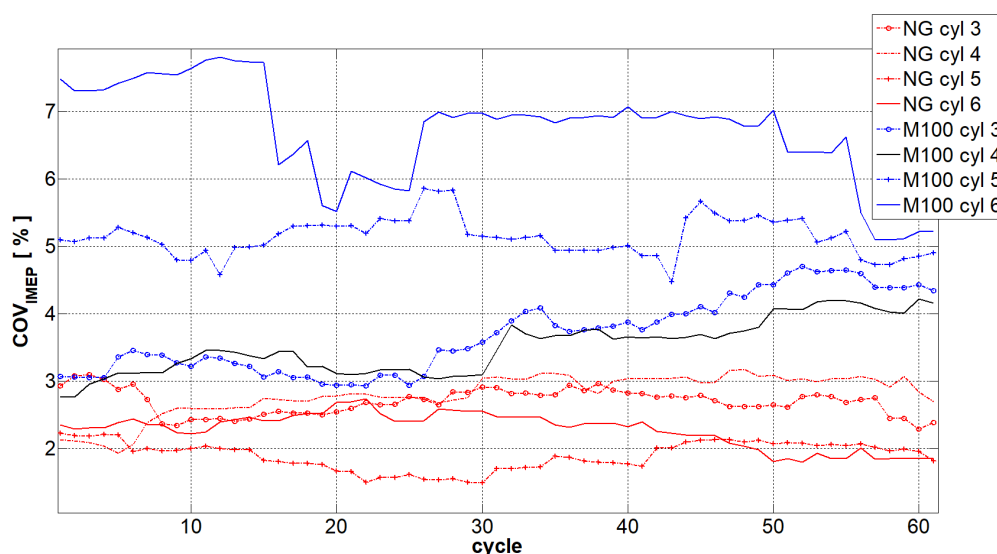


Figure 4.9: COV values of NG and methanol at 375 kWe and 20 °CA BTDC ignition from Kibox (M=30 for every COV point)

Figure 4.9 contains the following information:

- All COV values at 375kWe and 20 °CA BTDC are under the unstable limit of 10 %.
- COV values of methanol fluctuate more than COV values of natural gas. And the COV values of methanol are almost all cycles higher than the COV values of natural gas.
- For methanol cylinder 5 and 6 variate up to 2.5 % of the COV values. For cylinder 3 and 4 COV values variate up to 1.5 %.
- COV values of methanol from cylinder 3 and 4 are higher but much closer to the COV values of NG compared to cylinder 5 and 6.

Now, having a closer look to the (black) line of cylinder four with methanol, in figure 4.9, this is clearly lower than cylinder 5 and 6, indicating higher stability. As already mentioned the injector of cylinder 4 was replaced and the calculated COV_{imep} was found lower compared to all other cylinders, as shown in table 4.3. Thus, the kibox COV values shown comparable results. Meaning the higher stability of cylinder 4 compared to all other cylinders is also found over more cycles with the Kibox.

In summary, looking at the tables 4.2 and 4.3 and figure 4.9 it can be seen that the stable combustion with methanol is gained at both loads on ignition timings between 16 - 24 °CA BTDC. All COV_{imep} values are under the unstable limit of 10 %, thus earlier calculated COV values are comparable. However, at all ignition timings, the COV values are higher with methanol than with NG. It showed in figure 4.9 that only cylinder 3 and 4 were close to the COV values of NG. With the knowledge that cylinder 4 had a clean injector, it is recommended to replace all injectors prior to the next performance tests. Expected is that stability COV values of methanol will then be closer or even lower compared to the COV values of NG.

4.3. Aftercooler temperature variation

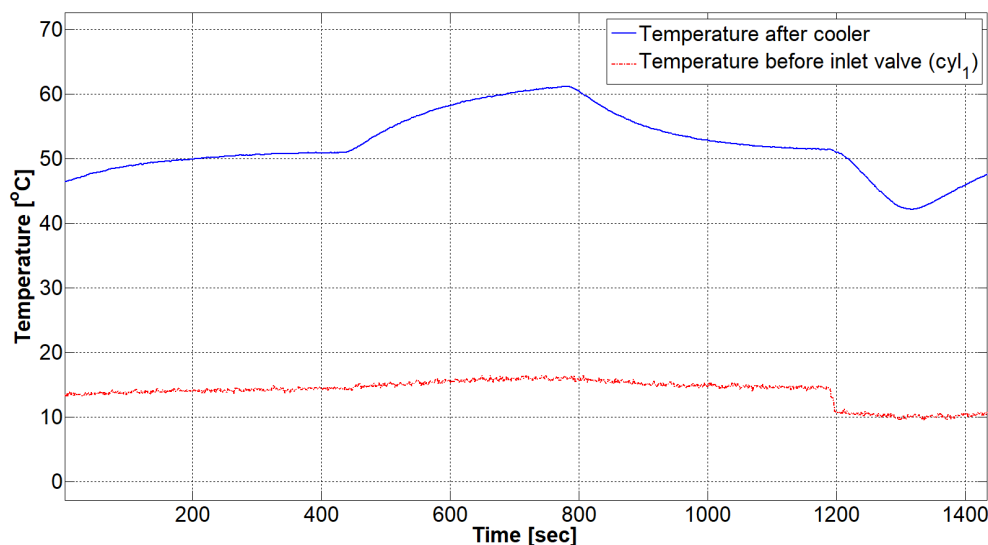


Figure 4.10: Temperature aftercooler variation between 40 °C and 60 °C

The temperature after the cooler, $T_{manifold}$, has been varied from 40 °C to 60 °C. This increases the in-cylinder inlet air temperature measured just before the inlet valve, $T_{inletvalve}$. This has been realized by manual closing the cooling valve to the air cooler. Increasing $T_{inletvalve}$ increases the fraction of fuel vaporized before entering the combustion chamber [15]. And due to the high heat of vaporization of methanol, it is expected that a higher $T_{inletvalve}$ will give a more homogeneous mixture at ignition [3]. And yet generally lower $T_{inletvalve}$ gives a lower maximum in-cylinder temperature, resulting in fewer NOx emissions [36]. The trade-off between these two effects with changing $T_{inletvalve}$ is unknown and therefore it is interesting to see how the engine responds to varying temperature settings. In the

following experiment, the temperature after the cooler is changed from 40 to 60 °C and back within a period of 20 minutes as shown in figure 4.10. The methanol flow and power were kept constant on 200 kg/hr and 375 kWe.

With increasing temperature after the cooler from 40 °C to 60 °C the λ climbed from 1.61 to 1.65 and the NO_x emissions drop from 170 ppm (= 500 mg/Nm³) to 117 ppm, which is shown in figure 4.11. This is an observation that is differently known from other fuel types. When normal increasing the temperature after the cooler the temperature of the air and fuel entering the cylinder will be higher and therefore more NO_x is shown with conventional fuels like diesel and natural gas [38]. However, increasing the temperature after the cooler by 20 °C, resulted not in a (trapped) in-cylinder temperature increase of 20 °C. The temperature at the inlet valve only went up from 13.5 °C to 16.0 °C, as shown in table 4.5. This small increase in temperature is expected to be due to the high heat of evaporation required for methanol, which is further explored in chapter 5.2.2.

Table 4.5: Important parameters with increasing aftercooler temperature at 375 kWe and constant fuel consumption

$T_{manifold}$ (°C)	$T_{inletvalve}$ (°C)	P (bar)	λ (-)	NOx (ppm)
40	13.5	1.42	1.61	170 (=500 mg/Nm ³)
60	16.0	1.51	1.65	117 (=344 mg/Nm ³)

In figure 4.12 the mean in-cylinder pressure is shown at a manifold temperature of 40 °C and 60 °C, this is the temperature after the outlet of the aftercooler. A clear difference is shown in the increasing pressure part. Where the manifold temperature is higher the pressure is increased at an earlier CA. However, at 20 °CA ATDC the pressure lines cross each other. Resulting in a almost equal peak pressures. To explain this, first, the trapped mass is investigated. With increasing temperature, the trapped pressure (p_1) will be compared at the moment of IVC (159 °CA BTDC). $p_1(40\text{ °C}) = 1.42$ bar and $p_1(60\text{ °C}) = 1.51$ bar. When looking at the difference of the pressure manifold following can be seen: $p_{manifold}(40\text{ °C})=0.72$ bar and $p_{manifold}(60\text{ °C})=0.78$ bar. Due to the ideal gas law (equation 5.3) and equal volume, this must result in more trapped mass or higher in-cylinder temperature. Equal mass of fuel is injected, but there is more air in the cylinder at the moment of IVC (λ went up). This is interesting to see because in appendix B.2 also higher lambda showed with lower NOx emissions. However, there it was combined with increased fuel consumption. In this analyse, with increasing temperature after the cooler, now higher lambda's are obtained, with equal fuel consumption resulting in lower NOx emissions.

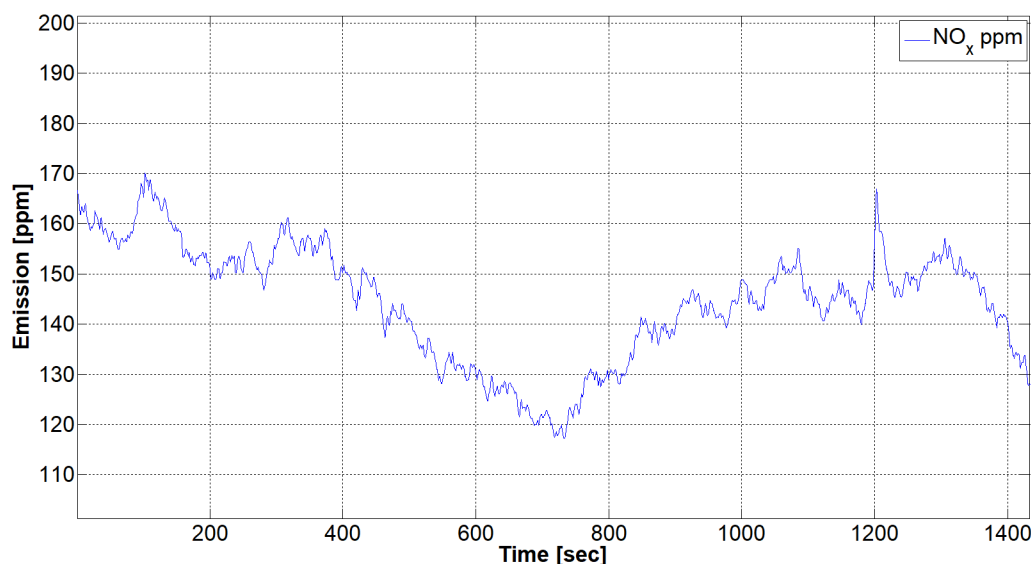


Figure 4.11: No_x emission during temperature increase to 60°C

Regarding the stability, the COV_{imep} for cylinder 3 and 4 decreased, indicating higher stability,

however, the COV_{imep} for cylinder 5 and 6 increased. COV_{imep} for cylinder 3 declined from 3.32 % to 3.17 %, and for cylinder 4 from 4.12 % to 4.07 %; COV_{imep} for cylinder 5 rose from 5.07 % to 5.72 %, and for cylinder 6 from 4.06 % to 5.77 %. Therefore, changes in the overall stability of the combustion with methanol with higher aftercooler temperature could not be concluded, because stability went up for cylinder 3 and 4 and went down for cylinder 5 and 6. More and steady state measurements are required to determine the stability change with varying manifold temperature. As stated in chapter 3, this test could only be conducted on 75 % load due to limited time, but testing at different loads is advised. It is also visible in figure 4.10 that it was a quick sweep from 40 to 60 °C and back. For better results regarding stability, a steady-state, longer period at 60 °C or even higher temperatures is recommended. With the model, the in-cylinder temperature will be investigated to see if it can be related to the lower NO_x emissions at higher manifold temperatures in chapter 6.

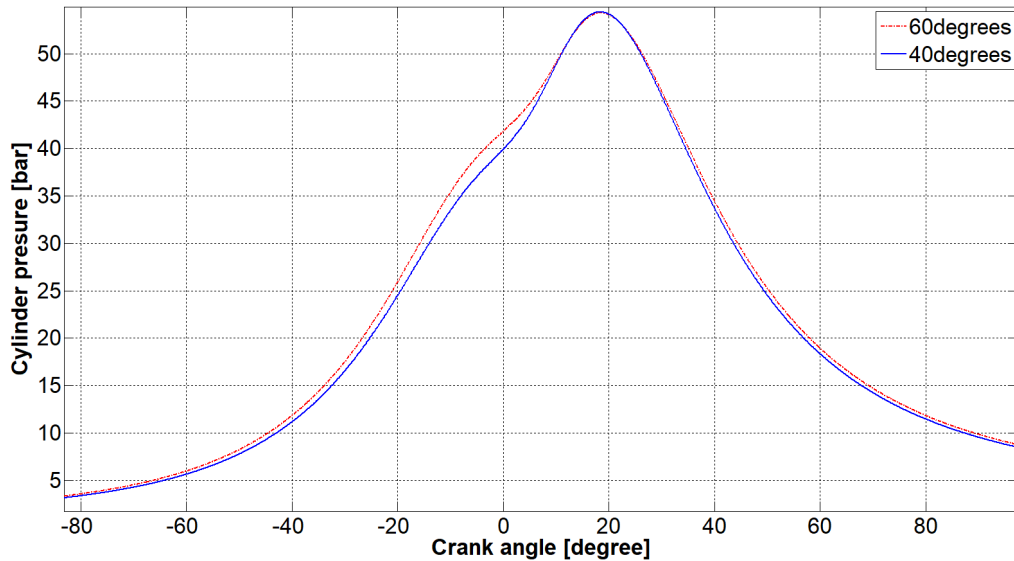


Figure 4.12: Mean in-cylinder pressure plots at a $T_{manifold}$ of 40 °C and 60 °C

4.4. Combustion duration

The combustion duration is a period of time within which combustion of the fuel is completed [15]. According to Verhelst, the faster premixed-combustion of methanol shortens the combustion duration, limiting the duration of high in-cylinder temperatures [42]. In chapter 6 a heat release comparison will be made between NG and methanol with the model. Within a heat release study often the combustion duration and centre of heat release rate (HRR) are seen as an important parameter [26]. These heat release values to determine the combustion duration are obtained from the Kibox data and will be shown in this section, to compare the combustion duration between NG and methanol.

Table 4.6: Mean of kibox CA10 CA50 and CA90 values in °CA ATDC of the four measured cylinders with methanol with varying ignition timing compared to natural gas

	NG 20 °CA BTDC	16 °CA BTDC	18 °CA BTDC	20 °CA BTDC	22 °CA BTDC	24 °CA BTDC
CA10	5.03	8.26	6.97	5.57	3.40	2.56
CA50	19.78	20.49	19.31	19.98	15.59	14.86
CA90	42.86	42.71	42.36	41.79	40.05	40.01
CA90-CA10	37.83	34.45	35.39	36.22	36.65	37.45

From the Kibox the crank angles can be found for 10 %, 50 %, and 90 % of mass fraction burned. For every measurement 60 values are given for every cylinder. These values are taken from the four measured cylinders and the mean value is taken. These mean values are compared for NG with an

ignition timing of 20 °CA BTDC and methanol at 16 °CA BTDC up to 24 °CA BTDC and shown in table 4.6. In this table 10% fuel mass fraction burned (CA10), centre of the heat release rate (CA50), end of combustion (CA90) and combustion duration (CA10-CA90) are shown for 375 kWe, 1500 rpm and 500 mg/nm³ NO_x. It shows that the combustion duration decreases with methanol with later ignition timing. In comparable settings (20 °CA BTDC) combustion duration of methanol is shorter than for NG with 1.61 °CA. The Kibox calculation for the CA10, CA50 and CA90 are calculated different compared to the model calculations and therefore further investigation and comparisons of the combustion duration will be done with the model in chapter 6.3.

According to Merker the most fuel consumption optimal operating point of CA50 is at 8 °CA ATDC [26]. This is almost independent of type of engine or combustion process. This optimal operating point of CA50 has been compared with data from 6 SI engines, in the work of Helmut Tschöke et al. [14]. They found an optimum at 8.65 CA ATDC for their 6 engines. In this research, the 8 °CA ATDC will be utilized as the fuel consumption optimal operating point of CA50. From table 4.6 can be seen that this optimal operating point is not obtained during the ignition variation, but with methanol at an ignition timing of 24 °CA BTDC, the CA50 value of 14.86 °CA ATDC is closest to this optimal operating point.

4.5. Effective (brake) engine efficiency

The effective (brake) engine efficiency of methanol is compared to NG and how this efficiency is calculated will be discussed in this section. First, fuel mass flow (\dot{m}) is required to determine the efficiency. Looking at methanol, the following is found from the experimental results concerning the fuel mass flow at 500 mg/nm³ NO_x and an ignition timing of 20 °CA BTDC :

- With 250 kWe generator power (50 % load) a methanol mass flow of 143.5 kg/hr is measured.
- With 375 kWe generator power (75 % load) a methanol mass flow of 200.0 kg/hr is measured.

Then, the brake power (P_b) is needed, but from the measurements only the generator power (P_{gen}) is known, therefor P_b is found with:

$$P_b = \frac{P_{gen}}{\eta_{generator}} \quad (4.7)$$

Next, the specific fuel consumption can be calculated with:

$$sfc = \frac{\dot{m}}{P_b} \quad (4.8)$$

Finally, the efficiency is determined with the following formulas from Stapersma [38] and is also known as the brake fuel conversion efficiency [15]:

$$\eta_e = \frac{1}{sfc \cdot h^L} \quad (4.9)$$

Where $h^L_{(methanol)}$ is the lower heating value (LHV) of methanol.

For methanol, the efficiency is calculated with a LHV = 19.9 MJ/kg from figure 2.3. A total (including generator) efficiency (η_{genset}) = 33.6 % at 375 kWe. Generator efficiency will be 95.5 % at 75 % load according to datasheet of the generator as shown in appendix G. With formula 4.9 and 4.7 the engine efficiency η_e (19.9 MJ/kg) = 35.5 % at 500 mg/nm³ NO_x, ignition timing of 20 °CA BTDC, and 375 kWe.

The engine efficiency with NG is gained from the datasheet of the engine as shown in appendix G. At 75 % load, 500 mg/nm³ NO_x, 18 °CA BTDC engine, an engine efficiency (η_e) of 33.9 % is received. For 50 % load, an engine efficiency (η_e) of 31.0 % is given by the manufacturer. Both efficiencies are calculated with a LHV of 34.5 MJ/m³. In table 4.7 the efficiency for methanol in the engine is given throughout the full ignition sweep at both (50 and 75 %) loads. At 18 °CA BTDC ignition and the LHV of 19.9 MJ/kg for methanol the efficiency for methanol will be compared with NG at both loads. The efficiency with methanol is around 2.2 % better at 250 kWe and 0.9 % better at 375 kWe than with natural gas already in these first performance tests. The engine efficiency increases up to a maximum of 35.9 % with changed ignition timing of 24 °CA BTDC at 375 kWe. Thus, the efficiency of the engine

improved by 2.0 % at 75 % load with advanced ignition timing while operating on 100 % methanol compared to natural gas. This improvement in engine efficiency at the advanced ignition of 24 °CA BTDC with 100 % methanol went up to 3.0 % at 50 % load.

In table 4.7 it shows the highest efficiency for methanol at the ignition timing of 24 °CA BTDC. In the previous section, a fuel consumption optimal operating point of CA50 was explained. In table 4.6 at an ignition timing of 24 °CA BTDC can be seen that from the Kibox the CA50 of 14.86 °CA ATDC is closest to 8 °CA ATDC. Thus, best efficiency found with an ignition timing of 24 °CA BTDC is compliant with the expectations of the CA50 closest to the fuel consumption optimal operating point of CA50 at 8 °CA ATDC. Further investigation and comparisons of fuel consumption optimal operating point of CA50 will be done with the model in chapter 6.3

Overall, the efficiency for methanol is higher compared to NG. These preliminary methanol engine results show that improvements in engine efficiency can be obtained from a retrofitted SI NG engine converted to operate on 100 % methanol without making any modifications to the geometrical engine specifications. According to Verhelst, this is expected to be gained from the increased charge density which leads to higher volumetric efficiency, shorter combustion duration and lower wall heat losses [42].

Table 4.7: Engine efficiency (η_e) of methanol with varying ignition timing compared with NG

Power	LHV (methanol) [MJ/kg]	NG 18 °CA BTDC	16 °CA BTDC	18 °CA BTDC	20 °CA BTDC	22 °CA BTDC	24 °CA BTDC
250 kWe	19.9	31.0 %	32.5 %	33.2%	33.6 %	33.8 %	34.0 %
375 kWe	19.9	33.9 %	34.4 %	34.8 %	35.5 %	35.7 %	35.9 %

4.6. Experimental sub-conclusions

Now the test setup in chapter 3 and the analyses of the experiments are described the first conclusions will be described by answering the sub-questions of this thesis:

- *Is it possible to run a CAT G3508A spark-ignited (SI) engine with port-injected methanol?*

Yes, it is possible to run the engine stable on 100 % methanol. The engine was able to operate after engine modifications were made to the fuel system, control system and aftercooler controls. Furthermore, safety systems and measurement systems were changed to make it possible to experiment on the 100 % methanol engine.

- *What challenges are faced when running the engine on methanol?*

During the first performance tests, it was not possible yet to start the engine on 100 % methanol and it still needed natural gas during a 5-second startup. Furthermore, 100 % load is not yet accomplished. Although it is expected that this will be possible at following performance tests after minor modification on the fuel system. The engine can operate, with the current fuel system, up to 430 kWe (86 % of maximum). Third challenge that must be noted is that the fuel injector of cylinder 4 needed to be replaced, prior to the measurements, due to dirt in the injector.

- *What data should be measured from the engine for modelling the in-cylinder combustion performance?*

During the experimental runs, the test plan could partly be conducted, only on 50 % and 75 % load, due to limited time and fuel. During these runs, the most important parameters for the input and validation of the model are received among interesting measurement data. The most important data that is received and necessary for modelling is in-cylinder pressure, crank angle, temperature measurements, pressure measurements, exhaust emissions (NO_x and O_2), engine power and fuel consumption.

- *What is the operation stability at 250 and 375 kWe with methanol compared to NG in terms of COV_{imep} and COV_{pmax} ?*

The engine runs stable on 100 % methanol at 250 kWe (50 % load) and 375 kWe (75 % load) between 16 °CA BTDC and 24 °CA BTDC ignition timing at 500 mg/Nm³ NO_x emission. Within

the ignition timings of 16-24 °CA BTDC, all COV_{imep} values stayed below the critical stability limit of 10 %. Compared to NG, COV_{imep} and COV_{pmax} showed higher values, indicating lower stability for methanol than for NG. Methanol showed less stability due to higher cylinder-to-cylinder variation. The expectation is that the higher cyclic variations are due to one or a combination of the following reasons: a.) Dirt in the injectors causing blocked injectors, b.) High evaporation heat of methanol and c.) Lower flame speed of methanol at the tested leaner air-excess ratios. The lower flame speed was not concluded with the experiments, because it was found that the combustion duration from Kibox for methanol was 1.6 °CA shorter than for NG at comparable settings of ignition timing (at 20 °CA BTDC), power (375 kW_e), engine speed (1500 rpm) and NO_x emission (500 mg/nm³).

- *When running with methanol on constant NO_x emissions of 500 mg/Nm³, what is the engine efficiency at 50 and 75 % load compared to NG?*

Efficiency improved by 2.2 % and 0.9 % at 50 % and 75 % load with methanol compared to natural gas at same test conditions of ignition timing and NO_x emissions. These preliminary methanol engine results show that improvements in engine efficiency could be obtained from a retrofitted SI NG engine converted to operate on 100 % methanol without making any modifications to the geometrical engine specifications such as cylinder or piston geometry. With advanced ignition timings of 24 °CA BTDC, the efficiency with methanol further increased up to 3 % and 2 % for 50 % and 75 % load, compared to NG with an ignition timing of 18 °CA BTDC.

And therefore the following hypotheses will hold or will be rejected:

- Hypothesis number 1 *"Engine efficiency is expected to be higher on methanol than on natural gas with the performed test loads of 50 % and 75 % load."*, will hold. Better efficiency at 50 % and 75 % load is shown with increasing efficiencies for methanol of 2.2 % and 0.9 % compared to NG.
- Hypothesis number 2 *"Better stability will be expected to be at an advanced ignition timing. With NG the standard ignition timing is at 20 °CA BTDC."*, will be rejected. The best stability initially has been found with methanol at 22 °CA BTDC. Also with the mean of the Kibox data the best COV stability values were found at 24 °CA BTDC. Nevertheless, the Kibox data showed lots of fluctuations in the COV values and also at moments better stability was found at 16 or 18 °CA BTDC. Therefore, this hypothesis will not hold.
- Hypothesis number 3 *"Better efficiency will be reached at an advanced ignition timing on methanol than the standard used ignition timing of NG. With NG the standard ignition timing is at 20 °CA BTDC."*, will hold. Within the ignition sweep, the best efficiency is found with an advanced ignition timing of 24 °CA BTDC.
- Hypothesis number 4 *"With increasing temperature after the cooler, there will be more evaporation before the inlet valve, which causes better in-cylinder condition and therefore with constant efficiency, a lower NO_x emission can be realized"* holds. With increasing aftercooler temperatures, lower NO_x emissions are shown at the same fuel consumption rate. Only aftercooler temperature variations of 40 °C up to 60 °C has been done in the performance test. Expected is that lower NO_x emissions can be obtained by further increasing the aftercooler temperature. Further testing of this hypothesis will show in chapter 6.

5

The model

This chapter describes the in-cylinder Heat Release (HR)-model. First, the original NG model is illustrated, including all sub-models and minor modifications for the use of methanol. Then, the major modifications to use the model for port-injected methanol are explained. Finally, the assumptions and pre-calculations in this model will be summarized.

5.1. The in-cylinder HR-model

The heat release model calculates the combustion reaction rate, including heat losses. The model is commonly used to calculate in-cylinder temperatures and three types of heat release rates (HRR), which will be explained in this chapter. This model requires cylinder pressure and the crank angle (α) as the input [8]. Both pressure and α are measured from the engine with the Kibox. All sub-models of the model will be discussed up to the point of HRR calculations. A block diagram of the whole process is given in figure 5.1. The sub-models or parts from the model that will be explained in the following order are volume, temperature, air excess ratio, mass balance and composition, properties library, heat of combustion (u_{comb}), heat loss (Woschni model), energy of fuel and finally the heat release calculations combustion reaction rate (CRR), gross apparent heat release rate (GAHRR) and the net apparent heat release rate (NAHRR).

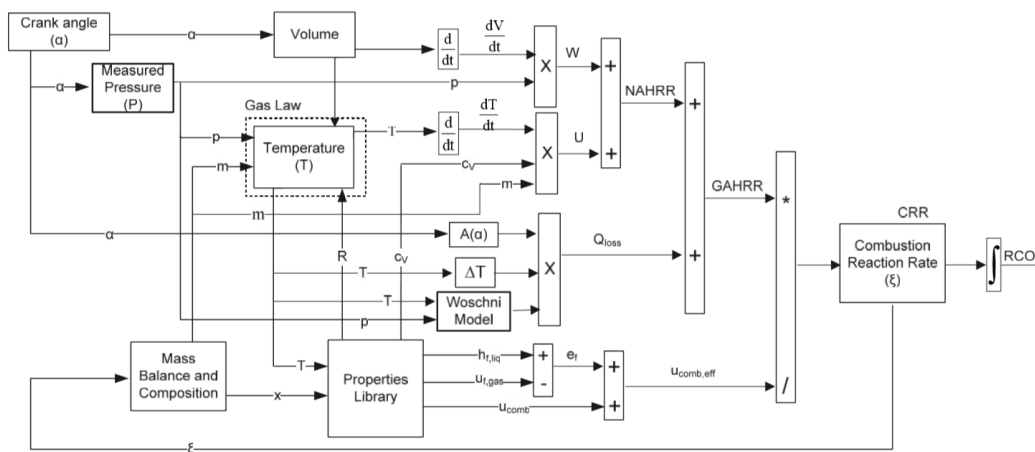


Figure 5.1: Blockdiagram of the "Heat release calculation model [8]"

5.1.1. Volume

To calculate work and temperature at every crank angle, the volume is needed. For every crank angle (α) the volume of the cylinder in m^3 is calculated as shown in equation 5.1 [8].

$$V(\alpha) = A_b \cdot L_s \cdot \left(\frac{1}{\epsilon - 1} \cdot \frac{1}{2} \cdot ((1 + \cos\alpha) + \frac{1}{\lambda_{cr}} \cdot (1 - \sqrt{1 - \lambda_{cr}^2 \cdot \sin^2\alpha})) \right) \quad (5.1)$$

Where A_b is the bore area in m^2 , L_s is the stroke length in m, ϵ is the geometric compression ratio, and the crank/rod ratio (λ_{cr}) is defined as [36]:

$$\lambda_{cr} = \frac{R_{cr}}{L_{cr}} = \frac{L_s/2}{L_{cr}} \quad (5.2)$$

Where R_{cr} is the radius of the connecting rod making on the crankshaft in m, L_{cr} is the length of the connecting rod in m, and L_s is the stroke length in m. The length of the stroke is equal to two times R_{cr} , equal to the maximum movement of the piston moving up and down on the crankshaft.

5.1.2. Temperature

The in-cylinder temperature is an interesting parameter in itself to investigate but is also needed in the model for internal energy, heat loss, and combustion heat calculations. The temperature will be calculated with the ideal gas law. The formula for the temperature in K is described in formula 5.3 [36].

$$T(\alpha) = \frac{p(\alpha) \cdot V(\alpha)}{m_1 \cdot R} \quad (5.3)$$

Where the pressure is the in-cylinder measured pressure in Pa, volume is the calculated volume by equation 5.1, m_1 is trapped mass in the cylinder in kg, which will be further explained in section 5.1.4, and R is the universal gas constant equal to 8.3145 kJ/(kmol K).

5.1.3. Air excess ratio

Before going further to the mass and composition balance first the air excess ratio is explained in more depth because this is input for the air mass balance. The engine is controlled by the air excess ratio and different values are observed at changing load or ignition timings. The air excess ratio for dry exhaust gas (λ_{tot}) is calculated with equation 5.4 [37]:

$$\lambda_{tot} = \frac{y_{O_2}^{da-in} - y_{O_2}^{dg-out} \cdot \frac{1}{4} \cdot \frac{x_H^f}{M_H} \cdot \frac{M_{da}}{\sigma_{da}}}{y_{O_2}^{da-in} - y_{O_2}^{dg-out}} \quad (5.4)$$

Where $y_{O_2}^{da-in}$ is assumed 20.95 %, $y_{O_2}^{dg-out}$ is the measured mol fraction of oxygen in the exhaust gas, molecular weight of hydrogen $M_h = 1.008$ g/mol, mixture molecular weight of dry air $M_{da} = 28.96$ g/mol and σ_{da} is the stoichiometric air/fuel ratio calculated with equation 5.5 [26, p178]:

$$\sigma_{da} = \frac{M_{a,da}}{y_{O_2}^{da-in}} \cdot \left(\frac{x_c^f}{M_c} + \frac{1}{4} \frac{x_h^f}{M_h} - \frac{1}{2} \frac{x_o^f}{M_o} \right) \quad (5.5)$$

Where x_c^f , x_h^f and x_o^f are the mass fraction in the fuel. M_c is the molecular weight of Carbon = 12.011 g/mol and M_o of Oxygen = 15.999 g/mol. For methanol the $\sigma_{da} = 6.41$, and for NG the $\sigma_{da} = 13.3$. To calculate the mass fractions, first the molecular weight of methanol ($M_{methanol}$) in g/mol is calculated with [19]:

$$M_{methanol} = M_c + 4 \cdot M_H + M_O = 12.011 + 4 \cdot 1.008 + 15.999 = 32.042 \quad (5.6)$$

And this gives the methanol mass fractions of $x_c = 37.48$ % for Carbon (C), $x_H = 12.58$ % for Hydrogen (H) and $x_o = 49.94$ % for Oxygen (O). For NG the mol fractions of every component are described in a analyse report shown in appendix I.1 and used to calculate $M_{NG} = 18.88$ g/mol.

Comparison of λ from Testo with outcome of formulas

With above formulas the measured λ_{testo} and the calculated λ_{tot} can be compared. For a given situation with methanol as fuel, the $y_{O_2}^{dg-out}$ is equal to 8.597 % and with the formula 5.4 the following λ_{tot} is calculated:

$$\lambda_{tot} = \frac{0.2095 - 0.08597 \cdot \frac{1}{4} \cdot \frac{0.1258}{1,008} \cdot \frac{28.96}{6.47}}{0.2095 - 0.08597} = 1.60 \quad (5.7)$$

When looking at the performance data, the λ can be found in the Testo-350 measured values. The Testo-350 measures the following lambda at 8.597 % [40]:

$$\lambda_{testo} = 1.63 \quad (5.8)$$

The λ_{testo} is 2 % higher than the calculated λ_{tot} , thus both close to each other. In the model, the calculated λ_{tot} with formula 5.4 will be used.

5.1.4. Mass and composition balance

The trapped mass (m_1) is the total mass in the cylinder at the moment the inlet valve is closed. For using m_1 in equation 5.3, all the partial in-cylinder masses at the moment the cylinder is closed, need to be known. The fuel mass is measured, but the air and residual gas that are both in the trapped mass are yet unknown. To calculate the m_1 , mass fraction of residual gas and fresh air are to be calculated with the following formula's.

Mass balance

First trapped mass (m_1) is calculated with the following formulas 5.9 [38]:

$$m_1 = m_{fresh} + m_{rg} \quad (5.9)$$

Where m_{fresh} is the newly added mass and calculated with equation 5.10. m_{rg} is the residual gas, remaining mass from the previous cycle, and calculated in 5.11 [38]:

$$m_{fresh} = m_{air(new)} + m_{fuel(new)} \quad (5.10)$$

$$m_{rg,t} = m_{air(old)} + m_{fuel(old)} \quad (5.11)$$

Therefore, combining the three equations will give equation 5.12 [38]:

$$m_1 = m_{air(new)} + m_{fuel(new)} + m_{rg} \quad (5.12)$$

Where the $m_{fuel(new),t}$ is known from measurements and $m_{air(new)}$ is calculated as follows [38]:

$$m_{air(new)} = \sigma_{da} \cdot \lambda_{tot} \cdot m_{fuel(new)} \quad (5.13)$$

Furthermore, to complete the mass balance the residual gas fraction (x_{rg}) will be calculated and is defined as [31]:

$$x_{rg,t} = \frac{m_{rg}}{m_t} \quad (5.14)$$

Composition balance and calculations of residual mass m_{rg}

Residual mass (m_{rg}) will be calculated at the moment of IVC. When using the ideal gas law from formula 5.3, at the moment of IVC, the m_1 can be calculated. Therefore, also m_{rg} is calculated with formula 5.12. The in-cylinder trapped mass is assumed to be constant without any crevice mass losses. With the pressure at IVC, the volume at IVC and $m_{fuel(new),t}$ known, only the temperature (T_1) must be calculated. The T_1 can be calculated with induced temperature and scavenge temperature as described in Stapersma [36, p.279]. The test engine in this research has no valve overlap of EVO and IVC, thus there is no scavenge period. Therefore, T_1 can be calculated for this engine as a combination of the induction temperature and the higher blowdown temperature of the residual gas with equation 5.15 according to Sapa [31]:

$$T_1 = \frac{1}{\frac{V_{IVC}-V_{IVO}}{V_{IVC} \cdot T_{ind}} + \frac{V_{EVC} \cdot p_{bld}}{V_{IVC} \cdot p_1 \cdot T_{bld}}} \quad (5.15)$$

Where the induction temperature (T_{ind}) is assumed equal to the measured temperature for the inlet valve. The p_1 is the trapped pressure at the moment of IVC and can be found in the measurements. The volumes at inlet valve close (IVC), inlet valve open (IVO), exhaust valve closed (EVC) are calculated with formula 5.1. The crank angles shown in 3.1 are used for these volumes and it must be noted that IVO has changed with 2 °CA up to 353.3 °CA. The reason and effects of this change are fully explained in appendix C.0.3. Blowdown temperature (T_{bld}) and pressure (p_{bld}) will be explained in following formulas. First T_{bld} is calculated with [36, p338]:

$$T_{bld} = \left(\frac{p_{bld}}{p_{EVO}} \right)^{\frac{n_e-1}{n_e}} \cdot T_{EVO} \quad (5.16)$$

Where p_{EVO} is the pressure at the moment of exhaust valve opening, n_e the polytropic exponent taken to be 1.30. The temperature exhaust valve open T_{EVO} is needed but was not measured during these performance tests. Therefore, an initial temperature of T_{EVO} , is taken from the experiments of Sapra [31]. And with iterating steps, this exhaust valve temperature is corrected. Actual blowdown pressure was not measured, but can be assumed to be the end pressure in the cylinder according to Stapersma with equation 5.17 [36, p338]:

$$p_7 = p_{bld} = p_{EVC} \quad (5.17)$$

Where the end pressure will be taken at the moment of exhaust valve closed from the in-cylinder pressure.

Furthermore, it must be noted that the calculation of $x_{rg,t}$ is sensitive to the inlet temperature. This temperature is measured close to the inlet valve but also has a sensor error. With a change of 1 °C of the inlet temperature the calculated $x_{rg,t}$ changes with 0.3 %, e.g. from 18.4 % to 18.7 %. But the uncertainty of the temperature sensors is already 1.5 °C, as shown in table 3.3. In the model, the analysis of HR-results are strongly dependent on the composition, and thus the value of the residual gas fraction $x_{rg,t}$. Therefore, the calculated $x_{rg,t}$ will be adjusted to the measured injected fuel mass. The measured fuel mass has an uncertainty of +/- 0.1 %, as shown in table 3.3. The injected fuel mass is defined in the model as:

$$m_{fuel(new)} = m_1 \cdot x_{gas} \quad (5.18)$$

Where the fuel fraction (x_{gas}) is defined as:

$$x_{gas} = 1 - x_{rg} - x_{air} \quad (5.19)$$

The calculated injected fuel mass (m_{ftr}) for methanol is always kept equal to the measured value. This has been done by changing x_{rg} until the measured value has been reached. But when changing the x_{rg} , the rest of the formulas must hold. Therefore in iterating steps, the T_{EO} will be adjusted according to the outcome of the model. After iterating steps of T_{EO} , with NG as fuel, a $x_{rg,t}$ of 17.2 % is calculated, at an ignition timing of 20 °CA BTDC. For methanol with the same ignition timing a $x_{rg,t}$ is calculated of 18.7 %, both being close to the +/- 15 % found by Sapra [31].

5.1.5. Properties library

In the properties library the following properties are used for calculations:

- Ambient condition. The ambient pressure and temperature is described here.
- Common properties. The universal gas constant and mol masses are described here.
- Fuel properties. The fuel properties are described here from common fuels. Methanol as fuel needs to be added and is described in chapter 5.2.
- Gas properties; describes the energy of the fuel. Due to the vaporization of methanol before the cylinder, this part must be adjusted as described in 5.2.
- Water properties. In this library, all properties of water are described.

- Engine properties. The specifications of the engine are given in table 3.1 and are similar to the values in the model files of the engine.

Except for the fuel properties and gas properties no significant changes are made in the properties library of the model. The modifications of the fuel and gas properties are explained in chapter 5.2.1.

5.1.6. Heat of combustion

The individual components of the heat release calculations will now be explained, starting with the heat of combustion. The combustion heat is a result of internal combustion in the cylinder. The combustion heat (\dot{Q}_{comb}) is calculated with equation 5.20 [36]:

$$\dot{Q}_{comb} = \zeta \cdot (u_{comb}^{ref} - \Delta u_{comb}^{ref}) \quad (5.20)$$

Where ζ is the combustion reaction rate (CRR) and u_{comb}^{ref} is the combustion value for a closed system. u_{comb}^{ref} is defined in equation 5.21 [36]

$$u_{comb}^{ref} = u_f^{ref} + \sigma \cdot u_a^{ref} - (1 + \sigma) \cdot u_{sg}^{ref} \quad (5.21)$$

And the change of internal energy of the species defined as equation 5.22 [36]:

$$\Delta u_{comb}^{ref} = (1 + \sigma) \cdot \Delta u_{sg} - \sigma \cdot \Delta u_a - \Delta u_f \quad (5.22)$$

Thus, the combustion value of the closed system is the sum of the internal energies of the mass composition in the combustion chamber.

5.1.7. Heat loss to cylinder walls (Woschni model)

During combustion heat loss to the surrounding metal should be taken into account, due to the large temperature difference between the combustion gas and cylinder wall. The heat loss is calculated with equation 5.23 [34]:

$$\dot{Q}_{loss} = \sum_{n=1}^3 \alpha_{g \rightarrow w} \cdot (T - T_{wall,i}) \cdot A_{wall,i} \quad (5.23)$$

With: $i=1$, cylinder wall, $i=2$, cylinder cover and $i=3$, piston crown, together these three temperatures are defined as the Woschni temperatures in this thesis.

It is very difficult to measure the surface temperature in these three places, therefore these Woschni temperatures will be estimated and kept constant during the combustion cycle. The heat transfer coefficient (α), in $W/(m^2K)$, will be estimated using the formula of Woschni as shown in equation 5.24 [34]:

$$\alpha = C_2 \cdot \frac{1}{D_b^{0.214}} \cdot \frac{p^{0.786}}{T^{0.525}} \cdot (C_3 \cdot c_m + C_4 \cdot \frac{p - p_0}{p_1} \cdot \frac{V_s}{V_1} \cdot T_1)^{0.786} \quad (5.24)$$

Note that the pressure must be in [bar], bore in [meter] and temperature in [Kelvin]. The C_2 value for NG is around 240 which has been found by Harsh Sapra [31] and is higher than the known value for diesel ($C_2=130$). The values used for the Woschni equation for this engine with methanol as fuel are adjusted with every data set as fine-tuning parameters, and will be further explained in chapter 5.1.10, but are in the order of:

$$\begin{aligned}
C2 &= 180 - 240 \\
C3 &= 2.28 + 0.308 \cdot \frac{w_t}{c_m} \\
\frac{w_t}{c_m} &= 5 \\
C4 &= 0.00324 \quad [m/(sK)] \\
T_{cyl\ wall} &= 320 - 362 \quad [K] \\
T_{piston\ crown} &= 450 - 515 \quad [K] \\
T_{cyl\ head} &= 450 - 510 \quad [K]
\end{aligned}$$

Note that " w_t " is the tangential swirl velocity and " c_m " is the piston stroke velocity and the C3 value for compression and expansion is used in the model and not the second C3 value for the gas exchange part.

5.1.8. Energy of fuel

The energy of fuel (\dot{E}_f) is equal to the difference of total enthalpy of the entering fuel and the internal energy of (gaseous) fuel in the cylinder. The energy fuel rate is given in equation 5.25 [8]:

$$\dot{E}_f = \dot{m}_f \cdot e_f = \dot{m}_f \cdot (h_{f,liquid} - u_{f,gas}) \quad (5.25)$$

This energy of fuel can also be seen as the heat flowing from the gas phase to the (liquid) fuel and required to heat up and evaporate the fuel before combustion ($\dot{Q}_{loss,fuel}$ in figure 5.3) [8]. The methanol fuel enters the cylinder partly as a fluid and partly as a gas due to the PFI. Therefore, this part must be changed in the model because the model assumes a gas state for NG. The modifications in this part of the model will be discussed in chapter 5.2.2.

5.1.9. Heat release calculations

In previous sections the individual components of the heat release calculations are explained, the heat release calculations of the model shall be given in this section. The heat release rate is defined with three equations 5.26, 5.27 and 5.28 [8].

(a) Net Apparent Heat Release Rate (NAHRR) in J/s:

$$NAHRR = \dot{Q}_{comb} - \dot{Q}_{loss} + \dot{E}_f = m \cdot c_v \cdot \frac{dT}{dt} + p \frac{dV}{dt} \quad (5.26)$$

Where m is in-cylinder mass, c_v is the specific heat at constant volume, T is temperature, t is time p is in-cylinder pressure and V is volume. With NAHRR calculation the heat loss (\dot{Q}_{loss}) is neglected. But as explained in chapter 5.1.7 the heat loss will be calculated with Woschni and therefore the NAHRR will not be the final heat calculation in the model.

(b) Gross Apparent Heat Release Rate (GAHRR) in J/s:

$$GAHRR = \dot{Q}_{comb} + \dot{E}_f = m \cdot c_v \cdot \frac{dT}{dt} + p \cdot \frac{dV}{dt} + \dot{Q}_{loss} \quad (5.27)$$

Where (\dot{Q}_{loss}) is calculated with Woschni.

(c) Combustion reaction rate (CRR) in kg/s:

$$CRR = \zeta = \frac{m \cdot c_v \cdot \frac{dT}{dt} + p \cdot \frac{dV}{dt} + \dot{Q}_{loss}}{u_{comb} + e_f} \quad (5.28)$$

The physical meaning of the right-hand side of the CRR are explained as follows [36]:

- $m \cdot c_v \cdot \frac{dT}{dt}$ represents the change of internal energy as a result of temperature change.
- $p \cdot \frac{dV}{dt}$ is the work interaction with the piston.

- \dot{Q}_{loss} is the heat loss to the walls.
- u_{comb} is the heat of combustion value for a closed system.
- e_f the energy needed to heat the fuel and evaporate (being a negative energy value).

NAHRR can directly be calculated from the pressure and temperature in the cylinder. Pressure is measured and temperature will be calculated by the ideal gas law.

GAHRR includes heat loss and indicated the heat produced by combustion. The heat loss will be calculated with equation 5.24. The accuracy of GAHRR is therefore dependent on the estimation of the heat loss.

The CRR is the final output of the HR-model. For the CRR also the effective combustion value ($u_{comb} + e_f$) must be known. For methanol, these values are discussed in chapter 5.2.1. CRR is heavily fluctuating because it is measured from the pressure signal. The integral of the CRR is the reaction coordinate (RCO) is an increasing function. The RCO divided by the initial injected fuel mass ($m_{fuel(new)}$) gives the normalized RCO X and is given in formula 5.29 [8].

$$X = \frac{RCO}{m_{fuel(new)}} = \int_{SOC}^{EOC} \frac{CRR}{m_{fuel(new)}} \cdot dt \quad (5.29)$$

Where SOC is the start of combustion and EOC is the end of combustion. X increases to 1 when all fuel is burned in the cylinder, with 100 % combustion efficiency. But this is an ideal case, and combustion efficiency is not 100 %. Therefore it should be computed with O₂, CO, and CO₂ exhaust emissions. In this study, this could not be done due to the incorrect emission measurements. Consequently, an assumption is made that for NG and methanol 98 % of the fuel mass is burnt at EVO. This is equal to a final RCO of 0.98 in the model.

5.1.10. Spark-ignited (SI) engine

The engine that is modelled has a spark plug and therefore the fuel is spark-ignited (SI). In this section will be explained how the model will be adjusted to the spark timing of the SI engine. From the experiments, the spark timing was known for every experiment and even adjusted as discussed in chapter 3. In the model, the spark ignition is checked with the moment the first fuel is starting to burn. This will be done with formula 5.29, where the normalized RCO represents the mass-burn fraction. Where the RCO goes from negative through zero for the first time is the CA where the fuel is starting to burn. The CA where the RCO intersects zero will be seen as the CA where the fuel starts to combust and thus the point where it is spark-ignited [31].

The Woschni parameters need to be adjusted and will be used as fine-tuning parameters for modelling this crossing of the RCO through zero at the CA of ignition. According to Ding [8] the RCO can be corrected with the values of Woschni after the correct TDC shift is made. Changing the C_2 constant of Woschni can change the end value of RCO and bring the burnt fuel to 98 %, due to its direct change in the amount of heat loss. After correcting the total burnt fuel it is found that when changing the temperature values of $T_{cyl\ wall}$, $T_{piston\ crown}$ and $T_{cyl\ head}$ the starting point of combustion will shift, without much influence on the end value of RCO. The temperature values have been used to set the start of combustion (RCO=0) equal to the spark timing. Thus, with changing the start of combustion with varying Woschni's temperatures, the engine model is calibrated on the spark ignition.

5.2. Modifications in the model for the engine on methanol

All parts of the original NG model are discussed in section 5.1, including already some minor input changes needed for methanol. An overview of this model was given in figure 5.1. These minor changes include single input value changes, however, did not include multiple values or changes in the Matlab Simulink model. Therefore, two major changes to convert the model into a methanol PFI model are still to be discussed. First, the fuel properties related to the methanol needs to be adapted. Secondly, the energy of fuel needs to be modified due to the PFI of methanol. The modifications for methanol as a fuel are described in the following sections: modification for the fuel, modification to the heat loss to liquid fuel sub-model, and the vaporization factor.

5.2.1. Modifications for the fuel

To use methanol as a fuel in the model two parameter files need to be adjusted, the gas properties and the fuel properties.

Gas properties

The "gas properties" parameter file describes the energy of every component in the combustion chamber. As stated in the energy of fuel equation 5.25, the total enthalpy of the entering fuel and the internal energy of the gaseous fuel is needed from methanol. Both enthalpy and internal energy are also dependent on temperature. To describe the temperature dependence of the internal energy and enthalpy used in the model the following formulas are needed from Stapersma [36, p635].

The change of internal energy relative to the reference temperature is the difference between the internal energy of stoichiometric gas (after combustion) and the air and fuel (before combustion) is given in equation 5.22:

$$\Delta u_{comb}^{ref} = (1 + \sigma) \cdot \Delta u_{sg} - \sigma \cdot \Delta u_a - \Delta u_f \quad (5.22 \text{ revisited})$$

The internal energy differences relative to there reference state are functions of temperature as shown in 5.30, 5.31 and 5.32 [37]:

$$\Delta u_{sg} = u_{sg} - u_{sg}^{ref} = \int_{T_{ref}}^T c_{v,sg} \cdot dT \quad (5.30)$$

$$\Delta u_a = u_a - u_a^{ref} = \int_{T_{ref}}^T c_{v,a} \cdot dT \quad (5.31)$$

$$\Delta u_f = u_f - u_f^{ref} = \int_{T_{ref}}^T c_{v,f} \cdot dT \quad (5.32)$$

Then the relation for C_p and C_v can be made with 5.33 [37]:

$$C_v = C_p - R \quad (5.33)$$

Where R is the universal gas constant ($R = 8.3145 \text{ kJ/kmolK}$).

Now with power series for specific heats at constant pressure (C_p) these internal energies can be evaluated at any temperature. The power series are described in equation 5.34 [39, p166]:

$$C_p = \sum_{k=1}^m a_k \cdot \theta^{(k-1)} \quad (5.34)$$

With temperature (θ) shifted to a non-zero point around the series and normalised in equation 5.36 [39]:

$$\theta = \frac{T - T_{shift}}{T_{norm}} \quad (5.35)$$

Where T_{shift} is the temperature to be shifted to a non-zero point. e.g. $T_{shift} = 273.15 \text{ K}$, but in this case, a $T_{shift} = 0 \text{ K}$ is used. T_{norm} is the normalized temperature, $T_{norm} = 1000 \text{ K}$;

The power series needed to calculate u_{fuel} (methanol), also used in Byungjoo Lee [21, p65] but original from Yaws [7], needs the coefficients for methanol that are shown in figure 5.2.

Formula	Name	a'_1	a'_2	a'_3	a'_4	a'_5
CH ₃ OH	Methanol	40.046	-3.8287E-02	2.4529E-04	-2.1679E-07	5.9909E-11
$C_p = a'_1 + a'_2 \cdot \theta + a'_3 \cdot \theta^2 + a'_4 \cdot \theta^3 + a'_5 \cdot \theta^4 \text{ (J/mol/k)}$						

Figure 5.2: The coefficients for the polynomial to calculate C_p for methanol"

The units for a_k' in figure 5.2 are in J/mol/K. Unit conversation from J/mol/k to J/Kg/K can be done by equation 5.36 [7]:

$$a_k = \frac{1000 \cdot a_k'}{M_{methanol}} \quad (5.36)$$

Where $M_{methanol}$ means the molar mass of methanol. The molar mass is described in the "fuel properties" parameter file.

Fuel properties

The "fuel properties" parameter file describes all other needed properties for methanol, which are needed in the model, e.g. the fuel density, temperature at injection, and the fuel specification in molecular mass. The overall molar mass (M) of methanol (CH₃OH) in g/mol is calculated with equation 5.6:

$$M_{methanol} = M_C + 4 \cdot M_H + M_O = 12.011 + 4 \cdot 1.008 + 15.999 = 32.042 \quad (5.6 \text{ revisited})$$

Then the mass fractions of Carbon (C), Hydrogen (H) and Oxygen (O) can be calculated with:

$$x_C = \frac{M_C}{M_{methanol}} = \frac{12.011}{32.042} = 0.3749 \quad (5.37)$$

$$x_H = \frac{4 \cdot M_H}{M_{methanol}} = \frac{4 \cdot 1.008}{32.042} = 0.1258 \quad (5.38)$$

$$x_O = \frac{M_O}{M_{methanol}} = \frac{15.999}{32.042} = 0.4993 \quad (5.39)$$

These mass percentage with 4 significant numbers are used for the model. With these known mass fractions the stoichiometric air to fuel ratio (σ) is calculated. Combined with the measured oxygen in the exhaust stream ($y_{O_2}^{dg-out}$) the air excess ratio (λ) can be calculated according to equation 5.7. Also, the lower heating value (LHV) is calculated with the molar mass of methanol.

Compared to the thesis of Byungjoo Lee the mass fractions are optimized. His study used mass fractions 38, 12 and 50 % from a reference table [21, p24], but these rounding errors give errors in the stoichiometric air to fuel ratio (σ), the molar mass of methanol ($M_{methanol}$), and the lower heating value (LHV), which are all related to the mass fractions of the fuel composition in the model. The old and new values from the model are shown in table 5.1.

Table 5.1: Significantly changed model values from changing mass fractions

mass fractions	σ [-]	$M_{methanol}$ [g/mol]	LHV [MJ/kg]
old ($x_C = 38.00\%$)	6.27	31.608	19.304
new ($x_C = 37.49\%$)	6.41	32.043	19.934

5.2.2. New sub-model: Heat loss to liquid fuel h-u (methanol)

In equation 5.25 the energy of fuel rate of the model is given and the modification will be discussed in this chapter.

$$\dot{E}_f = \dot{m}_f \cdot e_f = \dot{m}_f \cdot (h_{f,liquid} - u_{f,gas}) \quad (5.25 \text{ revisited})$$

The model assumes that the fuel will be injected into the combustion chamber as liquid fuel and will evaporate with a dwelling time equal to zero (i.e. the injection rate and the evaporating rate are the same). In figure 5.3 the control volume of the in-cylinder model is shown. The energy of fuel is indicated as " $Q_{loss,fuel}$ " in figure 5.3 and can be seen as the heat that is needed to heat up and evaporate the fuel.

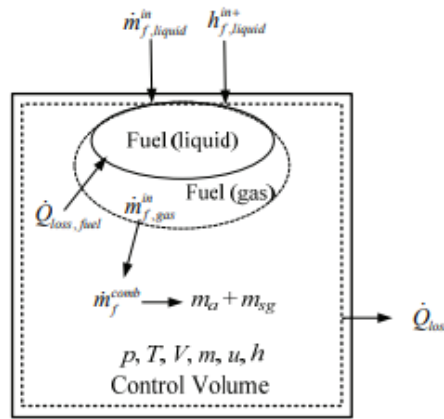


Figure 5.3: Scheme of the control volume of the in-cylinder model [34]

Model for the engine on NG

The sub-model "Heat loss to liquid fuel $h-u$ ", which calculates the energy of fuel rate with equation 5.25, was removed from the model of Harsh Sapra. It was removed because NG already is in a gaseous state when it enters the combustion chamber. For the NG analysis in chapter 6 the sub-model "Heat loss to liquid fuel $h-u$ " will not be used.

Model for the engine on methanol

Methanol enters the combustion chamber as a liquid, therefore the sub-model "Heat loss to liquid fuel $h-u$ (methanol)" is placed back into the model with two modifications. First, the sub-model will be further explained and then the modification will be clarified.

The sub-model, shown in figure 5.5, calculates the losses due to the injection of fuel, the losses that are needed to heat and vaporize the fuel (with equation 5.25) until it is in a gaseous state [8]. The injection pressure energy calculates the kinetic energy with the pressure difference from the in-cylinder pressure and injection pressure. The liquid fuel-specific energy ($h_{f,liquid}$) is a function of the temperature and pressure. The fuel specific energy ($u_{f,gas}$) is a function of temperature. Both ($h_{f,liquid}$) and ($u_{f,gas}$) are thus strongly dependent on (maximum) in-cylinder temperature. The denominator from equation 5.28, ($u_{comb} - e_f$), is called the 'the effective heat of combustion'. Ding shows a figure with the temperature vs specific heat of combustion for diesel as fuel [8, p.25], shown in figure 5.4, concluding that the 'effective heat of combustion' is considerably lower than the 'heat of combustion', in particular at higher a temperature. This difference is due to the temperature-dependent energy of fuel formula calculated in this sub-model.

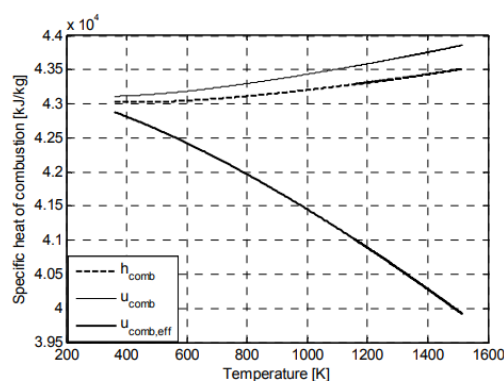


Figure 5.4: Temperature dependence of heat of combustion for diesel [9]

The first modification that is made in the sub-model is in the part containing the injection pressure calculations. When DI is used with e.g. diesel this part must be taken into account. But due to the port fuel injection (PFI) with methanol, this energy loss will not be in the combustion chamber. This is

made visible with figure 5.6, where must be noted that the in-cylinder calculations are done with p_{cyl} and not p_{fuel} . Also must be noted that the injection pressure with PFI is much lower than DI, therefore the injection pressure energy loss is much lower when it would be taken into account. In figure 6 it is shown that this part is "comment-out" in the Simulink model, and therefore not taken into account with the models HRR calculations.

The second modification in the sub-model is that it now assumes that the fuel will enter the combustion chamber as 100 % liquid. But with PFI the fuel is already heated and partly evaporated before it enters the combustion chamber. The original sub-model calculates the energy loss for evaporating 100 % methanol. This was done with the energy of fuel formula from 5.25, which calculates the difference of total enthalpy of entering (liquid) fuel and the internal energy of (gaseous) fuel present in the cylinder. The modification in the sub-model is that it will be multiplied with a factor $(1-x_{vapor})$. This evaporation factor represents the fuel part that is already in a gaseous phase at the moment that the inlet valve closes (IVC) and will be further explained in chapter 5.2.3. The following formula represents the modified energy of fuel rate calculation including the evaporation loss:

$$\dot{E}_f = \dot{m}_f \cdot e_f \cdot (1 - x_{vapor}) = \dot{m}_f \cdot (h_{f,liquid} - u_{f,gas}) \cdot (1 - x_{vapor}) \quad (5.40)$$

The second modification in the sub-model is shown in the red circle in figure 5.5.

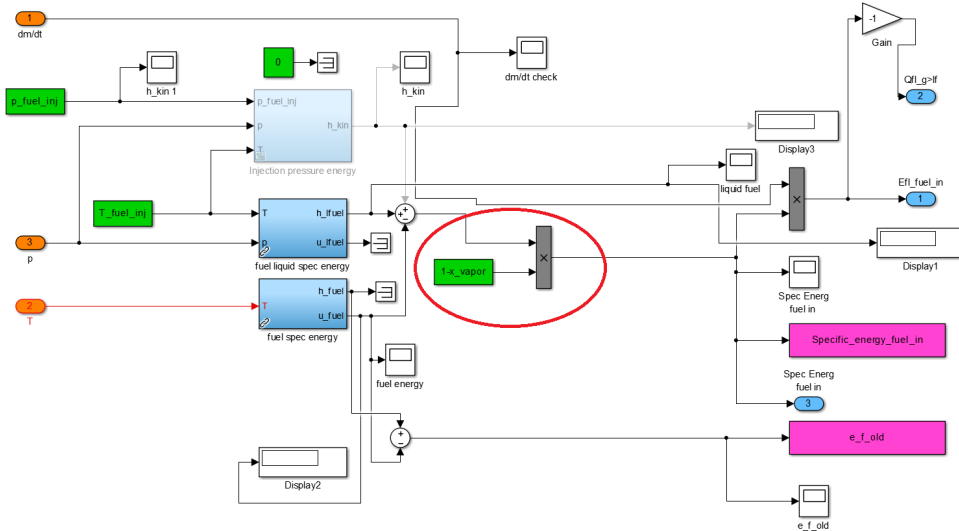


Figure 5.5: Modifications in the Simulink sub-model "heat loss to liquid fuel"

5.2.3. The vaporization factor

The vaporization factor (x_{vapor}) is a value between 0 and 1 and represents the fraction of fuel that is evaporated before the inlet valve closes (IVC). Before IVC the (liquid) fuel is injected before the combustion chamber. The fuel mixes with the air as shown in 5.6 before it enters the combustion chamber. The model calculates with the in-cylinder pressure and takes into account the energy losses for vaporization within the combustion chamber. Therefore, it is required to first calculate the fuel part that is already in vapor phase when entering the combustion chamber. This is called the vaporization factor (x_{vapor}) in the model. When $x_{vapor}=0$ it represents a 100 % liquid fuel, and when $x_{vapor}=1$ it represents a 100 % gaseous fuel, as is shown in formula 5.41:

$$x_{vapor} = \frac{m_{fuel-vapor}}{m_{fuel-liquid} + m_{fuel-vapor}} \quad (5.41)$$

To calculate the vaporization factor a Eulerian (stationary fixed in space) control volume has been made in the port inlet, as shown in figure 5.6.

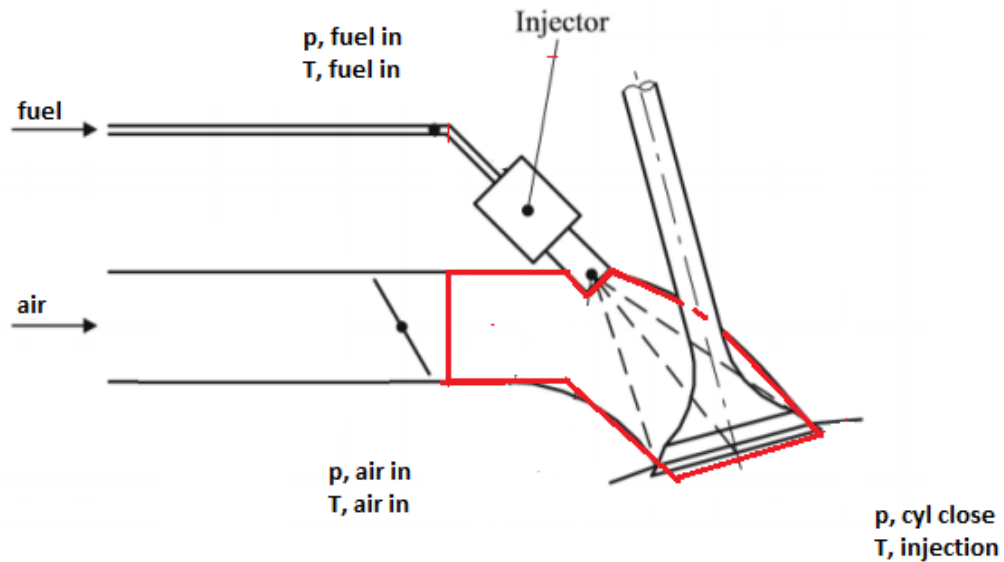


Figure 5.6: Control volume used to calculate x_{vapor}

From the experiments, the pressure and temperature of incoming flows in the control volume are known. For the outgoing flow, the in-cylinder pressure and the temperature after the injector are known from the measurements. Therefore, these (measured) quantities are shown in figure 5.6. Within this control volume, the conservation of mass equation and conservation of energy equation must hold. The formula of conservation of mass is given in 5.42:

$$\frac{dm}{dt} = 0 \quad (5.42)$$

$$\frac{dm}{dt} = (m_{air,in} + m_{fuel,in}) - (m_{fuel,vapor,out} + m_{fuel,liquid,out} + m_{air,out}) \quad (5.43)$$

The incoming mass of fuel for every cycle is known by measurements, the incoming mass of air will be calculated with λ and σ . When combining formula 5.42 and 5.43 outgoing mass can be calculated with the formula 5.44.

$$m_{fuel,in} * (1 + \lambda \cdot \sigma) = m_{fuel,vapor,out} + m_{fuel,liquid,out} + m_{air,out} \quad (5.44)$$

Next to the formula for conservation of mass also the formula for conservation of energy must hold for the control volume. The formula of conservation of energy for the control volume is given in 5.45 [33, p84]:

$$Energy_{out} = Energy_{in} + generation - consumption - accumulation \quad (5.45)$$

Where the energy can exist in many forms, e.g. as potential energy, kinetic energy, internal energy, work, heat, or electric energy. Generation and consumption will occur with chemical reactions and accumulation for non-steady-state reactions [33, p84].

Because this is a new part of the model two methods of calculating the vaporization factors will be described. After evaluation one of the two methods will be used in the model. First, a method with a heat balance, with the heat of vaporization, also used in the *single component model fuel*. The second method is with an enthalpy (energy) balance. With enthalpy, the work and internal energy are combined ($H = U + Pv$). For both methods the following assumptions are made:

- The process is adiabatic. The heat transfer from/to the walls is zero.
- Phase equilibrium is assumed. This means phase transition is much faster than the vapor transport into the cylinder.
- Process is in steady-state (therefore, accumulation = 0).
- Change of flow speed is neglected, therefore change in kinetic energy is assumed 0.

Energy calculations by heat balance

The first way the vaporization factor will be calculated is with the heat of vaporization (from single component model fuel) and the temperature change of the fuel and the air. In the book, *Mixture formation in internal combustion engine* from Baumgarten a single component model fuel is described [3, p140]. For this sub-model, the end state at IVC is of importance, therefore, the single component model fuel is more than sufficient. The first formulas for this model will be used to complete the conservation of energy formula.

The temperature change of a liquid fuel droplet can be obtained from following energy balance in formulas 5.46, 5.47 and 5.48 [3]:

$$\dot{Q}_{drop} = \dot{Q}_{heating} + \dot{Q}_{evap} \quad (5.46)$$

$$\dot{Q}_{heating} = m_{drop} \cdot c_{p,l} \cdot \frac{dT_{drop}}{dt} \quad (5.47)$$

$$\dot{Q}_{evap} = h_{evap} \frac{dm_{evap}}{dt} \quad (5.48)$$

The single model fuel will use these formulas to describe the size of a fuel droplet and the evaporating time. Equation 5.46 will be used to determine the vaporization factor (x_{vapor}) at the moment of IVC. Therefore, the heat needed to heat up the fuel (Q_{fuel}) is assumed to be the sum of the heat needed to use all droplets with formula 5.46. This is described in formula 5.49:

$$\dot{Q}_{fuel} = \sum \dot{Q}_{drop} = \dot{m}_f \cdot c_p \cdot (1 - x_{vapor}) + \dot{m}_f \cdot h_{evap} \cdot x_{vapor} \quad (5.49)$$

For changing the energy balance formula 5.45 in to a heat balance formula the following is assumed:

- The pressure influence is not taken into account (isobaric process).
- The heat is coming from the cooling of the air, therefore temperature difference (δT) will be taken from $T_{manifold} - T_{inlet}$.
- Kinetic and potential energy are neglected.

Now with these assumptions, the energy balance formula 5.45 is rewritten to the following heat balance formula, as shown in 5.50 [33]:

$$\frac{dQ}{dt} = \dot{Q}_{fuel} + \dot{Q}_{air} + \dot{Q}_{walls} = 0 \quad (5.50)$$

Because an adiabatic process is assumed the Q_{walls} term will be 0. Q_{air} is to be calculated with:

$$\dot{Q}_{air} = m_{air(new),t} \cdot c_{p,air} \cdot \delta T \quad (5.51)$$

Combining formulas gives us now a way to calculate the mass of fuel vapor and therefore with formula 5.41 the vaporization fraction:

$$\dot{Q}_{fuel} = \dot{Q}_{air} \quad (5.52)$$

$$\dot{m}_f \cdot c_p \cdot (1 - x_{vapor}) + \dot{m}_f \cdot h_{evap} \cdot x_{vapor} = m_{air(new),t} \cdot c_{p,air} \cdot \delta T \quad (5.53)$$

$$m_{fuel-vapor} = \frac{m_{air(new),t} \cdot c_{p,air} \cdot \delta T - m_{fuel-liquid} \cdot c_{p,l} \cdot \delta T}{h_{evap}} \quad (5.54)$$

The vaporization factor (x_{vapor}) is calculated with measurement data at 40 °C and 60 °C after the cooler from the temperature variation performance test. The temperatures before the inlet valve were respectively 13.5 °C and 16 °C. $c_{p,air}$ and $h_{vaporization}$ values are taken averaged over the temperatures. The vaporization factor (x_{vapor}) found for 40 °C and 60 °C after the cooler is respectively 24.7 % and 41.5 %.

Energy calculations with enthalpy balance

One of the shortcomings from previous calculations is that it is known that the process is not isobaric because a pressure decrease is seen at IVC compared to the pressure in the manifold. The fuel is also injected with a higher pressure of 5 bar.

Therefore, the energy balance equation 5.45 will be rewritten to an enthalpy equation to get more accurate results. When kinetic and potential energy are neglected, equation 5.45 simplifies to [33, p87]:

$$H_2 - H_1 = Q - W \quad (5.55)$$

This means that in our (adiabatic, steady-state) control volume, the work will be assumed to be zero, the difference in enthalpy will be used for the heat of vaporization.

To use formula 5.55 the enthalpy of the air and fuel is calculated before and after injection with the measured temperatures and pressures. Enthalpy values are taken from Refprop and shown in appendix H. For methanol, after injection the enthalpy for liquid is used and the enthalpy for vapor is calculated with the heat of vaporization added to the enthalpy of liquid. The total equation for the enthalpy balance then becomes:

$$\begin{aligned} & h_{air_{in}}(T_{air_{in}}, p_{air_{in}}) \cdot m_{air_{in}} + h_{fuel_{in}}(T_{fuel_{in}}, p_{fuel_{in}}) \cdot m_{fuel_{in}} = \\ & h_{air_{out}}(T_{air_{out}}, p_{air_{out}}) \cdot m_{air_{out}} + h_{fuel_{vapor}}(T_{fuel_{out}}, p_{fuel_{out}}) \cdot m_{fuel_{in}} \cdot x_{vapor} + \\ & h_{fuel_{liquid}}(T_{fuel_{out}}, p_{fuel_{out}}) \cdot m_{fuel_{in}} \cdot (1 - x_{vapor}) \end{aligned} \quad (5.56)$$

Where the total mass in is equal to total mass out according to formula 5.44, but the changing enthalpy, by changing pressure and temperature gives the vapor-liquid state. $p_{fuel_{out}}$ and $p_{air_{out}}$ are equal to p_{cyl} close in the control volume as shown at figure 5.6 and $T_{fuel_{out}}$ and $T_{air_{out}}$ are equal to $T_{injection}$ in the outgoing flow of the control volume. Now with interpolation, the vaporization factor (x_{vapor}) can then be found. The x_{vapor} found with equation 5.2.3 for 40 and 60 °C after the cooler is respectively 18.0 % and 37.7 %.

With formula 5.2.3 a few assumptions are made which gives an uncertainty. The following assumptions are made:

- The energy needed for mixing the gasses is not taken into account.
- Flow velocity is neglected.
- Adiabatic process is assumed.
- In-cylinder pressure is equal to the pressure at the end of the control volume.
- Temperature measured before the inlet valve is equal to the temperature at the end of the control volume.

With an aftercooler temperature of 60°C, the heat calculation gives a x_{vapor} of 41.5 %, the enthalpy balance gives a x_{vapor} of 37.7 %. Here the difference is 4 %. At 40°C the heat calculation gives a x_{vapor} of 24.7 %, the enthalpy balance gives a x_{vapor} of 18.0 %. Here the difference is bigger, almost 7 %. In both cases, the x_{vapor} is calculated to be lower with the enthalpy balance. Both measurements give a significant increase of almost 20 % more vapor when the temperature after the (air)cooler is increased from 40°C to 60 °C. A higher temperature after the (air)cooler is possible but not done with the experiments.

After the evaluation of both methods, the enthalpy balance method was chosen to be used in the models. The calculations in the enthalpy balance is a better estimate compared to the heat balance calculation because it also takes the changing pressure into account. The model will now be used with a vapor factor of 18 % at 40 °C after the cooler and a vapor factor of 37.7 % at 60 °C after the cooler will be used for the model.

5.3. Assumptions & pre-calculations used in model

Now the original NG model is described and all modification in the model needed for methanol are described, in this section, a summation of the assumptions and pre-calculated values within these two model are given and the order in which the parameters are changed for every data set. Starting with the assumptions and pre-calculations for both models, unless stated otherwise:

- Air and stoichiometric gases are considered to be ideal gases, the internal energy and enthalpy of in-cylinder gases are functions of temperature.
- A residual mass fraction (x_{rg}) of 12.4 % up to 18.7 % is calculated and is corrected with the measured fuel mass in the model.
- No crevices (heat) losses are assumed.
- For the methanol model, a vapor factor (x_{vapor}) of 18 % is calculated with 40 °C after the cooler at the moment of IVC. A vapor factor of 37.7 % is calculated for methanol with 60 °C after the cooler.
- There is zero delay in the model. Dwelling time of fuel and fuel vapor in-cylinder is equal to zero, only combustion gas phase is considered.
- The mass of fuel burnt at the end of the in-cylinder process could not be measured due to the incorrect emission measurements. Therefore, for NG and methanol, the mass fuel burnt is assumed at 98 % (equal to RCO(end)=0.98 in the model).
- The fuel starts to combust at the CA where the spark is ignited (equal to RCO=0 in the model)
- The internal energy for methanol is calculated with a power series, making the calculated combustion heat with methanol, temperature dependant in the model.

The order in which the parameters are changed could influence the output. The model input parameters change for every data set. Changing the parameters into the correct values are done in following order: 1) vapor factor (x_{vapor}) 2) Inlet temperature (varied due to manual control of temperature), 3) Calculated λ , 4) Mass flow and x_{sg} , 5) Iterating the found temperature at EVO (T_{EVO}) for correcting trapped temperature (T_1), 6) RCO at 98 % end value for both fuels, 7) Woschni temperature parameters for fine-tuning the CA of RCO=0 at the ignition timing.

6

Analysis of the model

In this chapter, the analysis of the model will be presented. In the analysis, the following in-cylinder indicators will be investigated in the corresponding section: pressure, power, heat release rate, and temperature. Every section will be divided into at least the following three analysis variants: NG compared to methanol, ignition variation, and aftercooler temperature variation. Furthermore, a validation will be shown for the model, by comparing it with the heat release from in the Kibox. In the last section, the conclusions regarding the model will be shown. But first, each analysis variant is further clarified in the following three sub-chapters.

6.0.1. Methanol compared to NG

The first analysis variant that is made with the models is the comparison between NG and methanol at 375 kWe, 500 mg/nm³ NO_x, ignition at 20 °CA BTDC and 1500 rpm. Two different models are used for this comparison. The methanol model modifications regarding fuel properties and the energy of fuel sub-model compared to the NG model, as has been explained in chapter 5. For the NG model, the NG fuel flow is not measured during the experiments. Therefore, the fuel flow is used from similar experiments. Two fuel flows are obtained: 127 m³/hr from the manufacturer and an almost -5 % lower value of 120 m³/hr from the experiments of H. Sapra's, both at an ignition timing of 20 °CA BTDC [32]. The fuel flow of 127 m³/hr for NG is utilized with a density of 0.80 kg/m³ at 15 °C at atmospheric pressure. Then a fuel mass $m_{fuel(new),t}$ is determined of 0.2833 g/cycle at the load of 375 kWe. The ρ of 0.80 kg/m³ at 15 °C is compliant with the (ρ) of 0.8469 kg/m³ (at 0 °C) from the NG composition in appendix I. In the following figures also a -5 % fuel mass for NG will be shown for comparison, which is close to the obtained experimental value of 120 m³/hr.

6.0.2. Ignition variation

The second analysis variant is performed for the ignition variation, using only the methanol model. The ignition timing was varied by retarding the spark-timing by steps of 2 degrees, at 375kWe, 500 mg/nm³ NO_x, and 1500 rpm. The ignition timing has been varied from 16 °CA BTDC to 24 °CA BTDC. For the ignition timing the 20 °CA BTDC is taken as normal ignition timing, 16 and 18 °CA BTDC are therefore retarded ignition timings and 22 and 24 °CA BTDC are advanced ignition timings.

6.0.3. Aftercooler temperature variation

In the last analysis variant, the aftercooler temperature varies from 40 °C to 60 °C with 100 % methanol. The following engine settings were kept constant: ignition timing at 20 °CA BTDC, engine speed at 1500 rpm, load at 375 kWe. In this aftercooler temperature variation, the λ and NO_x emissions also differed. In the performance analysis (chapter 4 lower NO_x emissions were visible at higher aftercooler temperatures and in this chapter, it will be investigated if it can be related to the in-cylinder parameters.

6.1. Pressure

In chapter 4 the average pressure signal of four cylinders has been analysed in depth. In the model, the pressure from only one cylinder has been used, namely cylinder four. First, is explained why this

cylinder has been chosen for the model. Following, the pressure analysis for the 3 analysis variants (methanol compared to NG, the ignition variation, and the aftercooler temperature variation) will be shown. Deviations and agreements with chapter 4 will be indicated.

6.1.1. The chosen cylinder

The choice of the used in-cylinder pressure signal for the model needs to be clarified. The in-cylinder model uses the average pressure data of 60 cycles from one cylinder. As shown in chapter 4 there were four cylinders measured and one out of these four needs to be chosen as input for the model. The data from cylinder 4 has been chosen to be used in the model analysis due to the lowest COV values for methanol. Cylinder 4 had the lowest COV values because of a new methanol injector just prior to the measurements. However, with this option, it is important to recall the results of cylinder 4 compared to the other measured cylinder 3, 5 and 6

- For methanol, at 75 % load, the average peak pressure of cylinder 4 was about 2 bar (4 %) higher than the average of the measured cylinder 3,4,5 and 6.
- For NG, at 75 % load, the average peak pressure was 4 bar (7 %) lower than the average of the 4 measured cylinders.

Although this contradiction in (peak) pressure between methanol and NG has been noticed, the best comparison between the two fuels is made by using the same cylinder pressure sensor. This way any errors due to the in-cylinder pressure measurement will be similar and can be excluded in a relative comparison between NG and methanol. For NG, it could be argued to choose another cylinder, e.g. cylinder 3, because of the low (peak) pressures with cylinder 4. Though for methanol, cylinder 3 has excessive-high pressures up to 68 bar at 375 kWe compared to the mean average pressure of the four cylinders of 55-60 bar. Cylinder 5 and 6 had considerably more cylinder-to-cylinder variation with methanol as shown in the COV values in chapter 4 and are therefore also seen as a lesser option. Accordingly, the choice is made to use the data of cylinder 4 for all analyses with the models.

6.1.2. Methanol compared to NG

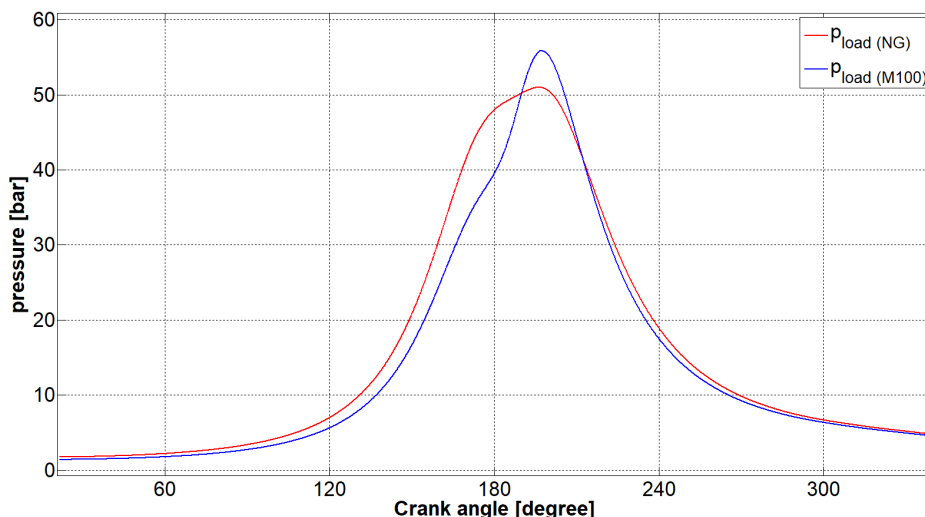


Figure 6.1: Pressure plot of cylinder 4 for NG and methanol at 375 kWe, both at an ignition timing of 20 °CA BTDC.

Figure 6.1 shows the in-cylinder pressure signals for both NG and methanol of cylinder 4. Methanol displays a higher maximum pressure compared to NG. Furthermore, it is visible that with methanol a steeper pressure increase is measured after TDC compared to NG. This indicates faster combustion after TDC and will be further investigated in section 6.3.

6.1.3. Ignition sweep

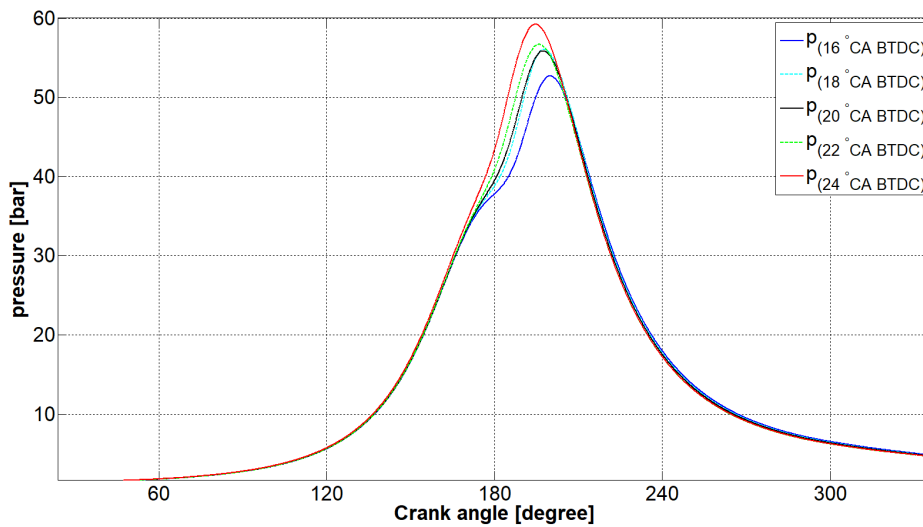


Figure 6.2: Pressure plot of cylinder 4 for methanol at 375 kW with changing ignition timings.

In figure 6.2 the pressure of cylinder 4 is visible with changing ignition timings. The maximum pressure increased and the position shifted closer to TDC, as ignition timing was advanced from 16 to 24 °CA BTDC. Furthermore, the figure indicates a higher rate of pressure rise with advanced ignition timing. This is compliant with the performance analysis where the average of four cylinders was taken, as shown in figure 4.7. In table 4.7 it was also visible that the effective engine efficiency increases with advanced ignition timing, with increasing maximum pressure closer to TDC.

6.1.4. Aftercooler temperature variation

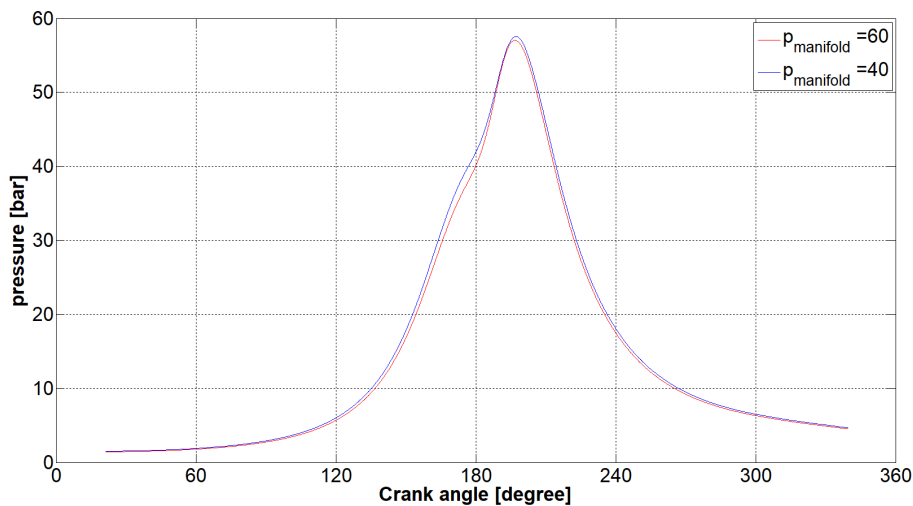


Figure 6.3: Pressure plot of cylinder 4 with varying manifold temperature at 375 kW, both at an ignition timing of 20 °CA BTDC.

Figure 6.3 shows the used pressure for the model of cylinder 4 of varying manifold temperature. It is almost similar to the pressure figure in the performance results, figure 4.12, only there the mean of the four measured cylinders is shown. Both figures show where the manifold temperature is higher, the pressure is increased at an earlier CA, starting from around 150 CA. However, around 200 CA the pressure lines cross each other resulting in a lower peak pressure with the manifold temperature of 60 °C. The small difference in peak pressure is here a little bit more compared to the mean of the four cylinders, but the position of the maximum pressure are in both figures at equal CA position.

6.1.5. Conclusion pressure

From the models and experiments, the following can be concluded regarding the pressure:

- Each measured cylinder had its drawbacks for selecting the best in-cylinder pressure signal, due to stability or pressure deviations from the mean pressure. Nevertheless, cylinder 4 is chosen to use in the models, because of the lowest COV values found with methanol.
- Methanol shows a steeper increase of pressure after TDC compared to NG, indicating faster combustion after TDC.
- The maximum pressure increased and the position shifted closer to TDC, as ignition timing was advanced from 16 to 24 °CA BTDC, leading to engine efficiency improvements as shown in table 4.7.
- In the aftercooler temperature variation, the pressure differences are small. However, around 20 °CA ATDC the pressure lines cross each other, resulting in a lower peak pressure with the manifold temperature of 60 °C.

6.2. Power

In this section, the closed cycle indicated power from the model is shown. Starting with the calculations for indicated power and the translation to brake power. Then, the influence of TDC shift on indicated power is discussed. Furthermore, the closed cycle power output from the model is presented for the three analyse variants.

6.2.1. TDC shift

To show the influence of a TDC shift in the model, first, the formulas that influence the indicated power will be shown. Starting from the measured generator power (P_{gen}), the brake power (P_b) is calculated with equation 4.7:

$$P_b = \frac{P_{gen}}{\eta_{generator}} \quad (4.7 \text{ revisited})$$

Where the $\eta_{generator}$ is 95,5 % at 375kW. The indicated power (P_i) and the brake power (P_b) are related with the mechanical efficiency ($\eta_{mechanical}$) according to the formula 6.1 [18, p200]:

$$\eta_{mechanical} = \frac{P_b}{P_i} = \frac{W_e}{W_i} \quad (6.1)$$

The indicated power of an engine can be found with formula 6.2 [18]:

$$P_i = W_i \cdot \frac{n_e \cdot i}{k} = \int_{cycle} p \cdot dV \cdot \frac{n_e \cdot i}{k} \quad (6.2)$$

Where i is the number of cylinders, n_e is the engine speed and constant $k=2$ for a 4-stroke engine. The pressure signal is the input and the volume is determined with formula 5.1 in the model, and thus dependent on the crank angle. Note that the model calculates the indicated work only for one cylinder and the brake power from measurements is for all 8 cylinders of the engine. Also must be noted that the model does not calculate the indicated power for the full cycle, but only for the closed combustion cycle. The full 4-stroke cylinder cycle exists of two parts, a pumping cycle and a combustion cycle. Therefore, the indicated power exist of indicated power of the combustion cycle ($P_{i_{cc}}$) and indicated power of the pumping cycle ($P_{i_{pc}}$), shown in equation 6.3:

$$P_i = P_{i_{cc}} + P_{i_{pc}} \quad (6.3)$$

To get an accurate indicated power calculated in the model, the pressure signal can be shifted to a different CA. However, the model is sensitive to shifting the pressure signal at a different °CA due to changing calculations of volume per CA as shown in formula 6.2. A 2 °CA shift changes the indicated power output with 5 kW (+/- 10 %) per cylinder. Ding stated that the TDC shift is limited to a small range up to a maximum of 1 °CA [8]. In figure 6.4, the pressure signal is shown for three shifts, 0 shift, -0.9 and -2.0, for methanol at 375 kWe and 20 °CA BTDC ignition timing.

To determine the needed TDC shift to get an accurate indicated power, two assumptions are made:

- First, it is assumed that the mechanical efficiency is constant, at 91 %, which is stated as a nominal value for a diesel engine [18]. Thus, assumed is that for NG and methanol the mechanical efficiency remains the same and does not change depending on the fuel.
- Secondly, it is assumed that the engine power is equally divided over 8 cylinders [18]

With these assumptions and the known generator power, the indicated power per cylinder can be determined, with above formulas. The brake power is around $(375/8/0.955)=49.08$ kW per cylinder. With the mechanical efficiency of 91 %, then the indicated power is calculated with formula 6.1. The indicated power for 1 cylinder at $49.08 \text{ kW}/0.91=53.94$ kW.

As explained in section 6.1 the choice is made to use the pressure signal of cylinder 4, for the model. Therefore, only for cylinder 4, the indicated power will be given here. With a TDC shift of -0.9 , the model calculated an indicated power for methanol with the model of $P_{i_{cc}} = 52.41$ kW (at 24 °CA BTDC) and $P_{i_{cc}} = 53.96$ kW (at 16 °CA BTDC) for cylinder 4. The model computes the indicated power over the combustion cycle, and not the full (4-stroke) cylinder cycle, as shown in 6.3. Therefore, the indicated power is actual to low and requires a higher TDC shift than the -0.9 °CA. At a TDC shift of 0, and an ignition timing of 16 °CA BTDC the models indicated power ($P_{i_{cc}}$) is 56.1 kW compared to $P_i = 50.6$ kW for the full cycle, calculated directly from the Kibox data.

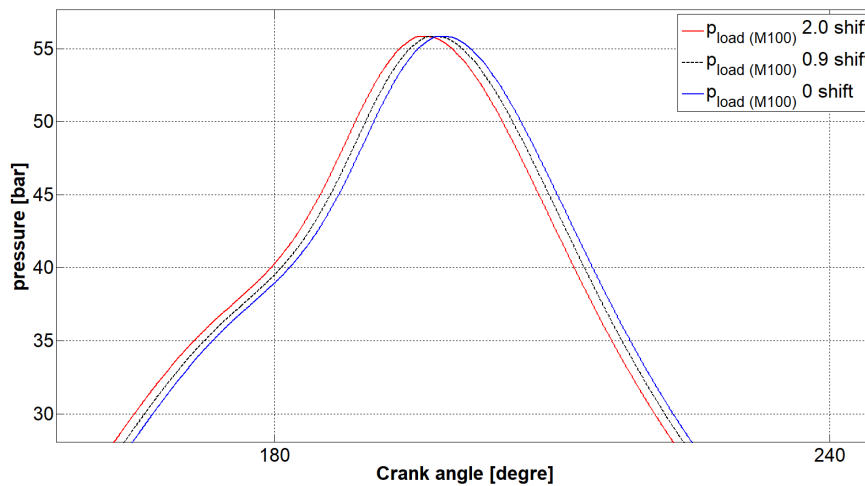


Figure 6.4: Pressure signal of methanol with three TDC shifts.

Shifting the signal more from -0.9 °CA shift towards 0 shift, as shown in figure 6.4, gives higher indicated powers, thus better representation of the indicated power. Although, this also has an influence on other parameters. One of those parameters is the input of the Woschni temperatures. The Woschni temperatures are varied to make sure that the RCO goes through zero at the start of combustion (SOC). After adjustment of SOC, for 0 °CA shift, the cylinder wall temperature is 215 K (-58 °C). Which is not representative of actual physical values. At least 80 °C from the cooling water is expected as wall temperature.

The Woschni temperatures are better represented at -2.0 °CA shift, e.g. the cylinder wall temperature is 465 K (192 °C), after fine-tuning the SOC. The downside of this shift is that the indicated power drops to $P_{i_{cc}} = 50.51$ kW (at 20 °CA BTDC ignition). This would come close to a mechanical efficiency of 100 %, thus no friction, which is also not physically possible. The decision is made to shift the pressure signal at -0.9 °CA, where thus the solution lies between two extremes, both the best representation of indicated power and the Woschni temperatures. With this shift, the best of both is chosen to model as close as possible to actual physical values. With NG the indicated power calculations are lower compared to methanol, but the shift is not executed differently with the NG model. The pressure sensor, the signal and Kibox TDC shift has not altered during measurements. Therefore, a TDC-shift should be done the same for all models. Shifting TDC has an influence on HRR shapes, combustion duration, etc. and will influence further analysis. The absolute values of combustion duration are seen as less important in this study than the comparison between the combustion duration at different settings of fuel, ignition timing and aftercooler temperature. Therefore, it is decided to keep the TDC shift constant

for all analysis at $-0.9\text{ }^{\circ}\text{CA}$, for both the methanol as the NG model.

6.2.2. Methanol compared to NG

Continuing the power analyses, now the in-cylinder indicated power will be analysed for NG compared to methanol. P_{icc} at this comparison is computed at 52.26 kW for methanol and for NG 48.61 kW. The indicated power for NG is 7 % lower than for methanol, based on cylinder 4. To verify, the pressure data of NG is compared to three other NG 375 kWe pressure data sets from the same measurement. Finding all indicated power calculation between 48.0 and 49.0 kW. The lower indicated power is assumed to be due to variation in pressure cylinder-to-cylinder variations as discussed in chapter 4.

Indicated power vs crank angle is shown for methanol and NG in figure 6.5. It is visible that maximum in-cylinder power is observed at an earlier CA. Furthermore, the negative power is smaller for methanol compared to NG. Negative power is computed with the in-cylinder pressure in the compression part of the graph until TDC. Higher pressures for NG compared to methanol at this part are shown in figure 6.1. Therefore, methanol has less total negative power calculated compared to NG.

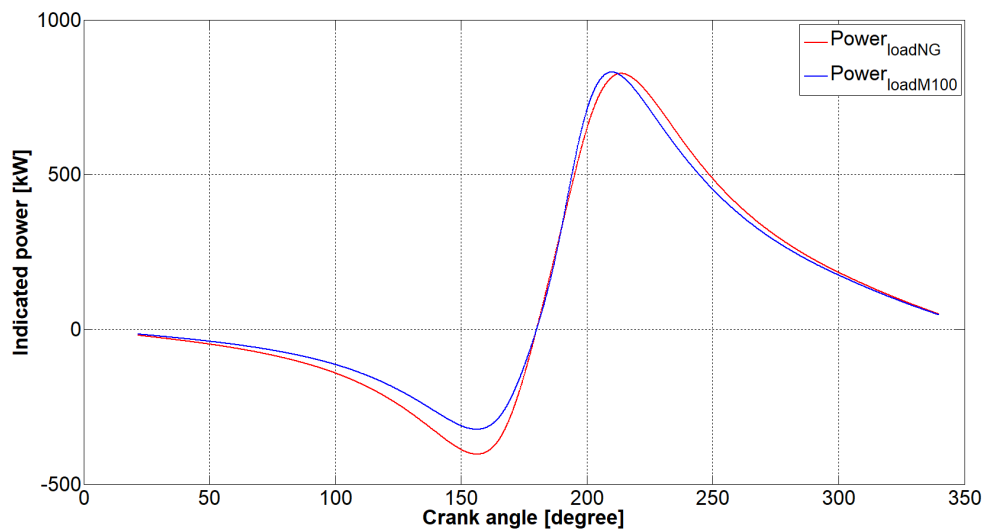


Figure 6.5: Indicated power plot of cylinder 4 for NG compared to methanol at 375 kWe.

6.2.3. Ignition variation

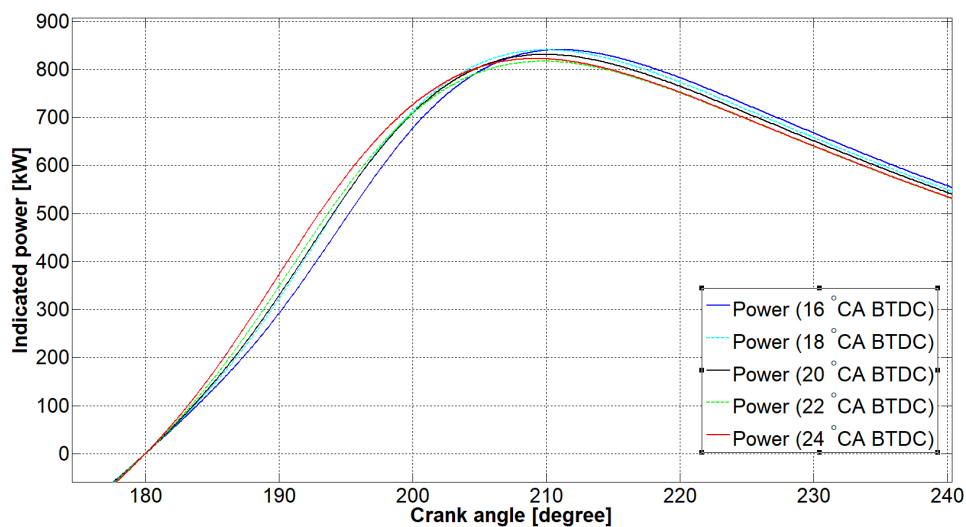


Figure 6.6: Indicated power of cylinder 4 with changing ignition timings at 375 kWe.

In figure 6.6 the indicated power is shown with changing ignition timing. With advanced ignition timings the maximum power is reached at earlier CA. The calculated combustion cycle indicated power, $P_{i_{cc}}$, varied between 52.41 kW (at 24 °CA BTDC), 53.26 kW (at 20 °CA BTDC) and 53.96 kW (at 16 °CA BTDC) at changing ignition timings with 375 kWe power. For clarity, the TDC shift was kept constant for all ignition timings. This could be an indication that the indicated power for the pumping loop ($P_{i_{pc}}$) changes with changing ignition timing. Because the model does not calculate the indicated power with the full cycle, but only the combustion cycle. The full cycle indicated power (P_i), is compared for 16 and 24 °CA BTDC, both being 50.6 kW, calculated from the Kibox values (at 0 TDC shift).

6.2.4. Aftercooler temperature variation

The indicated power calculated by the model, $P_{i_{cc}}$, is 53.4 kW for the manifold temperature of 40 °C and 53.9 kW for the manifold temperature of 60 °C. P_i were closer to each other with 50.57 kW for the manifold temperature of 40 °C and 50.66 kW for the manifold temperature of 60 °C. This is compliant with expectations because both measurements were done at 375 kWe output, and therefore the total indicated power is expected to be the same.

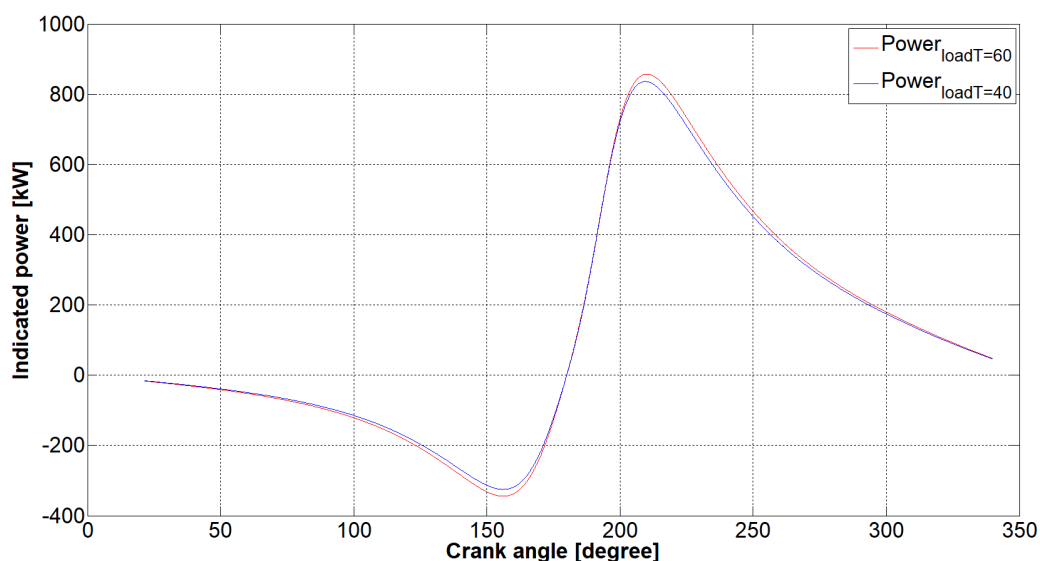


Figure 6.7: Indicated power plot of cylinder 4 with varying manifold temperature.

In figure 6.7 the in-cylinder indicated power is shown for varying aftercooler temperature. More negative power at higher manifold temperatures is shown. The higher amount of negative power is expected to be from more in-cylinder mass for higher manifold temperatures. However, these negative powers are compensated with higher maximum powers during combustion, after TDC.

6.2.5. Conclusion Power

From the models and experiments, the following can be concluded regarding the indicated power:

- The indicated power is best represented at higher TDC shift. Woschni temperatures were best represented with lower TDC shift. To be closest to actual physical values, of both indicated power and Woschni temperatures, a TDC shift of -0.9 °CA is chosen.
- The model computes a higher indicated power with methanol for cylinder four compared to NG. Cylinder 4 had with methanol higher pressures compared to the mean pressure of the four measured cylinders, influencing the indicated power calculations.
- The calculation of indicated power from the model is calculated with the combustion cycle and not the full cycle, resulting in deviations in indicated power. This was specifically visible with the ignition sweep, where the indicated power was decreasing with advanced ignition timing.

6.3. Heat release

The heat release rate graphs and fuel mass burn fraction (RCO) graphs will be shown for the NG compared to methanol, the ignition variation and the aftercooler temperature variation. For the comparison between methanol and NG, and for the ignition variation, also the combustion duration will be analysed. Furthermore, the start of combustion and end of combustion will be analysed for the ignition sweep.

In the calculation of the model, the end of RCO is assumed at 98 %. This means that at the end of the in-cylinder cycle 98 % of the fuel is burned. Similarly, it is stated that the fuel starts to burn at the ignition timing. However, the combustion rate for methanol compared to NG is shown in this section.

The literature study reveals in figure 2.14 how the heat release typically looks. The heat release curve typically can be divided in four phases: ignition delay, premixed combustion, diffusive combustion and late combustion. Before going to the actual analyse one more heat release figure will be shown from Heywood for diesel in figure 6.8, here is the part of fuel vaporization visible as a negative dip just before ignition [15, p.511]. This negative dip is also expected for methanol because methanol has almost 4 times the heat of vaporization compared to diesel as shown in figure 2.3. Note that the shown crevices losses in the figure are not calculated in this model.

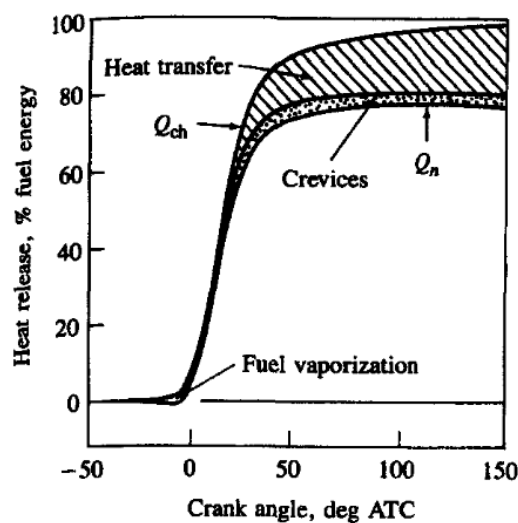


Figure 6.8: Heat-release during combustion for DI diesel [15].

6.3.1. Methanol compared to NG

In figure 6.9 the heat release of methanol and NG is shown at 375 kWe, 500 mg/nm³ NO_x, ignition at 20 °CA BTDC and 1500 rpm. It is visible that maximum heat release takes place earlier after top dead centre for methanol compared to NG. Indicating faster combustion for methanol.

In the performance analyse, the Kibox results show faster combustion for methanol with equal conditions as presented in table 4.6. In figure 6.9 this also looks to be the result due to an earlier maximum of heat release. Meaning considerably more fuel is burned in the premixed combustion phase with methanol compared to NG. And compared to typical diesel hr curves, shown in 2.14, methanol combustion does not show any diffusive combustion, only premixed combustion and late combustion.

The fuel mass burn fraction (RCO) is displayed in figure 6.10. From this figure, it becomes more clear that 10 % and 50 % of the fuel is burnt much faster with methanol compared to NG. However, 90 % fuel is burnt at almost equal CA. In the RCO is also the -5 % fuel measurement for NG shown, as discussed in section 6.0.1. The -5 % fuel measurement is almost equal at CA10 and CA50 compared to NG 20 °CA BTDC, but the CA90 is at 5.0 °CA earlier. To calculate the combustion duration the crank angle where 90 % fuel is burnt minus the crank angle where 10 % fuel is burnt (CA90 - CA10) is taken, and also the CA50 point is found and shown in table 6.1. It is found that CA10 and CA50 are much faster with methanol compared to NG. It also shows that the combustion duration (CA90-CA10) is 61.5 °CA, and therefore 7.2 °CA shorter for methanol compared to NG.

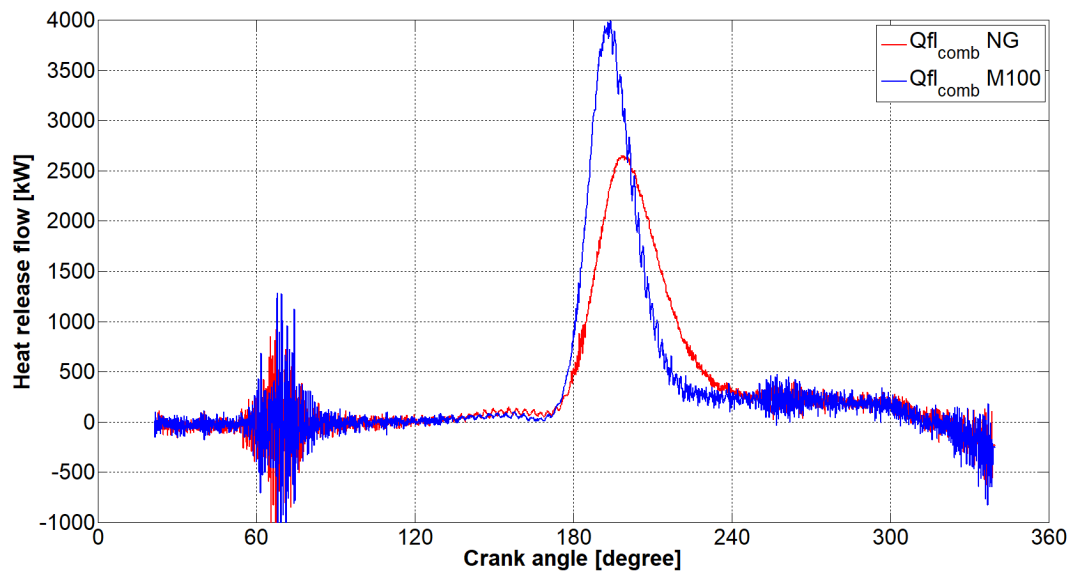


Figure 6.9: HRR plot of cylinder 4 with NG and Methanol at 375 kW both at an ignition timing of 20 °CA BTDC.

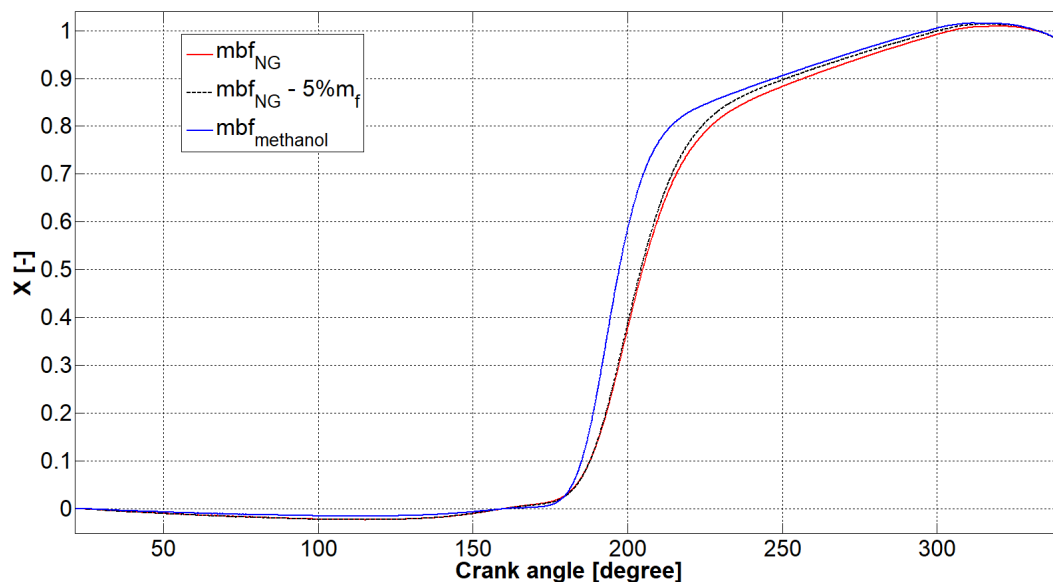


Figure 6.10: RCO plot of cylinder 4 with NG and methanol at 375 kW both at an ignition timing of 20 °CA BTDC

Table 6.1: CA10 CA50 and CA90 values of the cylinder 4 from the RCO for NG compared to methanol

	NG 20 °CA BTDC - 5%	NG 20 °CA BTDC	methanol 20 °CA BTDC
CA10	187.8°	187.8°	185.1 °
CA50	204.3°	204.8°	197.2°
CA90	251.4°	256.5°	246.6°
CA90-CA10	63.6°	68.7°	61.5 °

The combustion duration from the Kibox data, in table 4.6, compared to the combustion duration from the model, in table 6.1, is almost twice as long. This indicates a different calculation method with the Kibox. From the Kibox settings could be found that the Kibox uses a resolution of 1 °CA and a maximum window of 120 °, which both should not make such a big difference possible. The Kibox does not take any heat loss into account, which makes the biggest difference in the combustion

duration calculations. To show this a comparison is made in table 6.2, where the combustion duration is computed in the model from the NAHRR, instead of the RCO, and compared to the combustion duration of the kibox. It clearly shows that the calculated CA90 and CA10 are more close to the kibox data, determined with the NAHRR. However, the heat loss should be included, therefore, the combustion duration from the model will be determined with the CA10 and CA90 of the RCO.

Combustion duration is dependent on the input of fuel consumption, heat loss coefficients etc. For the NG it must be noted that it is an assumption from other experiments, and also dependent on the density (ρ) that is used. In table 6.1 the 5 % lower fuel consumption the NG combustion duration is already almost equal of duration compared to the combustion duration with methanol. However, the earlier CA50 and CA10 for methanol compared to NG stay visible. Most variation is in CA90 for NG with changing the fuel consumption of NG.

Table 6.2: Combustion duration (CA90-CA10) from NAHRR with methanol compared to the Kibox calculations

	Kibox methanol 20 °CA BTDC	NAHRR methanol 20 °CA BTDC
CA10	5.57°	3.6°
CA90	41.8°	38.7°
CA90-CA10	36.2°	35.1°

Both the performance analyses (Kibox data) and the model show faster combustion for methanol compared to NG. The faster combustion of methanol is not what was expected from the literature. With lean mixtures as shown in figure 2.9 methanol has a lower laminar flame speed than methane (NG main component), thus slower combustion was expected. Within this laminar flame speed comparison the in-cylinder effects, such as higher temperature, pressure and turbulence, were not taken into account and could make the difference seen in this experiment.

According to Merker the most fuel consumption optimal operating point of CA50 is at 8 °CA ATDC [26], which was further explained in section 4.5. In table 6.1 it shows this has been reached closer with methanol compared to NG at an ignition timing of 20 °CA BTDC, where for methanol a CA50 of $197.2 - 180 = 17.2$ °CA ATDC is calculated. This is indicating a better fuel consumption optimal operating point for methanol, thus higher efficiency with methanol at this operating point.

In section 4.2 it was argued that one of the three possible reasons for the lower stability with methanol compared to NG could be due to lower combustion rates. This is not shown in these first comparison results. Combustion rates are almost equal or even higher for methanol compared to NG.

6.3.2. Ignition variation

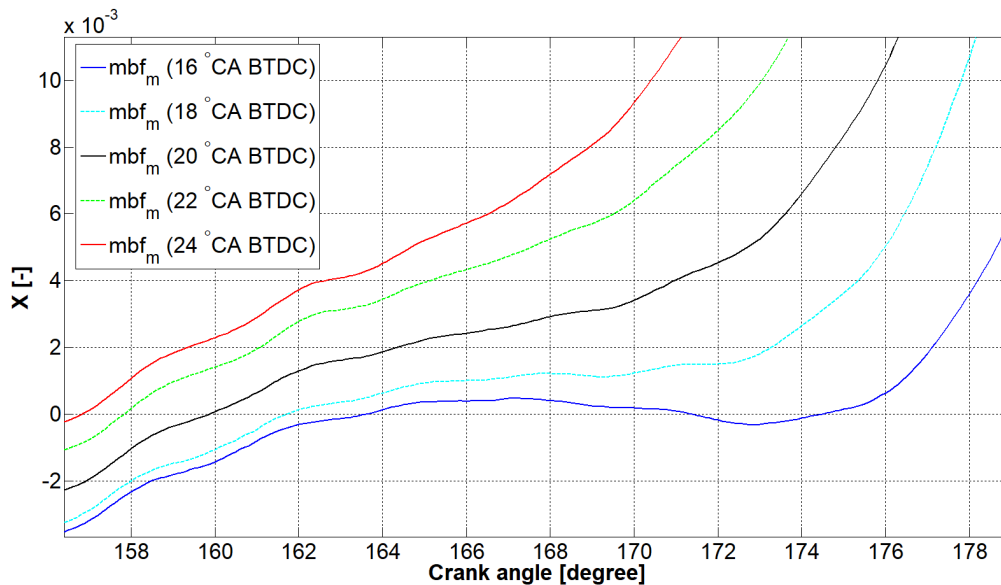


Figure 6.11: The fuel mass burn fraction (RCO) with changing ignition timing, with a closer look at the start of ignition

The heat release analysis with varying ignition timing will start with having a closer look at the start of combustion (SOC). SOC is at all points where the RCO=0 and made equal to ignition timing. This is visible in figure 6.11. Only with retarded ignition timings of 16 °CA BTDC, it shows a dip through zero after ignition, expected to be from the fuel vaporization as shown in figure 6.8. A fuel vaporization dip as shown with diesel just before SOC is not seen in all the heat release figures with methanol. This dip was expected due to the four times high heat of vaporization with methanol. The lack of fuel vaporization dip could be due to one or a combination of the following reasons:

- The lower boiling point of 65 °C with methanol compared to 180-360 °C with diesel as shown in figure 2.3. Lower boiling point could indicate that the methanol is evaporated earlier in the process than with diesel.
- A fast and high premixed combustion period. Methanol compared to NG and diesel, is dominating in the premixed combustion phase. This is shown in the first 10 % of burnt fuel (CA10) value. For methanol, a CA10 is calculated at 185.1 °CA with a spark timing of 20 °CA BTDC. Meaning 10 % of fuel is burnt in 25.1 °CA after the spark, compared to a 27.8 °CA for NG.
- PFI gives more time for evaporation of the methanol compared to DI. With PFI methanol can vaporize already just after the moment of IVC, while with diesel DI less time is available for vaporization of diesel. For a typical Diesel DI, the injection of fuel is in the order of 5 °CAs earlier before ignition starts [p.506] [15]. For methanol with PFI, shown in these experiments, it had around 160 °CAs before ignition.

Wei also shows hr curves with PFI methanol blending with DI injected diesel [44]. In these experiments methanol/diesel ratios were used up to 1.54 (mass flow methanol/mass flow diesel). When more methanol is added with diesel in his experiments, smaller evaporation dips are shown in the hr-curves, and no dip is visible anymore with the 1.54 ratio. Furthermore, in formula 5.40 it is stated that the energy of fuel is calculated with the mass of fuel burned. Although this gives a decent energy calculation for vaporizing and heating the fuel. For methanol it does not seem to be a good representation over time in the evaporation of the fuel.

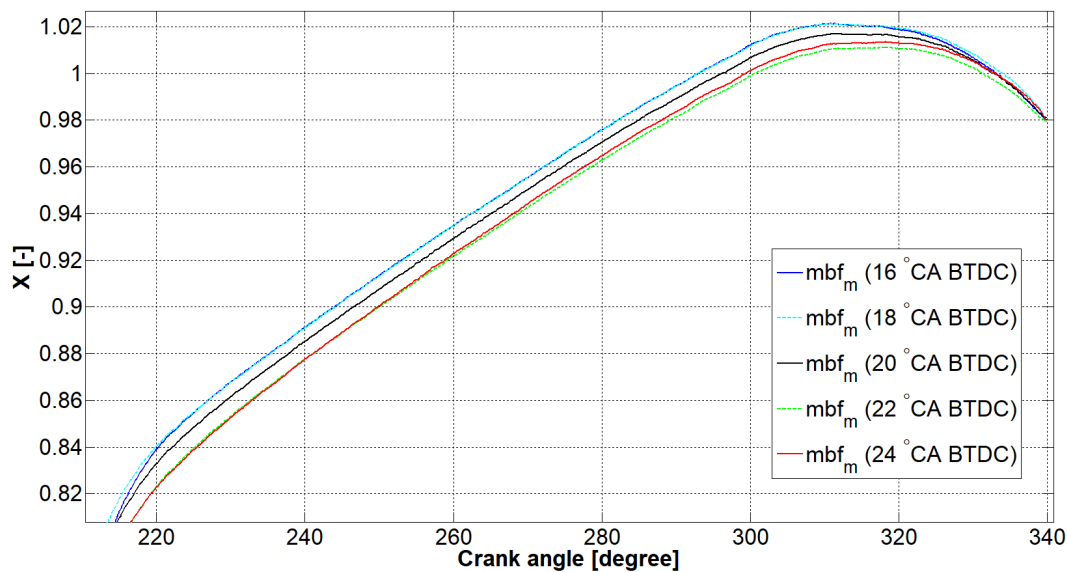


Figure 6.12: The fuel mass burn fraction (RCO) for changing ignition timing, with a closer look at EOC

The end of RCO is set to 98 % for all ignition timings, and this is made visible in figure 6.12. The combustion rate is interesting when looking at figure 6.13 and changes with changing ignition timings. Due to changing combustion rates, the combustion duration, CA10, CA50 and CA90 will change with varying ignition timing. First of all, the RCO is determined with formula 5.29, which results in a maximum RCO of 1.02 around 310 °CA. This results in an overshoot before decreasing back to the end value of 98 %. Due to the decreasing temperature and decreasing heat loss in formula 5.28 in the last 30 °CAs before EVO (=340.1 °CA), the RCO decreases after it's maximum. Pressure also decrease but

the $p \cdot dv/dt$ part will go near to zero but will not go negative in the NAHRR calculations. The engine has a relative late moment of EVO, therefore, this overshoot in RCO is visible for this engine. Similar overshoot was visible with the research with NG and hydrogen on this engine [30]. This overshoot is not visible in an engine with an earlier moment of EVO, e.g. the MAN 4 L20/27 diesel engine used with an EVO at 300 °CA from the research of Ding [8] does not show overshoot in RCO.

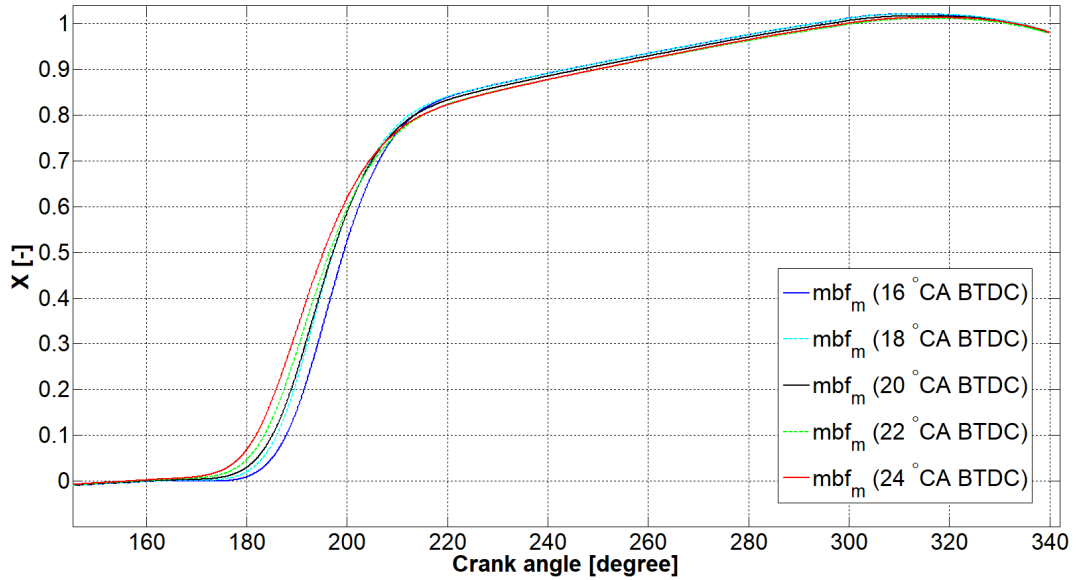


Figure 6.13: The fuel mass burn fraction (RCO) for changing ignition timings

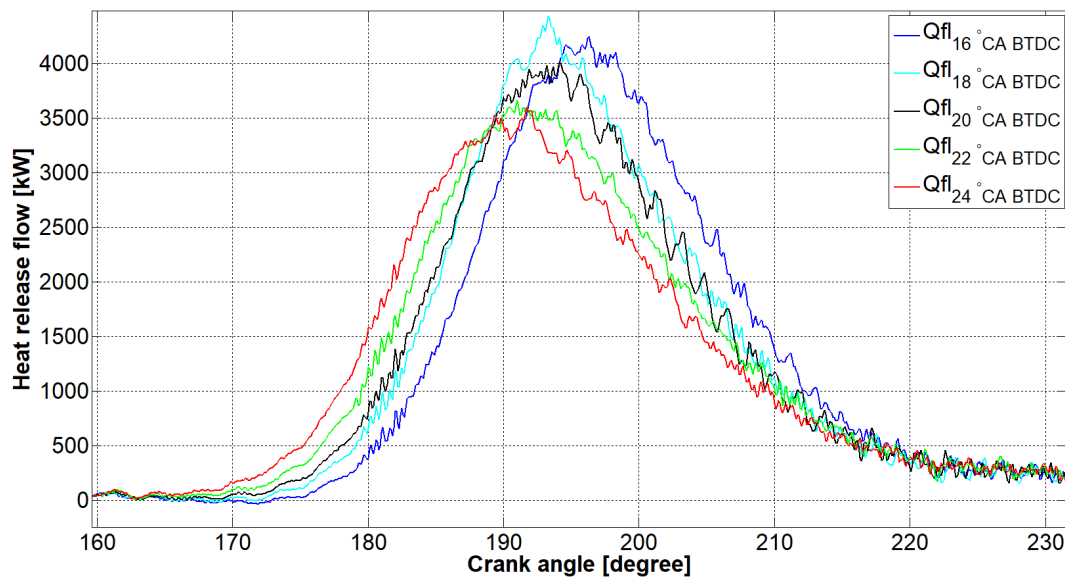


Figure 6.14: The heat release flow for changing ignition timing

From figure 6.12 and 6.14 can be seen that with retarded ignition timing e.g. an ignition timing of 16 °CA BTDC, the end of combustion (CA90) is also retarded. The peak heat release also looks to increase with retarded ignition, but this can not be fully confirmed due to the peak with the ignition timing of 18 °CA BTDC line compared to the peak of the ignition timing of 16 °CA BTDC.

To have a better understanding of the combustion performance with changing ignition timing the CA10, CA50, CA90 and combustion duration (CA90 - CA10) is calculated for varying ignition timings and shown in table 6.3.

Table 6.3: CA10, CA50 and CA90 values of the cylinder 4 from the model with varying ignition timings

	16 BTDC	°CA	18 BTDC	°CA	20 BTDC	°CA	22 BTDC	°CA	24 BTDC	°CA
CA10	187.8°		185.9°		185.1°		183.5°		181.8°	
CA50	199.3°		197.2°		197.2°		196.5°		195.2°	
CA90	244.0°		244.0°		246.6°		250.0°		249.7°	
CA90-CA10	56.2°		58.1°		61.5°		66.5°		67.9°	

Table 6.3 shows that with advanced ignition timing, the combustion duration increases. This same trend was visible with the Kibox values shown in table 4.6. However, the Kibox values have computed a shorter combustion duration, as discussed in section 6.3.1, because it does not take heat losses into account.

According to Merker the most consumption optimal operating point of CA50 is at 8 °CA ATDC [26]. In table 6.3 it is shown that this point was not reached but closest to it was the ignition timing of 24 °CA BTDC, with a CA50 of 15.2 °CA ATDC. The results of the best consumption optimal operating point match with what is found in section 4.5, where the highest engines brake efficiency is also calculated at an advanced ignition timing of 24 °CA BTDC. Further investigation of efficiencies found in the model is done in appendix B.3.

6.3.3. Aftercooler temperature variation

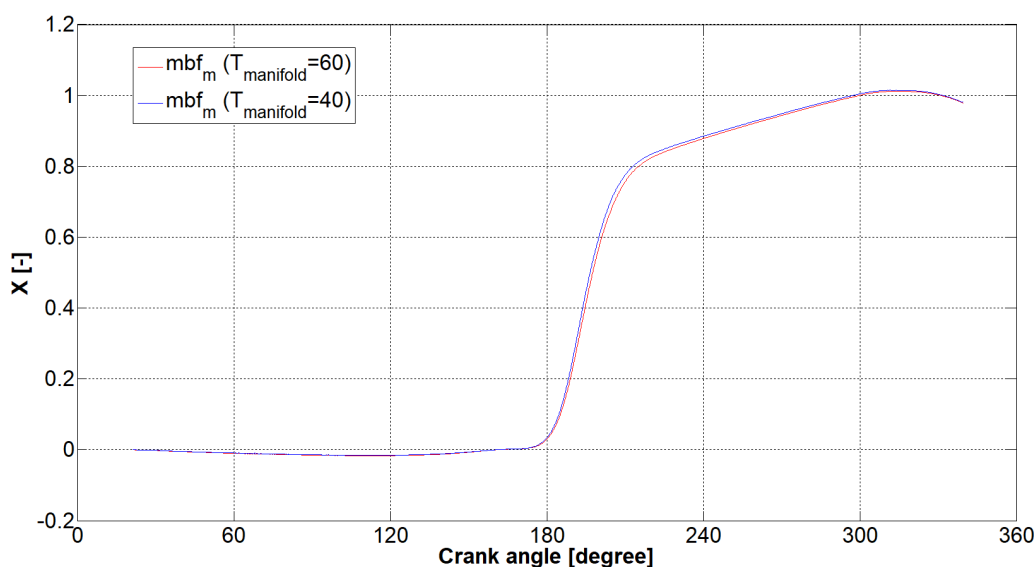


Figure 6.15: The fuel mass burn fraction (RCO) for varying aftercooler temperatures

In figure 6.15 the fuel burnt is shown for varying aftercooler temperatures at equal power and fuel consumption. The SOC is set at 20 °CA BTDC, equal to the ignition timing, for both manifold temperatures. At the end, 98 % of fuel is burnt for both manifold temperatures. Furthermore, both lines are near each other, meaning no significant changes in combustion duration and combustion rate.

6.3.4. Conclusion heat release

From the models and experiments, the following can be concluded regarding the heat release:

- Methanol shows 7.6 °CAs earlier CA50 and 2.7 °CAs earlier CA10 compared to NG. Indicating faster (premixed) combustion. However, due to late CA90, the combustion duration is almost equal with only 1.6 °CA shorter combustion duration for methanol at the lower mass of fuel used for NG. At the higher fuel flow for NG, the combustion duration is 7.2 shorter for methanol.

- With changing ignition variation combustion duration changed. Advanced ignition timing of 24 °CA BTDC showed a combustion duration increases of 11.7 °CA compared to an ignition timing of 16 °CA BTDC.
- With changing ignition variation the fuel consumption optimal operating point was found at an ignition timing of 24 °CA BTDC.
- With changing temperature after the cooler there were no significant changes calculated in the CA10, CA50, CA90 and the combustion duration.

6.4. Temperature

The in-cylinder temperature will be analysed for the NG compared to methanol, the ignition variation and the temperature variation. The in-cylinder temperature is calculated with formula 5.3 as described in chapter 5.

6.4.1. Methanol compared to NG

In this analysis, the in-cylinder temperature for methanol will be compared to NG. In figure 6.16 the in-cylinder temperature variation of cylinder 4 is given at 375 kWe, 500 mg/nm³ NO_x, ignition at 20 °CA BTDC and 1500 rpm is shown for methanol and NG. The model with 5 % less fuel for NG was very similar to the NG model in the temperature graph and is therefore not shown in the figure.

It is visible that the maximum temperatures are almost equal and figured to be both above 1400K, with methanol 30 K higher. But the maximum temperature is reached at an advanced CA with methanol compared to NG. Furthermore, it shows with methanol a steeper, increase and decrease, to the maximum temperature, indicating a shorter period in the maximum temperature compared to NG. The λ for NG was higher with 1.62 compared to 1.56 for methanol. NO_x emissions are strongly dependent on (maximum) in-cylinder temperatures, as shown in figure 4.11. But also depends on the duration at this maximum temperature and the air-excess-ratios (λ). That the maximum in-cylinder temperatures for methanol compared to NG are close to each other is expected, due to the fact the engine was controlled at an equal NO_x emission level of 500 mg/nm³ NO_x.

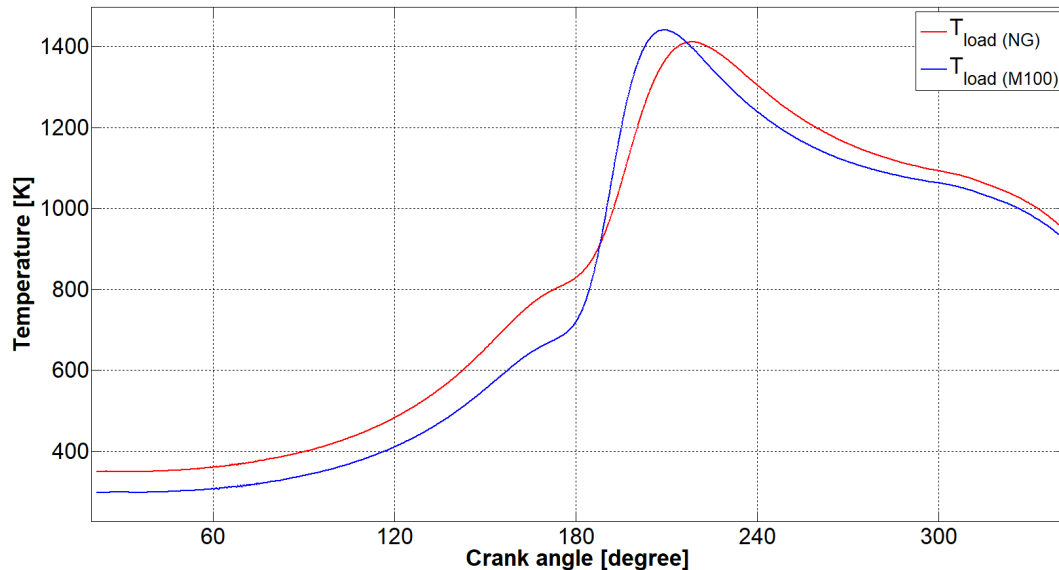


Figure 6.16: Temperature plot of cylinder 4 with NG vs M100 at 375 kWe

In figure 6.16 is visible that the in-cylinder temperatures for methanol are lower from the beginning at IVC. The lower temperature is due to the lower fuel temperature and the high heat of vaporization of methanol. The measured temperature before the inlet, equal to T_{ind} , was around 50 °C lower for methanol compared to NG. The model calculates temperature (T_1) with formula 5.15, strongly dependent on T_{ind} . At 0 CA, the temperature plot starts at T_1 . Thus, the measured temperature difference is visible at the beginning of the figure. However, due to the steep increase around TDC (180 °CA)

the temperature of methanol will become higher just after TDC, and the maximum temperature is at an earlier CA than NG. From formula 5.3 it is known that the temperature is computed with the in-cylinder pressure. The steep increase of temperature must therefore also be visible as a steep increase in pressure, as was shown in section 6.1. This faster increase of temperature for methanol compared to NG is an indication of combustion taking place faster than with NG under equal conditions. The steeper temperature rise, which is a function for the measured pressure, has an effect on the combustion duration and the heat release, which are shown in section 6.3.

The shape after the maximum temperature looks similar only shifted. Due to the earlier reached CA where methanol reached the maximum temperature, the temperature will decrease in advance compared to NG. Therefore, methanol will have a lower maximum temperature at the moment of EVO compared to NG. Heywood reports that lower (in-cylinder) exhaust temperatures have an effect to reduce the in-cylinder heat losses and efficiency will, therefore, increase [15]. However, the in-cylinder exhaust gas is used by the turbocharger. This difference in exhaust temperatures will also affect the turbocharger, therefore, the effect on the overall engine efficiency is hard to determine only from the in-cylinder temperature differences.

It must be noted that the model is sensitive to the temperature, due to the calculation it makes with the ideal gas law from the input pressure. The trapped temperature (T_1) is an important input parameter to show the best representation of the temperature plot. For methanol, the measured fluctuation in temperature before the inlet was in the order of 0.5 °C. For NG, the measurement of the temperature at the inlet fluctuated +/- 10 °C. A 10 °C higher T_1 will affect the maximum calculated in-cylinder temperature with an approximate 40 °C. But the CA where maximum temperature is achieved will not change with changing the initial temperature T_1 .

6.4.2. Ignition variation

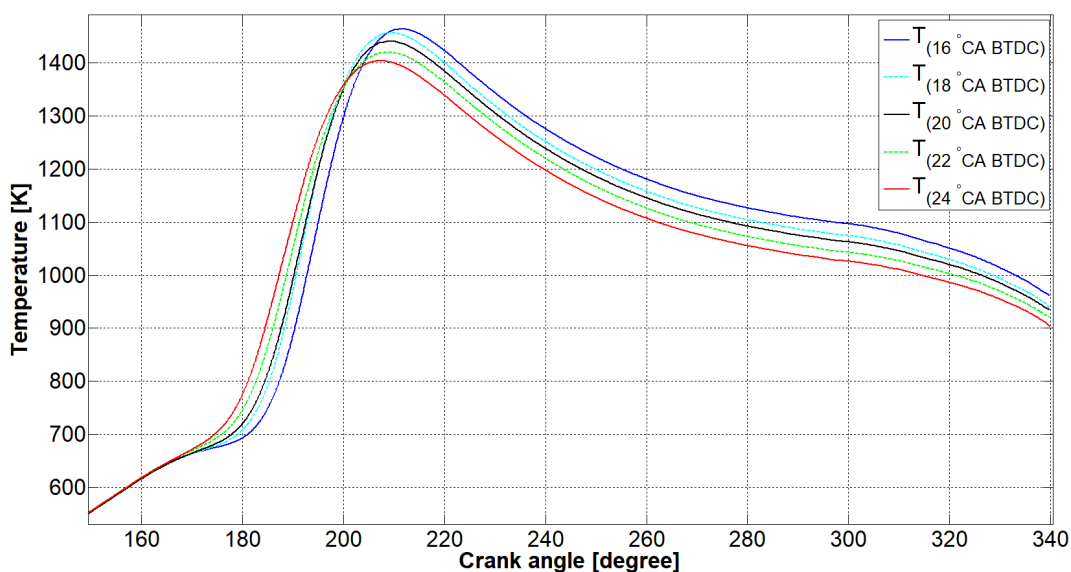


Figure 6.17: Temperature plot of cylinder 4 with changing ignition timings at 375 kWe

In figure 6.17 the in-cylinder temperature is shown with changing ignition timings at 375 kWe (75 % load). With retarded ignition timing the maximum temperature is at a later CA. This is also expected due to a later CA where the maximum pressure is measured as shown in figure 6.2, and as earlier mentioned the computed temperature is a function of the measured pressure and calculated volume.

Advanced ignition timings (22 and 24 °CA BTDC) show lower maximum temperatures than retarded ignition timings. The calculated higher temperatures are not due to a higher pressure, because at 24 °CA BTDC the highest pressure is measured. The higher temperatures at retarded ignition timings are due to a bigger volume at the CA of maximum pressure. The volume of maximum pressure with 16 °CA BTDC is 13.5 % bigger than the volume at the moment of maximum pressure with 24 °CA BTDC.

The (in-cylinder) exhaust temperatures are taken at the end of the in-cylinder temperature calcu-

lations. At an ignition timing of 24 °CA BTDC an (in-cylinder) exhaust temperatures of 902 °C has been computed. At an ignition timing of 16 °CA BTDC an (in-cylinder) exhaust temperatures of 960 °C has been calculated. Thus, with retarded ignition timing, higher (in-cylinder) exhaust temperatures are determined, at constant NO_x emission settings.

With advanced ignition timings, it is visible that the temperature increases at an earlier CA resulting in decreasing at an earlier CA. At the end of the in-cylinder process, when the exhaust valves opens, this results in a lower (in-cylinder) exhaust temperature. Lower exhaust temperatures could indicate an increase in efficiency, due to lower heat loss [15]. In table 4.5 the best efficiency is calculated at an advanced ignition timing of 24 °CA BTDC, which corresponds with the lowest (in-cylinder) exhaust temperature.

6.4.3. Aftercooler temperature variation

In the third analyse variant the temperature after the cooler is changed between 40 °C to 60 °C. The methanol flow and power was kept constant at 200 kg/hr and 375 kWe. With the increase of the temperature after the cooler by 20°C the temperature at the inlet valve is only increased from 13.5 °C to 16.0°C, due to the vaporization of methanol. The model calculated the in-cylinder temperature for both variants, and is shown in figure 6.18 from ignition (160 °CA) until just after the maximum temperature has been reached.

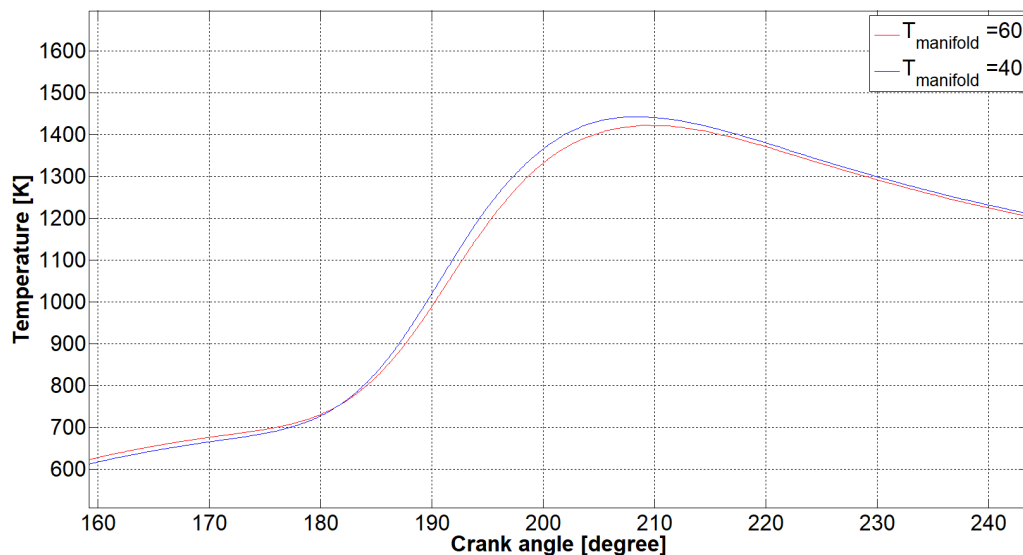


Figure 6.18: Temperature plot of cylinder 4 with changing temperature manifold at 375 kWe

A maximum temperature of 1169 °C has been figured for the $T_{manifold} = 40$ °C. For the $T_{manifold} = 60$ °C a maximum temperature of 1148 °C has been calculated. Interesting to see is that an initially higher inlet temperature will lead to lower maximum in-cylinder temperatures. The lower maximum temperature at a higher manifold temperature matches with the lower NO_x emission, which is seen in the performance results, as shown in figure 4.11. The main reasons for the lower maximum temperature is the higher λ combined with more vaporization of methanol before the inlet. The higher manifold temperature ($T=60$ °C) had a higher λ of 1.70 compared to a λ of 1.66 for the lower manifold temperature ($T=40$ °C). The determined vapor factors at IVC are 37.7 % for the higher manifold temperature and 18 % for the lower manifold temperature.

The (in-cylinder) exhaust temperatures are taken at the end of the in-cylinder calculations. For $T_{manifold} = 40$ °C an (in-cylinder) exhaust temperatures of 928 °C has been computed. For the $T_{manifold} = 60$ °C an (in-cylinder) exhaust temperatures of 919 °C has been determined. These two calculated exhaust temperatures are close upon each other when compared to the ignition sweep or the where NG was compared with methanol.

6.4.4. Conclusion Temperature

From the models and experiments, the following can be concluded regarding the temperature:

- Almost equal maximum in-cylinder temperatures were reached just above 1400 K for NG and methanol, as expected due to fixed NOx emission settings with both measurements. Only with methanol maximum temperature was reached about 20 °CA earlier.
- Maximum temperatures at an earlier CA results in a lower (in-cylinder) exhaust temperature. Lower (in-cylinder) exhaust temperatures are shown for methanol compared to NG, and with the ignition variation at an advanced ignition timing of 24 °CA BTDC.
- A decrease of 21 °C in maximum in-cylinder temperatures calculated at an increase of manifold temperature from 40 to 60 °C, at equal power output and equal fuel consumption. Lower in-cylinder temperatures are expected to be the reason of lower measured NOx emissions. Increasing the manifold temperature further could give better in-cylinder performances until 100 % vapor is reached at the moment of IVC. However, increasing manifold temperature would also increase the thermal loads on the materials in the inlet port (e.g the inlet valve).

6.5. Validation of the models with Kibox HR & HRR

For validation of the NG and methanol models, the heat release and heat release rate from the Kibox are compared to the NAHR and NAHRR. First, the values of NAHR for the methanol model and the HR from the Kibox are compared, then the NAHR for the NG model is compared with the HR from the Kibox, and finally, for both models, the NAHRR is compared to the HRR of the Kibox.

6.5.1. Validation of the NAHR for the methanol model

In this section, the calculated NAHR of the methanol will be compared with the NAHR calculated in the Kibox. This way the model will be validated. The Kibox computes the heat release between 30 °CA BTDC and 90 °CA ATDC. The Kibox determines the heat release with a 1th law of thermodynamics algorithm and is not including any heat losses. This way it is comparable with the NAHR of the models, where also the heat losses are not included, according to equation 5.26. The shown NAHR in equation 6.4 is the integral of the formula 5.26.

$$NAHRR = \dot{Q}_{comb} - \dot{Q}_{loss} + \dot{E}_f = m \cdot c_v \cdot \frac{dT}{dt} + p \frac{dV}{dt} \quad (5.26 \text{ revisited})$$

$$NAHR = \int NAHRR \quad (6.4)$$

Where the NAHRR is in J/s and the NAHR is in J. According to the thesis report of combustion drive, the heat release in the Kibox in J/CA is calculated with formula 6.5[1]:

$$\frac{\delta Q_{ch}}{d\theta} = \frac{\gamma}{\gamma - 1} \cdot p \cdot \frac{\delta V}{d\theta} + \frac{1}{\gamma - 1} \cdot V \cdot \frac{\delta p}{d\theta} \quad (6.5)$$

Where γ is C_p/C_v , p is pressure, V is the volume, θ is the crank angle. Then, the heat release in the Kibox (I) is the integral of the heat release rate (Q):

$$HR_{Kibox} = I = \int \frac{\delta Q_{ch}}{d\theta} \quad (6.6)$$

In figure 6.19 and 6.20 the NAHR of the methanol model is compared to the Kibox HR. This comparison is at 375 kWe, ignition of 20 °CA BTDC, with the used TDC shift of -0.9 and without a TDC shift. It is visible that the NAHR from the Kibox does not show a fuel vaporization dip as shown for diesel in figure 6.8. Furthermore, the Kibox HR initially follows the -0.9 shifted NAHR line from the model. But from 40 °CA ATDC it is closer to the unshifted NAHR line. When looking into the closer look around TDC in figure 6.20, it shows that the HR from the Kibox starts to increase at 150°CA, 30 °CA BTDC. This is unreliable because the ignition timing is set at 20 °CA BTDC.

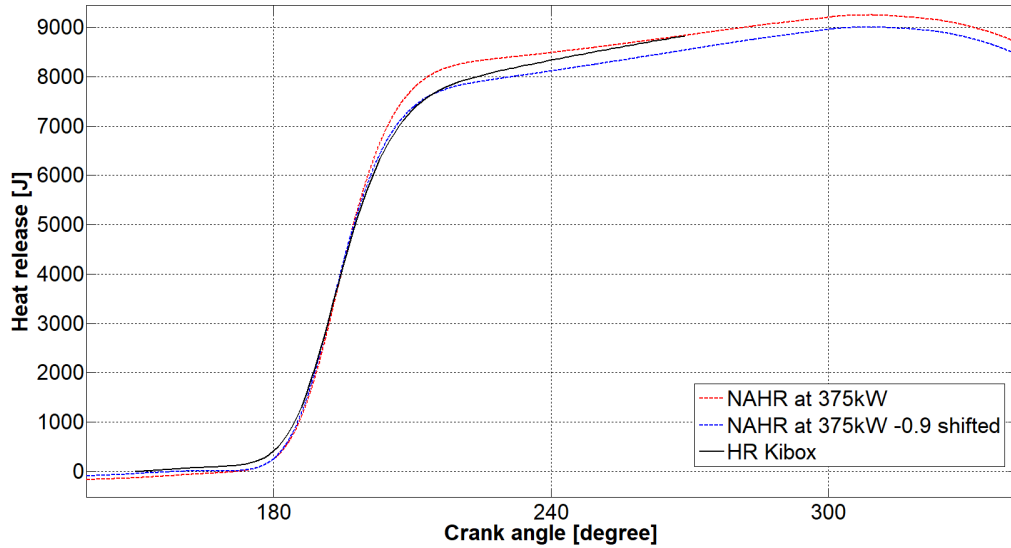


Figure 6.19: Net apparent heat release methanol model compared to Kibox hr

When looking at the end values of all three heat release calculations, the heat release per cycle is given. It is expected that this value is lower than Q_{fuel} calculated with equation B.5, which is approximate:

$$Q_{fuel} = 0.55555[gram] \cdot 19.9[kJ/gram] = 11.0 \quad [kJ]$$

The NAHR is expected to be lower because from the Q_{fuel} the heat losses, combustion losses and the energy to fuel must be subtracted to get the NAHR. The heat release per cycle is shown in table 6.4.

The heat release per cycle from the NAHR in table 6.4 show that the end values are best represented in the model without shift. The shifted value is almost 4 % lower. This complies with what is found with the TDC shift that the found indicated power was also better without shifting the signal. The model has been shifted because better values of heat loss, meaning more realistic Woschni temperatures were found. In figure 6.20 a closer look from ignition and TDC is shown to see the benefits of the TDC shift. Both NAHR signals have been adjusted with Woschni temperatures to have the RCO go through zero at 20 °CA BTDC. The shifted signal is in the region of the start of combustion (SOC) and just after TDC more compliant with the Kibox HR signal and still has the SOC in the NAHR at 160 °CA BTDC. Just as the RCO it is expected that the NAHR starts to increase from zero at the moment of ignition, thus best shown in the NAHR with a TDC shift of -0.9.

Table 6.4: Heat release per cycle comparison between model and Kibox

	heat released at 90 °CA ATDC [J]
Model: NAHR no shift	8830
Model: NAHR with -0.9 shift	8537
Kibox: HR	8827

Concluding that the HR signal from the Kibox and the NAHR from the methanol model are almost similar. Also, it becomes more clear that the chosen TDC shift is a trade off between, a good calculated indicated power or total heat release in this case, and a better representation of the in-cylinder heat loss and combustion rate.

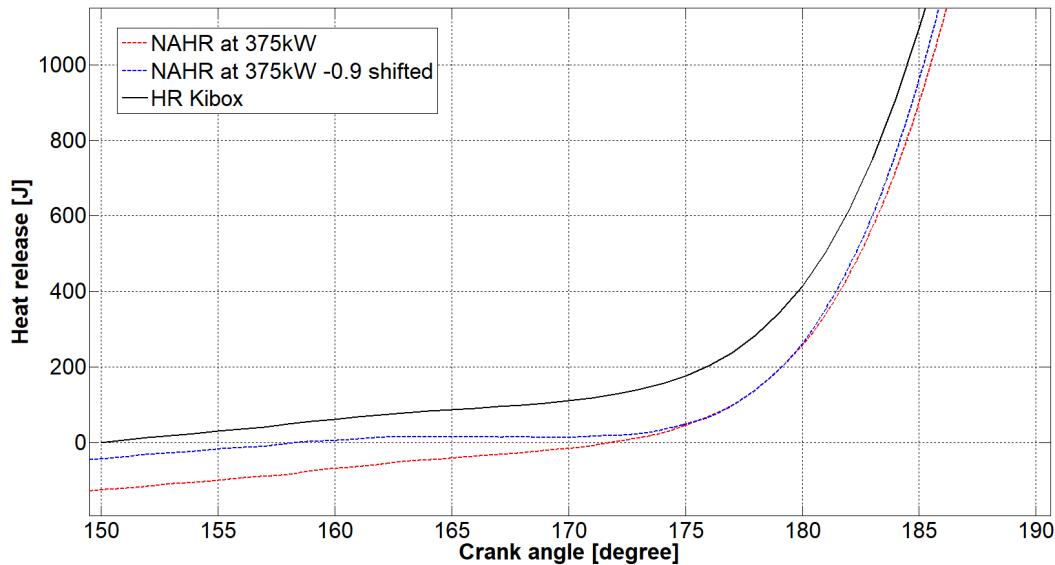


Figure 6.20: Net apparent heat release methanol model compared to Kibox hr. close look around TDC

6.5.2. Validation of the NAHR for the NG model

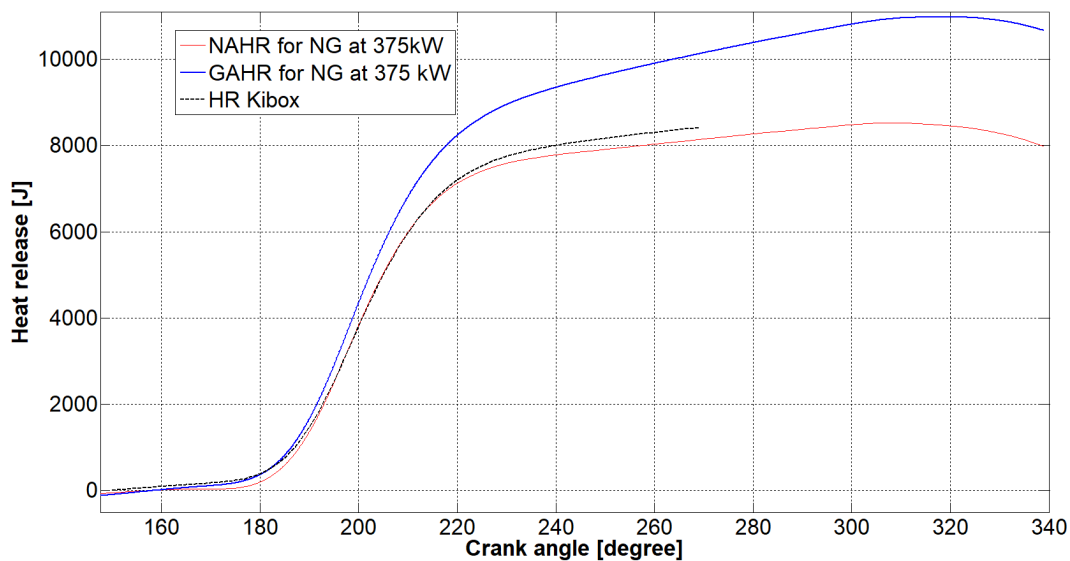


Figure 6.21: Net apparent heat release NG model compared to kibox HR

Similar validation, as been done for the methanol model, will be done here for the NG model. In figure 6.21 the NAHR for NG at 375 kWe is shown with the 127 m/hr fuel flow and -0.9 TDC shift as has been used throughout this chapter for the comparison with methanol. Besides the NAHR, also the GAHR from the model is shown. The GAHR will be shown for comparison and to show the influence of taking heat loss into account in the models.

It is found that:

- NAHR and HR from Kibox are approximately the same from 190 to 220 °CA.
- Between 160 and 185 °CA, the GAHR is closer to the HR from the Kibox than the NAHR.
- HR from Kibox is higher from 220 °CA and ends 3.5 % higher with 8423 J at 270 °CA.
- GAHR is showing higher results due to the included heat loss, as expected. The GAHR is 33.7 % higher than the NAHR, with a final value of 10670 J. Indicating that 33.7 % of the energy is lost

due to heat losses and energy to fuel. According to Ding, Heat losses are in order of 20-30 % [8].

- Longer combustion duration calculated by the model compared to the Kibox results is shown here as a result of the included heat loss calculations. The GAHR shows, after 8000 J at 215 CA, a long slow increasing curve, resulting in found CA for 90 % burnt fuel (CA90) at a later °CA.

Furthermore, the following was found after changing settings of fuel flow and TDC shift:

- Found that heat release from Kibox more comparable with the higher fuel flow of 127 m³/hr compared to the -5 % fuel flow. Both fuel flows were used in comparison with methanol and explained in section 6.0.1.
- Found that without TDC shift, the end of NAHR is more compliant with the model. With the -0.9 TDC shift, the first part of NAHR is more compliant with NAHR, similar to what was found with the methanol model.

Concluding that the NAHR also for the NG model is comparable with the HR from the model. Also, the GAHR compared to the NAHR is showing the desired effect of including heat losses in the model.

6.5.3. Heat release rate validation

Until now only the heat release (I) from the Kibox is shown, but the Kibox also has a heat release rate (Q), which will be used to compare with the NAHRR from the model. The heat release rate (Q) and NAHRR for methanol are shown in figure 6.22 in J/CA. The heat release rate NAHRR from the methanol model looks compliant to that what is found from the Kibox HR.

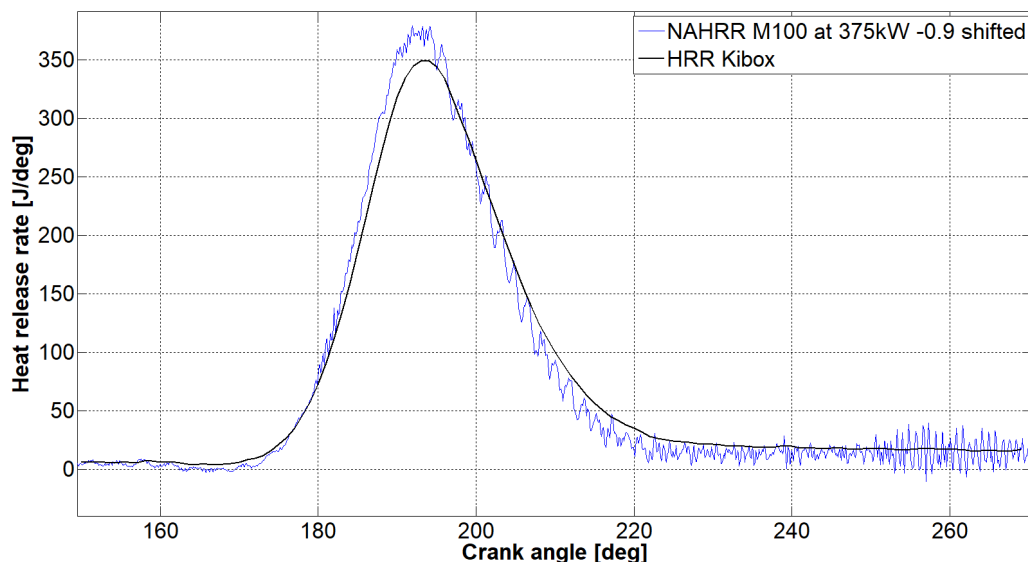


Figure 6.22: Net apparent heat release rate methanol model compared to Kibox HRR

For the NG model, this similar figure of heat release rate is shown in figure 6.23. HRR signals shown comparable graphs. For the methanol NAHRR, a lower maximum is found in the Kibox HRR, with 349 J/CA compared to the model, with 378 J/CA. For methanol, this is an error of 8.3 %. This error increases, when a 0 °CA TDC shift is used, up to 12.0 %, indicating that NAHRR is better represented with a TDC shift. For NG a lower maximum heat release rate is found in the Kibox, with 258 J/CA, compared to the calculated value in the model with 269 J/CA. Furthermore, the maximum HRR is at 14 °CA ATDC for the Kibox HRR and 13 °CA ATDC for the NAHRR with the -0.9 °CA TDC shift, as expected because both are a function of the same pressure signal. For NG maximums are found at 19 °CA ATDC for the Kibox and 18 °CA ATDC for the NAHRR from the NG model. HRR signals from Kibox shows similarity with the NAHRR for the NG and methanol model.

Concluding that the HR and HRR from the Kibox and the NAHR and NAHRR from the NG model and methanol model are almost identical. Small differences found are expected, due to different calculations and assumptions in the model, e.g. the adjustment of the SOC in the model and the TDC-shift. The

HR curves from the Kibox and NAHR from the model are showing similar results within a margin of 4 %. The HRR curves show results within a margin of 8.3 % for the difference in maximum heat release rate, thus the NG model and methanol model are validated.

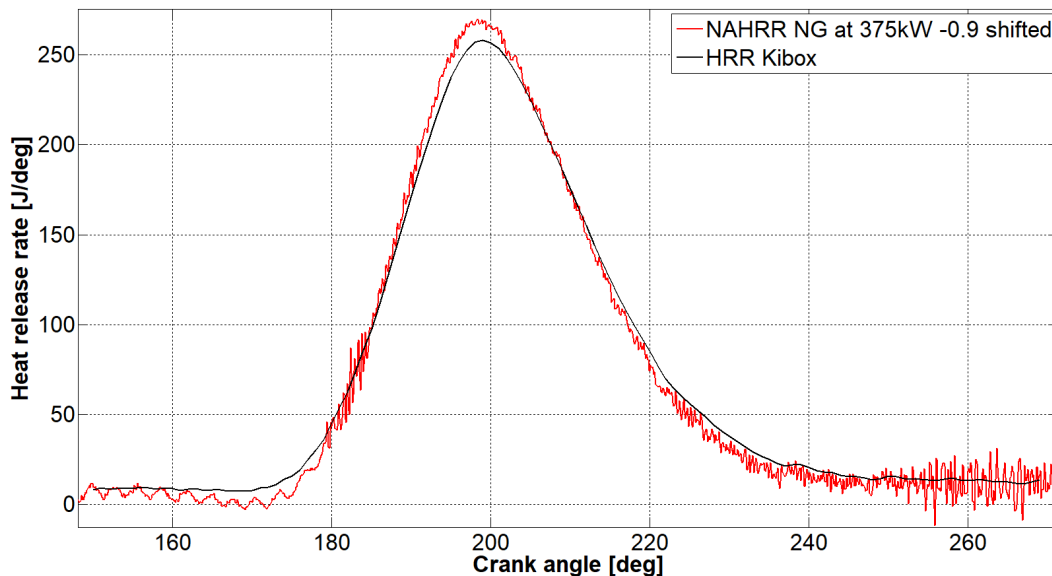


Figure 6.23: Net apparent heat release rate NG model compared to Kibox HRR

6.6. Modelling sub-conclusions

Every section already has its own sub-conclusion but here the answers will be given to the last remaining sub-question of the thesis:

- *Which heat release model is used for the methanol engine and what needs to be changed in the model?*

A modified in-cylinder heat release rate model is used to model the PFI of methanol. The model has been modified at two parts. The first part is the fuel modifications; the properties of the fuel and the gas properties are modified in the model to have correct calculations of combustion heat. The second part is the energy to liquid fuel sub-model that has been modified. It has been adjusted with a vaporization factor to simulate the part that already is vaporised in the inlet valve before the combustion chamber is closed. The methanol model, including the modifications, are validated when comparing the results with the Kibox heat release.

- *Will the model give comparable performance characteristics as found in the experimental data?*

The following characteristics from the model are found to be comparable with the experimental data:

- Both model and performance results shown best fuel consumption optimum point with methanol at advanced ignition timings of 24 °CA BTDC.
- Higher manifold temperatures showed lower NO_x emissions in performance data. In the model, the higher manifold temperature shown lower in-cylinder maximum temperature, which could result to lower NO_x emissions as found in the literature.
- Both the model and the experimental data showed faster combustion for methanol compared to NG. However, almost twice as long combustion duration was calculated with the model, this was a result of the heat losses that are taken into account with the model.

The following characteristics from the model are found not to be comparable with the experimental data:

- The calculation of indicated power from the model is calculated with the combustion cycle and not the full cycle, resulting in deviations in indicated power compared to the effective power. This was specifically visible with the ignition sweep, where the effective power was increasing with advanced ignition timing, the indicated power was decreasing with advanced ignition timing.
- In the model, the best representation of indicated power is shown without a TDC shift, but heat loss temperatures in the Woschni formula are best represented with a TDC shift of -2.0 °CA. Both could not be made exactly comparable with the performance characteristic. A TDC shift of -0.9 °CA is chosen to be closest to both expected values of indicated power and Woschni (heat loss) temperatures.



Conclusions & recommendations

The main objective of the thesis is to compare the performance of 100 % methanol with Natural Gas (NG) in a spark-ignited (SI) internal combustion engine (ICE) with the purpose of using methanol in a maritime environment. First experimental performance runs are executed and analysed following a modelling analysis. The following was concluded and recommended from the analyses of the experiments and the modelling.

7.1. Conclusions

This study presented the ability to stably run a CAT G3508A spark-ignited (SI) engine with port-injection of 100 % methanol. The engine was able to operate with the new fuel after engine modifications were made to the fuel system, control system and aftercooler controls. Furthermore, safety systems and measurement systems were changed to make it possible to experiment on the 100 % methanol engine. Three major challenges were encountered during the performance tests. First, it was not possible yet to start the engine on 100 % methanol and it still needed natural gas during a 5-second startup. Furthermore, 100 % load is not yet accomplished but expected that this will be possible at following performance tests after modifications on the fuel system. The engine can operate, with current fuel system, up to 430 kW_e (86 % of maximum load). The third challenge that must be noted is that the fuel injector of cylinder 4 needed to be replaced, prior to the measurements, due to dirt in the injector.

During the experimental runs, the test plan could only be partially executed, on 50 % and 75 % load, due to limited time and fuel. During these runs, the most important parameters for the input and validation of the model are received among interesting measurement data. The most important data that is received and necessary for modelling is in-cylinder pressure, crank angle, temperature measurements, pressure measurements, exhaust emissions (NO_x and O₂), engine power and fuel consumption.

A modified in-cylinder heat release rate model is used to model the PFI of methanol. The original NG model has been modified in two parts. The first part is the fuel modifications; the properties of the fuel and the gas properties are modified in the model to have correct calculations of combustion heat. The second part is the energy to liquid fuel sub-model that has been modified. It has been adjusted with a vapor factor to simulate the part that already is vaporised in the inlet before the combustion chamber is closed. The NG and methanol model are validated by comparing the results with the Kibox heat release and heat release rate.

After successfully performance testing and data collecting, the performance and model analysis provided conclusions about the stated hypotheses. The following hypotheses will hold:

1. *"Engine efficiency is expected to be higher on methanol than on natural gas with the performed test loads of 50 % and 75 % load."*

Efficiency improved by 2.2 % and 0.9 % at 50 % and 75 % load with methanol compared to natural gas at the same test conditions of ignition timing and NO_x emissions. These preliminary methanol

engine results show that improvements in engine efficiency could be obtained from a retrofitted SI NG engine converted to operate on 100 % methanol without making any modifications to the geometrical engine specifications such as cylinder or piston geometry. The hr model also shows, for methanol, a CA50 at 17.2 °CA. The CA50 for methanol compared to NG is 7.6 CA closer to the consumption optimal operating point of CA50 at 8°CA ATDC, due to faster premixed combustion.

2. *"Better efficiency will be reached at an advanced ignition timing on methanol than the standard used ignition timing of NG. With NG the standard ignition timing is at 20 °CA BTDC."*

The performance analysis showed a decrease of bsfc with advanced ignition timing, due to the lower amount of needed fuel with equal power. The hr model also reveals, with an advanced ignition timing of 24 °CA BTDC, a CA50 at 15.3 °CA ATDC, to be closest to the consumption optimal operating point of CA50 at 8°CA ATDC. Optimum efficiency was found for both loads at an ignition timing of 24 °CA BTDC, which was the most advanced ignition timing used in the performance tests.

3. *"With increasing temperature after the cooler, there will be more evaporation before the inlet valve, which causes better in-cylinder condition and therefore with constant efficiency, a lower NO_x emission can be realized"*

It is calculated that the (in-cylinder) evaporation of methanol at IVC increased from 18.0 % vapor to 37.7 % with increasing temperature after the cooler from 40 °C to 60 °C. In the performance analyse it showed a decrease of NO_x emissions at constant load and fuel consumption. Supported by the model which shows a decrease in maximum in-cylinder temperature, with increasing temperature after the cooler. However, it should be noted that the air excess ratio also increased (more in-cylinder mass) and that the measurements were not in steady state.

And the following hypothesis will be rejected:

- *"Better stability will be expected to be at an earlier ignition timing. With NG the standard ignition timing is at 20 °CA BTDC."*

Advanced or retarded ignition timings did not give a clear trend in optimising the stability (COV values). But, the engine runs stable on 100 % methanol at 250 kWe (50 % load) and 375 kWe (75 % load) between 16 °CA BTDC and 24 °CA BTDC ignition timing at 500 mg/Nm³ NO_x emission. Within the ignition timings of 16-24 °CA BTDC, all COV_{imep} values stayed below the critical stability limit of 10 %. Compared to NG, COV_{imep} and COV_{pmax} showed higher values, indicating lower stability for methanol than for NG. Methanol showed less stability due to higher cylinder-to-cylinder and higher cycle-to-cycle variations. The expectation is that the higher cyclic variations are due to one or a combination of following reasons: a.) Dirt in the injectors causing blocked injectors, b.) High evaporation heat of methanol and c.) Lower flame speed of methanol at the tested leaner air-excess ratios. The lower flame speed, expected from the literature study, was not concluded with the experiments. It was found that the combustion duration (without heat loss included) from Kibox for methanol was 1.6 °CA shorter than for NG at comparable settings of ignition timing (at 20 °CA BTDC), power (375 kWe), engine speed (1500 rpm) and NO_x emission (500 mg/nm³). The model supported the faster combustion for methanol. With 1.1 °CA shorter combustion duration compared to NG, calculated with the NAHRR (without heat losses). Taken into account the heat losses, with GAHRR, the combustion duration was up to 6.6 °CA shorter compared to NG. Both calculations indicate that the laminar flame speed is not dominant in the combustion chamber. Thus, for comparing in-cylinder flame speeds of methanol and NG more in-cylinder parameters need to be considered e.g. temperature, pressure and turbulence.

Regarding the heat release of methanol, it was found that methanol reveals 7.0 °CAs earlier CA50 and 2.6 °CAs earlier CA10 compared to NG at 75 % load. Indicating faster premixed combustion. However, due to late CA90, the combustion duration is almost equal with only 1.1 °CA shorter combustion duration for methanol. Furthermore, with changing ignition variation combustion duration changed. Advanced ignition timing of 24 °CA BTDC showed a combustion duration increase of 11.4 °CA compared to an ignition timing of 16 °CA BTDC.

As mentioned before, most characteristics from the model were found comparable with the experiments. The following characteristics from the model are found not to be comparable with the experimental data:

- In the model, the best representation of indicated power is shown without a TDC shift. Heat loss temperatures in the Woschni formula are best represented with a TDC shift of -2.0 °CA. Both could not be made exactly comparable with the performance characteristic. With a chosen TDC shift of -0.9 °CA, it was found to be closest to both actual physical values of indicated power and cylinder wall temperatures. The choice of TDC shift has much influence on the absolute values of HR and HRR, but limited influence when the comparison is made between the fuels with the same TDC shift.
- The calculation of indicated power from the model is calculated with the combustion cycle and not the full cycle, resulting in deviations in the indicated power. This was specifically visible with the ignition sweep, where the indicated power calculated by the model was decreasing with advanced ignition timing.

In the introduction of this study, the following primary question was deposited:

"What is the effect on the engine performance when 100 % methanol is used as fuel for a spark-ignited port fuel injected engine compared to premixed injection of natural gas?"

Summarizing the conclusions, this question can now be answered with:

The engine operates stably on methanol at 50 % and 75 % load within ignition timings of 16-24 °CA BTDC, but less stable than with NG. Heat release indicates an almost similar combustion duration, but shorter combustion duration is shown for methanol. Also with methanol, the crank angle where 50 % of fuel is burnt (CA50) is shown earlier compared to NG. The faster premixed combustion, combined with a better found fuel consumption operating point, resulted in higher efficiencies for methanol compared to NG for the tested 50 % and 75 % load at comparable operating conditions.

7.2. Recommendations

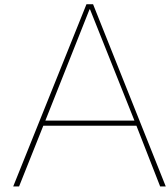
For the engine and test setup it is recommended to:

- Change the methanol injectors and check if the COV values drop for cylinder 5 and 6. Then also the cylinder-to-cylinder variation becomes lower with methanol, thus, increasing the stability.
- Increase manifold temperature up to maximum vaporization of methanol and/or engine limits to increase stability and efficiency (or lowering NOx emissions at constant efficiency).
- Test more advanced ignition timings than 24 °CA BTDC, to further improve fuel consumption. From the performance results, it was concluded that the highest efficiency is reached with an ignition timing of 24 °CA BTDC. However, more advanced ignition timings are not tested yet.
- Investigate if the engine can perform on a propeller load (with varying engine speed) instead of the generator load (with constant engine speed).
- Investigate the emissions when running on methanol, including CO₂, CO, HC and formaldehyde emissions. This also can improve the model, because then the combustion efficiency can be calculated instead of assumed at 98 %.
- Use the setup for ethanol as a fuel instead of methanol and compare results. It was found that ethanol should have comparable performances, with higher LHV, but no projects are known to use ethanol on marine size engines. The current engine setup can be used for ethanol.

For the model it is recommended to:

- Make predictive methanol models to forecast behavior with changing engine settings, such as engine speed, loads, etc. The current methanol model has been used to explain and better understand what is found in experiments. To obtain a predictive model it is advised to find the Wiebe or Seiliger parameters with the modified methanol model.

- Minimize the uncertainties in the model. The TDC-shift could not represent the physical values for both the indicated power as the wall temperatures of the cylinder, indicating that there are uncertainties in the model. Improvements in the accuracy of the model should be searched in:
 - Adding delay and improve evaporation rate. The current single-zone model assume the evaporating rate to be equal to the combustion rate. Meaning that the evaporation rate is now dependent on in-cylinder burned fuel mass flow, which works for a decent estimate of energy needed for the fuel. But this does not give a good representation of evaporation in time. The current single zone model also simulates combustion from SOC equal to the spark timing and to be equal in the entire combustion chamber. To improve the modelling accuracy of methanol combustion, it is recommended to use multi-zone modeling including delay times to obtain better results.
 - Add crevices (heat) losses. In current model, the crevices losses were assumed to be zero. To have a better representation of the in-cylinder masses the crevices losses should be taken into account.
 - Improve heat loss coefficients of Woschni for methanol as a fuel. In this research, only the C2 and temperatures in the Woschni equation has been altered to fine-tune the SOC. The values of C3 and C4 are not changed but should be more adjusted for methanol as a fuel. This will create a better formula for in-cylinder heat losses.
- Validate the vaporization factor, build in the model, before further use of the model. In this research was found that most used models choose to assume 100 % vapor in the model. Better results are shown in this research but not yet validated. The vaporization factor is only compared with another calculation, which shown comparable results.



Engine modifications

The following systems are changed on the G3508A SI GI engine to make an 100% methanol injected engine:

- Modified fuel system (including fuel storage, fuel pump, filters, piping, special designed fuel rail, adjusted port injection system with high flow methanol injectors and valves).
- Modified charged air cooling system. New three way valve and modified control system to adjust the temperature after the cooler. This was done because the cylinder inlet temperature (T_1) changes by load due to the heat of vaporization of methanol after the cooler.
- New designed control system to control primary and secondary engine control systems.
- A vapor detection system is installed (safety). Inside the test bed a continuous methanol vapor detection is available.
- A inert gas system is installed (safety). Nitrogen gas is used to clean the fuel system.
- Special measurement system and adjusted sensors (research purpose only).

A picture of the modified engine on the test bed is shown in A.1. In this appendix the modified sub-systems will be discussed in more depth.



Figure A.1: Test bed

A.1. Fuel system

In this chapter the methanol fuel system, as shown in figure A.2, will be discussed. The fuel system will partly be outside in a closed area and partly inside the building where the test area is for the engine. The safety considerations need to be taken into account when designing the fuel system. Also the expected fuel flow, \dot{V}_{fuel} , needs to be known during the designing process. The fuel flow of NG is known to be $150 \text{ m}^3/\text{hr}$ at full load. The \dot{V}_{fuel} with methanol is almost 300 L/hr at maximum power calculated with equation A.1.

$$\dot{V}_{methanol}[\text{L/hr}] = \frac{\rho_{NG(gas)}}{\rho_{methanol(liquid)}} * \frac{LHV_{Methanol}}{LHV_{NG}} * 1000 * \dot{V}_{NG}[\text{m}^3/\text{hr}] \quad (\text{A.1})$$

With these design conditions known now the following fuel subsystems will be described.

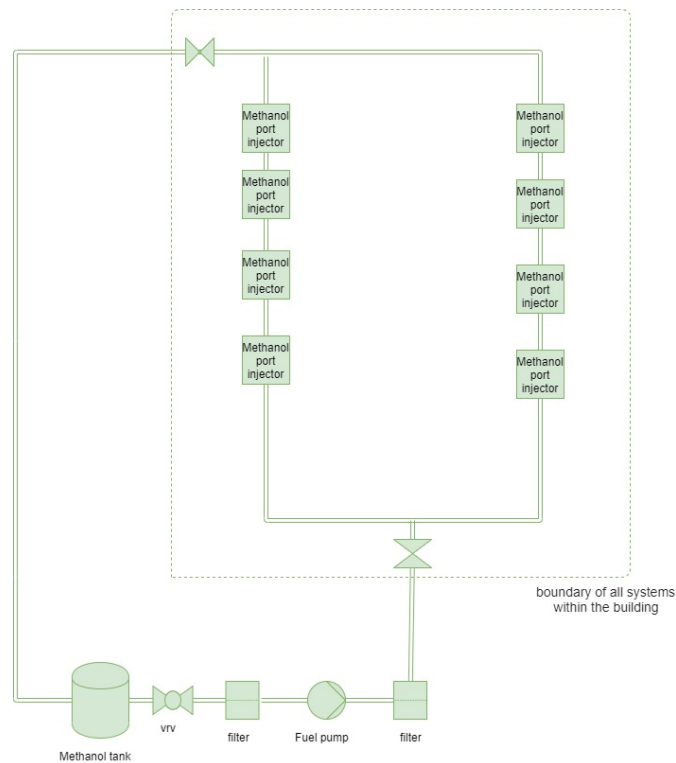


Figure A.2: Schematic of the fuel system

A.1.1. Fuel hoses / piping



Figure A.3: Rubber hose

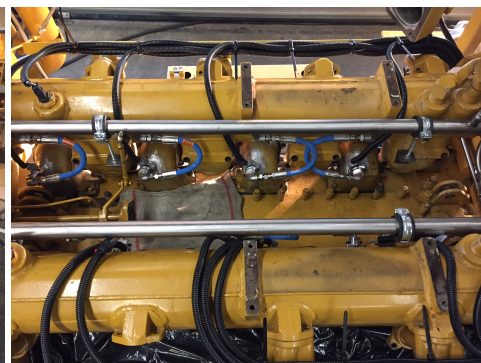


Figure A.4: Stainless steel fuel lines

Choosing a fuel pipe depends on the following characteristics: strength, thermal stability, availability, pricing, chemical resistance and \dot{V}_{fuel} . The required diameter depends on \dot{V}_{fuel} , a minimum diameter of 20 mm is used for the fuel hoses and piping.

Stainless steel (SST) meets the requirements and is therefore suitable to use for methanol transport. Stainless steel pipe is a strong material but not flexible to move like PTFE, EPM or Rubber hose. A hose is less resistant to heat of the engine and therefore less suited at higher temperatures ($T > 100\text{ }^{\circ}\text{C}$) than stainless steel. EPM or Rubber hose are also chemical resistant and widely available.

Due to the comfort of flexibility a rubber hose is used with a double braided steel wire inserts for extra strength for outside and inside as shown in figure A.3. Due to the less temperature resistance character the hose will be used from the fuel storage tank up to 1 meter from the engine. Within one meter of the engine stainless steel tubing is mainly used. From the double walled SST fuel rail to the injector high temperature resistant rubber hose is used as shown in figure A.4.

A.1.2. Fuel storage



Figure A.5: Dip tray with Methanol IBC container used as fuel tank

The expected fuel needed for the engine is around 300 L/hr of methanol at full power. Due to start-up of the engine and low load operations a maximum daily consumption of 1000L/day is expected. Due to safety reasons a total amount of 3000L will be stored at PON Power. In the standard delivery methods of methanol is in bulk (max 20.000L) or in intermediate bulk container (IBC) of 1000L.

In this project 3 IBC's of 1000L are used and put on a fuel drip tray. With regards to safety the dip tray and IBC container are outside in a shielded territory where no unauthorized personal is allowed during operations. One of the three IBC's is used as fuel tank and is connected to the engine as shown in A.5

For this project the expected time the engine will be available for performance tests will be a maximum of 2 weeks. For longer duration of a similar projects a more sustainable solution is preferred like an external double walled tank. Due to the costs and the size this solution is not chosen for this project.

A.1.3. Fuel pump

The fuel pump needs to keep the fuel rails under pressure. The fuel pump will be placed outside and close to the fuel storage. A fuelab fuel pump "41402-c (-sp)" has been chosen. The pump has proven to be an good methanol fuel pump in automotive and has a $\dot{V}_{pump} = 500\text{ L/hr}$, which is enough for this engine at full power ($\dot{V}_{max} = 300\text{ L/hr}$).

A.1.4. Fuel filters

There will be two filters used in the system. One direct after the fuel tank and one direct after the fuel pump. A fuel straining filter with a 75 micron particle rating will be used after the storage tank to protect the pump. After the pump a fuel filter with 10 micron particle rating is used to remove all small particles and to ensure this pollution will not enter the engine.

A.1.5. Fuel rail

A double walled fuel rail has been designed and placed at the engine as shown in figure A.4. A double walled rail has been used for leakage indication and safety reasons. It will not be used for cooling or heating the fuel. The fuel rail will be placed above the engine and therefore a main concern could be that the temperatures of the fuel rail can become higher than the boiling point of methanol. But this engine has water cooled air outlets. The hot outlet air of +/- 1000°C will be cooled with 85°C water on an outer tube. Due to this cooling, heating of the fuel lines above boiling point is not expected.

A.1.6. Fuel injection & ignition



Figure A.6: Port fuel injection holders



Figure A.7: Fuel injectors



Figure A.8: Available spark plugs

A.1.7. Fuel injectors

The used fuel injectors are Bosch EV14 2200cc injectors, that have multiple holes and a conical type spray. The fuel injectors will be placed just above the cylinder air inlet valves, better known as port fuel injection (PFI). The holders for the injectors and the injector itself are shown in figure A.6 and A.7. With PFI you will have quicker transient behavior than premixed injection before the air cooler as has been used with natural gas. Also due to the port injection the air/methanol flow will not pass aluminium parts from the engine that are vulnerable for methanol/water. PFI provides a good fuel-air mixture before ignition compared to direct injection which minimizes the risk of droplets of fuel. This better mixture is due to longer mixing time before combustion. PFI also has the advantages to operate at lower pressures, 3-5 bar, compared to common injection methods.

A.1.8. Spark plug

With the use of methanol as a fuel in the automotive industry the "pre-ignition" is the limiting factor instead of knock. The change on knock is low due to the high octane number. The change on pre-ignition is high due to the low minimal ignition energy. Pre-ignition can lead to damage of the piston and spark plug [13, p64].

The spark plug electrode is one of the hottest parts in the combustion chamber and can be the source of a pre-ignition. The material of the spark plug is therefore important. With platinum electrode the change on pre-ignition is lower than with non-platinum electrodes. A even better solution is to replace a standard iridium-electrode with electrodes with a copper core [13, p66].

The standard spark plug in the G3508A SI NG engine is a "J" gap spark plug, shown on the right of figure A.8. It has a iridium alloy on the tip of the center electrode. The tip of the ground electrode has a platinum alloy. Also the use of pre-chamber spark plugs, shown in the middle of figure A.8 must be considered optional. The pre-chamber spark plug has multiple holes which increase the flame speed of the fuel mix. With high flame speed the engine can run with less fuel and more air. This will reduce the NOx emission. The pre-chamber spark plug is specially designed to satisfy the NOx emission regulation.

This project will start with a "J" gap spark plug because already a higher flame speed is expected with methanol than with NG. A change of the spark plug is recommended when experiencing pre-ignition problems (spark plug with copper core) or efficiency/flame speed increase is wanted (pre-chamber spark plug).

A.1.9. Safety and control valves

A valve after the fuel tank is used and a safety valve is needed inside the test area at the incoming line before the engine. These fuel valves will close automatically when the emergency button will be used. Also two valves are placed where the SST line connects to the rubber hoses.

To prevent vacuum suction in the system a pressure relief valve is needed to control the pressure in the system.

A.2. Cooling system

The charged air cooling and engine cooling modifications will be discussed in this section.

A.2.1. Charged air cooling system before modifications

The charged air cooling system on the 3508A SI NG engine is an aftercooler which is placed after the turbo's and before inlet receiver. The aftercooler cools the hot compressed air combined with the natural gas. The regulator will keep the combined air and natural gas flow in the receiver at a temperature of 35°C. The air cooling system is separate from the internal engine cooling system.

A.2.2. Modification on the air cooling system



Figure A.9: Cooling three-way valve



Figure A.10: Cooling three-way valve placed with electric motor

Due to the PFI the temperature of the air inlet will be changed just before the cylinder inlet valve. This temperature change is due to the heat of vaporisation of methanol. The air temperature can not be kept on a constant temperature after the air cooler because with methanol injection the temperature after the air cooler is load dependent. Therefore a three-way valve is placed before the cooler instead of the previous constant temperature regulator. The three way valve will be opened and closed by a

electric motor which will be regulated by a PLC. The cooling valve and the electric motor are shown in figure A.9 and A.10.

A.2.3. Engine cooling system

The engine cooling system will maintain the temperature of the engine around 80 °C. When the engine is cold there is no preheating system available for the engine. When experiencing cold start problems the engine will be preheated with starting up on natural gas. When no start up fuel is available then preheating the engine block should be considered and can be done by heating up the engine cooling system.

When experiencing to cold inlet air on constant load operations, due to the heat of vaporization of methanol, than connecting the engine cooling ($T_{engine} = 80^{\circ}C$) with the air cooling system ($T_{air} > 35^{\circ}C$) should be considered. To be clear for this project no actual changes will be done on the engine cooling system but only the options with the engine cooling system are given in this paragraph.

A.3. Control system

There are several electric systems on the engine. The main control system is designed and delivered by Woodward. The secondary control systems are made by PON power. In this chapter I will give an overview of all designed, made and existing electric systems that will be used on the engine.

A.3.1. Woodward LECM

A large engine control module (LECM) will be delivered and designed by Woodward to PON specification. The LECM will control the following engine's operations:

- Speed/load control.
- Air/fuel ratio control.
- Air flow control.
- Ignition or injector control.
- Misfire and knock detection.

The LECM will control the air throttle, methanol pressure, methanol injectors and ignitors to do these operations. The LECM will use the air throttle and methanol pressure for initial speed/load control. The LECM will use the pressure sensors in the cylinder heads and the control over timing of the individual methanol injectors for optimizing load control over the different cylinders. Initially the LECM will have a mapping for the injection time and ignition of every cylinder which will be adjusted during the first operations to get stable load conditions.

A.3.2. Engine PLC

A PLC will be designed by PON Power to control all other secondary engine systems, e.g. the cooling system. The PLC system is placed in a Rittal control cabinet together with the LECM. This cabinet will be placed on the engine and connected to a HMI. The following functionalities to control and monitoring of all secondary systems are taken into the PLC:

- Engaging/disengaging of sub systems.
- Controlling manifold temperature.
- N2 fuel line purging system.
- N2 fuel storage blanketing system.
- Handling of system alarm.
- Registration of system events.

A.4. Safety system

A.4.1. Vapor detection system

Methanol makes its presents above (10 times) safety limits for humans. Therefore a vapor detection system is needed for this experiment. Initially a full vapor detection sweep must be done over the whole new fuel system. After that continuously vapor detection is recommended within the test bed

room when operating with methanol. Two Oldham MX32 2120001 OLCT vapour detectors has been used to determine (0-1000) ppm methanol vapour in the air.

A.4.2. Inert gas system: Nitrogen

When working on ships a inert gas system is necessary according to Lloyd's classification rules. The inerting of all fuel piping during normal operation and emergency shutdown activation and inerting of methanol-fuelled consumers is necessary [?]. For this project due to safety concerns a nitrogen inert system is used:

The Nitrogen needs to be able to fill all the available space in the methanol tank, therefore a nitrogen bottle containing at least 1000L gas fill is necessary. This is possible with a 30L or 50L bottle with regulator.

In this project four 50L bottles for six weeks are rented by the company Air Liquide. The regulator needed to be purchased and was set at a operating pressure of 2 to 3 bar. Due to the short duration of this project the chose was made to rent the nitrogen bottles. The nitrogen system is shown in figure A.11.



Figure A.11: Used nitrogen bottles with pressure regulator

A.4.3. Extra safety systems

The following safety system were already available at the test side, but these systems were checked or modified to work with methanol:

- fire detection
- fire extinguishers
- emergency shutdown buttons

A.5. Measurement systems

A.5.1. Dewetron measurement & adjust sensors

At the engine there will be an Dewetron Dewe-2600 measurement system installed to collect all measurement data during the test runs. The temperature and pressure sensors needs to be adjust before using the system. The sensors will be rejected when the measurement is outside the given tolerance according to the manufacturer e.g. for a TE 1260 thermocouple the tolerance is 1,5 °C. To get the best results from temperature sensors out of the dewetron measurements the temperature sensors are calibrated at 40 and 135 °C and the pressure sensors are calibrated at 0 and 10 bar. The calibration report of all sensors are given in appendix E. Remarkable is that the thinner temperature sensors are 1 °C lower at the 90 °C setpoint, and the thicker sensors are all 1 °C higher at the 90 °C setpoint. To make correct measurements as much as possible we must try to use the same sensortype in a sub-system.

Also remarkable is that the 10 bar pressure sensors are more accurate than the 2,5 bar pressure sensors when testing at 50% max pressure. Therefore the 10 bar pressure sensors should be preferred. All other measurement systems that are connected on the Dewe-2600 are calibrated external or earlier in the project. e.g. the exhaust gas measurement system that is calibrated by the manufacturer.

A.5.2. Kibox

A Kibox-to-go (2893A) is used to determine crank angle and in-cylinder pressure. The pressure sensors used during the tests are 5064C type with a operating range up to 250 bar. The sampling rate was set to 20kHz. The sensitivity of the sensors are 81,78 pC/bar. The pressure sensors are water cooled, the cooler is shown the bottom right of figure A.12. The kibox further needs a crank angle measurement and has a crank angle decoder for this measurement. The kibox software then enables a TDC correction. The TDC correction factors are set at 226,65 TDC shift and 0.23 deviation.

A.5.3. Testo-350

A Testo-350 system is used to determine the emissions in the exhaust. The system is connected to the Dewetron system to have a continuous data storage. The measurement sensor was in a fixed mount at the exhaust pipe. The Testo measurement computer is shown in figure A.13.



Figure A.12: Dewetron measurement system

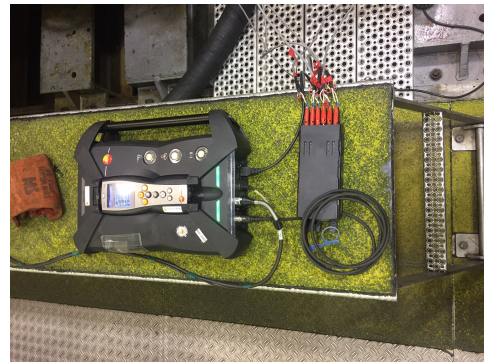


Figure A.13: Testo-350

B

Extra analysis

The following analyses were executed to have a better understanding of the engine running on methanol or to be able to execute later performance runs. There are interesting findings described in this appendix, but they did not contribute to the final conclusions of the research and are therefore placed here in the appendix. These include the missing performance tests as described in the executed plan in table 3.2. This appendix will describe the findings from the stable loads runs, the performance analysis of the NO_x variations, and the efficiency calculated by the model.

B.1. Stable load runs

The performance run on methanol shown in table 3.2 are performed on 22-01-20, except for the stable load runs. Before that date the engine was already a few days on the test bed. During this period there are some points of interest that need to be known before the data will be interpreted. The following characteristics were found during these days before the performance tests:

- First days were needed to get stable load runs on methanol by filling the lambda (control) table in the Woodward control system.
- Mean pressure variations between the cylinders were shown on the first days. The (mean) pressure at cylinder 4 decreased. At a given moment the injector at cylinder 4 was not injecting any fuel due to dirt in the injector. Before following performance tests the injector was replaced and the pressures of cylinder 4 looked normal again after replacement.
- In total there was 3000 liter methanol available during the test period. The first 1000 liter was used to get stable load runs. For the performance tests 2000 liter of methanol was used. At a 75% load this is around 8 hours of testing before the fuel is used.
- Maximum load test has been done and at a 430 kWe (86% of maximum engine power) the engine stopped. The engine stopped due to the reaching of the maximum of the fuel pump capacity.
- The performance test done on 22-01-20 are done at 50% and 75% load due to limited time and fuel. Maximum power and 25% load performance test as shown in table D.1 are therefore not done during the tests on 22-01-20.
- CO emissions shown were high (+/- 2x up to 4x more than with NG) and not reliable (shown zero output long periods of time).
- The temperature of the manifold can be controlled automatically or manually with the secondary control system. Due to the large amount of temperature variation on automatic control we controlled the air temperature of the manifold manually by adjusting the amount of cooling water through the aftercooler. The temperature of the manifold is kept manually at 40°C.
- Significant more water production at the crankcase was shown. This resulted in too much water in the return line before the filter to the air inlet. It resulted in a clogged filter. After isolating the return line and cleaning the filter the water/air got well back to the inlet air filter.

B.2. NO_x variation

The NO_x setting has been varied, with the main reason being the tightening emission legislation in the maritime sector. It is therefore interesting to see how the engine responded to varying NO_x settings.

At a load of 250 kWe and a ignition timing at 24 CA BTDC the NO_x has been varied between 250 and mg/nM³. λ changed from 1.68 to 1.52 with increasing NO_x from 250 up to 1000 mg/nM³. The mean pressures of all cylinders is plotted in figure B.1. It is clearly visible that the changing NO_x settings have less impact on the pressure plot than the changing ignition timings. With higher NO_x settings we have richer settings (λ is lower) and we see this back in the plot with higher peak pressures.

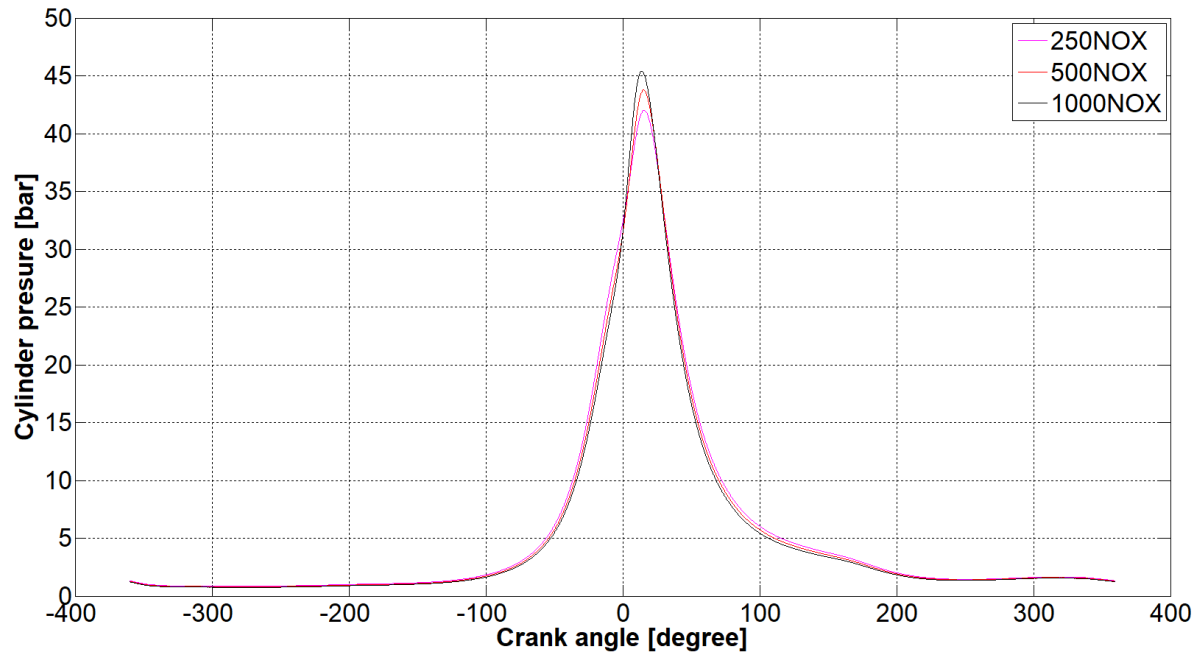


Figure B.1: Mean pressure of all cylinders with changing NO_x settings at a load of 250 kWe

At a load of 375 kWe similar NO_x settings has been varied between 250 and 1000 mg/nM³. With settings of 250 mg/nM³ the engine shut down do to reaching its operating limit.

From this experiment can be concluded that the engine can run with methanol on NO_x settings from 250 up to 1000 mg/nM³ at 250 kWe and on NO_x settings from 500 up to 1000 mg/nM³ at 375 kWe. For lower NO_x more air is needed and therefore λ increased from 1.52 up to 1.68 to reach the NO_x settings of 250 mg/nM³ at 250 kWe.

B.3. Efficiency

In this section, the efficiencies calculated by the model will be explained and compared for the three sets of performance tests. First the brake down into the partial efficiencies will be given. The model calculates the indicated specific fuel consumption (isfc). Isfc is computed in the model with the indicated power according to formula:

$$isfc = \frac{\dot{m}}{P_{indicated, closedcycle}} \quad (B.1)$$

The deviations found in the indicated power, given in chapter 6.2, are therefore also valid for the isfc and indicated efficiency. Indicated power is related to work with formula 6.2.

$$P_{indicated} = W_i \cdot \frac{n_e \cdot i}{k} = \int_{cycle} p \cdot dV \cdot \frac{n_e i}{k} \quad (6.2 \text{ revisited})$$

The effective efficiency (η_e) can be written as an function of work and heat [18, p200]:

$$\eta_e = \frac{W_e}{Q_f} \quad (\text{B.2})$$

The effective efficiency (η_e) can also be written as four partial efficiencies [18, p202]:

$$\eta_e = \eta_m \cdot \eta_i = \eta_m \cdot \eta_{comb} \cdot \eta_q \cdot \eta_{td} \quad (\text{B.3})$$

Where η_i is the indicated efficiency, η_m is the mechanical efficiency, η_{comb} is the combustion efficiency, η_q is the heat input efficiency and η_{td} the thermodynamic efficiency.

The indicated efficiency is calculated in the model as the ratio of indicated work and heat input[18]:

$$\eta_i = \frac{W_i}{Q_f} \quad (\text{B.4})$$

Indicated efficiency calculation with a heat input (Q_f) that is assumed to be equal to the fuel injected per cycle m_f times the lower heating value (h^L in J/kg) of the fuel[18]:

$$Q_f = m_f \cdot h^L \quad (\text{B.5})$$

The first indicated efficiency calculation in the model has a fixed LHV calculated with the enthalpy of formation and is 19.9 MJ/kg for methanol. The second indicated efficiency calculation in the model is with the temperature dependent heat of combustion value, from the power series explained in formula 5.34. The heat of combustion, with this power series, is +/- 20.7 MJ/kg for methanol, depending on in-cylinder temperature, but from this value the heat loss to fuel value need to be subtracted to get a net heat input. Thus, in the model the following equation is calculated for the heat input from the fuel [8]:

$$Q_{comb_{eff}} = Q_{comb} + E_f \quad (\text{B.6})$$

Then efficiency calculated with the effective heat of combustion will give comparable efficiency, than calculated with the LHV. This efficiency is shown in this chapter, due to the fact that all other previous calculation shown are also done with this temperature dependent effective heat of combustion.

The first partial efficiency is the mechanical efficiency η_m and previous defined as:

$$\eta_m = \frac{W_e}{W_i} \quad (\text{6.1 revisited})$$

The second partial efficiency is the combustion efficiency:

$$\eta_{comb} = \frac{Q_{comb}}{Q_f} \quad (\text{B.7})$$

The third partial efficiency is the heat input efficiency (η_q), the ratio of combustion heat to heat input, is calculated with [18]:

$$\eta_q = \eta_{hl} = \frac{Q_{in[1]}}{Q_{comb_{eff}}} \quad (\text{B.8})$$

Where $Q_{in[1]}$ is the heat that is put into the cycle process [18]:

$$Q_{in[1]} = \eta_{comb} \cdot \eta_q \cdot Q_f \quad (\text{B.9})$$

:

And the last partial efficiency is the thermodynamic efficiency (η_{th}), which is calculated with [18]:

$$\eta_{th} = \frac{W_i}{Q_{in[2]}} \quad (\text{B.10})$$

Where the input heat $Q_{in[2]}$ is defined as:

$$Q_{in[2]} = \int_{combustion} T \cdot dS \quad (\text{B.11})$$

An overall figure of the energy losses in an engine is given in figure B.2.

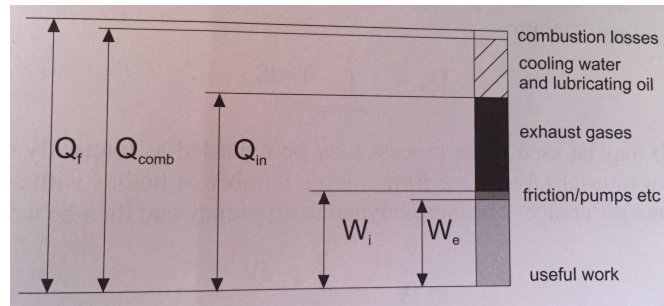


Figure B.2: Energy losses in an engine (taken from Klein Woud et al. [18])

B.3.1. Methanol compared to NG

The efficiencies calculated by the model are shown in table B.1. The NG mass flow was gained from other experiments and could give a wrong indicated efficiency, due to the calculation with the mass flow in equation B.1 and B.5. Therefore, in the table again a -5% mass flow for NG is shown for comparison. The comparison is made at 375 kW_e, 20 °CA and 500 mg/nm³ NO_x.

Table B.1: Efficiency values of cylinder 4 from the model for NG compared to methanol at 375 kW_e

	indicated ef- ficiency	thermodynami efficiency	heat loss ef- ficiency
NG	0.365	0.488	0.748
NG -5% fuel	0.384	0.487	0.789
Methanol	0.392	0.501	0.865

Compared to the effective brake engine efficiencies calculated in chapter 4.5 there are some differences. In the performance analyse a effective efficiency increase was shown for methanol from $\eta_e = 34.8\%$ compared to $\eta_e = 33.9\%$ for NG at an ignition timing of 18 °CA. At 20 °BTDC a effective efficiency of $\eta_e = 35.5\%$ was calculated for methanol. The model calculated the indicated efficiencies for the closed cycle of both fuels at an ignition timing of 20 °CA. Furthermore, the model is not adjusted to get high quality efficiency calculations. Deviations could be found due to following reasons: 1) Cylinder-to-Cylinder variations, only 1 cylinder is calculated by the model. 2) Unknown losses in pumping cycle, only closed combustion cycle is calculated in the model. 3) TDC shift not optimised on power output.

Although, the experimental efficiencies show inequalities with the model efficiencies, it is visible that methanol has higher heat loss efficiencies compared to NG in table B.1. The absolute values may not be correct, but the increased efficiency with methanol is compliant with what is expected from Verhelst. According to Verhelst higher efficiencies is expected to be gained from the increased charge density which leads to a higher volumetric efficiency, shorter combustion duration and lower wall heat losses [42]. The lower wall heat losses are shown in the increased heat loss efficiency. Therefore, in this comparison between NG and methanol it shows the efficiency gain as seen in the experimental analysis comes mainly from the increase in heat loss efficiency.

B.3.2. Ignition variation

The partial efficiencies from the model will be shown and compared with the performance efficiencies, for methanol with varied ignition timing. In the performance analyse it is shown that the efficiency increases with advanced ignition timing at 24 °CA BTDC. The efficiencies from the model will be shown in table B.2.

Table B.2: Efficiency values of cylinder 4 from the model with methanol and ignition variation

	isfc [g/kWh]	indicated ef- ficiency	thermodynamic ef- ficiency	heat loss ef- ficiency
16 °CA BTDC	455.6	0.396	0.494	0.883
18 °CA BTDC	454.9	0.397	0.506	0.870
20 °CA BTDC	460.6	0.392	0.502	0.862
22 °CA BTDC	469.3	0.385	0.504	0.844
24 °CA BTDC	468.0	0.387	0.508	0.840

With the ignition sweep a decrease of indicated power was computed by the model with advanced ignition timing, therefore, lower efficiencies at advanced ignitions. This is not compliant with what is found in the experimental efficiencies calculated in chapter 4.5. The decrease in the indicated efficiency corresponds to the decrease of the model's calculated indicated power. It should be noted here that the indicated power is calculated with the combustion cycle, and not with the full cycle.

A trend is visible in the increased thermodynamic efficiency with advanced ignition timings. The increase in efficiency with advanced ignition timing is also shown in chapter 4.5, but with the model braking down the efficiencies, it now shows that the overall increase of efficiency is partly due to the thermodynamic efficiency increased with advanced ignition timing.

B.3.3. Aftercooler temperature variation

With the performance test the efficiencies with an aftercooler temperature of 40 °C and 60 °C were similar. The advantage shown with higher aftercooler temperature was the decrease in NOx. The model efficiency output is shown in table B.3.

Table B.3: Efficiency values of cylinder 4 from the model for varying the aftercooler temperature

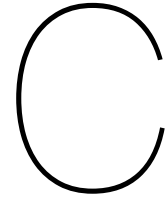
	isfc [g/kWh]	indicated ef- ficiency	thermodynami efficiency	heat loss ef- ficiency
$T_{Aftercooler}$: 40 °C	459.1	0.378	0.504	0.861
$T_{Aftercooler}$: 60 °C	453.2	0.383	0.503	0.845

As expected from the performance analyse the efficiencies shown in table B.3 are than close to each other. This was expected, due to the constant fuel consumption during these experiments.

B.3.4. Conclusion efficiency

From the models and experiment the following can be concluded regarding the efficiency:

- The calculation of indicated power from the model is done with the combustion cycle and not the full cycle, resulting in deviations from efficiencies shown in the performance analyses.
- The efficiency increase for methanol compared to NG, could largely be a result from the increased heat loss efficiency. To validate this the model should be more adjusted to get better efficiency calculations.
- Thermodynamic efficiency increase was shown with advanced ignition timing leading to a better overall efficiency at advanced ignition timings with methanol. Nevertheless, increase of isfc with more advanced ignition timing was not compliant with what was found with the performance results.
- Efficiencies shown with varying aftercooler temperature were similar, as expected due to constant fuel consumption.



Validations and deviations

In this chapter, extra validations and data will be shown to validate or extra check the data. The following subsections will be validated and explained in more depth in this appendix:

- Validation of own COV values calculated compared to Kibox values.
- Stability increase after replacement of the injector of cylinder 4.
- Check the influence of 2 degrees difference in IVO.

C.0.1. Validation COV values calculated compared to Kibox COV values.

In this section the COV_{imep} and COV_{pmax} calculations of the Kibox will be compared with the used calculations in this thesis.

COV_{imep}

Before comparing the COV_{imep} calculations first as a reminder the equation 4.3, 4.4, 4.5 and 4.6 are given:

$$COV_{imep} = \frac{std_{imep}}{imep_{avg}} \cdot 100\% \quad (4.3 \text{ revisited})$$

$$std_{imep} = \sqrt{\frac{\sum_{i=1}^m (imep_i - imep_{avg})^2}{m - 1}} \quad (4.4 \text{ revisited})$$

$$imep = p_{mi} = \frac{W_i}{V_s} = \frac{\int_{cycle} p \cdot dV}{V_s} \quad (4.5 \text{ revisited})$$

$$imep_{N,Kibox} = imep_H + imep_L \quad (4.6 \text{ revisited})$$

The Kibox gives for every cycle a COV value. For example the COV values of cylinder 3 at 20 °CA BTDC at 375 ekW are used. The Kibox gives 61 values with a minimum value of 2.93 and a maximum value of 4.69. The own calculated COV_{imep} is calculated with formula 4.3, and thus an average over the 60 cycles. For this measurement the own calculated COV_{imep} is equal to 4.02. This value could not be found in the 61 values. But what are we actually comparing? To get more insight we first need the settings in the Kibox. These settings and are shown in figure C.4 from the Kibox-cockpit under Administration / Signal types / Cylinder pressure / Indicated mean effective pressure.

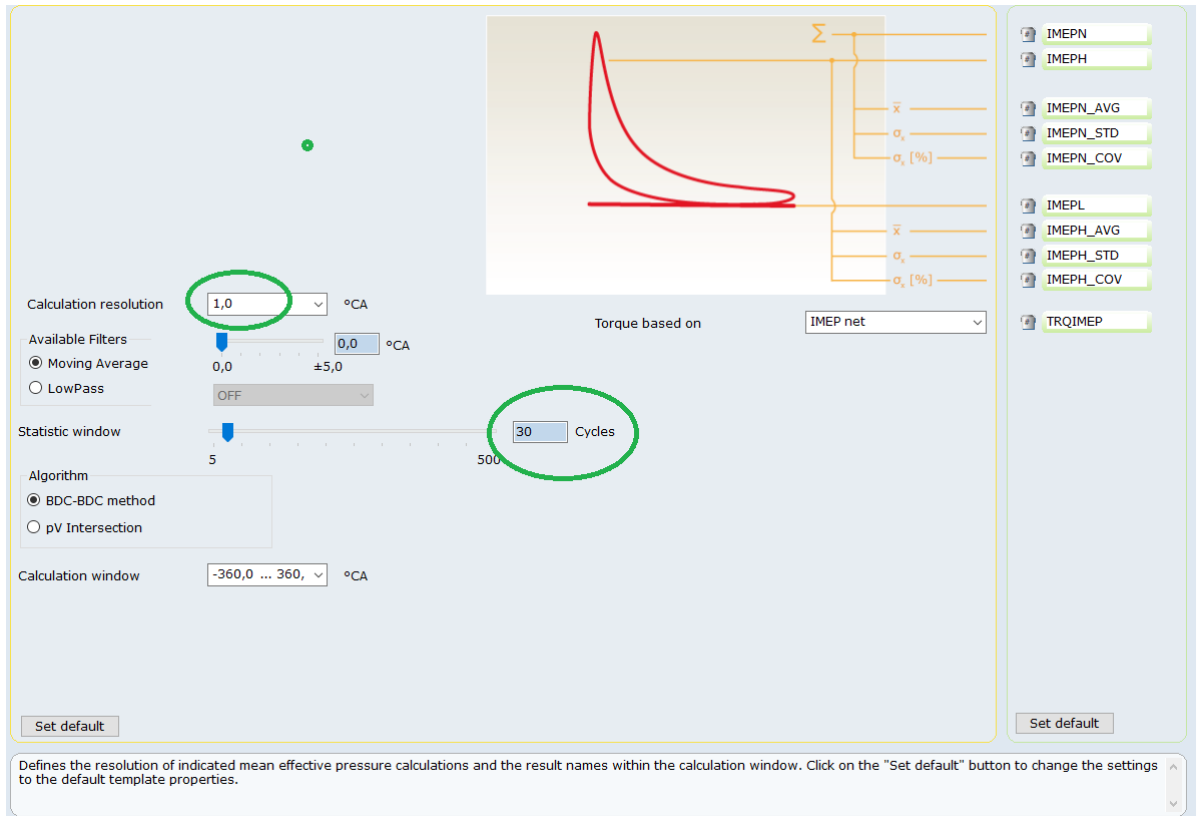


Figure C.1: Kibox settings of IMEP

Figure C.4 shows that the (standard used) setting of the Kibox is to calculate the COV_{IMEP} with 30 cycles, as shown after "statistic window". My calculations of $IMEP_{avg}$ and COV_{IMEP} are conducted with 60 cycles. Now for the validation, my calculations will also be carried out with the first 30 cycles from these 60 cycles. Then, the calculated $COV_{imep}(M=30)$ is equal to 3.57. Looking back at the data of the Kibox this is exactly equal to the 30th value of the COV values of cylinder 3. The Kibox gives, therefore, a COV_{IMEP} value on every cycle, calculated with the last 30 cycles.

For the comparison of the COV_{IMEP} values of all cylinders with the calculation of formula 4.3 with $m=60$ and $m=30$ cycles are shown in table C.1. Also is shown in the table the 30th cycle of the Kibox data. The minimum and maximum values from the Kibox are also shown.

In table C.1 the values of COV_{imep} from Kibox are compared to my calculated COV_{imep} .

Table C.1: COV_{imep} at 375kW for 100%methanol with own calculations and (standard) Kibox calculations

	$COV_{imep}(m=60)$	$COV_{imep}(m=30)$	Kibox (30 th)	Kibox min-max
Cylinder 3	4.0233%	3.5768%	3.5768 %	2.93 - 4.70 %
Cylinder 4	3.7183%	3.0965%	3.0976 %	2.76 - 4.22 %
Cylinder 5	4.9676%	5.1496%	5.1444 %	4.47 - 5.86 %
Cylinder 6	6.1063%	6.9721 %	6.9704 %	5.10 - 7.81 %

When using 30 cycles in formula 4.3 and compared to the 30th Kibox COV_{IMEPN} value then the same value with an error up to 0.1% is calculated. This small error can be explained due to the used calculation resolution of the Kibox. The Kibox used a resolution of 1 CA. In formula 4.3 all measurement points are used resulting in a resolution of 0.1 CA.

Based on table C.1 another point of interest is noticed. The range of min-max values of the COV_{IMEP} with 30 cycles varies up to 2.7% at cylinder 6. This is in my opinion a large range which can be lowered when using more cycles in the calculation. In Heywood [15] it is stated that more accurate IMEP and thus also more accurate COV_{IMEP} are given when more than 100 cycles are used. With this statement and the large range, the standard Kibox 30 cycles is shown to be low to get an accurate value of

the COV_{IMEP} . Even the 60 I used might be too low, however, a trend or comparison might still be available. Also because the Kibox gives the COV values for all 60 cycles and not for 1 cycle. First, the COV values for NG and M100 at 375 ekW are compared in figure C.2 and C.3. The figures show clearly higher COV_{IMEP} for methanol over the full 60 cycles compared to NG. For cylinder 3 and 4 with methanol lower COV_{IMEP} are shown constantly compared to cylinder 5 and 6. All cylinders fluctuate for methanol around 2 percent in value. For NG fluctuations are in order of 1 percent.

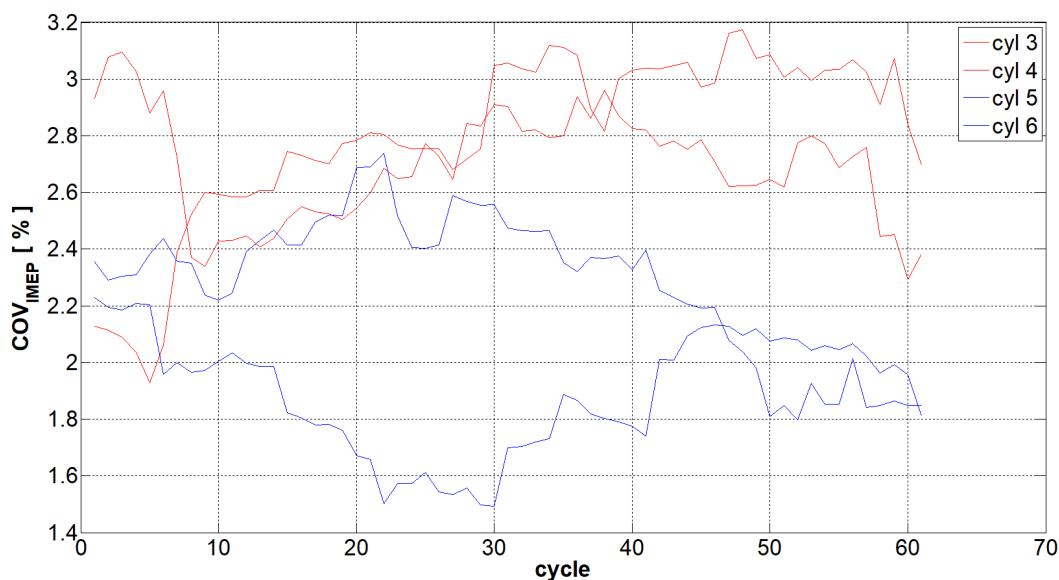


Figure C.2: COV values with NG at 375ekW

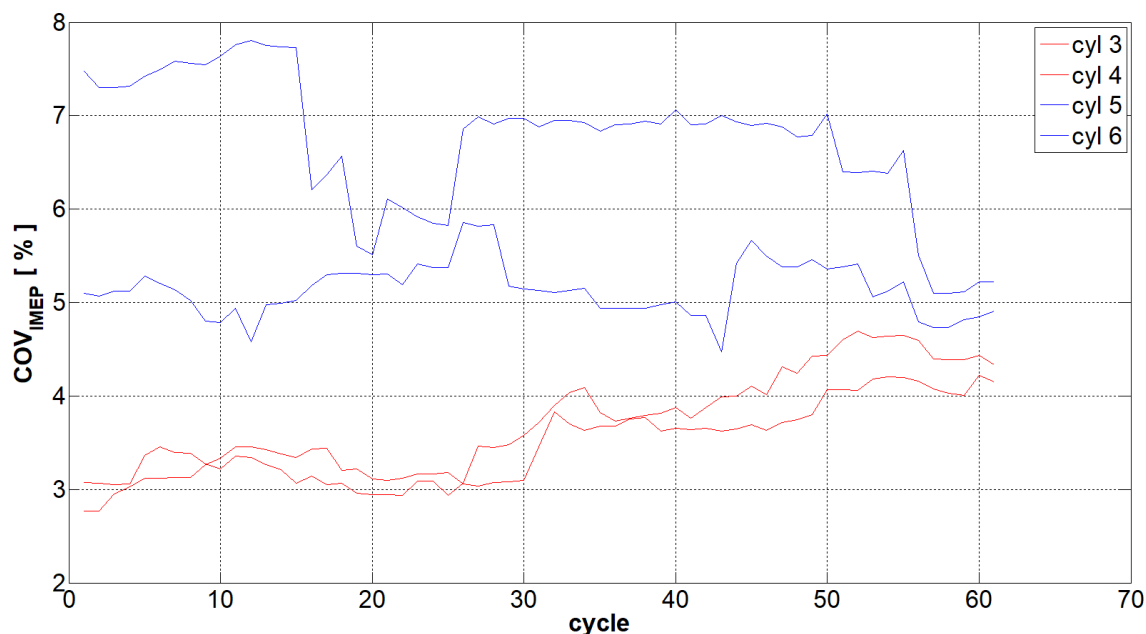


Figure C.3: COV values with Methanol at 375 ekW

COV_{pmax}

Before comparing the COV_{pmax} , the formulas 4.1 and 4.2 from chapter 4 are given here again:

$$COV_{pmax} = \frac{std_{pmax}}{Pmax_{avg}} \cdot 100\% \quad (4.1 \text{ revised})$$

$$std_{pmax} = \sigma_{pmax} = \sqrt{\frac{\sum_{i=1}^m (P_i max - Pmax_{avg})^2}{m - 1}} \quad (4.2 \text{ revised})$$

Now to compare these calculations with the Kibox calculations the settings of the Kibox are needed. These can be found in the Kibox-cockpit under Administration / Signal types / Cylinder pressure / Maximum and are shown in figure.

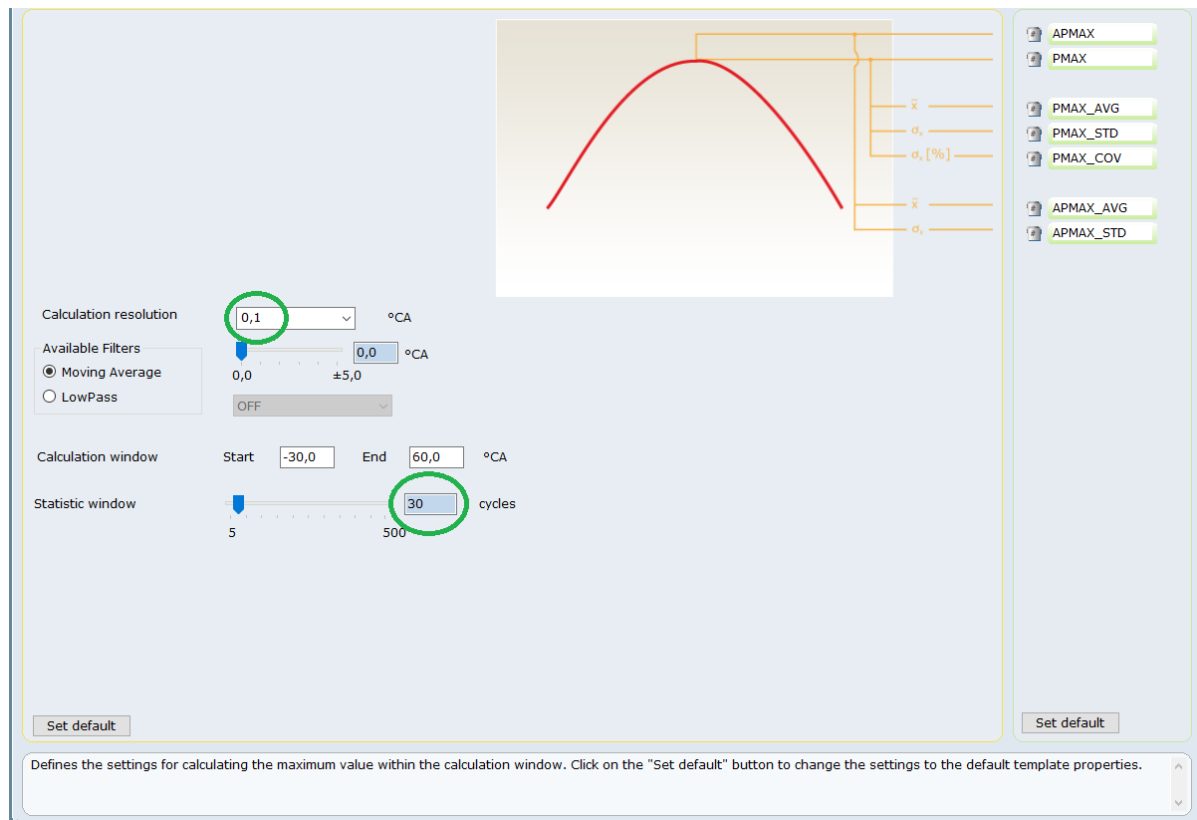


Figure C.4: Kibox settings of IMEP

Again is found that the Kibox calculation is based on 30 cycles, but the resolution is different as compared to the IMEP calculations from Kibox. The resolution is 0.1 °CA used by Kibox similar to my own calculations. In table C.2 the values of COV_{pmax} from Kibox are compared to my own calculated COV_{pmax} .

Table C.2: COV_{imep} at 375 ekW for 100 % methanol with own calculations and (standard) Kibox calculations

	$COV_{pmax}(m=60)$	$COV_{pmax}(m=30)$	Kibox (30 th)	Kibox min-max
Cylinder 3	11.5732 %	11.2500 %	11.2500 %	9.52 - 12.74 %
Cylinder 4	11.1485 %	10.5598 %	10.5598 %	9.62 - 12.64 %
Cylinder 5	11.9649 %	12.5411 %	12.5411 %	11.13 - 13.42 %
Cylinder 6	14.6725 %	15.6003 %	15.6003 %	12.98 - 19.04 %

From table C.2 can be seen that when the amount of cycles used is lowered to 30 in my own calculation (m=30), than the calculated COV_{imep} is exactly equal to the 30th value of the Kibox. This may also be expected because now the resolution and the amount of cycles are equal. The only variable that has not been found in the Kibox data is the way the standard deviation was calculated,

but with these exact similar results it may now be stated that the Kibox used the same formula as stated in formula 4.2 .

C.0.2. Stability increase after replacement of the injector of cylinder 4

This section will validate that the cylinder 4 has the best stability performance due to the replacement of the injector before the performance tests. Measurements carried out on the performance test day of 22-01 will be compared with earlier measurements. On 21-01 on 16:04 the injector of cylinder 4 is replaced due to dirt in the injector. The dirt made the engine stop at a second attempt to reach maximum engine power. On the first attempt a maximum of 430 ekW was reached. On 21-01 at 12:46 and 12:48 two measurements were taken just before 375 ekW engine power was reached. The load step was from 330 ekW to 375 ekW. The ignition timing was at 20 °CA BTDC. To get a valid comparison the COV_{imep} values of all cylinders are compared in table C.3 where both values approximately reached 375 ekW, 20 °CA BTDC, +/- 500 NO_x. Following are the first two measurements before replacement of the injector at cylinder 4 and the third measurement after the replacement of cylinder 4.

Table C.3: COV_{imep} at 375 ekW for 100 % methanol before and after replacement of injector cylinder 4

	COV_{imep} (CYL3)	COV_{imep} (CYL 4)	COV_{imep} (CYL 5)	COV_{imep} (CYL 6)
Before replacement 21-01 12:46	3.15 %	10.59 %	4.40 %	5.21 %
Before replacement 21-01 12:48	3.37 %	17.70 %	3.86 %	5.17 %
After replacement 22-01	4.02 %	3.72 %	4.97 %	6.11 %

In table C.3 we see at cylinder 3, 5 and 6 stable but slightly lower COV_{imep} values before replacement of the injector of cylinder 4. This variation of +/- 1% has also been seen with changing ignition timings and within the data set of the Kibox itself. Also the circumstances were different because the data set before replacement was not a stabilized measurement at 375 ekW but more a quick measurement between load steps to get to the maximum load.

But the COV_{imep} of cylinder 4 is significantly higher with 10.59 and 17.7% before replacement than after the injector replacement with 3.72 %. In Heywood [15, p417] it is stated that when COV_{imep} exceeds 10% the ICE in automotive will cause driveability problems. For our engine this is also valid because 3 hours after this measurement was taken the engine failed and the injector of cylinder 4 needed replacement. After the replacement, some dirt was found in the injector of cylinder 4. After the replacement of injector 4 a much lower COV_{imep} was calculated. The COV_{imep} value of cylinder 4 is lowest after the injector replacement, while all other COV_{imep} values increased. This could suggest that there are also (smaller) dirt particles in the injector of cylinder 3, 5 and 6.

To further investigate the effect of the injector replacement also the COV_{pmax} values are given in table C.4.

Table C.4: COV_{pmax} at 375 ekW for 100 % methanol before and after replacement of injector cylinder 4

	COV_{pmax} (CYL3)	COV_{pmax} (CYL 4)	COV_{pmax} (CYL 5)	COV_{pmax} (CYL 6)
Before replacement 21-01 12:46	9.84 %	9.20 %	13.64 %	14.73 %
Before replacement 21-01 12:48	8.63 %	9.28 %	11.85 %	13.77 %
After replacement 22-01	11.57 %	11.15 %	9.28 %	14.67 %

The variation in maximum pressure as shown in the COV_{pmax} can not be proven to indicate a stability problem as shown in table C.4. But the value of (maximum) pressure itself can give a better insight into the injector of cylinder 4 not working appropriately. This is shown in figure C.5. Here the mean pressure of 60 cycles is shown. The mean pressure of cylinder 4 is compared to the mean pressure of all four measured cylinders. It is clearly significantly lower than for all other cylinders.

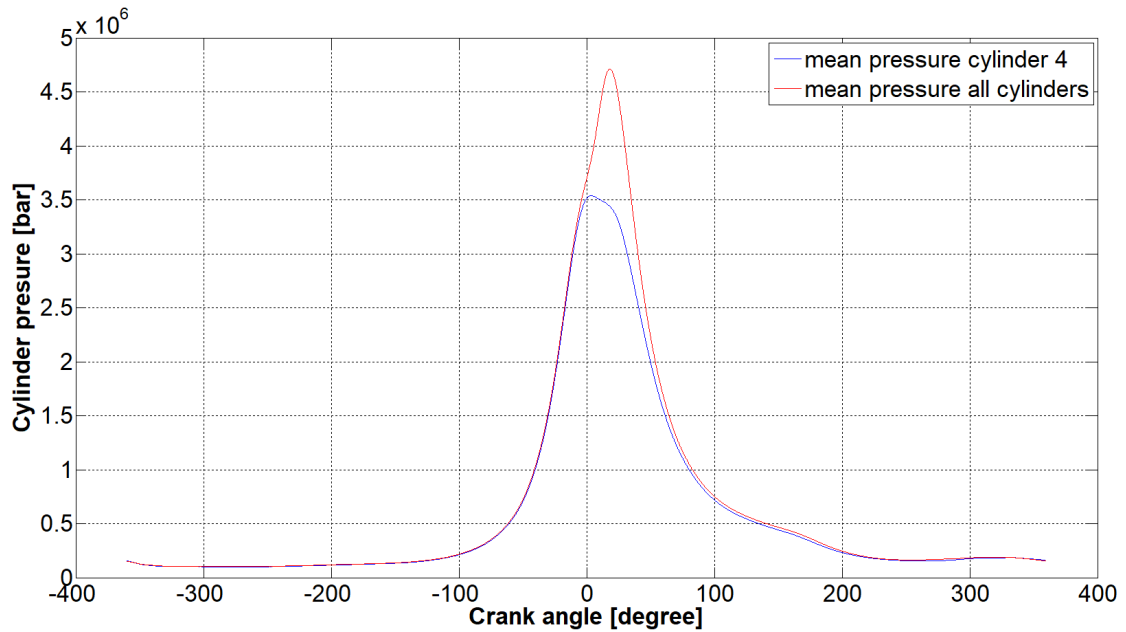


Figure C.5: Mean pressure of cylinder 4 compared to the mean pressure of cylinders 3,4,5, and 6

Now going back to the COV_{imep} . In C.6 the COV_{imep} values from the Kibox are shown. Clearly is visible that before replacement the COV values for most of the cycles show to be above the unstable limit of 10%. And the improvement of the COV value after replacement of the injector of cylinder 4 is visible. The COV_{imep} after replacement stays clearly far below the unstable limit of 10%. The COV_{imep} values are slightly different from the one calculated above, the alternative calculating method of the Kibox will be described in C.0.1.

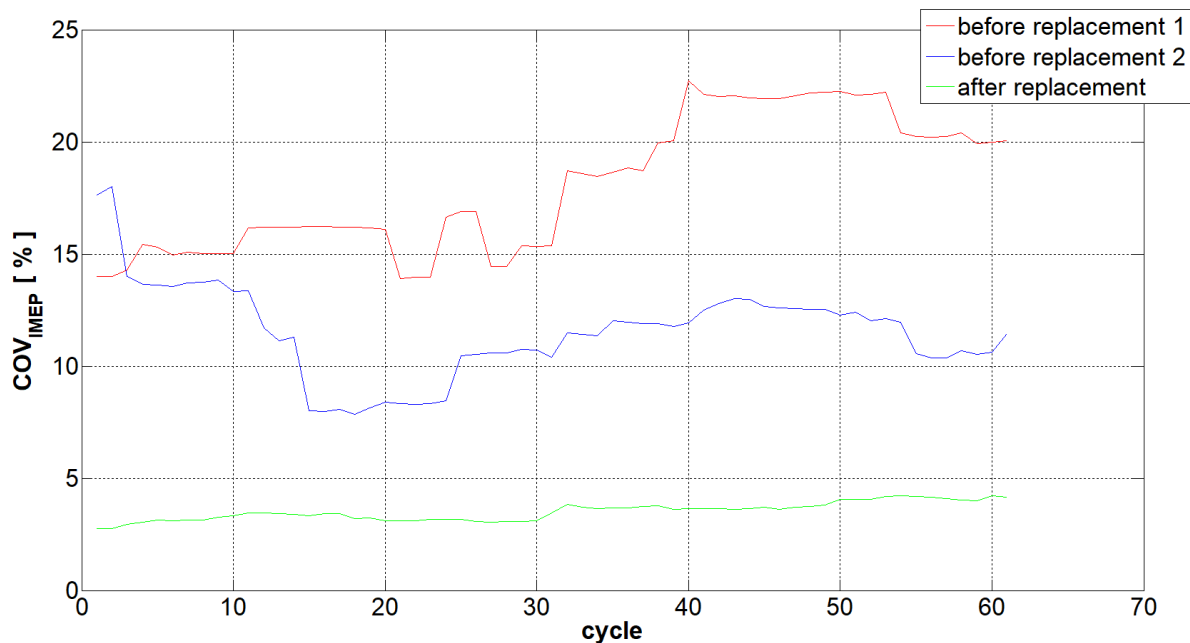


Figure C.6: COV values of cylinder 4 from Kibox before and after replacement.

C.0.3. Check the influence of 2 degrees difference in IVO

The valve timings are retrieved from a old piece of paper where the values are unclear written/printed. An interpretation error exists in the inlet valve open (IVO) timing. Where some of us interpret the

number as an 8 others read a 6. This results in an IVO of $360-6.7=353.3$ °CA BTDC or $360-8.7=351.3$ °CA BTDC. In this section the influence of this 2-degrees error will be discussed.

In the *CAT3508.m* engine parameter file the inlet valve open is stated as IO and will be changed by 2 degrees. The changes are carried out on both models, the original NG engine model and the modified methanol model. Nevertheless, only shown here in this evaluation for the NG model. The impact is expected to be visible in the calculated volume (IV and V_1), trapped temperature (T_1) and trapped mass (m_1) and will be shown in table C.5.

Table C.5: Influence of 2 degrees change in IVO

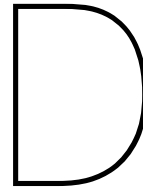
	Inlet volume (IV) (m ³)	Volume inlet close (V_1)(m ³)	T_1 (K)	m_1 (kg)
IVO at 353.3 °CA BTDC	4.1975e-04	0.0045715	3.26314e+02	0.008154
IVO at 351.3 °CA BTDC	4.0850e-04	0.0045715	3.27158e+02	0.008175
Difference in %	2.68 %	0 %	0.26 %	2.59 %

As can be seen from table C.5 that this small error has more than 2% effect on the inlet volume and m_1 . V_1 is not influenced due to the fact it has been calculated with the crank angle at inlet valve close and not with the inlet valve open. T_1 is only changing by 0.26%.

Due to these changes in the initial conditions of the model this will have a effect on the final results, a few of those will be shown in table C.6. Here the small change of 2 °CA is recognized to have a maximum of 0.26% effect in the end at final results of the model.

Table C.6: Influence of 2 degrees change in IVO on final results of the model

	thermodynamic efficiency (%)	isfc (g/kWh)	Max temperature (K)
IVO at 353.3 °CA BTDC	50.85	218.0	1466.3
IVO at 351.3 °CA BTDC	50.83	218.2	1470.1
Difference in %	0.04 %	0.09 %	0.26 %



Test plan for the engine on methanol

For the performance tests with the G3508A engine on 100% methanol a test plan is made. In this test plan a step by step action plan is made to make sure the test will be conducted safely and efficient during the 2 weeks of testing on the engine. This plan can be executed when the engine is on the test bed. Before this plan is executed the task risk analyse (TRA) needs to be known for all collaborators and is shown in Appendix F.

First step: safety checks

Fuel system

- First check system on leakage with compressed air.
- After successful check fill fuel system with methanol.
- With protective gear (clothes, air mask and gloves) check system with mobile vapor detection system. Or check installed vapor system before entering the room. Check fuel system with step by step increased pressure.

Control systems

- Check where possible all options on the secondary control system to work.
- Check where possible all options on the primary control system to work.

First run the engine on natural gas

- Before first start of the engine on methanol first start the engine on NG to check if all (sub)systems are working correct. Make use of standard checklist to start engine on NG.
- When all sub systems are working, shut down the engine and change all systems to be able to start on methanol.

Second step: first performance runs on methanol

- When starting the engine for the first time on methanol make sure no one is in the engine room and remote start the engine from the control room.
- The first starts will be done at 0% load, connected to the generator with the following conditions:
 - Fuel: 0,0982 g/cycle. (with $\rho = 784.5 \text{ g/l}$) = 0.125 CC/cycle. (15% of fuel flow at max load).
 - Airflow, stoichiometric (AFR=6.5): 0,638 g/cycle.
 - Pressure of fuel: 3 bar
 - Injection time: 3,41 ms (calculated with 2200CC/min injectors).
 - Deadtime to be included: 0,45-0,525 ms at 14 Volt and 3 bar (unknown at 24V).
 - Throttle positioning: controlled at constant engine speed of 1500 RPM.
 - Ignition moment: 18 degrees before TDC.
 - End of injection: Inlet valve open.

Table D.1: Overview of performance tests

Engine load:	25%	50%	75%	100%	Important parameters
Initial performance runs(step 2)					
Stable 0% load run					p, CA, HR, $T_{exhaust}$
Stable load runs					p, CA, HR, $T_{exhaust}$
Ignition timing at 18 DB TDC	-	-	-	-	p, CA, HR, NO_x , $T_{exhaust}$
Ignition timing at 16 DB TDC	-	-	-	-	p, CA, HR, NO_x , $T_{exhaust}$
Ignition timing at 14 DB TDC	-	-	-	-	p, CA, HR, NO_x , $T_{exhaust}$
Ignition timing at 12 DB TDC	-	-	-	-	p, CA, HR, NO_x , $T_{exhaust}$
Ignition timing at 10 DB TDC	-	-	-	-	p, CA, HR, NO_x , $T_{exhaust}$
NOx 500 mg/nm3	-	-	-	-	p, CA, HR, dp/dt
NOx 400 mg/nm3	-	-	-	-	p, CA, HR, dp/dt
NOx 300 mg/nm3	-	-	-	-	p, CA, HR, dp/dt
NOx 200 mg/nm3	-	-	-	-	p, CA, HR, dp/dt
NOx 100 mg/nm3	-	-	-	-	p, CA, HR, dp/dt
NOx 1000 mg/nm3	-	-	-	-	p, CA, HR, dp/dt
NOx 2000 mg/nm3	-	-	-	-	p, CA, HR, dp/dt
NOx 3000 mg/nm3	-	-	-	-	p, CA, HR, dp/dt
Max AFR	-	-	-	-	p, CA, HR, NO_x
Temperature variation T_1	-	-	-	-	p, CA, HR, NO_x
Optimisation runs (step 3)					
End of injection + 2 degrees	-	-	-	-	p, CA, HR, NO_x
End of injection + 4 degrees	-	-	-	-	p, CA, HR, NO_x
End of injection + 6 degrees	-	-	-	-	p, CA, HR, NO_x
End of injection + 8 degrees	-	-	-	-	p, CA, HR, NO_x
End of injection TBD degrees	-	-	-	-	p, CA, HR, NO_x
End of injection TBD degrees	-	-	-	-	p, CA, HR, NO_x
End of injection TBD degrees	-	-	-	-	p, CA, HR, NO_x
End of injection TBD degrees	-	-	-	-	p, CA, HR, NO_x
Changed spark plug (a few tests from above again)	-	-	-	-	p, CA, HR, NO_x
Optimizing efficiency steps	-	-	-	-	p, CA, HR, NO_x

- Next run stable at 25, 50, 75 and 100% load by changing lambda, ignition timing and manifold temperature. The lambda table in the control system must be adjusted for running stable engine operations.
- After stable running on 25% load determine the optimised ignition moment. Start at 18 degrees before TDC and change in steps of 2 degrees at all possible loads to determine best injection moment. Determine after these first series if going lower than 10 degrees or above 18 degrees TDC is optional. Ignition moment is performed at a constant NO_x emission of 1000 mg/nm³ (equal to +/- 680 ppm).
- Then the engine must run stable on constant NOx emission. Determine at which constant NOx emissions the engine can run. Vary settings for mg NOx from 500/400/300/200/100 mg/nm³. And from 500/1000/2000 and 3000 at 25% engine load. For every step perform the measurements at 50,75 and 100% load. Choose a NOx setting for further tests. Also determine available working area by searching maximum AFR at 25%, 50%, 75% and 100% engine load.
- Determine the effect of changing temperatures (T_1) by increased or decreased cooling in the aftercooler.
- Repeat above test and switch between test until stable and reliable measurements are shown.

Third step: optimising performance runs on methanol

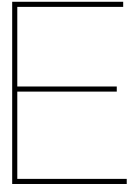
- Injection moment has been set at end of injection equal to opening inlet valve at all loads. Varying this injection moment and make measurements at 25, 50, 75 and 100% load. Start with small steps of + 2 degrees after opening inlet valve. Determine after a few runs the next steps. The inlet valve is open for around 180 degrees crank angle.
- Change spark-plugs and repeat above essential tests.
- Optimize efficiency by varying all above parameters at all load steps.

Due to the short testing period of 2 weeks I expect that not all tests of the third step can be done. To give a clear picture of how many tests can be done an overview is made for all planned performance tests in table D.1. When taking a 30 minutes for every test, then already 30 hours of testing is needed for the initial runs.

Analyses during performance tests

Pressure and crank angle (CA) are important parameters as input for the model. Heat Release (HR), specific brake power (SBP) and emissions are important parameters to compare the model with the performance tests. This comparison will be done on a later stage than the performance test. The HR-curve of the Woodward control and Kibox measurement system does not take heat losses into account and therefore is not suited to compare the HR with other (diesel) engines. But it gives directly a good indication of the combustion process. During the tests the following must be observed with the Woodward control system and the Kibox measurement system:

- Pmax measurements: It is possible that the in cylinder pressure signal will fluctuate at maximum pressure due to the location of the pressure sensor. It does not directly have to mean that it is due to knocking of the engine. The placement of the pressure sensor in the cylinder is very important for expecting this fluctuations. When the sensor is placed in a gap more fluctuations are expected. In the model the pressure signal can be made smooth with mathematic algorithms. The pressure range (0-150 bar) and the error in the pressure sensor are also important for the measurements. With the pressure curve and Pmax the detonation/knocking, misfire and efficient burning of the fuel can be detected.
- Crevice effects: As the cylinder pressure increases the gas flows into crevices, such as the region between the piston, piston rings and cylinder wall. During ignition it is possible that the fuel in this gas flow will not burn. At expansion a fraction can go into the crankcase but most of it will leave the engine with the exhaust. This unburned gas mix is expected to be a few percent. Due to the zero valve overlap of the engine no new fuel can go directly to the exhaust valve.
- Incomplete combustion: When combustion of the cylinder charge is incomplete then the exhaust gases contain more than normal combustible species. Due to the crevice effect a good operating SI engine has hydrocarbon emissions 2 to 3 percent of the fuel mass [15, p362]. When increased hydrocarbon emissions are measured incomplete combustion is expected. In the HR curve this can be seen due to a lower peak and a more flat late combustion part in the curve.
- Maximum in cylinder temperature: With increasing temperature in the cylinder the NO_x emissions will increase. The (maximum) temperature will not be measured in the cylinder but the peak in the HR-curve will give an indication of the peak temperature.
- Outside temperature vs coldstart problems. Cold start problems are expected with a T₁ temperature <-1 °C. Monitor outside temperatures at start.
- Pmax position after TDC. Optimizing this position will give better performance and efficiency.



Sensors and calibrationreports

An overview of the calibration of the Dewetron sensors is given in table E.1 and E.2

Kalibratie van Dewesoft id.nr. 2016-28

Sensornaam	Kabel	Sensor	Input in Dewesoft	Opmerkingen
Thermocouple (TC) 3 mm			[16]	Setpoint: 40 // 90 //135 [oC]
			Channel:	
Temperature(T) air filter R	1	1	0	40,3//90,9//135,2
T air filter L	2	2	1	40,4//90,9//135,2
T Gas R before cooler (BC)	3	3	2	40,2//90,7//135,0
T Gas L BC	5	5	3	40,3//91,0//135,3
T Gas NC	6	6	4	40,2//90,3//135,1
T Oil ENG IN	8	8	5	40,2//90,5//134,9
T OIL Sump	9	9	6	39,7//90,5//139,9
T Methanol	10	10	7	40,1//90,4//134,8
spare	11	11	7	40,2//90,5//134,5
			[EPAD2-TH8]	
TC 1 mm			Channel:	
Extern (E1)	80	80	0	39,7//89,3//135,1
E2	81	81	1	39,6//89,1//134,5
E3	82	82	2	39,6//89,0//134,6
E4	83	83	3	39,6//89,2//135,1
E5	84	84	4	39,5//88,8//134,1
E6	85	85	5	39,5//88,8//134,4
E7	86	86	6	39,5//88,8//134,3
E8	87	87	7	39,4//88,5//133,7
E9	88	88	8	39,5//89,0//134,8
E10	89	89	9	39,6//89,2//135,1
NB: 135 graden Celsius in RvA gekalibreerde droogblokken id.2006-417 90 graden Celsius in RvA gekalibreerde vloeistofbad id. 2006-355 40 graden Celsius in RvA gekalibreerde vloeistofbad id. 2006-355				
			[DAQP]	
Pressure sensor 10 bar			Channel	Setpoint: 0 // 10 [bar] test: 5[bar] *
P1	1	61	6	3,895 mA // 19,865 mA // 5,013 bar
P2	2	62	7	3,973 mA//19,865 mA // 5,015 bar
P3	3	63	8	3,942 mA// 19,876 mA // 5,016 bar
P4	4	64	9	3,948 mA// 19,823 mA // 5,012 bar
P5	4	65	10	3,932 mA// 19,861 mA // 5,013 bar
P6	4	66	11	3,947 mA// 19,844 mA // 5,012 bar
P7	4	67	12	4,006 mA// 19,900mA // 5,00 bar
P8	4	68	13	4,022 mA// 19,894 mA // 4,993 bar

Figure E.1: Calibratie sensoren dewetron(1/2)

			[DAQP]	
Pressure sensor 2,5 bar			Channel	Setpoint: 0 // 2,5 [bar] test: 1,25 [bar]
70	1	70	6	3,912 mA // 19,883 mA //1,2548 bar
71	1	71	7	3,9266 mA // 19,864mA // 1,2550 bar
72	1	72	8	3,9276 mA // 19,894 mA // 1,2545 bar
73	1	73	9	3,9087 mA // 19,867 mA // 1,2552 bar
<p>* op setpoint 0 and 10 bar mA is afgesteld zodat Dewesoft en kalibratie drukgenerator gelijk staan NB: Drukkalibraties uitgevoerd met de RvA-gekalibreerde drukgenerator (id.2012-401) Gekalibreerd door: 26-9-2019 J.J. Bosklopper</p> <p>Onder supervisie van: 26-9-2019 Rene van Eck</p>				

Figure E.2: Calibratie seensoren dewetron (2/2)

F

Task risk analysis




Taak Risico Analyse

<i>Projectnaam</i>	Green <u>Maritime</u> Methanol Project		
<i>Omschrijving werkzaamheden</i>	Test G3508 met methanol		
<i>Testperiode</i>	8 januari tot 24 januari 2020		
<i>Locatie</i>	Proefstand Pon Power, Ketelweg 20, 3356 LE Papendrecht		
<i>Projectorganisatie</i>	Project Manager	Wim van Sluijs	06-10344510
	Analyse	Jurian Bosklopper	
	<u>Woodward</u> Engineer	Marc Smeets	
	Test Bench Engineer	Jurgen van der Velden	06-22397236
	Service Manager Workshop	Patrick Korevaar	06-51170569
	QHSE Manager	Jacco Klijn	06-22123217
	BHV Coördinator	Pim Zijderveld	06-22799852
Alarmnummer Pon Power 078-6420444			
<i>Voorschriften</i>	<ul style="list-style-type: none"> • Algemene veiligheidsvoorschriften Pon Power BV • Beschikking Methanol 1 november 2019 • MSDS Methanol • IBC met methanol aangesloten op de proefstand dient te voldoen aan de PGS 31:2018 versie 1.1 voorwaarden zoals beschreven in paragraaf 4.1 en 4.2 met uitzondering van voorschrift 4.2.2 (zie beschikking) • Methanol safe handling manual - health and safety module 		
<i>Datum</i>	4-12-2019		
<i>Opgesteld door</i>	Wim van Sluijs		
<i>Goedgekeurd door</i>	Jacco Klijn		

Figure F.1: Task risk analyse (1/6)



Nr.	Taakstap of activiteit	Gevaren	Beheersmaatregelen	Actie door
1.	Toegepaste brandstof methanol	<ul style="list-style-type: none"> • Flam. Liq. 2 H225 Licht ontvlambare vloeistof en damp. • Acute Tox. 3 H301 Giftig bij inslikken. • Acute Tox. 3 H311 Giftig bij contact met de huid. • Acute Tox. 3 H331 Giftig bij inademing. • STOT SE 1 H370 Veroorzaakt schade aan organen. 	<ol style="list-style-type: none"> 1. Methanol toepassen in een gesloten systeem 2. Gevarenaanduiding op IBC's en leidingen <p>Gevarenpictogrammen</p>  <p>GHS02 GHS06 GHS08</p> <ol style="list-style-type: none"> 3. Voor goede ventilatie/afzuiging in de werkplaatsen zorgen. 4. Blootstelling via inslikken, contact met de huid en inademing voorkomen. 	Project Manager
2.	Veiligheidsbriefing voor start werkzaamheden	Geen	<ul style="list-style-type: none"> • Project Kick off over veiligheidsmaatregelen • Taak Risico Analyse doornemen met alle betrokkenen (zie projectorganisatie in header) 	Project Manager
3.	Plaatsen van 1.000 liter IBC met methanol achter bij proefstand	<ul style="list-style-type: none"> • Lekkage methanol • Methanol brand • Blootstelling methanol 	<ul style="list-style-type: none"> • Plaatsen IBC volgens plattegrond vergunning • Overige 2 IBC's staan in de vatenkast Expeditie • Maximale opslag 3 IBC's met methanol op het terrein • Afstand IBC's tot gasflessen minimaal 5 meter • Methanol pomp staat buiten opgesteld • Noodknop methanol pomp → indrukken = stop pomp • IBC's voldoen aan: <ul style="list-style-type: none"> - Metaal (31A, 31B en 31N) of 	Project Manager

2 / 6

Figure F.2: Task risk analyse (2/6)



			<ul style="list-style-type: none"> - Kunststof (31H1 en 31H2) • IBC is opgesteld achter hek met poort • IBC's worden geplaatst op een metalen lekbak • Daartoe heeft de opvangvoorziening een opslagcapaciteit van tenminste 110 % van de inhoud van de grootste verpakking • IBC's die als tijdelijke tankopslag worden gebruikt, zijn geëtiketteerd volgens het ADR of de Europese CLP-verordening • Indien een IBC moet worden geleegd en rechtstreeks wordt gekoppeld aan een procesinstallatie, moet worden voorkomen dat de gevaarlijke vloeistof terug kan stromen in de IBC. 	
4.	Aansluiten en testen van de methanol brandstofleidingen.	<ul style="list-style-type: none"> • Lekkage methanol • Methanol brand • Blootstelling methanol <div style="border: 1px solid black; padding: 5px; width: fit-content;"> <p>LOW RISK OF VAPOR/ LOW RISK OF VOLUME SPLASH Fire retardant clothing Gloves (Silvershield or disposable nitrile) Safety glasses with side shields Full boot cover</p> </div>	<ul style="list-style-type: none"> • PBM's bij het werken aan het brandstofsysteem met methanol: <ul style="list-style-type: none"> - veiligheid laarzen of schoen cover - Nomex overall - Ansell Handschoenen Sol-Vex 37-185 - Volgelaatsmasker met AX filter • Noodstop methanol pomp in proefstand ruimte. • Brandblusser AFFF • Minimaal worden een sluitende veiligheidsbril en nitril handschoenen gedragen • Chemisch bestendige materialen omvatten butyl rubber of nitril rubber. • Gebruik een chemische bril wanneer er een potentieel is voor oogcontact met methanol, inclusief damp. Een volledig gezichtsscherm kan over een veiligheidsbril worden gedragen voor extra bescherming, maar niet als vervanging voor een bril. • Chemisch bestendige kleding / materialen moeten worden gedragen indien herhaald 	Project Manager

3 / 6

Figure F.3: Task risk analyse (3/6)



			of langdurig huidcontact met methanol wordt verwacht. Deze omvatten rubberen laarzen, resistente handschoenen en andere ondoordringbare en resistente kleding.	
5.	Proefstand	<ul style="list-style-type: none"> • Lekkage methanol • Methanol brand • Blootstelling methanol 	<ul style="list-style-type: none"> • Toegang test cel uitsluitend na toestemming Project Manager (deur standaard op slot) • Wideband IR vlam detectie in testruimte en bij methanol opslag. • Brandblusser(s) buiten en in testruimte. • > 200 ppm gas detectie alarm • Gelaatsmasker met AX filter. • Rubber handschoenen. • Overall • Ventilatie in testruimte • Recirculatie ventilatie proefstand uitzetten • Aarding motorblok • Vanwege de ontvlambaarheid van methanoldamp kan statische elektriciteit ontstaan en ontbranden. Daarom moeten aarding altijd worden toegepast wanneer er een potentieel is voor statische elektriciteit en is vereist voor alle apparatuur. • Bij een concentratie in de lucht < 200 ppm is geen adembescherming nodig • Brandblussers Koolzuur (2x) 	
6.	Testdraaien op proefstand	<ul style="list-style-type: none"> • Lekkage methanol • Methanol brand • Blootstelling methanol 	<ul style="list-style-type: none"> • Controle installatie voor aanvang van werkzaamheden • H2 gasdetector voor in de testruimte. • Ventilatie niet op circuleren. • Veiligheidsinspectie uitvoeren • Brandblusser paraat • Noodknop achterzijde, proefstand en controlekamer 	Project Manager

4 / 6

Figure F.4: Task risk analyse (4/6)



			<ul style="list-style-type: none"> - Gehele testcel verlaten - Testcel entry mangatbewaking • Ontruimingsprocedure Pon Power (Evacuatie Gebouw 1 en 2) via alarmnummer 078-6420(444) of alarmknop 	
7.	Uit bedrijf nemen van methanol voorziening (dagelijks aan het einde van de werkdag)	<ul style="list-style-type: none"> • Lekkage methanol • Methanol brand • Blootstelling methanol 	<ul style="list-style-type: none"> • Toevoer dichtzetten en leidingen leegdraaien. • Purgen met stikstof • Brandblusser paraat 	Project Manager
8.	Vervangen IBC container	<ul style="list-style-type: none"> • Lekkage methanol • Methanol brand • Blootstelling methanol 	<ul style="list-style-type: none"> • Uit bedrijf nemen van methanol voorziening (zie stap 7) • Vervisselen IBC met heftruck 	Project Manager
9.	Uit bedrijf nemen van methanol voorziening na einde test: <ul style="list-style-type: none"> • Leidingen leegmaken en buiten laten uitdampen • Leidingen verwijderen • Methanol IBC container laten ophalen door leverancier 	<ul style="list-style-type: none"> • Lekkage methanol • Methanol brand • Blootstelling methanol 	<ul style="list-style-type: none"> • Uit bedrijf nemen van methanol voorziening (zie stap 7) • Afvoeren IBC met heftruck 	Project Manager
10.	Eerste hulp maatregelen	Lekkage, vrijkomen methanol	<p>Na het inademen:</p> <ul style="list-style-type: none"> • Verse lucht of zuurstof toedienen; deskundige medische hulp inroepen. Bij bewusteloosheid ligging en vervoer in stabiele zijligging. • Slachtoffer in de open lucht brengen en rustig neerleggen. <p>Na huidcontact:</p> <ul style="list-style-type: none"> • Onmiddellijk met water en zeep afwassen en goed naspoelen. • Wanneer de huid geïrriteerd blijft, een dokter raadplegen. <p>Na oogcontact:</p>	Project Manager

5 / 6

Figure F.5: Task risk analyse (5/6)



			<ul style="list-style-type: none"> Ogen met open ooglid een aantal minuten onder stromend water afspoelen en dokter raadplegen. Oogdouche bij toiletten kantine Binnendienst <p>Na inslikken:</p> <ul style="list-style-type: none"> Geen braken teweegbrengen Een brakende, op zijn rug liggende persoon op zijn zij leggen Deskundige medische hulp invoeren Zie sectie 4. Eerste hulp maatregelen MSDS Methanol MSDS Methanol op papier beschikbaar op lokatie 	
11.	Brandbestrijding	Lekkage, vrijkomen methanol, brand	<ul style="list-style-type: none"> Geschikte blusmiddelen: CO2, bluspoeder of waterstraal. Grotere brand met waterstraal bestrijden of met schuim, dat tegen alcohol bestand is. Brandblusmaatregelen op omgeving afstemmen. Zie sectie 5. Brandbestrijdingsmaatregelen MSDS Methanol MSDS Methanol op papier beschikbaar op lokatie 	Project Manager
12.	Maatregelen bij het accidenteel vrijkomen van methanol	Blootstelling aan methanol	<ul style="list-style-type: none"> Zie sectie 6. Maatregelen bij het accidenteel vrijkomen van methanol MSDS Methanol op papier beschikbaar op lokatie 	Project Manager

Figure F.6: Task risk analyse (6/6)



Engine and Generator datasheet

In figure G.1 the efficiencies of the engine are given with NG as a fuel at 100, 75 and 50% load. In figure G.2 the efficiency is shown of the generator.

CATERPILLAR GAS ENGINE DATA		28 JUL, 1993	ID NUM: APERFAB30	
ARRANGEMENT	OPERATION			
ENGINE MODEL:	3508	FUEL	NATURAL GAS	
ENGINE SPEED:	1500	AFTERCOOLER (DEG.C)	32	
COMPRESSION RATIO:	12:1	JACKET WATER (DEG.C)	127	
COOLING SYSTEM	2 & 3 CIRCUIT	MIN. FUEL PRESSURE (KPAg)	10	
FUEL SYSTEM	LPG DELTEC	MIN. METHANE NUMBER	75	
COMBUSTION	LEAN BURN	MAX. AMBIENT CONDITIONS	150m @ 25 C	
EMISSION LEVEL	TA LUFT (NOx, CO)			
LOAD		100%	75%	50%
RATING AND EFFICIENCY				
LHV OF FUEL	MJ/Nm3	34.5	34.5	34.5
ENGINE POWER	BKW	517	388	259
ENGINE EFFICIENCY	%	35.2	33.9	31.0
THERMAL EFFICIENCY	%	46.1	48.4	53.0
TOTAL EFFICIENCY	%	81.3	82.2	84.0
HEAT BALANCE DATA				
LHV INPUT	KW	1469	1145	834
HEAT REJ. TO JACKET	KW	316	263	225
HEAT REJ. TO A/C	KW	99	59	25
HEAT REJ. TO ATMOSPHERE	KW	78	65	52
HEAT REJ. TO LUBE OIL	KW	89	74	64
HEAT REJ. TO EXH. (LHV to 25	KW	370	296	209
HEAT REJ. TO EXH. (120 C)	KW	272	216	153
EXHAUST STACK TEMP.	DEG C	426	428	429
EXHAUST GAS FLOW	Nm3/BKW-hr	4.42	4.65	4.92
EXHAUST MASS	kG/BKW-hr	5.53	5.81	6.14
ENGINE DATA				
FUEL CONSUMPTION	MJ/BKW-hr	10.23	10.63	11.61
AIR FLOW	Nm3/BKW-hr	4.12	4.33	4.57
INLET MAN. PRESS.	KPAa	223	170	121
EXHAUST O2 (DRY)	%	8.2	7.9	7.7
LAMBDA		1.56	1.55	1.51
TIMING	DEG. BTDC	18	18	18
NOISE - MECH @ 1 M	dB (A)	98	97	96
NOISE - EXH @ 1.5 M	dB (A)	109	108	107
NOx EMISSION (corr. 5% O2)	mg/Nm3	500	500	500
CO EMISSION (corr. 5% O2)	mg/Nm3	650	650	650
CONDITIONS AND DEFINITIONS				
TOTAL JACKET WATER HEAT:				
COMBINED = JACKET HEAT + OIL COOLER HEAT				
2- CIRCUIT AND 3- CIRCUIT = JACKET HEAT				
TOTAL AFTERCOOLER HEAT:				
COMBINED AND 3-CIRCUIT = AFTERCOOLER HEAT x A/C HEAT REJ. FACTOR				
2-CIRCUIT = AFTERCOOLER HEAT x A/C HEAT REJ. FACTOR + O/C HEAT				
THERMAL EFFICIENCY:				
32 TO 54 DEG. C SCAC = JACKET HEAT + O/C HEAT+ EXH. HEAT TO 120C				
70 DEG. C SCAC = JACKET HEAT + O/C HEAT+ EXH. HEAT TO 120C + A/C HEAT				
TOTAL EFFICIENCY = ENGINE EFF. + THERMAL EFF.				
ENGINE PERFORMANCE OBTAINED AND PRESENTED IN ACCORDANCE WITH ISO 3046/1				
CONSULT ALTITUDE CURVES FOR AMBIENT CONDITIONS ABOVE THE STATED MAXIMUM				

Figure G.1: Motor datasheet

GENERATOR DATA**FEBRUARY 03, 2020**For Help Desk Phone Numbers [Click here](#)

Selected Model				
Engine: 3508	Generator Frame: 685	Genset Rating (kW): 490.0	Line Voltage: 400	
Fuel: Natural Gas	Generator Arrangement: 6I3095	Genset Rating (kVA): 490.0	Phase Voltage: 230	
Frequency: 50	Excitation Type: Permanent Magnet	Pwr. Factor: 1.0	Rated Current: 707.3	
Duty: CONTINUOUS	Connection: SERIES STAR	Application: EPG	Status: Current	
<small>Version: 38901 /38433 /38285 /4455</small>				
Spec Information				
Generator Specification		Generator Efficiency		
Frame: 685	Type: SR4	No. of Bearings: 1	Per Unit Load	
Winding Type: FORM WOUND	Flywheel: 521.0		kW	
Connection: SERIES STAR	Housing: 00		Efficiency %	
Phases: 3	No. of Leads: 6	0.25	122.5	
Poles: 4	Wires per Lead: 4	0.5	245.0	
Sync Speed: 1500	Generator Pitch: 0.6667	0.75	367.5	
		1.0	490.0	
		1.1	539.0	
			91.2	
			93.9	
			95.4	
			96.0	
			96.2	
Reactances		Per Unit	Ohms	
SUBTRANSIENT - DIRECT AXIS X''_d		0.0671	0.0219	
SUBTRANSIENT - QUADRATURE AXIS X''_q		0.1504	0.0491	
TRANSIENT - SATURATED X'_d		0.1023	0.0334	
SYNCHRONOUS - DIRECT AXIS X_d		1.5049	0.4914	
SYNCHRONOUS - QUADRATURE AXIS X_q		0.7430	0.2426	
NEGATIVE SEQUENCE X_2		0.1090	0.0356	
ZERO SEQUENCE X_0		0.0034	0.0011	
Time Constants		Seconds		
OPEN CIRCUIT TRANSIENT - DIRECT AXIS T_{d0}		3.9310		
SHORT CIRCUIT TRANSIENT - DIRECT AXIS T'_d		0.2670		
OPEN CIRCUIT SUBTRANSIENT - DIRECT AXIS T''_{d0}		0.0101		
SHORT CIRCUIT SUBTRANSIENT - DIRECT AXIS T''_d		0.0074		
OPEN CIRCUIT SUBTRANSIENT - QUADRATURE AXIS T''_{q0}		0.0196		
SHORT CIRCUIT SUBTRANSIENT - QUADRATURE AXIS T''_q		0.0149		
EXCITER TIME CONSTANT T_c		0.1090		
ARMATURE SHORT CIRCUIT T_A		0.0455		
Short Circuit Ratio: 0.82		Stator Resistance = 0.0048 Ohms		
		Field Resistance = 1.476 Ohms		
Voltage Regulation		Generator Excitation		
Voltage level adjustment: +/-	5.0%	No Load	Full Load, (rated) pf	
Voltage regulation, steady state: +/-	0.5%		Series	Parallel
Voltage regulation with 3% speed change: +/-	0.5%	Excitation voltage:	7.53 Volts	17.0 Volts
Waveform deviation line - line, no load: less than	5.0%	Excitation current	1.97 Amps	3.66 Amps
Telephone influence factor: less than	50			

Selected Model

Engine: 3508	Generator Frame: 685	Genset Rating (kW): 490.0	Line Voltage: 400
Fuel: Natural Gas	Generator Arrangement: 6I3095	Genset Rating (kVA): 490.0	Phase Voltage: 230
Frequency: 50	Excitation Type: Permanent Magnet	Pwr. Factor: 1.0	Rated Current: 707.3
Duty: CONTINUOUS	Connection: SERIES STAR	Application: EPG	Status: Current

Version: 38901 /38433 /38285 /4455

Figure G.2: Generator datasheet



refprop datasheets

The refprop data shown in H.1 is used to calculate the vaporization percentage before entering the cylinder in chapter 5.41.

1b: Air: Specified state points (75,571,2691/23,16)																		
	Temperature (K)	Pressure (MPa)	Density (kg/m ³)	Liquid Phase Density (kg/m ³)	Vapor Phase Density (kg/m ³)	Enthalpy (kJ/kg)	Liquid Phase Enthalpy (kJ/kg)	Vapor Phase Enthalpy (kJ/kg)	Entropy (kJ/kg-K)	Liquid Phase Entropy (kJ/kg-K)	Vapor Phase Entropy (kJ/kg-K)	Cv (kJ/kg-K)	Liquid Phase Cv (kJ/kg-K)	Vapor Phase Cv (kJ/kg-K)	Cp (kJ/kg-K)	Liquid Phase Cp (kJ/kg-K)	Vapor Phase Cp (kJ/kg-K)	Heat of Vapor. (kJ/kg)
1	289.00	0.078000	0.94031	Superheated	0.94031	289.30	Superheated	289.30	6.9043	Superheated	6.9043	0.71761	Superheated	0.71761	1.0059	Superheated	1.0059	Undefined
2	289.00	0.142000	1.7123	Superheated	1.7123	289.14	Superheated	289.14	6.7318	Superheated	6.7318	0.71778	Superheated	0.71778	1.0070	Superheated	1.0070	Undefined
3	333.00	0.780000	8.1606	Superheated	8.1606	332.34	Superheated	332.34	6.3821	Superheated	6.3821	0.72137	Superheated	0.72137	1.0167	Superheated	1.0167	Undefined
4	333.00	0.142000	1.4853	Superheated	1.4853	333.48	Superheated	333.48	6.8746	Superheated	6.8746	0.72016	Superheated	0.72016	1.0088	Superheated	1.0088	Undefined
5	313.00	0.780000	8.6907	Superheated	8.6907	312.00	Superheated	312.00	6.3192	Superheated	6.3192	0.72031	Superheated	0.72031	1.0170	Superheated	1.0170	Undefined
6	313.00	0.142000	1.5805	Superheated	1.5805	313.31	Superheated	313.31	6.8121	Superheated	6.8121	0.71890	Superheated	0.71890	1.0078	Superheated	1.0078	Undefined
7																		

8: methanol: Specified state points												
	Temperature (K)	Pressure (MPa)	Density (kg/m ³)	Liquid Density (kg/m ³)	Vapor Density (kg/m ³)	Enthalpy (kJ/kg)	Liquid Enthalpy (kJ/kg)	Vapor Enthalpy (kJ/kg)	Entropy (kJ/kg-K)	Liquid Entropy (kJ/kg-K)	Vapor Entropy (kJ/kg-K)	Heat of Vapor. (kJ/kg)
1	292.00	0.142000	792.13	792.13	Subcooled	-120.94	-120.94	Subcooled	-0.38444	-0.38444	Subcooled	Undefined
2	292.00	0.151000	792.14	792.14	Subcooled	-120.94	-120.94	Subcooled	-0.38445	-0.38445	Subcooled	Undefined
3	350.00	0.100000	1.1359	Superheated	1.1359	1139.4	Superheated	1139.4	3.3761	Superheated	3.3761	Undefined
4												

2: Air: Specified state points (75,571,2691/23,16)																	
	Temperature (K)	Pressure (MPa)	Density (kg/m ³)	Liquid Phase Density (kg/m ³)	Vapor Phase Density (kg/m ³)	Enthalpy (kJ/kg)	Liquid Phase Enthalpy (kJ/kg)	Vapor Phase Enthalpy (kJ/kg)	Entropy (kJ/kg-K)	Liquid Phase Entropy (kJ/kg-K)	Vapor Phase Entropy (kJ/kg-K)	Cv (kJ/kg-K)	Liquid Phase Cv (kJ/kg-K)	Vapor Phase Cv (kJ/kg-K)	Heat of Vapor. (kJ/kg)		
1	313.00	0.172000	1.9145	Superheated	1.9145	313.25	Superheated	313.25	6.7569	Superheated	6.7569	0.71897	Superheated	0.71897	Undefined		
2	333.00	0.178000	1.8619	Superheated	1.8619	333.41	Superheated	333.41	6.8095	Superheated	6.8095	0.72023	Superheated	0.72023	Undefined		
3																	

Figure H.1: refprop used data



Natural gas analyse

The used NG is very dependent on the composition of the natural gas. The used natural gas is from the Dutch grid and composition is given in this appendix.



ANALYSERAPPORT

Blad 1 van 2

Datum rapport : 20 februari 2018
 Projectnummer : 18-0041 HC

Gegevens opdrachtgever

Naam : Pon Power BV
 Adres : Ketelweg 20
 Woonplaats : 3356 LE Papendrecht
 T.a.v. : Dhr. L. Goedhart

Doel analyse

Analyse van een gasmonster op hoofdcomponenten.

Werkwijze

De analyse is uitgevoerd op basis van ISO-6974 deel 1 t/m 3; "Natural gas - Determination of hydrogen, inert gases hydrocarbons up to C8 - Gas chromatographic method".

De berekeningen zijn uitgevoerd conform ISO-6976; "Natural gas - Calculation of calorific value, density and relative density".

Omschrijving monster

Monsternr	Cilindernr	Datum	Tijd	Monsternaam
M52011	91005	06-12-2017	08:30 uur	Aardgas Papendrecht

Monsternemer : W. Sluijs

Toegepast meetstelsel

Fabrikant : Interscience Thermo Scientific
 Type : Trace 1300 Gas Chromatograph
 Serienummer : s/n 714530067
 Bouwjaar : 2014

Analyse gegevens

Datum analyse : 15-02-2018
 Analyse door : M. Veldkamp
 Resultaat analyse : Zie blad 2
 Paraaf analist :

Paraaf lab coördinator :
 Ing B.J. Gerritsen

Kiwa Technology B.V.
 Postbus 137
 7300 AC Apeldoorn Nederland

Fysisch Chemisch Laboratorium
 Wilmersdorf 50
 7327 AC Apeldoorn

Telefoon 088 998 3521
 Fax 088 998 3223
 www.kiwatechnology.nl

Dit rapport mag alleen in het geheel en met toestemming van de opdrachtgever gereproduceerd worden en heeft alleen betrekking op het voor dit onderzoek uitgenomen of afgeleverde gas

Figure I.1: Analyse of used NG (1/2)



ANALYSERAPPORT

Blad 2 van 2

Naam monster : Aardgas Papendrecht, 06-12-2017 08:30 uur
 Monsternummer : M52011
 Projectnummer : 18-0041 HC

Resultaat

De analyseresultaten en de berekende fysische grootheden uit de samenstelling hebben de onderstaande waarden. De m³ wordt gedefinieerd bij 0°C (meetcondities) en 1013.25 mbar. De energie in MJ is herleid van de thermodynamische waarden van 25°C (verbrandingscondities) tot 0°C en bij 1013.25 mbar volgens ISO 6976.

Component	Molprocenten	Onzekerheid (mol%)	
Helium	0.0418	0.0005	
Argon	0.0069	0.0002	
Waterstof	0.01	0.02	
Zuurstof	-	-	
Stikstof	13.1	0.1	
Kooldioxide	1.46	0.01	
Koolmonoxide	-	-	
Methaan	80.5	0.1	
Ethaan	3.79	0.03	
Propaan	0.690	0.006	
Isobutaan	0.122	0.001	
Butaan	0.131	0.001	
neo-Pentaaan	0.00481	0.00005	
isoPentaaan	0.0348	0.0004	
n-Pentaaan	0.0310	0.0003	
cyclopentaaan + 2,3-dimethylbutaan	0.00336	0.00003	
2,2-dimethylbutaan	0.00420	0.00004	
2-methylpentaan	0.00725	0.00006	
3-methylpentaan	0.00399	0.00004	
n-Hexaan	0.00900	0.00009	
C7-KWS	0.0168	0.0002	
C8-KWS	0.00681	0.00008	
Benzeen	0.0194	0.0004	
Tolueen	0.00182	0.00004	
Fysische grootheden:			
Calorische onderwaarde	32.48	0.04	MJ/m ³
Calorische bovenwaarde	35.97	0.05	MJ/m ³
Wobbe-index (inf.)	40.13	0.07	MJ/m ³
Wobbe-index (sup.)	44.45	0.08	MJ/m ³
Dichtheid t.o.v. lucht	0.6550	0.0006	-
Soortelijke massa	0.8469	0.0008	kg/m ³
- < 0,001 mol%			
De fysische grootheden hebben een onzekerheid van maximaal 0.2 % relatief (k=2).			
Controle Kaarten volgens Kiwa Technology WI403.			
Datum laatste kalibratie: januari 2018. Primair Referentie Materiaal: NPL2013100302-01/-09			

Kiwa Technology B.V.
 Postbus 137
 7300 AC Apeldoorn Nederland

Fysisch Chemisch Laboratorium
 Wilmersdorf 50
 7327 AC Apeldoorn

Telefoon 088 998 3521
 Fax 088 998 3223
 www.kiwatechnology.nl

Dit rapport mag alleen in het geheel en met toestemming van de opdrachtgever gereproduceerd worden en heeft alleen betrekking op het voor dit onderzoek uitgenomen of afgeleverde gas

Figure I.2: Analyse of used NG (2/2)

Bibliography

- [1] T. Adams, M; Jacobse, L; Vermeulen, M; Lelieveld. Combustion drive thesis. 2018.
- [2] B Anicic, P Trop, and D Goricanec. Comparison between two methods of methanol production from carbon dioxide Comparison between two methods of methanol production from carbon dioxide. *Energy*, 77(June 2016):279–289, 2014. ISSN 0360-5442. doi: 10.1016/j.energy.2014.09.069. URL <http://dx.doi.org/10.1016/j.energy.2014.09.069>.
- [3] Carsten Baumgarten. Mixture Formation in IC Engines. pages 215–230, 2006.
- [4] J Bomanson, P Molander, J Ellis, E Errestad, and H Klintonberg. Final Report GreenPilot – Pilot Boat with Minimal Environmental Impact.
- [5] Stijn Broekaert, Joachim Demuyne, Thomas De Cuyper, Michel De Paepe, and Sebastian Verhelst. Heat transfer in premixed spark ignition engines part I: Identification of the factors influencing heat transfer. *Energy*, 116:380–391, 2016. ISSN 03605442. doi: 10.1016/j.energy.2016.08.065. URL <http://dx.doi.org/10.1016/j.energy.2016.08.065>.
- [6] Mariska Buitendijk. Methanol as a marine fuel on the rise as Stena Germanica hits milestone - SWZ Maritime, 2020.
- [7] Carl L. Yaws. *Handbook of Thermodynamic Diagrams, Volume 1*. 1996.
- [8] Y. Ding. *Characterising Combustion in Diesel Engines: Using parameterised finite stage cylinder process models*. 2011. ISBN 9789065622891. URL <https://repository.tudelft.nl/islandora/object/uuid{%}3A10e25404-4b8e-443b-9f16-5e6e5c2a7444?collection=research>.
- [9] Yu Ding, Douwe Stapersma, The Netherland, Henk Knoll, and Hugo Grimmelius. Characterising Heat Release in a Diesel Engine: A comparison between Seiliger Process and Vibe Model. *CIMAC Congress 2010*, 2010.
- [10] Youness El Fouih and Chakib Bouallou. Recycling of carbon dioxide to produce ethanol. *Energy Procedia*, 37:6679–6686, 2013. ISSN 18766102. doi: 10.1016/j.egypro.2013.06.600. URL <http://dx.doi.org/10.1016/j.egypro.2013.06.600>.
- [11] Joanne Ellis and K Tanneberger. Study on the use of ethyl and methyl alcohol as alternative fuels in shipping. 46(0):8–31, 2015.
- [12] M. Ghaderi Masouleh, K. Keskinen, O. Kaario, H. Kahila, S. Karimkashi, and V. Vuorinen. Modeling cycle-to-cycle variations in spark ignited combustion engines by scale-resolving simulations for different engine speeds. *Applied Energy*, 250:801–820, sep 2019. ISSN 03062619. doi: 10.1016/j.apenergy.2019.03.198.
- [13] Maarten Van De Ginste and Louis Sileghem. Methanol als brandstof voor moderne vonkontstekingsmotoren : Rendementstudie. page 163, 2011.
- [14] Prof. Dr.-Ing. Dr. h. c. helmut tschöke Is. Thermodynamic Optimization Criteria for Ignition Timing Calibration of Advanced SI Engines. pages 52–57.
- [15] John B. Heywood. *Internal Combustion Engine (ICE) Fundamentals*, volume 21. 2015. ISBN 007028637X. doi: 10.1002/9781118991978.hces077.
- [16] International Maritime Organization (IMO). Nitrogen Oxides (NOx) – Regulation 13, 2008. URL [http://www.imo.org/en/OurWork/Environment/PollutionPrevention/AirPollution/Pages/Nitrogen-oxides-\(NOx\)---Regulation-13.aspx](http://www.imo.org/en/OurWork/Environment/PollutionPrevention/AirPollution/Pages/Nitrogen-oxides-(NOx)---Regulation-13.aspx).

- [17] Methanol Institute. Methanol Safe Handling Manual. (October), 2008.
- [18] D. Klein Woud, J; Stapersma. *Design of propulsion and electric power generation systems*. 2002.
- [19] Avinash Kumar, Agarwal Anirudh, Gautam Nikhil, Sharma Akhilendra, and Pratap Singh. *Methanol and the Alternate Fuel Economy Energy, Environment, and Sustainability Series Editors: Avinash Kumar Agarwal · Ashok Pandey*. ISBN 9789811332869. URL <http://www.springer.com/series/15901>.
- [20] David R. Lancaster, Roger B. Krieger, and John H. Lienesch. Measurement and analysis of engine pressure data. *SAE Technical Papers*, 84:155–172, 1975. ISSN 26883627. doi: 10.4271/750026.
- [21] Byungjoo Lee. The effects of methanol fuel on combustion in premixed dual fuel engine. 2016.
- [22] Jun Li, Chang Ming Gong, Yan Su, Hui Li Dou, and Xun Jun Liu. Effect of injection and ignition timings on performance and emissions from a spark-ignition engine fueled with methanol. *Fuel*, 89(12):3919–3925, 2010. ISSN 00162361. doi: 10.1016/j.fuel.2010.06.038. URL <http://dx.doi.org/10.1016/j.fuel.2010.06.038>.
- [23] Kun Liang and Richard Stone. Laminar burning velocity measurement of hydrous methanol at elevated temperatures and pressures. *Fuel*, 204:206–213, 2017. ISSN 00162361. doi: 10.1016/j.fuel.2017.05.060. URL <http://dx.doi.org/10.1016/j.fuel.2017.05.060>.
- [24] Fanhua Ma, Yu Wang, Haiquan Liu, Yong Li, Junjun Wang, and Shangfen Ding. Effects of hydrogen addition on cycle-by-cycle variations in a lean burn natural gas spark-ignition engine. *International Journal of Hydrogen Energy*, 33(2):823–831, 2008. ISSN 03603199. doi: 10.1016/j.ijhydene.2007.10.043.
- [25] TNO Maritime Knowledge Centre and TU Delft. Public final report-Methanol as an alternative fuel for vessels Project data. page 24, 2018. URL <https://platformduurzamebiobrandstoffen.nl/wp-content/uploads/2018/02/2018{ }MKC{ }TNO-TU-Delft{ }Methanol-as-an-alternative-fuel-for-vessels.pdf>.
- [26] Guenter Merker, Chirstian Schwarz, Gunnar Stiesch, and Frank Otto. *Simulating Combustion: Simulation of combustion and pollutant formation for engine-development*. Number 1. 2014. ISBN 9780874216561. doi: 10.1007/s13398-014-0173-7.2.
- [27] Methanex. Methanex monthly average regional posted contract price history. 2020.
- [28] B. Overmaat. <https://engineered.thyssenkrupp.com/en/world-environment-day-smarter-refueling-with-green-methanol/>, 2018.
- [29] Harsh Sapra, Milinko Godjevac, Peter De Vos, Wim Van Sluijs, Youri Linden, and Klaas Visser. MODELLING HYDROGEN-NATURAL GAS COMBUSTION : FROM EXPERIMENTS TO.
- [30] Harsh Sapra, Youri Linden, Wim van Sluijs, Milinko Godjevac, and Klaas Visser. Experimental investigations of performance variations in marine hydrogen-natural gas engines. In *Cimac Congress 2019*, pages 1–17, 2019. doi: 10.1016/B978-0-323-39396-6.00001-4.
- [31] Harsh Sapra, Milinko Godjevac, Peter De Vos, Wim Van Sluijs, Youri Linden, and Klaas Visser. Hydrogen-natural gas combustion in a marine lean-burn SI engine: A comparative analysis of Seiliger and double Wiebe function-based zero-dimensional modelling. *Energy Conversion and Management*, 207(January):112494, 2020. ISSN 01968904. doi: 10.1016/j.enconman.2020.112494. URL <https://doi.org/10.1016/j.enconman.2020.112494>.
- [32] Harsh Sapra, Jelle Stam, Jeroen Reurings, Lindert Van Biert, Wim Van Sluijs, Peter De Vos, Klaas Visser, Aravind Purushothaman Vellayani, and Hans Hopman. SOFC-ICE Integration for maritime applications. *To be Published*, pages 1–50, 2020.
- [33] Ray Sinnott and Gavin Towler. *Chemical engineering design*. 2008. ISBN 9780750684231.

- [34] D Stapersma. *Diesel Engines Volume 4 Emissions and Heat transfer April 2010*, volume 4. 2010. ISBN 0693485000.
- [35] D Stapersma. *Diesel Engines Volume 5 Thermodynamical Principles I*, volume 5. 2010. ISBN 0693485000.
- [36] D Stapersma. *Diesel Engines Volume 3 Combustion April 2010*, volume 3. 2010. ISBN 0693485000.
- [37] D Stapersma. *Diesel Engines Volume 6 Thermodynamical Principles II April 2010*, 2010.
- [38] D Stapersma. *Diesel Engines Volume 1 Performance Analysis. Lecture notes WB4408A*, 1 (January), 2010.
- [39] D Stapersma. *Diesel Engines, Volume 2 Turbocharging. Tu Delft*, 2(January):–, 2010.
- [40] TESTO. Instruction manual testo 350. *Science*, os-1(8):84–84, 1880. ISSN 0036-8075. doi: 10.1126/science.os-1.8.84-d.
- [41] Jorrit Harmsen (TNO). Green Maritime Methanol Project Plan. pages 1–14, 2018.
- [42] Sebastian Verhelst, James WG Turner, Louis Sileghem, and Jeroen Vancoillie. Methanol as a fuel for internal combustion engines. *Progress in Energy and Combustion Science*, 70:43–88, 2019. ISSN 03601285. doi: 10.1016/j.pecs.2018.10.001.
- [43] Ying Wang, Jingjing Zhang, Qingli Qian, Bernard Baffour Asare Bediako, Meng Cui, Guanying Yang, Jiang Yan, and Buxing Han. Efficient synthesis of ethanol by methanol homologation using CO₂ at lower temperature. *Green Chemistry*, 21(3):589–596, 2019. ISSN 14639270. doi: 10.1039/c8gc03320j.
- [44] Lijiang Wei, Chunde Yao, Quangang Wang, Wang Pan, and Guopeng Han. Combustion and emission characteristics of a turbocharged diesel engine using high premixed ratio of methanol and diesel fuel. *Fuel*, 140(X):156–163, 2015. ISSN 00162361. doi: 10.1016/j.fuel.2014.09.070. URL <http://dx.doi.org/10.1016/j.fuel.2014.09.070>.
- [45] Yanju Wei, Shenghua Liu, Fangjie Liu, Jie Liu, Zan Zhu, and Guangle Li. Formaldehyde and methanol emissions from a methanol/gasoline-fueled spark-ignition (SI) engine. *Energy and Fuels*, 23(6):3313–3318, 2009. ISSN 08870624. doi: 10.1021/ef900175h.
- [46] Desmond E. Winterbone and Ali Turan. Combustion and Flames. *Advanced Thermodynamics for Engineers*, pages 323–344, 2015. doi: 10.1016/b978-0-444-63373-6.00015-0.
- [47] La Xiang, Enzhe Song, and Yu Ding. A two-zone combustion model for knocking prediction of marine natural gas SI engines. *Energies*, 11(3), 2018. ISSN 19961073. doi: 10.3390/en11030561.
- [48] Fang-xi Xie, Xiao-ping Li, Xin-chao Wang, Yan Su, and Wei Hong. Research on using EGR and ignition timing to control load of a spark-ignition engine fueled with methanol. *Applied Thermal Engineering*, 50(1):1084–1091, 2013. ISSN 1359-4311. doi: 10.1016/j.applthermaleng.2012.08.003. URL <http://dx.doi.org/10.1016/j.applthermaleng.2012.08.003>.
- [49] Dong Wei Yao, Xin Chen Ling, and Feng Wu. Evaporate prediction and compensation of intake port wall-wetting fuel film for spark ignition engines fueled with ethanol-gasoline blends. *Journal of Zhejiang University: Science A*, 13(8):610–619, 2012. ISSN 1673565X. doi: 10.1631/jzus.A1200068.
- [50] Ke Zeng, Zuohua Huang, Bing Liu, Liangxin Liu, Deming Jiang, Yi Ren, and Jinhua Wang. Combustion characteristics of a direct-injection natural gas engine under various fuel injection timings. *Applied Thermal Engineering*, 26(8-9):806–813, 2006. ISSN 13594311. doi: 10.1016/j.applthermaleng.2005.10.011.